Università Politecnica delle Marche
Scuola di Dottorato di Ricerca in Scienze dell'Ingegneria
Curriculum in Ingegneria Civile, Ambientale, Edile e Architettura

---

Elasto-plastic models for the response of passive rigid piles

Ph.D. Dissertation of:
Caferri Leonardo

Tutor:
Prof. PASQUALINI ERIO

Co-tutor:
Prof. BELLEZZA IVO

Curriculum Advisor:
Prof. LENCI STEFANO

XV edition - new series

Università Politecnica delle Marche
Dipartimento di Ingegneria Civile, Ambientale, Edile e Architettura
Via Brecce Bianche — 60131 - Ancona, Italia

ABSTRACT

The use of piles to stabilise active landslides or to prevent future instabilities has been successfully applied in the past and is nowadays a widely accepted technique.

However, while the stabilising piles are usually designed with the aim of reducing the soil displacement rate, the design strategies commonly adopted in engineering practice apply to the ultimate state only, not taking into account any realistic interaction mechanism between pile and soil, and are not capable of predicting the effectiveness of the pile and soil displacement magnitude.

The goal of the present investigation is to propose a practical displacement-based numerical methodology for the analysis and design of passive rigid piles in different ground conditions. The developed method considers both a free-head and an unrotated-head rigid pile, embedded in a Winkler type soil and subjected to the sliding of a surrounding soil. The Winkler approach allows to consider a layered soil stratigraphy and to use the horizontal displacement of the surrounding soil as an input to evaluate the associated lateral deflection of the pile as well as the acting shear forces and bending moments in function of the external ground displacement. A FORTRAN computer program has been written to implement the numerical procedure.

The proposed method seems to be suitable for being implemented in traditional Limit Equilibrium Methods or more in general in any decoupled approach method. Moreover, non-dimensional design charts have been developed for simplified soil stratigraphies, in which the required shear force offered by the pile is plotted over the sliding surface depth, as a function of the pile head deflection, the maximum bending moment and the external soil displacement.

LIST OF TABLES

LIST OF FIGURES

TABLE OF CONTENTS

NOTATION

N = normal force
T = shear force
M = bending moment
D = pile diameter
F_d = total of the disturbing actions along a slip surface
F_r = total of the resisting actions along a slip surface
M_R = total of the resisting bending moments along a slip surface
M_d = total of the disturbing bending moments along a slip surface
SF = factor of safety of a unreinforced slope
SF_T = factor of safety of a pile-reinforced slope
SF_{target} = target factor of safety for a pile-reinforced slope
RF = slope stabilising contribution provided by the piles
N_p = ultimate undrained lateral bearing capacity factor
s = centre-to-centre pile spacing in a row
d = clear spacing between the piles in a row
μ = pile-soil adhesion factor
s_1 = critical pile spacing
N_{p1} = ultimate undrained lateral bearing capacity factor
p_y = yielding soil-pile pressure [FL-2]
$p(z)$ = elastic force per unit length of the pile at the depth z [FL-1]
p_u = ultimate force per unit length of the pile [FL-1]
K_p = Rankine passive pressure coefficient
φ' = internal friction angle of the soil
c' = effective cohesion of the soil
φ_R = reduced internal friction angle of the soil
c_R = reduced cohesion of the soil
Su = undrained shear strength of soil
σ'_{v0} = initial vertical effective stress
γ = total unit weight of the soil
γ' = effective soil unit weight of the soil
h = load transfer reduction factor

k_h = coefficient of subgrade reaction of a soil mass [FL^{-3}]
E_s = subgrade reaction modulus or elastic spring modulus [FL^{-2}]
L = pile length
L_s, L_1 = sliding surface depth (βL)
L_0 = first layer thickness (λL)
L_2 = firm layer thickness
β = ratio between sliding depth and pile length Ls/L
λ = ratio between first layer thickness and pile length L_0/L
E_p = Young's modulus of the pile
J_p = Moment of inertia of the pile section
I = characteristic pile length [L]
z,z_n = depth and the normalised depth z/L, respectively
$y_{p(z)}$ = pile deflection at the depth z
y_0 = pile head's deflection at ground level
y_{0n} = normalised pile head's deflection at ground level Y_0/L
ω = pile rotation angle
M_0 = bending moment on pile head for the unrotated head fixity condition
M_{0n} = normalised bending moment on pile head for the unrotated head fixity condition
T = shear force
T_n,T_m = normalised shear force
M = bending moment
M_n = normalised bending moment
M_y = yielding moment of the pile section
$y_s(z)$ = soil movement at the depth z
y_{s0} = soil free-field movement at ground surface
y_{s0} = normalised soil free-field movement at ground surface Y_{s0} /L
θ = angle of linear variation of the free-field soil movement
η = ratio between soil displacement at ground level and at Ls
Y(z) = relative soil-pile displacement at a generic depth of z
Δy_0 = relative soil-pile displacement at ground level
Δy_{0n} = normalised relative soil-pile displacement at ground level
Δtan = relative soil-pile tangent of rotation angle

k = ratio between E_s or p_u of stable and unstable soils

α_0 = ratio between modulus of subgrade reaction at ground level and at L_s or L_0 when linearly varying with depth

k_0 = ratio between p_u at ground surface and stable and at $z=L_0$

m = gradient of the ultimate force per unit length of the pile (FL^{-2})

m_1,m_2 = gradient of p_u for unstable and stable layer

X = ratio of gradients of p_u ($X = m_1/m_2$)

n = gradient of the horizontal subgrade reaction modulus (FL^{-3})

N_y = Proportionality constants in the elastic solutions

N_t = Proportionality constants in the elastic solutions

$N_{\Delta y}$ = Proportionality constants in the elastic solutions

$N_{\Delta t}$ = Proportionality constants in the elastic solutions

N_M = Proportionality constants in the elastic solutions

D = Proportionality constants in the elastic solutions

a = coefficients of a six order governing equations for failure mode B, B1, BY and B2

1. Introduction

When subjected to a lateral force due to the horizontal movements of the surrounding soil, piles are defined as passive piles, in opposition to active piles, i.e. being part of piled walls, subjected to applied forces. Obviously, both kinds of situations are governed by the same series of parameters as the deformability of the pile and the soil and the ultimate soil resistance, all governed by the interaction soil-pile.
Anyway, active piles transmit lateral loads to the soil due to a horizontal load applied on it, being the horizontal soil movements the consequence of their action. They are frequently used for supporting axial and lateral loads for different structures, cases in which the horizontal loads governs the design of the piles. The problem of active piles either in clay or sand has already been treated by several authors (Broms [1], Matlock and Reese [2], Zhang L. [3]), by using different approaches.

On the contrary, piles which are subjected to lateral loading along their length caused by horizontal movements of the surrounding soil are instead defined as passive piles. Passive load on the piles may occur every time changes in the surrounding soil stress state provoke a movement in the soil mass, for example those installed close to embankments, tunnels or earthworks. Typical cases are piles solicited by the installation of adjacent others or crossing liquefying layers subjected to earthquakes.
Another common example is the use of shaft in unstable slopes to prevent or reduce the occurrence of slope failures. The use of piles to stabilise active landslides or to prevent future events has been successfully applied in the past, due to the easy installation in slopes which does not disturb or compromise the equilibrium of the land.
However, there remain uncertainties on the design of passive piles, and an agreement on how to model passive piles has still to be reached, due to the complex phenomena ruling the soil-pile interaction and the several factors affecting it.

The presented research work has the primary goal of developing a reliable and representative design method that accounts for the effect of the soil and pile properties on the performance of passive piles based on the soil-pile interaction.
The method results to be capable to analysis and design passive piles, estimating the pile reaction as a function of the external soil displacement acting on it as well as predicting the complete pile deflection and stress state.
In particular, several different soil stratigraphy and pile boundary conditions are analysed and relative elastic or elasto-plastic solutions of the soil-pile system are developed. The proposed design approach was also compiled into a computer program for the analysis of pile-soil system.
In addition, examples of practical design charts are also shown as results of the implemented methodology.

2. Analysis methods of passive piles

The definition of active piles refers to a pile subjected to an external horizontal force and, eventually, a bending moment applied on its head. On the other hand, if subjected to a soil movement, piles are known as passive piles (Figure 2-1).

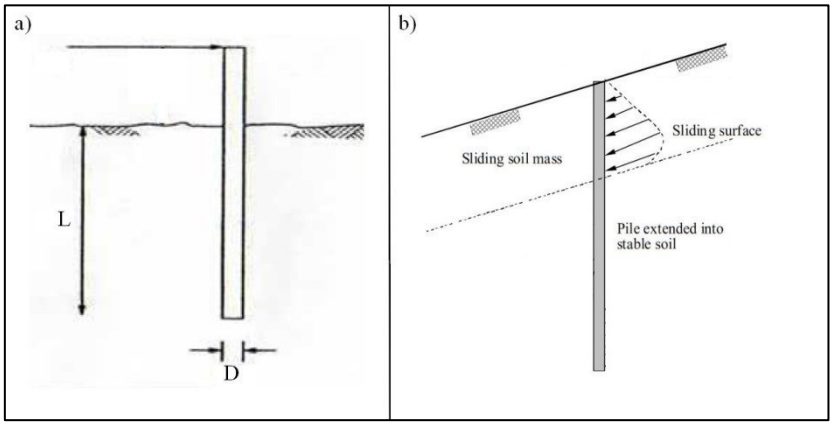

Figure 2-1:Schematic sections of : a) Active pile with length L, diameter D. b) Passive pile embedded in a surrounding sliding soil

Driven or drilled piles work as passive piles whenever they are installed to prevent or at least reduce the likelihood of slope failure or are subjected to a lateral force due to the horizontal movements of the surrounding soil if changes in the stress state provoke a movement in the soil mass.

Soil movement is also encountered in practice when piles are placed in an unstable slope, landslides, adjacent to deep excavation, tunnel operation, marginally stable riverbank with high fluctuating water level and also in piles supporting bridge abutment adjacent to approach embankments.

This chapter attempts to present an overview mainly for single pile in different topics: pile-supported embankment, piles adjacent to deep excavation, pile

subjected to horizontal soil movement as used for slope stabilisation. It aims to be only an overview and brief description of the contributions given by various researchers and to present the discussion mainly to emphasise the significance of past researches on passive piles used as stabilising system.

2.1. Pile-supported embankments

The consolidation of embankments on clay can produce significant vertical and horizontal movements of the adjacent soil. Piles supporting bridge abutments might then be axially and laterally loaded by these soil movements. The assessment of the resulting axial force and movement, bending moment and lateral deflection developed in the piles are then fundamental for the design of the piles. Figure 2-2 shows a schematic section through such a structure, illustrating the forms of interaction which tend to increase lateral structural loading and displacement, and hence may result in unserviceable behaviour of the abutment or bridge deck.

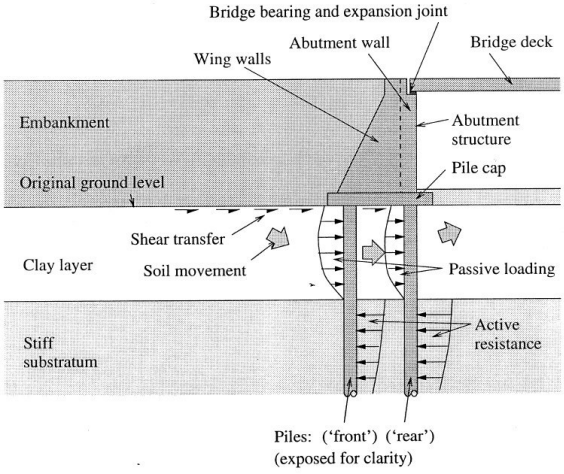

Figure 2-2: Schematic section through a full-height piled bridge abutment constructed on soft clay [4]

De Beer & Wallays [5] proposed a simple semi-empirical method to estimate the maximum bending moment for piles subjected to asymmetrical surcharges. They assumed that a constant lateral pressure distribution acted on the pile in the soft layer and assessed the magnitude of this lateral pressure as a function of the total vertical lithostatic pressure, friction angle and the slope of a fictitious embankment of material. They suggested that the lateral loading was caused by horizontal consolidation and creep, involving that their method was primarily intended to design piles in the long term. Otherwise, the method cannot be used to calculate the variation of bending moment with depth along the pile. Therefore, they conservatively recommended that the piles should be reinforced over their whole length to carry the maximum calculated bending moment. After calibrating the method against a few case studies, they demonstrated that the method is only suitable if a large margin of safety is provided against the overall instability of the soil mass.

The effects of vertical drains in the clay layer within embankments was investigated by Ellis [6] through a series of geotechnical centrifuge tests of full-height piled bridge abutments examining the effect of soft clay layer depth and the rate of embankment construction. The results confirmed the existence of established interaction effects due to lateral displacement of clay past piles.

Following this, Ellis and Springman [4] presented an accompanying series of plane strain finite element analyses for the same series of geotechnical centrifuge tests to study the soil-structure interaction effects. Although some aspects of the structure do not conform to a plane strain analysis (most notably the piles), success of the method is illustrated by good comparison with the centrifuge test results.

For piles to support a retaining wall, the recommendations of Terzaghi et al. [7] embodied in charts, are based on the use of the equivalent-fluid method and show the importance of the selection of an appropriate material for the backfill. A comparison of values from theory with values from the charts shows that the charts are close to those from Rankine's theory for active earth pressure. Therefore, the assumption is implicit in the Terzaghi charts that the wall is capable of some

movement without distress if the pressures from the backfill were greater than the chart values.

Finally, it is worth to be noticed the work made by Poulos [8], who reviewed some available design methods of piles through embankment and presented comparison between these methods for maximum bending moment in the piles, lateral pile head deflection, maximum axial force in pile and axial pile head settlement. Some of the methods being reviewed are the method of De Beer and Wallays [9], an approach used by a road authority in Australia, a simplified analysis of pile downdrag and design charts developed from boundary element analyses of pile-soil interaction. It is interesting that the author concludes that none of the previously available methods appears able to provide a consistent means of estimating the lateral response of piled embankment.

2.2. Piles adjacent to deep excavation

In dense urban environment where buildings are closely spaced, deep excavation for basement construction and other underground facilities is unavoidable. These deep excavations would cause lateral soil movement behind the excavation, which would in turn induce lateral loading on adjacent pile foundations and consequently additional bending moment and deflection.

For example, Finno et al. [10] reported the analyses of performance of groups of piles located adjacent to a 50-ft-deep tieback excavation. Evaluation of effects of movements on the adjacent piles was then carried out using a plane strain finite element code. However, accuracy of the approach could not be clearly verified due to less certainty with the selection of soil parameters, especially the soil's modulus because of the lack of detailed laboratory or in situ testing.The uncertainty of modelling the equivalent bending stiffness of the pile group in plane strain resulted in lower and upper bound solution.

Poulos & Chen [11] did a two stage analysis by use of the finite-element method and the boundary-element method to analyse the response of piles due to unsupported excavation-induced lateral soil movement in clay. Initially, a plane strain finite element method was used to simulate the excavation procedure and to generate free-field soil movements, that is the soil movement that would occur. These generated soil movements are then used as input into a boundary element method to analyse the pile's response.

On the contrary, Goh et al. [12] presented the results of an actual full-scale instrumented study carried out to examine the behaviour of an existing pile due to nearby excavation of a 16m deep excavation with an in-soil inclinometer installed about 6m away . The instrumented existing pile was discretized into a finite number of discrete (linear elastic) beam elements. The interaction between the soil and the pile is modelled by a series of non-linear horizontal springs represented by a hyperbolic equation.

Recent efforts in centrifuge modelling of passive piles adjacent to unsupported excavation were done by Leung et al. [13] who presented the results of centrifuge tests of a single pile behind a stable and failed wall of a deep excavation in dense sand. The research also investigates the influence of head fixity and shows that behind the stable wall, the pile head deflection and maximum bending moment for the free-headed pile decrease exponentially with increasing distance from the wall. Subsequently, he extended the centrifuge test to pile groups, incorporating the effects of interaction factors between the piles with different head fixities [14]. Further investigation was done for single pile behind stable wall [15] and unstable wall [16] in clay. It is concluded that calculated pile response is in good agreement with the measured data if correct shear strength obtained from post-excavation was used in numerical analysis. The numerical analysis was based on a simplified model and was used to back-analysed the responses of single pile subjected to lateral soil movements in clay. In this model, the pile is modelled as a series of linear elastic beam elements and the soil is idealised using the modulus of subgrade reaction. This numerical method has been also adopted successfully to back-analyse the centrifuge model tests on a single pile in sand.

2.3. Passive piles to increase slope stability

At present, simplified methods based on crude assumptions are used to design the driven or drilled piles needed to stabilise the slopes of embankments or to reduce the potential for landslides from one season to another. The major challenge lies in the evaluation of lateral loads (pressure) acting on the piles/pile groups by the moving soil and in the development of a representative model for the soil-pile interaction above and below the failure surface, both required to reflect and describe the actual distribution of the soil-pile pressure along the length of the pile.

The different mechanisms of failure and factors can be considered in the evaluation of the resistance contribution a pile can transmit implicate a distinction between two groups of methods used to describe soil-pile interaction: analytical methods, like pressure or displacement-based ones, and numerical methods, such as finite elements and finite differences. Nevertheless, it is important to highlight that a similarity of the applicability of method of analysis by using plane strain finite element method, subgrade reaction or elastic continuum formulation is that a specified free-field soil movement have to be inputted in the numerical method to analyse the response of the piles in terms of deflection.

2.3.1.Numerical methods

Over the last few years, the progress in computing and software power led to a wide application of the finite-element (FE) and finite differences (FD) methods, which provide the ability to model complex three-dimensional geometries and to run coupled analysis of soil-structure interaction such as pile group effects (Chow [17]; Cai and Ugai [18]; Won et al.[19]; Wei and Cheng [20];) as 2D analysis do not capture some aspect of the problem as soil arching. However, the applications of numerical methods in three dimensions are rather unattractive for practitioners as they are complex, computationally expensive and time-consuming.

Among all, Chow [17] presented a numerical approach in which the piles are modelled using beam elements and the surrounding soil using an average modulus

of subgrade reaction. The theory of elasticity is therefore used to simulate the soil-pile-soil interaction while the sliding soil movement profile is assumed according to field measurements. The same method has been used later by Cai and Ugai [18] for the same scope.

More recently, Kourkoulis et al. 2011 [21], [22] developed a hybrid methodology for the design of slope-stabilizing piles aimed at reducing the amount of computational effort usually associated with 3D soil-structure interaction analyses. This method involves all the steps for evaluating the required lateral resisting force per unit length of the slope, needed to increase the safety factor to the desired value by using the results of a conventional slope stability analysis, and for estimating the pile configuration that offers the required force for a prescribed deformation level using a 3D finite element analysis. This approach computes the lateral capacity of the piles by numerically three-dimensionally simulating only a limited region of soil around the piles and imposing a uniform displacement profile into the model boundary.

2.3.2. Analytical methods

The analytical methods used for the analysis of passive piles can generally be classified into two different types: pressure-based methods and displacement-based methods.

The pressure-based methods (Broms [1]; Viggiani[23]; Randolph and Houlsby, [24]; Ito and Matsui [25]) are centred on the analysis of passive piles that are subjected to the ultimate lateral soil pressure. The most notable limitation of pressure-based methods is that they apply to the ultimate state only (providing ultimate soil-pile pressure) and do not give any indication of the development of pile resistance with soil movement (mobilised soil-pile pressure). Therefore, their application should be limited to already stable soil configurations, in which piles are called to give a contribution to reach a mandatory higher factor of safety.

In displacement-based methods (Poulos [26]; Lee et al. [27]), the lateral soil movement above the failure surface is used as an input to evaluate the associated

lateral response of the pile. These methods are superior to the pressure-based ones as they can provide the mobilised pile resistance by considering the soil external movement as the input of the calculation. In addition, they reflect the true mechanism of soil-pile interaction. For this reason, this kind of methods better fit with analysis of slopes where a soil movements are already acting: the free-field soil movements that can be evaluated by monitoring the landslide or by modelling the slope behaviour can be used as an input for the calculation of the piles response, making possible to optimise their design according to the admissible displacements of the retaining piles wall or of the ground.

Due to this advantages, the analytical displacement-based approach has been chosen for the development of the method object of the present dissertation.
However, in the following paragraph a list of the more interesting methods is given in order to provide a review of the methods available in literature

2.3.3. Pressure-based methods

Analysing different soil-pile failure modes with depth, Broms [1] suggested the several equations to calculate the ultimate soil-pile pressure p_u for a single pile both in sand, as a function of the Rankine passive pressure coefficient K_p, and in cohesive soils, as function of the undrained shear strength Su and of a bearing capacity factor N_p varying with depth.
Viggiani [23] proposed a simplified method in which the maximum shear force provided by a single unrestrained pile is derived assuming that soil movements are great enough to fully mobilise the limiting soil pressure above and/or below the sliding surface. With this assumption, Viggiani derived dimensionless solutions for the ultimate lateral resistance of a pile in a two-layer purely cohesive soil profile. These solutions provide the pile shear force at the slip surface and the maximum pile bending moment as a function of the pile length and the ultimate soil-pile pressure p_u in stable and unstable soil layers. With this assumption, six failure modes were analysed and dimensionless solutions for shear force and maximum bending moment are derived for each potential failure mechanism (Chmoulian [28]). The solution of Viggiani is applicable only to soil in undrained condition

with an ultimate lateral pressure constant with depth in the stable and unstable layer.

Among all, Guo [29] proposed pressure-based pile–soil models and developed their associated solutions to capture response of rigid piles subjected to soil movement. The impact of soil movement was schematized as a fixed distributed loading over a sliding depth, and load transfer model was adopted to mimic the pile–soil interaction. The soil is modelled according to a Winkler approach with an assumption of a constant subgrade reaction modulus with depth. The solutions are presented in explicit expressions and can be readily obtained. It should be noticed that, along the length subjected to the soil displacement, both the fixed distributed external loading and the reaction pressure due to the soil-pile interaction are acting on the pile at the same time.

2.3.4.Displacement-based methods

In displacement-based methods (Poulos, [26]; Lee et al., [27]), the lateral soil movement above the failure surface is used as an input to evaluate the associated lateral response of the pile. The superiority of these methods over pressure-based methods is that they can provide mobilised pile resistance by soil movement. In addition, they reflect the true mechanism of soil-pile interaction.
Poulos [26] in particular presented a method of analysis of a row of passive piles practically as improvement of the solutions already provided by Viggiani [23], aiming to describe the full soil-pile interaction and not only the ultimate lateral state. For this reason, the pile is modelled as an elastic beam and the soil as an elastic continuum and the calculation carried out by using a finite-difference method (Figure 2-3), so that the model can evaluate the maximum shear force that each pile can provide based on an assumed free-field soil movement input and also compute the associated lateral response of the pile. Poulos assumes that a large volume of soil (the upper portion) moves downslope as a block over a relatively thin zone undergoing intense shearing in the “drag” zone (Figure 2-4). It is assumed an elasto-plastic model for both the pile and the soil: the soil close to the pile interface can undergo elastic strains until the limit pressure is reached (both the

elastic modulus and the limit pressure of the soil are assumed as varying along pile length).

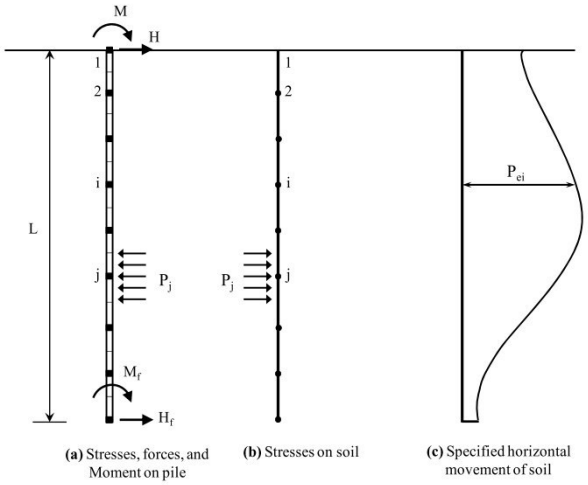

Figure 2-3: Model for piles in soil undergoing lateral movement [26]

It should be noticed that, while the pile and soil strength and stiffness properties are taken into account to obtain the soil-pile pressure, the group effects, namely pile spacing, are not considered in the analysis of the soil-pile interaction.

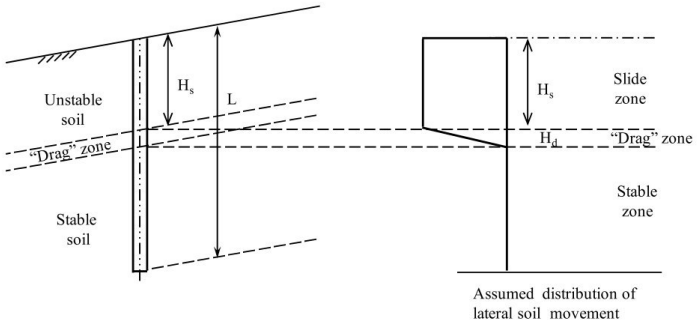

Figure 2-4: Free-field soil movement [26]

The analysis revealed the following failure modes, basically the same found by Viggiani [23]:

-The “flow mode” (or Mode C), when the depth of the failure surface is shallow and the sliding soil mass becomes plastic and flows around the pile (see Figure 2-5a). In this case, the pile deflection is considerably less than the soil movement.
-The “intermediate mode” (or Mode B), when the depth of the failure surface is relatively deep and the soil strength along the pile length in both unstable and stable layers is fully mobilised (see Figure 2-5b). In this mode, the pile deflection at the upper portion exceeds the soil movement and a resisting force is applied from downslope to this upper portion of the pile.
-The “short pile mode” – when the pile length embedded in stable soil is shallow and the pile will experience excessive displacement due to soil failure in the stable layer (Figure 2-5c).
-The “long pile failure” – when the maximum bending moment of the pile reaches the yields moment (the plastic moment) of the pile section and the pile structural failure takes place ($M_{max} = M_y$).This mechanism can be associated with any of the others, even if experience suggests that it is most likely to occur with the intermediate mode.

What it is worth to be highlighted is that the maximum shear force in the pile is always developed at the level of the slip surface; its maximum value occurs when the soil slide depth is about 0.5-0.6 times the pile length. Moreover, For practical uses, the author endorsed the flow mode as it creates the least damage from soil movement on the pile. Otherwise, as maximum shear forces and bending moments are developed under the intermediate mode, slope stabilising piles should be designed so that this mode of behaviour occurs.

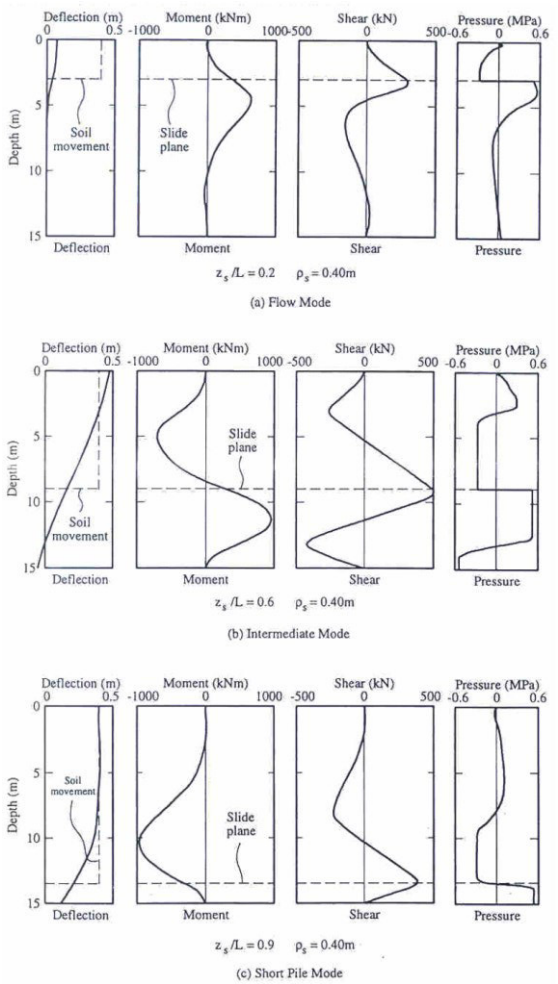

Figure 2-5: Pile behaviour characteristics for various modes with the hypothesis of constant soil movement in the slide zone, no "drag" zone, pile length of 15m and diameter 0.5m. Sliding soil with Su=30kPa and firm soil with Su=60kPa [26]

3. Passive pile in a linear elastic soil: a displacement-based model for passive pile in a linear elastic soil

Elastic solutions for laterally loaded piles are utilised successfully to predict the behaviour of passive piles. Recent studies suggest that the response of rigid passive piles is dominated by elastic pile–soil interaction [30]. They reveal that about one-third of limiting pressure on passive piles is induced by an elastic interaction. According to Chen and Poulos [31], relatively small soil movements, generally of the order of 5% of the pile diameter, are sufficient to fully mobilise the pile response obtained by mean of an elastic soil behaviour.

For this reason, the present work proposes a displacement-based model for the design of stabilising piles and develops their associated elastic solutions targeting the response in terms of shear force and bending moment along a rigid pile subjected to horizontal soil movement. Therefore, in comparison with available solutions for the ultimate state, the research aims at the development of a general framework focusing on the response of a pile to free-field soil movements, based on purely elastic soil behaviour and considering any stage of ground movement. The only static response is deemed. The analysis is designed to be subsequently improved to incorporate the nonlinear stress-strain relationships of soils and ultimate states, as described in next chapters.

More in particular, the analysing method considers a single rigid pile embedded in a sliding mass. Avoiding an initial assumption on the soil impact pressure on the shafts, the lateral displacement of the moving soil interesting the shaft is used as an input to evaluate the associated lateral deflection and strain state of the pile, according to the sliding depth and the ground and pile strengths. The method can consider a general linear free field soil movement with extreme cases represented by a uniform and an inverse triangular variation with depth. In light of a Winkler model [32], the pile-soil reaction is given by the coefficient of subgrade E_s and is represented by force per unit length. The solutions of the equilibrium equations

between the soil-pile pressures calculated both above and below the sliding surface are developed in explicit expressions for calculating bending moments, shear forces and deflection.
Different soil stratigraphies and pile boundary conditions are analysed to encompass the more common design configurations, as the presented result seems to be suitable for being implemented in traditional Limit Equilibrium Methods or more in general in any decoupled approach method, whenever the analysed slope presents an active landslide.

3.1. Overview of the Winkler model

Research on analysis of passive piles started more than five decades ago. As a consequence of such sustained research, several analysis methods have been developed and can be used for the design (an account of the salient available methods has been provided in chapter 2). While solutions for the ultimate lateral resistance of a pile do not give any indication of the development of pile resistance with soil movement and take into account only the limiting soil pressure, in a displacement based analysis the soil strain and stress levels are linked to the relative soil-pile displacement through an appropriate constitutive model.
In the presented research work, the governing equations for the deflection of passive rigid piles are obtained by using a beam-on-elastic-foundation (or Winkler) approach. It illustrates how simple idealisations of the pile-soil interaction can be used to derive the equations for layered, elastic foundations and to develop the analytical equations.

According to the Winkler approach [32], the resistance of a subgrade against external forces can be assumed to be proportional to the ground deflection. In other words, the ground can be represented by a set of elastic springs so that the compression (or extension) of the springs (which is the same as the deflection of the ground) is proportional to the displacement of a beam (or a pile) under an applied load (Figure 3-1).

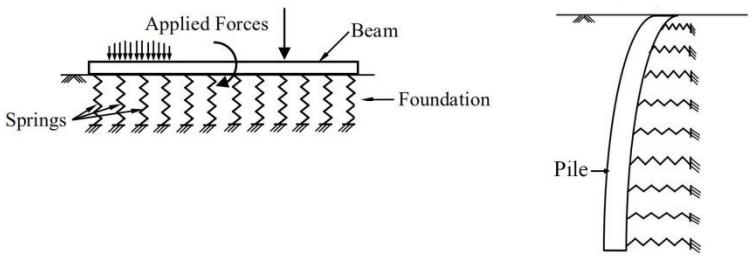

Figure 3-1: a) A beam on an elastic foundation; b) A pile on a bed of springs

The springs coefficient represents the stiffness of the ground (foundation) against the applied loads. It is important here to specify that the spring coefficient unit for a soil-pile system, in which the resistance is expressed per unit pile length, is [FL^{-2}] (F = force, L = length), while the spring coefficient unit of a conventional spring is [FL^{-1}].
The Winkler approach is also called subgrade-reaction approach as the foundation springs coefficient can be related to the coefficient of subgrade reaction of a soil mass k_h [FL^{-3}] (Terzaghi [33]): if the pressure at a point between the ground and the beam is *p* and if, because of *p*, the deflection of the point is y, then the modulus of subgrade reaction is given by *p*/y and has a unit of FL^{-3} (see Figure 3-2).

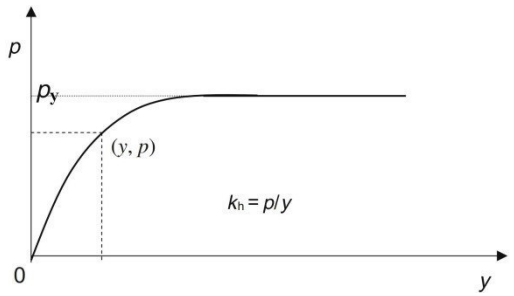

Figure 3-2: Soil reaction p and pile displacement y relationship

If k_h is multiplied by the width of the pile, gives the subgrade modulus E_s [FL^{-2}], considered as the spring modulus that multiplied by the spring deflection produces the resistive force of the soil per unit pile length.

$$E_s = k_h \cdot D \quad [FL^{-2}] \qquad (3\text{-}1)$$

Therefore, the spring modulus E_s is often estimated directly by experimental test, e.g. by performing a plate load test, or through correlations with soil strength parameters (a deeper explanation is given in Paragraph 3.3).
The solution provided in the present chapter only consider a linear elastic behaviour of the soil-pile interaction. Anyway, it has to be considered that the soil reaction (p) and pile displacement relation is nonlinear (Figure 3-2), particularly

near the top part of the pile. In order to simplify the problem, the soil can be assumed to be linear elastic-perfectly plastic [34]. In this case the empirical modulus of horizontal subgrade reaction E_s has to be estimated as a secant value in order to represent the real decreasing trend with increasing pile displacement.
In addition, as the pile movement increases to a certain level, the limit soil resistance p_u [FL^{-1}] will be reached: the p_u value is related to the limit yield pressure of the soil and to the relative pile-soil interaction.

The input parameters required are the elastic modulus and geometry of the beam, the spring modulus of the foundation (soil) and the magnitude and distribution of the soil movement. As a result, the beam deflection, bending moment and shear force along the length of the pile can be determined.

3.2. Problem definition and model hypotheses

The presence of a sliding mass over a firm stratum represents a typical and generalised condition for a passive loading on a pile, i.e. if used as a stabilising system.
The developed methods models the problem by considering a single rigid pile of length L and diameter D embedded in a moving soil to a depth of $L_s=\beta L$ (Figure 3-3). For simplicity, the ground and the slip surface are assumed to be horizontal.

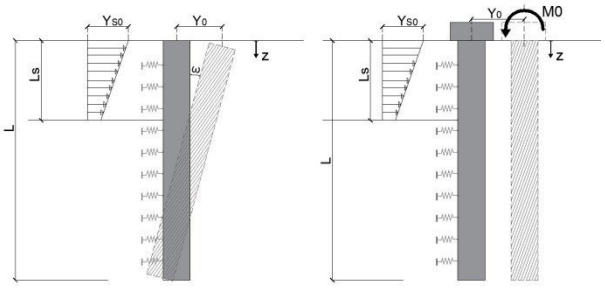

Figure 3-3: A Free—Head rigid and a unrotated-head pile subjected to a soil movement with a generic profile

Two cases for fixity condition of the pile head have been considered, namely: the free-head (rotation and displacement, Figure 3-3a), unrotated-head (displacement without rotation, $\tan\omega = 0$, Figure 3-3b). In the second case, the fixity condition is represented by the bending moment M_0 applied on the pile head.
More specifically, the presented displacement-based pile–soil interaction model, also based on the Winkler approach, is underpinned by the following hypotheses:

- The soil movement $y_s(z)$ has a magnitude of y_{s0} at the ground surface and follows a linear inverse decreasing with depth. It is defined through parameters Y_{s0} and the angle θ (Figure 3-4): y_{s0} represents the soil displacement at ground surface while its variation with depth is expressed by the θ angle, as described in the following formulation:

$$y_s(z) = y_{s0} - \tan\theta \cdot z \qquad 0 < z < Ls \qquad (3\text{-}2)$$

$$y_s = 0 \qquad Ls < z < L \qquad (3\text{-}3)$$

With:

$$tan\,\theta = (1-\eta)\frac{y_{s0}}{L_s} \qquad (3\text{-}4)$$

in which the ratio η is defined as:

$$\eta = \frac{y_s(z = L_s)}{y_{s0}} \qquad (3\text{-}5)$$

The soil movement distribution can vary from an inverse triangular variation with depth when no displacement occurs in correspondence of the slip surface (η=0) to a uniform distribution of the displacement when the unstable soil layers slide down as a single mass block (η=1). Intermediate values of η describe a generic trapezoidal profile of the soil movement.

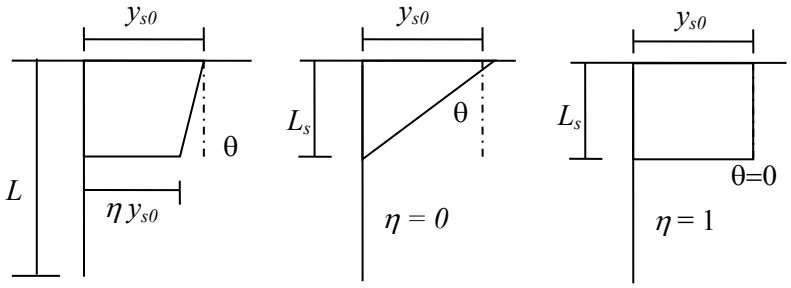

Figure 3-4:Distribution of the soil movement: a) generic distribution; b) inverse triangular variation with depth η=0; c)uniform distribution with depth η=1

- The kinematics of passive piles is complex and vary depending on its type.

Since piles subjected to soil movement are transversely loaded, the pile may rotate, bend or translate (Viggiani [35]), depending on the interaction between the pile and the soil. If the pile is long and slender, then it bends because of the applied load. These piles are called flexible piles. If the pile is short and stubby, it will not bend much but will rotate or even translate, and they are called rigid piles or shafts (Figure 3-5).

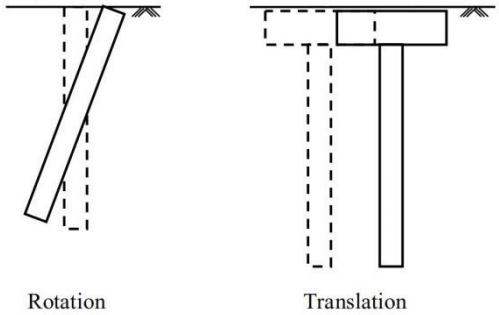

Figure 3-5: Kinematics of rigid piles

The proposed method is only applicable to rigid piles or shafts. This assumption results to be particularly suitable since the passive piles used as slope stabilising systems are generally rigid, with a big diameter in comparison to their length.

Several methods are available for determining whether a pile would behave as a rigid pile or not, including those by Broms [1], Matlock & Reese [2], Davisson and Gill [36]. Usually, to behave as a rigid one, the pile embedment length to diameter ratio should be smaller than 6. For a pile in a soil with a constant subgrade reaction modulus E_s, it can be considered to be rigid for practical purposes if the following condition is satisfied:

$$\frac{L}{I} \leq 2 \qquad (3\text{-}6)$$

in which $I = \sqrt[4]{4E_pJ_p/E_s}$, L is the length of the pile, and E_pJ_p is the bending stiffness of the pile [35].
For soils with a modulus of horizontal subgrade reaction E_s which vary linearly with depth, a different formulation is available:

$$I = \sqrt[5]{E_pJ_p/n_h} \qquad (3\text{-}7)$$

where n_h is the gradient of the modulus of horizontal subgrade reaction ($E_s = n_h\, z$).
In the case of different moduli within the sliding layer, an average value over the sliding layer thickness can be calculated and used in the formulation.

- Being the pile considered to be rigid, so that the yield moment of its section is higher than the bending moments acting upon it. It results that the displacement of the pile at the ground surface is a consequence of its head movement and its rotation around a point located at some depth below the ground surface. This assumption let fully describe his deflection $y_p(z)$ with depth by using two parameters y_0 and tanω:

$$y_p(z) = y_0 - z\tan\omega \qquad (3\text{-}8)$$

where y_0 is the pile head's movement and ω his angle of rotation around a generic point (Figure 3-3)

- The pile–soil interaction is modelled by a series of elastic springs along the pile length (note shear force at the bottom of the pile is ignored). Each spring has a constant coefficient of subgrade reaction E_s, depending on the soil stratigraphy and properties under consideration.

The pile has a displacement-dependent on-pile force profile (with a specific upper limit) and similarly is derived the impact of the moving soil on the piles. The soil strain above and below the slip surface is linked to the relative soil-pile

displacement $y_{(z)}$; based on the assumed lateral soil movement, the relative soil-pile displacement at a generic depth of z above the slip surface is calculated as follows

$$\Delta y(z) = y_p(z) - y_s(z) \qquad (3\text{-}9)$$

where $y_p(z)$ is the pile deflection at a generic depth of z. Below the slip surface, in the firm soil, the relative soil-pile displacement is considered to be the same as the pile deflection:

$$\Delta y(z) = y_p(z) \qquad (3\text{-}10)$$

The relative soil pile displacement is also expressed as:

$$\Delta y(z) = y_p(z) - y_s(z) = (y_0 - y_{s0}) - (\tan\omega - \tan\theta) = \Delta y_0 - \Delta tan \qquad (3\text{-}11)$$

Where

$$\Delta y_0 = y_0 - y_{s0} \qquad (3\text{-}12)$$

is the relative soil-pile displacement at ground level and

$$\Delta tan = \tan\omega - \tan\theta \qquad (3\text{-}13)$$

the difference between the soil-pile tangents of the respective rotation angle.

- According to the Winkler model assumed, the soil pressure p(z) per unit length is:

$$p(z) = -E_s(z) \cdot [y_p(z) - y_s(z)] \qquad (3\text{-}14)$$

The integral of the pressures along the pile length gives the equilibrium equations system.

- A major advantage of the model is that the solutions of the equilibrium equations system are then derived in a normalised explicit form for calculating bending moments, shear forces and pile deflection.

In particular, the normalised external soil displacement $y_{son} = {}^{y_{s0}}/_{L}$ results to be proportional to the pile deflection parameters, through several specific proportionality constants, determined separately for every single case under investigation, as function of non-dimensional coefficients which describe the soil stratigraphy.
Different expressions are derived for the boundary conditions of free-head pile and unrotated-head pile and reported in the tables below. In addition, also the shear forces and bending moments profiles are expressed in an explicit normalised form, once again as a function of the same proportionality constants and coefficients.

	Expressions
Normalised pile head's deflection at ground level	$y_{0n} = \frac{y_0}{L} = \frac{N_y}{D} y_{s0n}$
Tangent of the pile rotation angle	$\tan\omega = \frac{N_t}{D} y_{s0n}$
Normalised relative soil-pile displacement at ground level	$\Delta y_{0n} = y_{0n} - y_{s0n} = \frac{N_{\Delta y}}{D} y_{s0n}$

Normalised relative rotation angle	$\Delta \tan = \frac{N_{\Delta t}}{D} y_{s0n}$
	$N_{\Delta y} = N_y - D$
	$N_{\Delta t} = N_t - D\frac{1-\eta}{\beta}$

Table 3-1: General normalised expressions for the calculation of a free-head pile deflection

	Expressions
Normalised pile head's deflection at ground level	$y_{0n} = \frac{y_0}{L} = \frac{N_y}{D} y_{s0n}$
Tangent of the pile rotation angle	$N_t = 0$
Normalised relative soil-pile displacement at ground level	$\Delta y_{0n} = y_{0n} - y_{s0n} = \frac{N_{\Delta y}}{D} y_{s0n}$
Normalised relative rotation angle	$\Delta \tan = \frac{N_{\Delta t}}{D} y_{s0n}$
Normalised moment for a unrotated-head pile	$M_{0n} = \frac{N_M}{D} y_{s0n}$

$$N_{\Delta y} = N_y - D$$

$$N_{\Delta t} = -D\frac{1-\eta}{\beta}$$

Table 3-2:General normalised expressions for the calculation of an unrotated-head pile deflection

- Five different soil stratigraphy profiles have been analysed by means of the presented method. They differ each other for the distribution of the subgrade reaction modulus, as showed in Figure 3-6. For every single case, both the free-head and the unrotated-head are investigated.

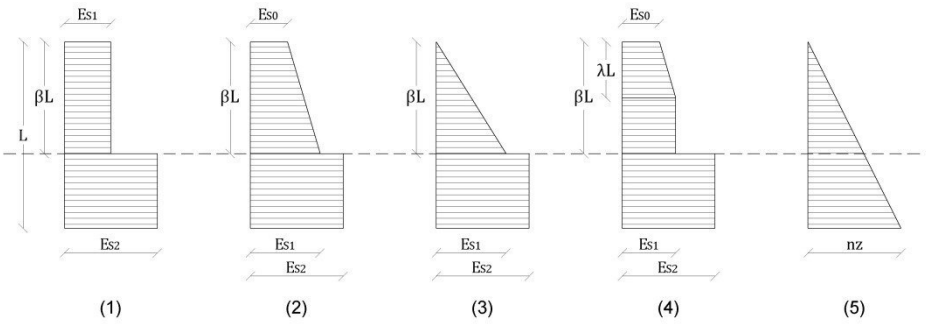

Figure 3-6: Analysed cases: Type-1) Two-layered soil with a constant subgrade reaction modulus. Type 2) Two layered soil with subgrade reaction modulus varying with depth. Type 3) Two layered soil with subgrade reaction modulus varying with depth. Type 4) Three layered soil. Type 5) Homogeneous soil with subgrade reaction modulus increasing with depth

3.3. Estimation of elastic soil parameters

The Winkler approach requests the assessment of E_s for the soil, properly defined as the product of the coefficient of subgrade reaction k_h and the width of the pile

$$Es = k_h \cdot D \quad [FL^{-2}] \qquad (3\text{-}15)$$

Whenever in-situ test measurements or pile load tests for the evaluation of k_h are not available, E_s is often estimated on the basis of correlations with soil strength parameters.
One of the most accepted distribution law for E_s is the one proposed by Palmer & Thompson [37] in the form of:

$$Es = Es_L \left(\frac{z}{L}\right)^f \qquad (3\text{-}16)$$

Where:
Es_L = the value of E_s at pile toe (z = L)
f = a coefficient greater or equal to zero
For overconsolidated clays, *f* is commonly taken as zero, so that E_s is constant with depth; in this case, E_s is typically correlated with S_u as:

$$E_s = \epsilon S_u \qquad (3\text{-}17)$$

where the value of ϵ typically lies between 150 and 400 ([38], [39]).

For sands and for normally consolidated clays under long-term loading, it is reasonable to assume that the modulus of horizontal subgrade reaction, E_s, varies linearly with depth (it means *f* is taken as unity). However, the most commonly used formulation for this case is:

$$E_s = n_h z \qquad (3\text{-}18)$$

where:
n_h = gradient of the horizontal subgrade reaction modulus [FL^{-3}]

This applies to cohesionless soils and normally consolidated clays where these soils indicate an increasing strength with depth due to the overburden pressure rising.

Soil Type	**n_h (kN/m^3)**	**Reference**
Soft NC Clay	163-3447	Reese and Matlock (1956)
	271-543	Davisson and Prakash (1963)
NC Organic Clay	179-271	Peck and Davisson (1962)
	179-814	Davisson (1970)
Peat	54	Davisson (1970)
	27-109	Wilson and Hilts (1967)
Loess	7872-10858	Bowles (1968)

Table 3-3: Typical values of n_h for cohesive soil

Table 3-3 summarises the typical values of n_h for cohesive soils by various authors, whereas typical values of n_h for saturated loose, medium and dense sands are 1.5, 5.0 and 12.5 MPa/m respectively (Decourt 1991 [40]). However, as n_h value for sand has been found to decrease with the increasing displacement of the pile, Bhushan K. et al. [41] proposed a n_h versus normalised pile displacement at ground surface relations for different sand relative density values (Figure 3-7). Their correlation has been later modified by Zhang L. [3] , who expressed the secant value n_h with the formulation:

$$\frac{n_h}{n_{h,max}} = 0.066\left(\frac{y_0}{D}\right)^{-0.48} \qquad (3\text{-}19)$$

Where $n_{h,max}$ is the maximum value determined at low strain in correspondence of the initial portion of the p–y curve (Figure 3-7).

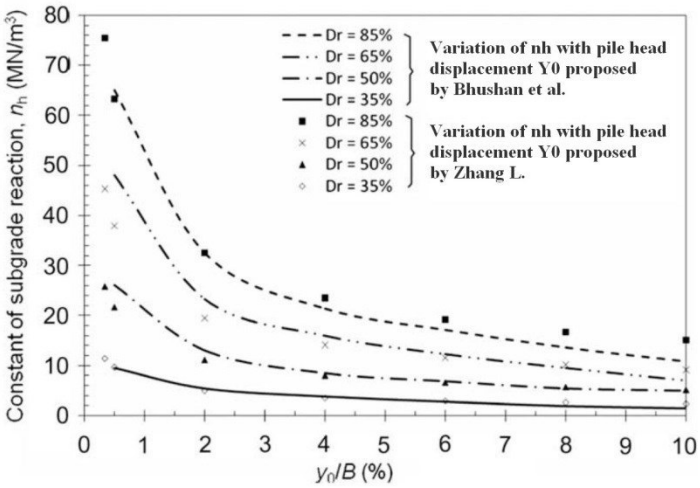

Figure 3-7: Variation of gradient n_h, with normalised pile head displacement y_0/D, according to Bhushan et al. [41] and Zhang L. [3]

3.4. Elastic solutions for a passive rigid pile in a two-layered cohesive soil with a constant subgrade reaction modulus

The presence of a sliding cohesive mass over a stiffer stratum represents a typical slope instability condition and is the same problem already investigated by Viggiani [23] by means of a simplified pressure-method for only the ultimate lateral resistance of a pile in a two-layer purely cohesive soil profile.
In the present paragraph, the same problem is investigated. In particular, it has been modelled a layer of soil of thickness $L_s=\beta L$, sliding on a firm underlying soil along a slip surface. Both soils are assumed to be saturated clays in undrained conditions, with a shear strength equals to S_{u1} above and to S_{u2} below the slip surface. A free-head rigid pile of length L crosses the sliding surface and is embedded in the stable underlying bed (Figure 3-8).

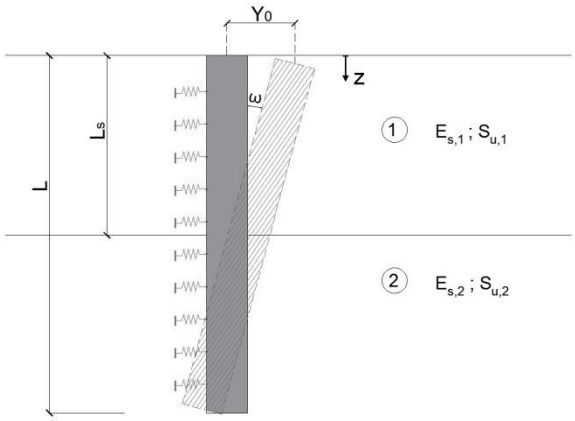

Figure 3-8: Soil profile and pile displacement geometry for a rigid pile in a two-layered cohesive soil

3.4.1.Estimation of elastic soil parameters

A different and constant value of the modulus of subgrade E_s is assigned to every soil layer (Figure 3-9), ideally correlated to their assumed constant shear strength, regardless of depth (cf. Paragraph 3.3 for over-consolidated cohesive soils): E_{s1} for the sliding stratum (through ground level to Ls) and E_{s2} for the stable layer :

$$E_s\,(z) = E_{s1} \qquad [FL^{-2}] \qquad 0 < z < Ls \qquad (3\text{-}20)$$

$$E_s\,(z) = E_{s2} = k * E_{s1} \qquad [FL^{-2}] \qquad Ls < z < L \qquad (3\text{-}21)$$

where k is a constant parameter defined as :

$$k = \frac{E_{s2}}{E_{s1}} \qquad (3\text{-}22)$$

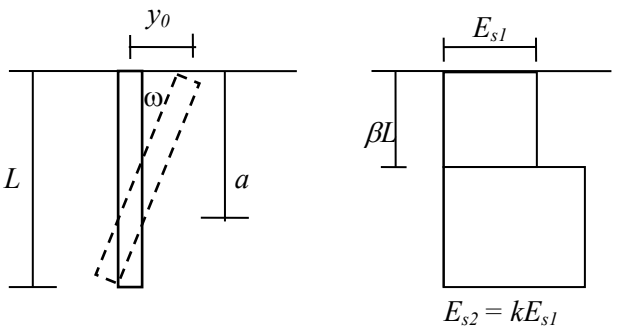

Figure 3-9: (a) A rigid pile; (b) Variation of Es with depth

The ratio k allow to parametrically vary the soil stiffness in order to obtain practical non-dimensional solutions. In particular, by imposing k=1 , the derived non-dimensional solutions can be adopted for a homogeneous soil with a constant

modulus of subgrade reaction. However, its value is assumed to be greater than unit; this is in agreement with Davisson [39] who suggested, in order to better model the plastic behaviour of the shallower soil, to consider a two layered stratigraphy, where the bottom layer is characterized by a modulus at least double than the top layer's one ([5], [23]).

3.4.2. Elastic solutions for the free-head condition

With the above assumptions and assuming there is no soil-yielding, the soil reactions along the whole length L of the pile can be expressed as:

$$p_{1(z)} = -E_{s1}\left(y_{0(z)} - y_{s(z)}\right) = -E_{s1}[(yY_0 - y_{s0}) - (\tan\omega - \tan\alpha)z] \quad [FL^{-1}] \quad 0 < z < Ls \quad (3\text{-}23)$$

$$p_{2(z)} = -E_{s2}[y_0 - \tan\omega\, z] \quad [FL^{-1}] \quad Ls < z < L \quad (3\text{-}24)$$

The global equations of the problem are obtained by imposing the horizontal force equilibrium and moment equilibrium around the head of the pile:

$$\int_0^{Ls} p_{1(z)}dz + \int_{Ls}^{L} p_{2(z)}dz = 0 \quad (3\text{-}25)$$

$$\int_0^{Ls} p_{1(z)}z dz + \int_{Ls}^{L} p_{2(z)}z dz = 0 \quad (3\text{-}26)$$

By substituting the expressions of the pressure $p_{(z)}$, the following two non-dimensional equations can be obtained:

$$\beta\Delta y_{0n} - \frac{1}{2}\beta^2\Delta\tan + ky_0(1-\beta) - \frac{1}{2}k\tan\omega\,(1-\beta^2) = 0 \quad (3\text{-}27)$$

$$\frac{1}{2}\beta^2\Delta y_{0n} - \frac{1}{3}\beta^3\Delta\tan + \frac{1}{2}ky_0(1-\beta^2) - \frac{1}{3}k\tan\omega\,(1-\beta^3) = 0 \quad (3\text{-}28)$$

What is interesting about the results in this paragraph is that they can be expressed in an explicit and normalised form; referring to Table 3-1 the profiles of pile displacement are expressed as function of the proportionality constants summarised in Table 3-4.

Proportionality constants	
	$D = \beta^4 + 2k\beta(1-\beta)\{2-\beta+\beta^2\} + k^2(1-\beta)^4$
$y_{0n} = \frac{N_y}{D} y_{s0n}$	$N_y = \beta^4(1-k) + 2k\beta(1+\eta) - k\beta^2(1+2\eta)$
$tan\omega = \frac{N_t}{D} y_{s0n}$	$N_t = \beta^3(1-k)(1-\eta) + 3k\beta(1+\eta) - 2k\beta^2(1+2\eta)$

Table 3-4: Proportionality constants for a passive free-head rigid pile in a two-layered cohesive soil

By means of the same constants and coefficients, shear forces and bending moments profiles at unstable and stable zones are deduced. Together with the maximum bending moment M_{max} and its depth z_n in both stable and unstable zones, they are provided in Table 3-5.

Depth (z_n)	Expressions
0 – β (unstable zone)	$\frac{T}{E_{s1}L^2} = -\Delta y_{n0} z_n + \frac{1}{2}\Delta tan \cdot z_n{}^2$
	$\frac{M}{E_{s1}L^3} = -\frac{1}{2}\Delta y_0 z_n{}^2 + \frac{1}{6}\Delta tan \cdot z_n{}^3$
	$z_{nM} = \frac{2\Delta y_{0n}}{\Delta \tan}$
	$\frac{\lvert M_{\max}\rvert}{E_{s1}L^3 y_{s0n}} = -\frac{2\lvert N_{\Delta y}{}^3\rvert}{3DN_{\Delta t}{}^2}$
$z_n = \beta$ (slip surface)	$\frac{T_\beta}{E_{s1}L^2} = \frac{k(1-\beta)}{2D}\left[2N_y - N_t(1+\beta)\right]y_{s0n}$
	$\frac{M_\beta}{E_{s1}L^3} = \frac{k(1-\beta)^2}{6D}\left[3N_y - N_t(2+\beta)\right]y_{s0n}$
β – 1 (stable zone)	$\frac{T}{E_{s1}L^2} = -ky_{0n}(z_n - 1) + \frac{1}{2}k\tan\omega(z_n{}^2 - 1)$
	$\frac{M}{E_{s1}L^3} = -ky_{0n}\left(\frac{1}{2}z_n{}^2 - z_n + \frac{1}{2}\right) + \frac{1}{2}k\tan\omega\left(\frac{1}{3}z_n{}^3 - z_n + \frac{2}{3}\right)$
	$z_{nM} = \frac{2y_{0n}}{\tan\omega} - 1$

$$\frac{M_{\max}}{E_{s1}L^3} = \frac{2k\left(N_t - N_y\right)^3}{3DN_t^{\,2}} y_{s0n}$$

Table 3-5: Elastic solutions for a passive free-head rigid pile in a two-layered cohesive soil

In each zone, the expression of the maximum bending moment is valid only if its depth z_n is within the relative interval. As a consequence, the maximum bending moment acting on the pile is:

$$\frac{M_{\max}}{E_{s1}L^3 y_{s0n}} = \max\left\{\left|\frac{2N_{\Delta y}^{\,3}}{3DN_{\Delta t}^{\,2}} y_{s0n}\right|; \left|\frac{2k\left(N_t - N_y\right)^3}{3DN_t^{\,2}} y_{s0n}\right|\right\} \qquad (3\text{-}29)$$

All the solutions provided highlight the proportionality between the soil movement and pile response. But by combining the expressions of T_β and M_{max} , it is possible to obtain the following expressions:

$$\frac{T_\beta}{E_{s1}L^2} = \frac{3(1-\beta)\left[2N_y - N_t(1+\beta)\right]}{4} \frac{N_{\Delta t}^{\,2}}{\left|N_{\Delta y}\right|^3} \frac{M_{1\max}}{E_{s1}L^3} \qquad (3\text{-}30)$$

$$\frac{T_\beta}{E_{s1}L^2} = \frac{3(1-\beta)\left[2N_y - N_t(1+\beta)\right]}{4} \frac{N_t^{\,2}}{\left|N_t - N_y\right|^3} \frac{M_{2\max}}{E_{s1}L^3} \qquad (3\text{-}31)$$

which demonstrates that even pile stresses are directly proportional to each other through a proportionality constant that is depending only on the geometry and soil stiffness.

The distribution profile of the pile shear forces and bending moments can then be obtained with the new solutions, concerning the depth of the sliding surface. The

normalised shear force $T_n = T/(L^2\, E_{s1} y_{s0n})$ and bending moment $M_n = M/(L^3 E_{s1} y_{s0n})$ are plotted in Figure 3-10, Figure 3-11, Figure 3-12 and Figure 3-13, for η equal to 1 and 0 and for a fixed k = 2.

It is evident that the normalised stress profiles shift with the normalised depth of the sliding surface β.

The case η = 1 corresponds to higher stress states on the pile, with T_n profile that has its maximum value in correspondence of the sliding surface, with a value almost identical for the different values of β. The case η = 0 corresponds to lower values of $T_{n,max}$, with two local extreme values which occur close to the pile's top and bottom (the latter with a negative value).

M_n generally has its maximum value for depths close to the middle of the pile, for both configurations. It has to be noticed that, while for η = 0 the bending moment on the pile is always positive, for η = 1 it is negative if β ≥ 6.

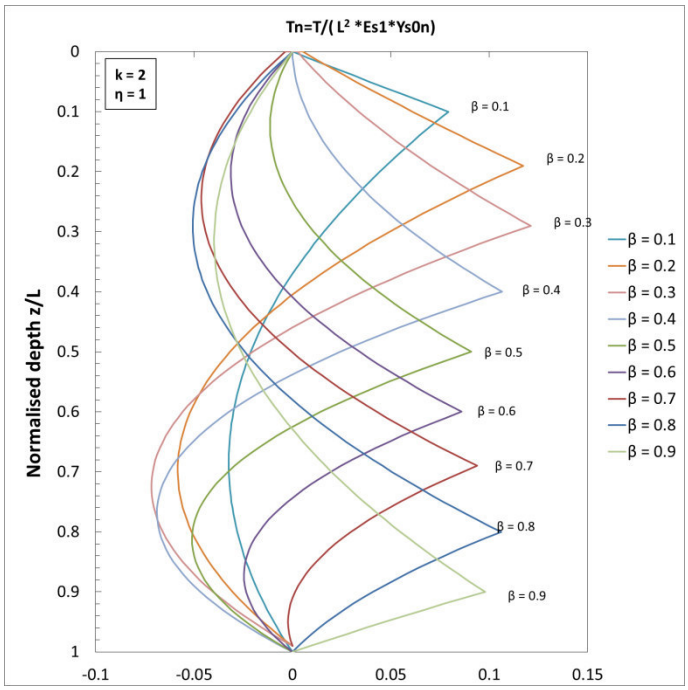

Figure 3-10: Normalised shear force with depth for k=2 and η=1

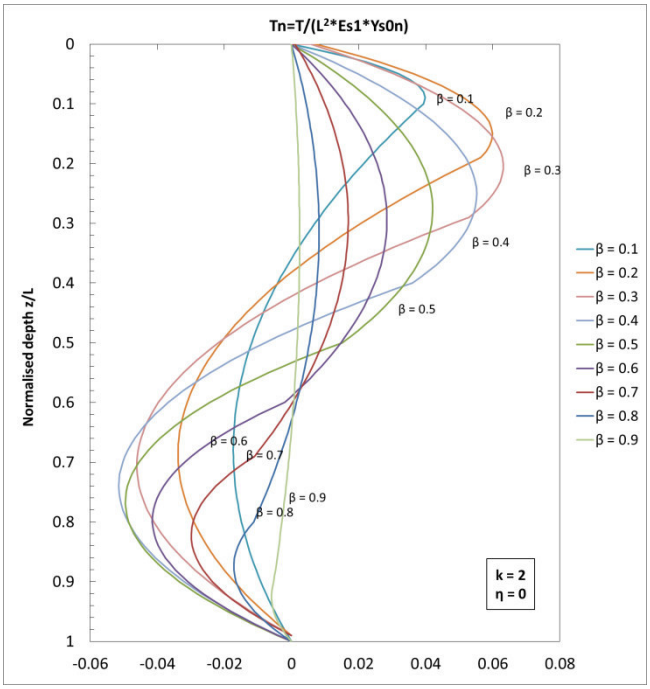

Figure 3-11: Normalised shear force with depth for k=2 and η=0

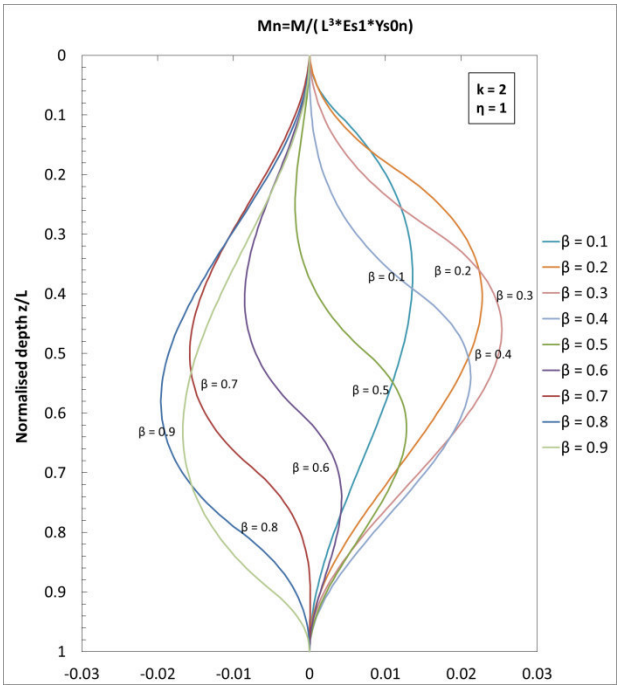

Figure 3-12: Normalised bending moment with depth for k=2 and η=1

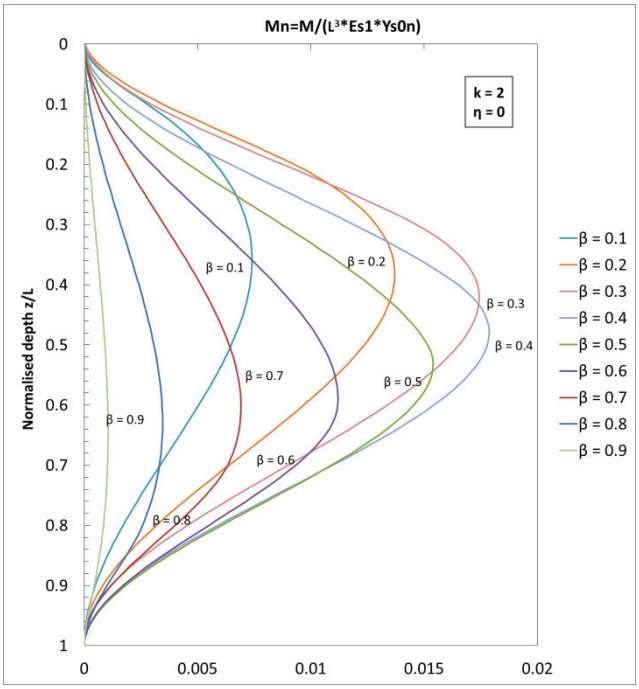

Figure 3-13: Normalised bending moment with depth for k=2 and η=0

3.4.3.Elastic solutions for the unrotated-head condition

The presence of a pile cap or a framing connecting the piles in a row, rigid enough to block the piles head rotation, changes the geometry and the behaviour of the problem, representing a different problem in the soil-pile interaction analysis. While the ground is assumed to have the same stratigraphy and properties than the previous case of the free-head pile, as consequence of the applied constrain the rigid pile cannot rotate and the angle ω is equal to zero, i.e. N_t =0 (Figure 3-14).

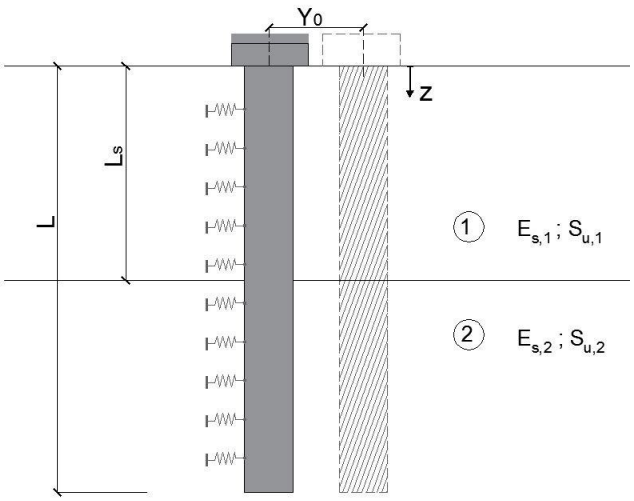

Figure 3-14: Soil profile and pile displacement geometry for a unrotated-head rigid pile in a two-layered cohesive soil

This assumption let adequately describe pile deflection $y_p(z)$ with depth by using the head's movement parameter y_0

$$y_p(z) = y_0 \qquad (3\text{-}32)$$

With the above assumptions, the soil reactions along the whole length L of the pile can be expressed as:

$$p_{1(z)} = -E_{s1}[(y_0 - y_{s0}) + z\ tan\,\theta] \qquad [FL^{-1}] \quad 0 < z < Ls \qquad (3\text{-}33)$$

$$p_{2(z)} = -E_{s2}(y_0) \qquad [FL^{-1}] \quad Ls < z < L \qquad (3\text{-}34)$$

The equations of the horizontal force equilibrium and moment equilibrium around the head of the pile, in a normalised form, are:

$$[\beta + k(1-\beta)]y_{0n} = \beta y_{s0n} - \frac{1}{2}\beta^2\ tan\theta \qquad (3\text{-}35)$$

$$-M_{0n} + \left[\frac{1}{2}\beta^2 + \frac{1}{2}k\left(1-\beta^2\right)\right]y_{0n} = \frac{1}{2}\beta^2 y_{s0n} - \frac{1}{3}\beta^3\ tan\theta \qquad (3\text{-}36)$$

The proportionally constants defining the profile of the pile deflection and the bending moment M_0 acting on its head are provided in Table 3-6

	Proportionality constants
	$D = \beta + k(1-\beta)$
$y_{0n} = \frac{N_y}{D} y_{s0n}$	$N_y = 0.5\beta(1+\eta)$

$M_{0n} = \frac{N_M}{D} y_{s0n}$	$N_M = \frac{1}{12}\beta\left\{\beta^2(1-\eta)+k(1-\beta)\left[3(1+\eta)+\beta(1-\eta)\right]\right\}$

Table 3-6: Proportionality constants for a passive unrotated-head rigid pile in a two-layered cohesive soil

Shear forces and bending moments profiles, maximum bending moment M_{max} and its depth z_n in both loading and non-loading zones are provided in Table 3-7

Depth (z_n)	Expressions
0 – β (unstable zone)	$\frac{T}{E_{s1}L^2} = -\Delta y_{n0} z_n + \frac{1}{2}\Delta \tan\cdot z_n^{\,2}$ $\frac{M}{E_{s1}L^3} = -M_{0n} - \frac{1}{2}\Delta y_0 z_n^{\,2} + \frac{1}{6}\Delta \tan\cdot z_n^{\,3}$
z_n = β (slip surface)	$\frac{T_\beta}{E_{s1}L^2} = \frac{k(1-\beta)}{D}\left[N_y\right] y_{s0n}$ $\frac{M_\beta}{E_{s1}L^3} = \frac{k(1-\beta)^2}{2D}\left[N_y\right] y_{s0n}$
β – 1 (stable zone)	$\frac{T}{E_{s1}L^2} = -k y_{0n}(z_n - 1)$

$$\frac{M}{E_{s1}L^3} = -ky_{0n}\left(\frac{1}{2}z_n{}^2 - z_n + \frac{1}{2}\right)$$

Table 3-7: Elastic solutions for a passive unrotated-head rigid pile in a two-layered cohesive soil

The maximum bending moment on the pile correspond to M_0 (acting on its head):

$$\frac{M_{max}}{E_{s1}L^3} = M_{0n} \qquad (3\text{-}37)$$

The distribution profile of the pile response can then be obtained with the new solutions, at varying of the depth of the sliding surface. The normalised shear force $T_n = T/(L^2\, E_{s1} y_{s0n})$ and bending moment $M_n = M/(L^3 E_{s1} y_{s0n})$ are plotted in the following figures, for η equal to 1 and 0 and for a fixed k = 2.

It is evident that the uniform soil movement distribution leads to a higher stress state acting on the pile; in particular T_n has its maximum value again in correspondence of the sliding surface and β values from 0.4 to 0.6 are those obtaining the higher response of the pile in terms of shear force.
The case η = 0 presents lower values of $T_{n,max}$, with peaks which occur at z_n generally upper than β.
M_n shows the same profile for both η = 0 and η = 1, with always negative values. As expected, the condition η = 1 results to give slightly higher values of $M_{n,ma}$.
Comparing these results with those relative to the free-head condition, it is evident that the unrotated-head pile condition corresponds to higher stresses acting on the pile. It leads to consider the restrained pile head condition as recommended whenever a high pile resistance at the sliding depth is preferable, as in case of pile used as stabilising systems, if the pile's stress state is verified.

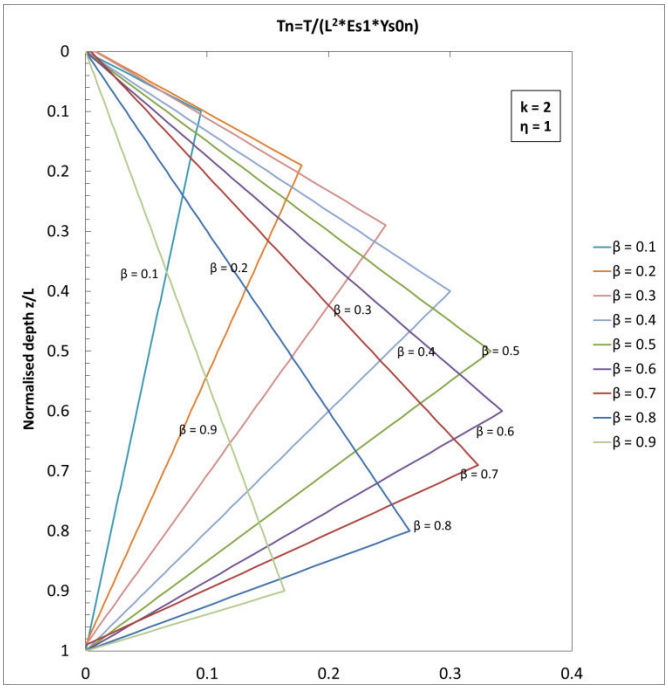

Figure 3-15: Normalised shear force with depth for k=2 and η=1

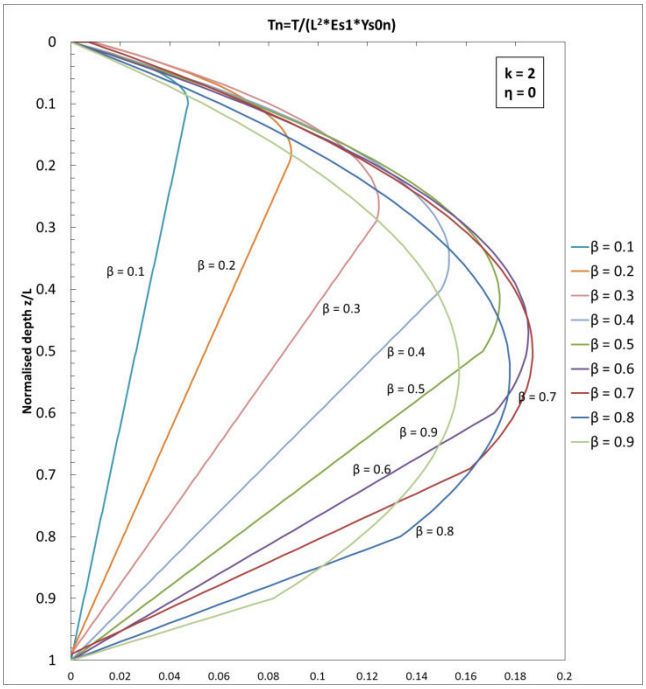

Figure 3-16: Normalised shear force with depth for k=2 and η=0

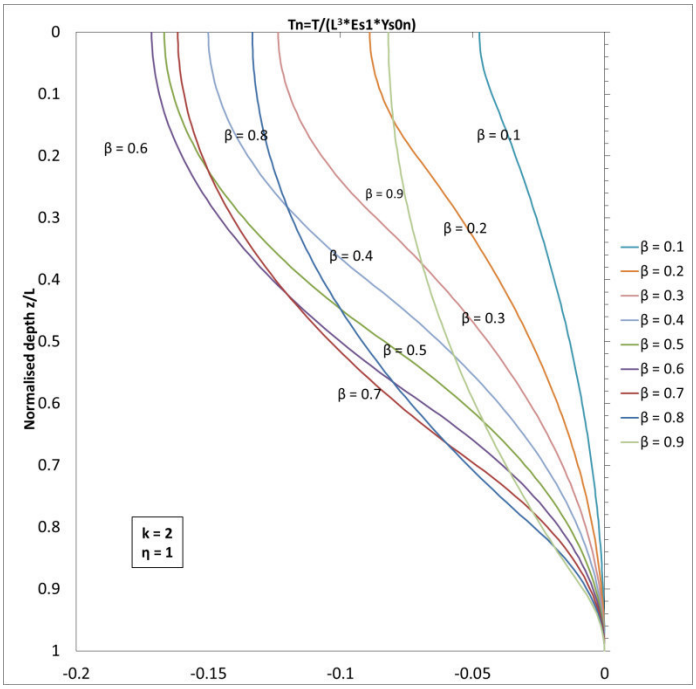

Figure 3-17: Normalised bending moment with depth for k=2 and η=1

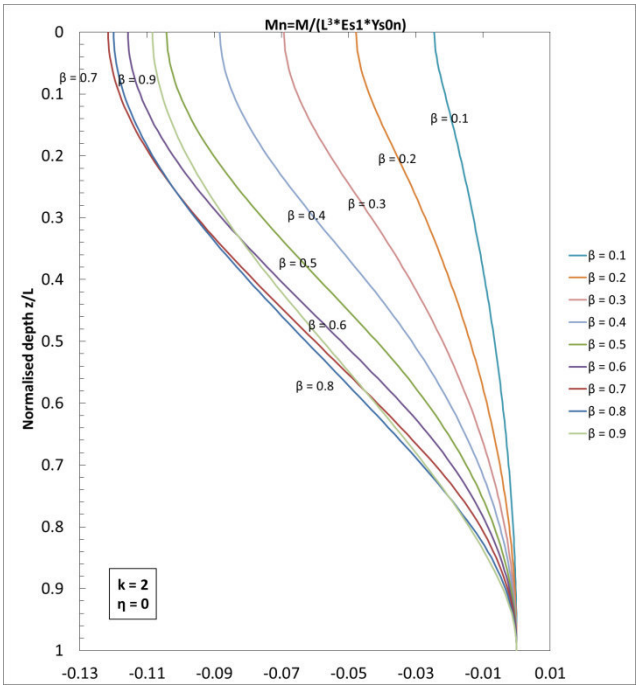

Figure 3-18: Normalised bending moment with depth for k=2 and η=0

3.4.4.Parametric analysis

The solution provided have been implemented in spreadsheets to carry out a parametric analysis of the problem.
The elastic solutions for a passive rigid pile in a two-layered cohesive soil with a constant subgrade reaction modulus are governed by the parameter k that represents the ratio between E_s values E_{s2} and E_{s1} respectively of the stable and unstable soils:

$$k = \frac{E_{s2}}{E_{s1}} \qquad (3\text{-}38)$$

And the parameter η that represents between soil displacement at ground level and at the sliding depth:

$$\eta = \frac{y_{s(z=Ls)}}{y_{s0}} \qquad (3\text{-}39)$$

The parametric analysis focuses on their effects on the normalised pile shear resistance at $z=L_s$:

$$T_{\beta,n} = \frac{T_{(z=Ls)}}{E_{s1}L^2 y_{s0,n}} \qquad (3\text{-}40)$$

Normalised bending moment at $z=L_s$:

$$M_{\beta,n} = \frac{M_{(z=Ls)}}{E_{s1}L^3 y_{s0,n}} \qquad (3\text{-}41)$$

Normalised maximum bending moment acting on the pile:

$$M_{n,max} = \frac{M_{max}}{E_{s1}L^3 y_{s0,n}} \qquad (3\text{-}42)$$

Normalised pile head displacement:

$$\frac{y_{on}}{y_{son}} = \frac{y_0}{y_{s0}} \qquad (3\text{-}43)$$

In every chart, values are plotted against the normalised depth of the sliding surface. The analysis concerns both the boundary conditions of free-head (Figure 3-19 through Figure 3-21) and unrotated-head (Figure 3-22 through Figure 3-24). Several considerations can be done on the showed results:

- The pile-head boundary condition considerably affects the pile response. The free-head piles present two local maximum values in the shear forces and bending moments profiles, where those corresponding to shallower sliding depth are the highers. The unrotated-head instead presents stress state profiles having only a global extrema. Moreover, it corresponds to higher stress states on the pile, with shear forces and bending moments at the sliding depth sensibly higher than those developed by the free-head condition, even associated to a lower pile head deflection. It leads to consider the restrained pile head condition as recommended in case low pile displacements are requested, or whenever a high pile resistance at the sliding depth is preferable, as in the case of pile used as stabilising systems, if the pile's stress state is verified. Both the boundary conditions, as reasonably expected, presents a pile head deflection proportionally increasing with β.
- Lateral soil movement profiles have been assessed as triangular (η=0),rectangular (η=1) and trapezoidal (η=0.25,0.5,0.75). The rectangular shape results in the largest stress state on the pile, followed in order by the trapezoidal and the triangular. Similarly, higher pile head deflection occurs for higher values of η. This result appears reasonable as the rectangular profile corresponds to a higher total soil displacement and consequently loading on the pile. It is worth to be noticed that the condition η=0 is the only one which corresponds to a negative shear force at the sliding surface for high values of β for the free-head condition.
- By varying k from 1 (corresponding to a homogeneous soil) to 10, several ratios between subgrade modulus of the stable and unstable soils have been

considered. This parameter has a scale effect on the pile stress state: the higher is assumed the k value, the higher results the value of shear forces and bending moments acting on the pile. However, a higher value of k corresponds to lower pile deflection, (except for some high β values if η=1) reasonably due to the stronger embedment given to the pile. Moreover, the extreme values of T_n and M_n occur in correspondence of deeper β if k is increased.

FREE-HEAD PILE

Effect of different η values:

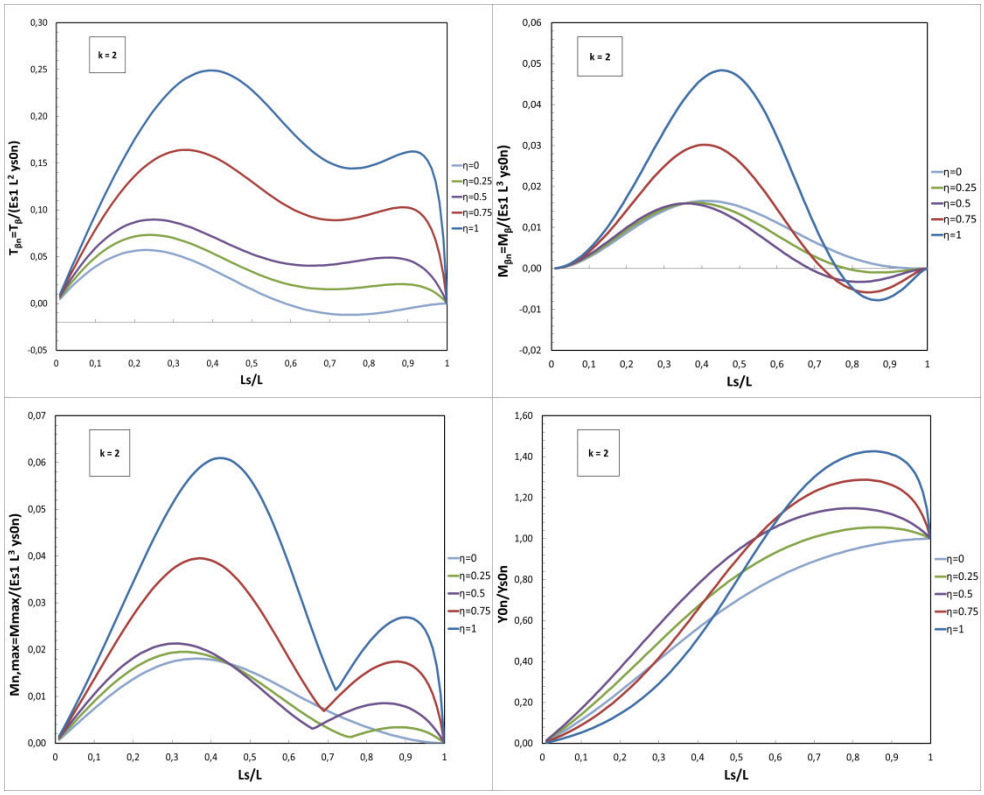

Figure 3-19: Normalised shear force at $z_n=\beta$, bending moment at $z_n=\beta$, maximum bending moment and pile head displacement versus L_s/L, for k=2 and different η values. Free-head condition

Effect of different k values (η=0):

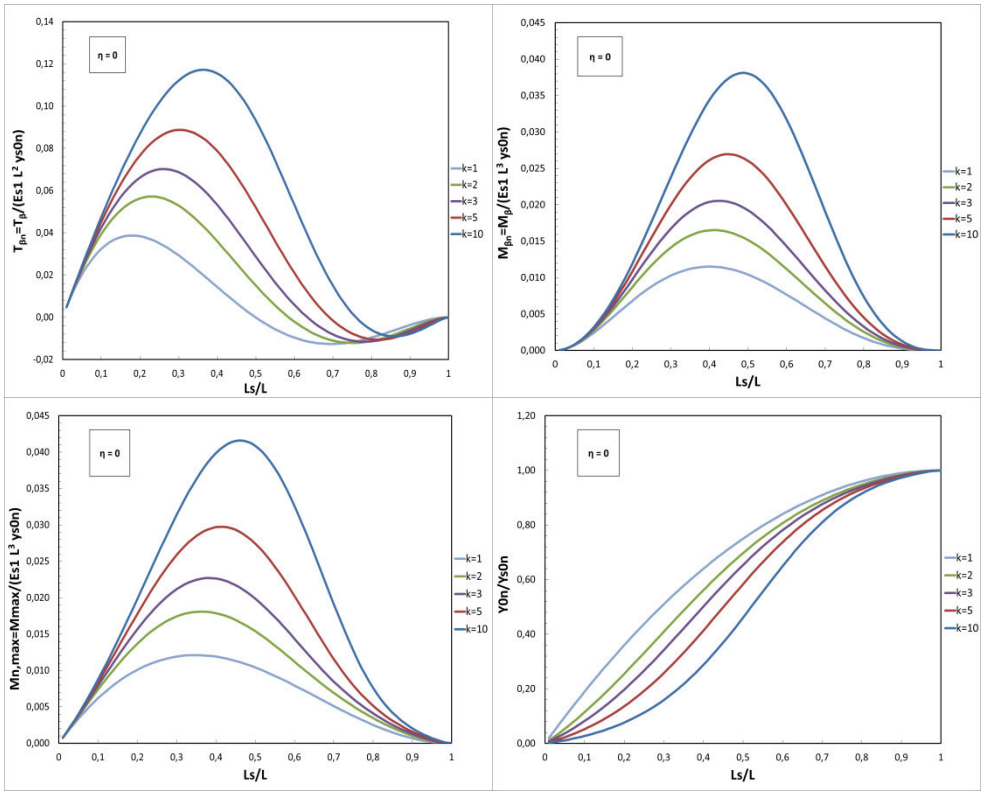

Figure 3-20: Normalised shear force at $z_n=\beta$, bending moment at $z_n=\beta$, maximum bending moment and pile head displacement versus L_s/L, for η=0 and different k values. Free-head condition

Effect of different k values (η=1) :

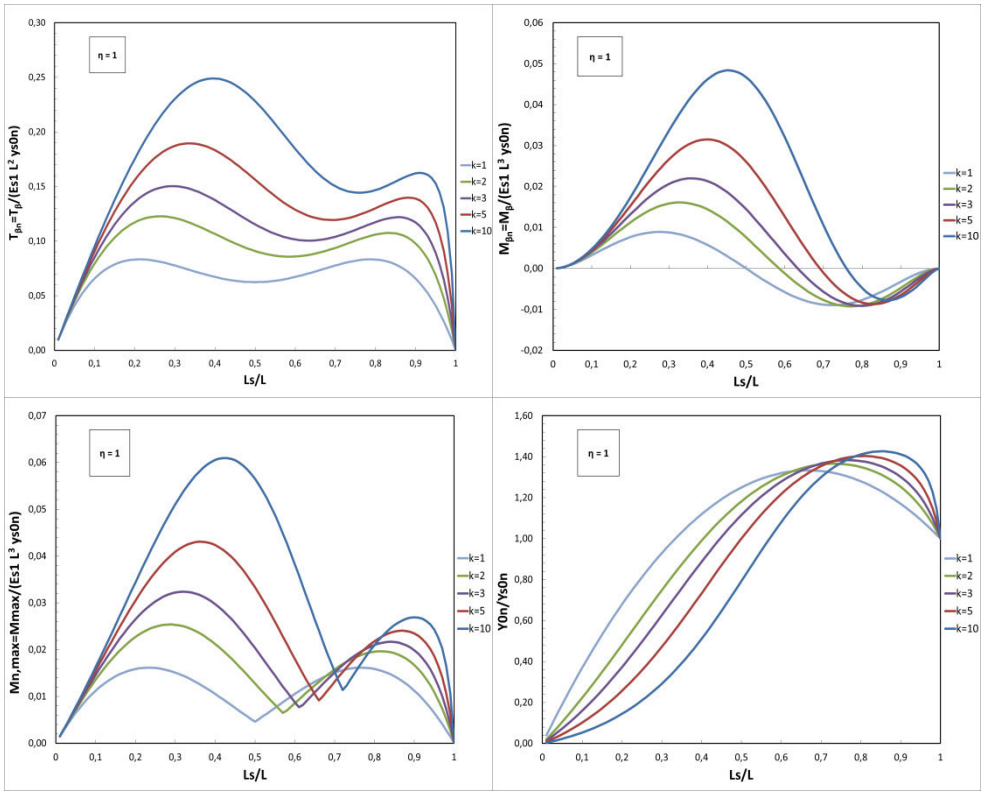

Figure 3-21: Normalised shear force at $z_n=\beta$, bending moment at $z_n=\beta$, maximum bending moment and pile head displacement versus L_s/L, for η=1 and different k values. Free-head condition

UNROTATED-HEAD PILE

Effect of different η values:

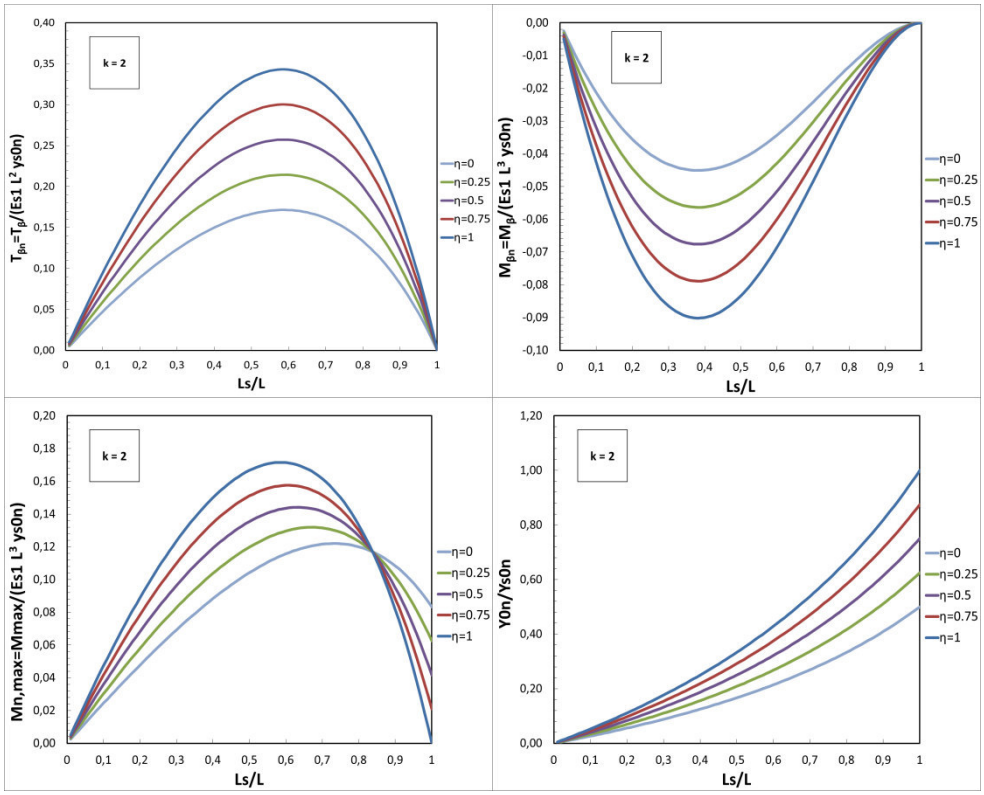

Figure 3-22: Normalised shear force at $z_n=\beta$, bending moment at $z_n=\beta$, maximum bending moment and pile head displacement versus L_s/L, for k=2 and different η values. Unrotated-head condition

Effect of different k values (η=0):

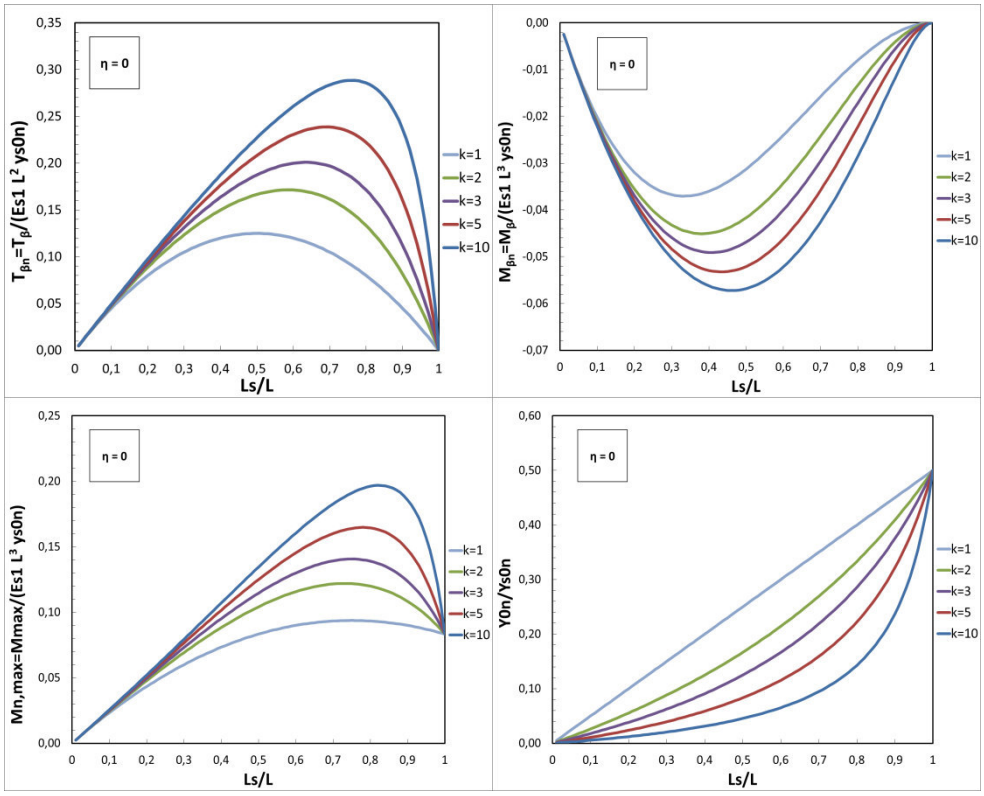

Figure 3-23: Normalised shear force at $z_n=\beta$, bending moment at $z_n=\beta$, maximum bending moment and pile head displacement versus L_s/L for η=0 and different k values. Unrotated-head condition

Effect of different k values (η=1) :

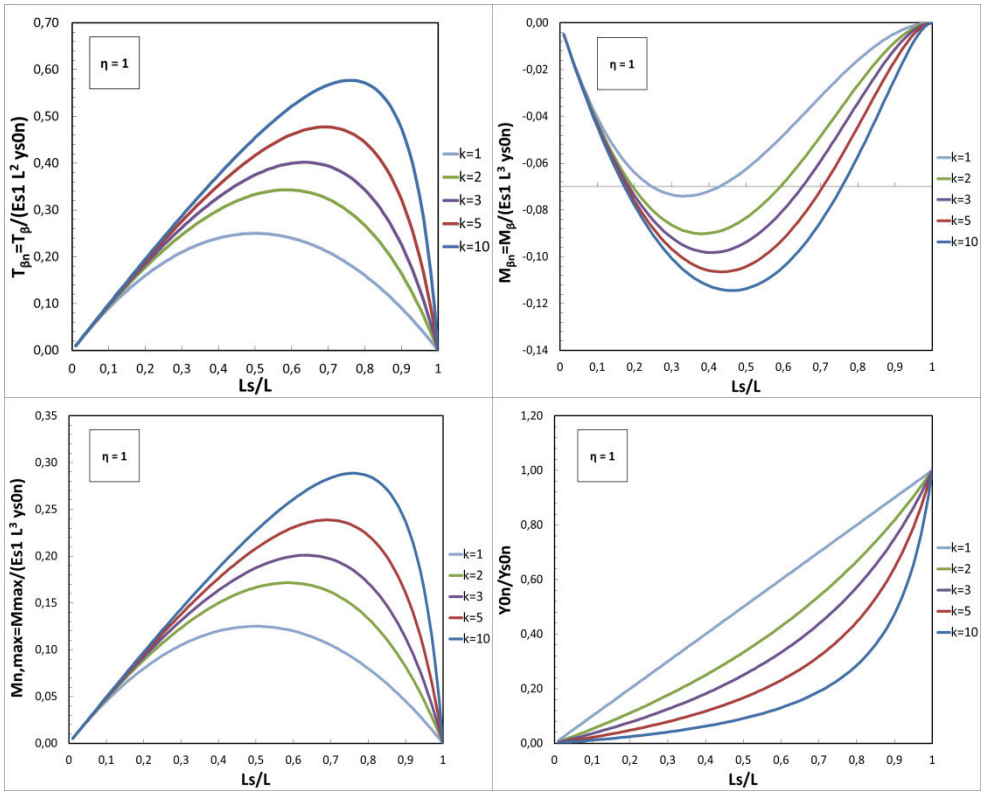

Figure 3-24: Normalised shear force at $z_n=\beta$, bending moment at $z_n=\beta$, maximum bending moment and pile head displacement versus L_s/L, for η=1 and different k values. Unrotated-head condition

3.5. Elastic solutions for a passive rigid pile in a two-layered soil with subgrade modulus varying with depth

3.5.1. Free-head condition

For some cohesive soil, the assumption of constant subgrade cannot be always appropriate. In this paragraph a linear variation of E_s with depth is assumed for the unstable layer: so that, if the sliding cohesive mass presents an undrained shear strength increasing with depth (i.e. a normally consolidated clay, see paragraph 3.3), the corresponding E_s modulus follows the same profile, with a linear trend from a value $E_{s0} = (\alpha_0 E_{s1})$ at ground level to E_{s1} at the bottom of the layer. At the same time, the underlying firm layer is assumed to have its own constant subgrade modulus E_{s2}, as k-ratio with E_{s1} (Figure 3-25).

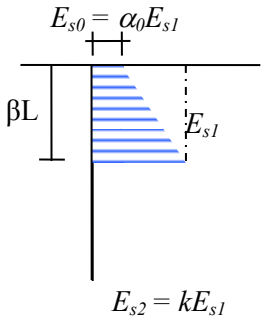

Figure 3-25: Variation of Es with depth for a free-head passive rigid pile in a normal consolidated cohesive soil

Similarly to the previous case investigated, it has been modelled a layer of soil of thickness Ls=βL, sliding on a firm underlying soil along a slip surface. Both soils are assumed to be saturated clays in undrained conditions, with a shear strength equals to $S_{u1(z)}$ increasing with depth above and to S_{u2} below the slip surface. A

free-head rigid pile of length L crosses the sliding surface and is embedded in the stable underlying soil (Figure 3-26).

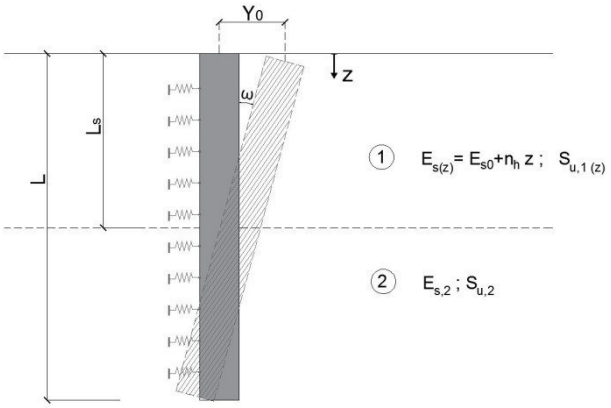

Figure 3-26: Soil profile and pile displacement geometry for a unrotated-head rigid pile in a two-layered cohesive soil

With the above assumptions, the soil reactions along the whole length L of the pile can be expressed as:

$$p_{1(z)} = -(E_{s0} + n_h z)[\Delta y_0 - \Delta \tan \cdot z] \qquad [FL^{-1}] \quad 0 < z < Ls \qquad (3\text{-}44)$$

$$p_{2(z)} = -E_{s2}(y_0 - z \tan \omega) \qquad [FL^{-1}] \quad Ls < z < L \qquad (3\text{-}45)$$

The global equations of the problem are obtained by imposing the horizontal force equilibrium and moment equilibrium around the head of the pile; in an explicit non-dimensional form, they are expressed as:

$$\left[-\frac{1}{2}\beta(1-\alpha_0)+\beta+k(1-\beta)\right]y_{0n}+\left[\frac{1}{6}\beta^2(1-\alpha_0)-\frac{1}{2}\beta^2-\frac{1}{2}k(1-\beta^2)\right]\tan\omega = \qquad (3\text{-}46)$$
$$\left[-\frac{1}{2}\beta(1-\alpha_0)+\beta\right]y_{s0n}+\left[\frac{1}{6}\beta^2(1-\alpha_0)-\frac{1}{2}\beta^2\right]\tan\theta$$

$$\left[-\frac{1}{6}\beta^2(1-\alpha_0)+\frac{1}{2}\beta^2+\frac{1}{2}k(1-\beta^2)\right]y_{0n}+\left[\frac{1}{12}\beta^3(1-\alpha_0)-\frac{1}{3}\beta^3-\frac{1}{3}k(1-\beta^3)\right]\tan\omega =$$
$$\left[-\frac{1}{6}\beta^2(1-\alpha_0)+\frac{1}{2}\beta^2\right]y_{s0n}+\left[\frac{1}{12}\beta^3(1-\alpha_0)-\frac{1}{3}\beta^3\right]\tan\theta \qquad (3\text{-}47)$$

The profile of the pile deflection is expressed as a function of the proportionally constants summarised in Table 3-8.

Proportionality constants	
	$D=\frac{1}{6}\beta^4\left(1+4\alpha_0+{\alpha_0}^2\right)+k^2(1-\beta)^4$ $+k\beta(1-\beta)\left[\beta^2-2\beta+2+\alpha_0\left(\beta^2+2\right)\right]$
$y_{0n}=\frac{N_y}{D}y_{s0n}$	$N_y=\frac{1}{6}\beta^4\left(1+4\alpha_0+{\alpha_0}^2\right)+\frac{1}{6}k\beta^2\left(1-\beta^2\right)\left[1-\eta+\alpha_0(\eta+5)\right]$ $+\frac{2}{3}k\beta(1-\beta)\left[1+2\eta+\alpha_0(2+\eta)\right]$
$tan\omega=\frac{N_t}{D}y_{s0n}$	$N_t=\frac{1}{6}\beta^3(1-\eta)\left(1+4\alpha_0+{\alpha_0}^2\right)+k\beta(1-\beta)\left[1+\eta(2-\beta)+\alpha_0(2+\eta+\beta)\right]$

Table 3-8: Proportionality constants for a free-head passive rigid pile in a normal-consolidated cohesive soil sliding on a firm layer

Shear forces and bending moments profiles, maximum bending moment M_{max} and its depth z_n in both loading and non-loading zones are provided in Table 3-9.

Depth (z_n)	Expressions
$0-\beta$ (unstable zone)	$\frac{T}{E_{s1}L^2} = -\alpha_0 \Delta y_{0n} z_n + \frac{1}{2}\alpha_0 \Delta tan\cdot z_n^{\,2} - \frac{1}{2}\frac{(1-\alpha_0)}{\beta}\Delta y_{0n} z_n^{\,2} + \frac{1}{3}\frac{(1-\alpha_0)}{\beta}\Delta tan\cdot z_n^{\,3}$
	$\frac{M}{E_{s1}L^3} = -\frac{1}{2}\alpha_0 \Delta y_{0n} z_n^{\,2} + \frac{1}{6}\alpha_0 \Delta tan\cdot z_n^{\,3} - \frac{1-\alpha_0}{6\beta}\Delta y_{0n} z_n^{\,3} + \frac{1-\alpha_0}{12\beta}\Delta tan\cdot z_n^{\,4}$
	$z_{nM} = \frac{3}{4}\left\{\frac{N_{\Delta y}}{N_{\Delta t}} - \left(\frac{\alpha_0\beta}{1-\alpha_0}\right) + \sqrt{\left(\frac{N_{\Delta y}}{N_{\Delta t}}\right)^2 + \frac{10}{3}\frac{N_{\Delta y}}{N_{\Delta t}}\left(\frac{\alpha_0\beta}{1-\alpha_0}\right) + \left(\frac{\alpha_0\beta}{1-\alpha_0}\right)^2}\right\}$
	$\frac{M_{\max}}{E_{s1}L^3} = \frac{1}{12} z_{1n}^{\,2}\frac{\Delta t}{\beta}\left\{-6\alpha_0\beta\frac{N_{\Delta y}}{N_{\Delta t}} + 2\left[\alpha_0\beta - (1-\alpha_0)\frac{N_{\Delta y}}{N_{\Delta t}}\right]\cdot z_{1n} + (1-\alpha_0) z_{1n}^{\,2}\right\}$
$z_n = \beta$ (slip surface)	$\frac{T_\beta}{E_{s1}L^2 y_{s0n}} = \frac{k(1-\beta)}{2D}\left[2N_y - N_t(1+\beta)\right]$
	$\frac{M_\beta}{E_{s1}L^3 y_{s0n}} = \frac{k(1-\beta)^2}{6D}\left[3N_y - N_t(2+\beta)\right]$
$\beta - 1$ (stable zone)	$\frac{T}{E_{s1}L^2} = -k y_{0n}(z_n - 1) + \frac{1}{2}k\tan\omega\left(z_n^{\,2} - 1\right)$
	$\frac{M}{E_{s1}L^3} = -k y_{0n}\left(\frac{1}{2}z_n^{\,2} - z_n + \frac{1}{2}\right) + \frac{1}{2}k\tan\omega\left(\frac{1}{3}z_n^{\,3} - z_n + \frac{2}{3}\right)$

$$z_{nM} = \frac{2y_{0n}}{\tan\omega} - 1$$

$$\frac{M_{max}}{E_{s1}L^3 y_{s0n}} = \frac{2k\left(N_t - N_y\right)^3}{3DN_t^{\ 2}}$$

Table 3-9: Elastic solutions for a free-head passive rigid pile in a normal-consolidated cohesive soil sliding on a firm layer

Once again, it has to be noticed that, in every zone, the expression of the maximum bending moment is only valid if its depth is within the relative interval.
The maximum bending moment all along the pile is clearly obtained as:

$$\frac{M_{max}}{E_{s1}L^3} = max\left\{\left|\frac{M_{max1}}{E_{s1}L^3}\right|;\left|\frac{M_{max2}}{E_{s1}L^3}\right|\right\} \qquad (3\text{-}48)$$

The distribution profile of the pile response can then be obtained with the new solutions, concerning the depth of the sliding surface. The normalised shear force $T_n = T/(L^2\, E_{s1} y_{s0n})$ and bending moment $M_n = M/(L^3 E_{s1} y_{s0n})$ are plotted in Figure 3-27, Figure 3-28, Figure 3-29, Figure 3-30, for η equal to 1 and 0 and for a fixed k = 2 and α_0=0.5.
The normalised stresses on the pile show similar trends than those showed for the previous case of a constant E_s value in the top layer: the shear force profiles present two local extrema, a positive one at upper parts of the piles and a negative at deeper depths.
In particular, for η = 1 T_n has its maximum value in correspondence of the sliding surface, once again with a value almost identical for the different values of β. The case η = 0 presents lower values of $T_{n,max}$, with peaks which occur closer to the pile's top and bottom. An almost null T_n at sliding depth corresponds to β=0.6, while a negative value occurs for higher β values.

M_n generally has its maximum value for depths close to the middle of the pile, for both configurations; anyway, while for $\eta = 0$ the bending moment on the pile is always positive, for $\eta = 1$ it is negative for $\beta \geq 6$.

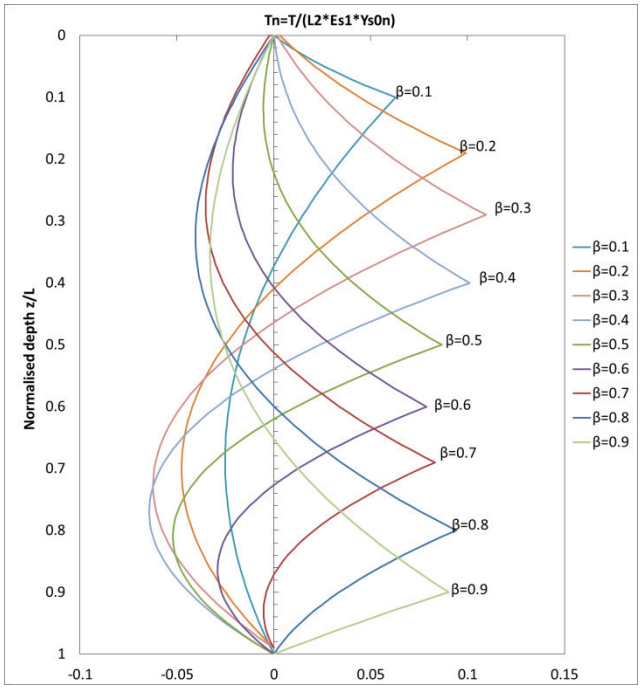

Figure 3-27: : Normalised shear force with depth for k=2, η=1 and α_0=0.5

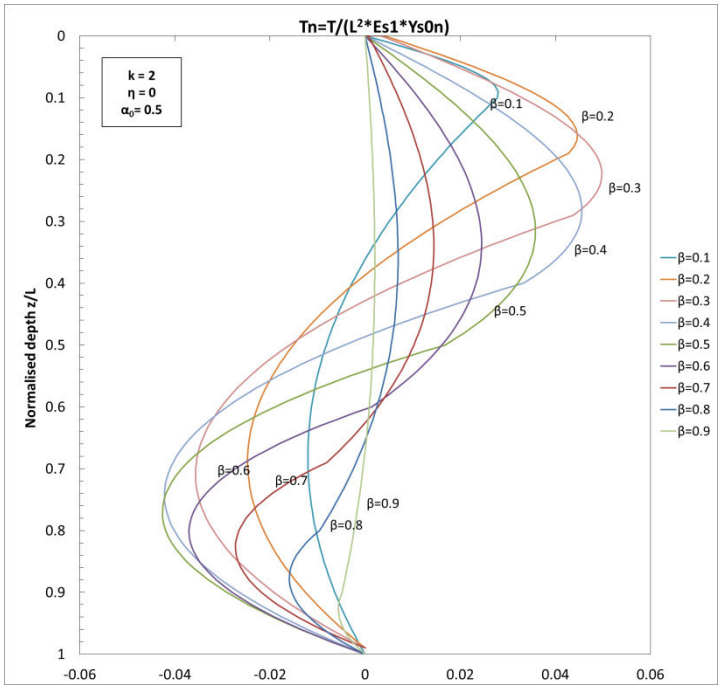

Figure 3-28: : Normalised shear force with depth for k=2 ,η=0 and α0=0.5

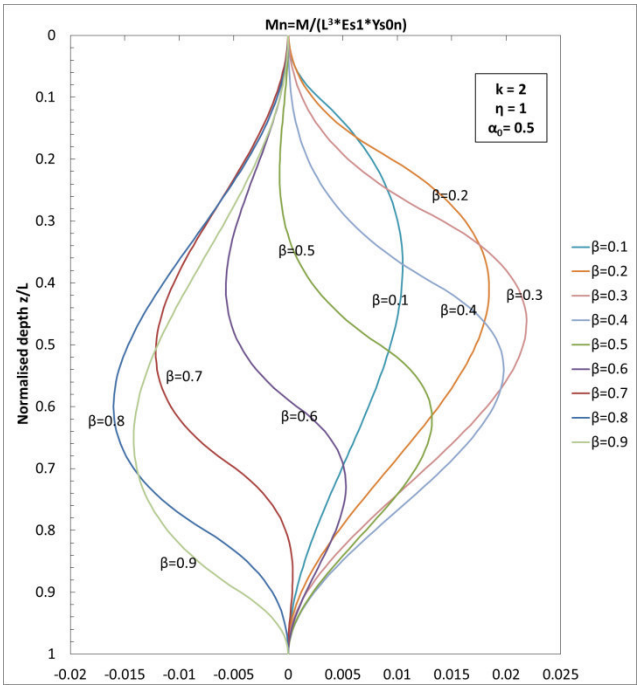

Figure 3-29: Normalised bending moment with depth for k=2, η=1 and α_0=0.5

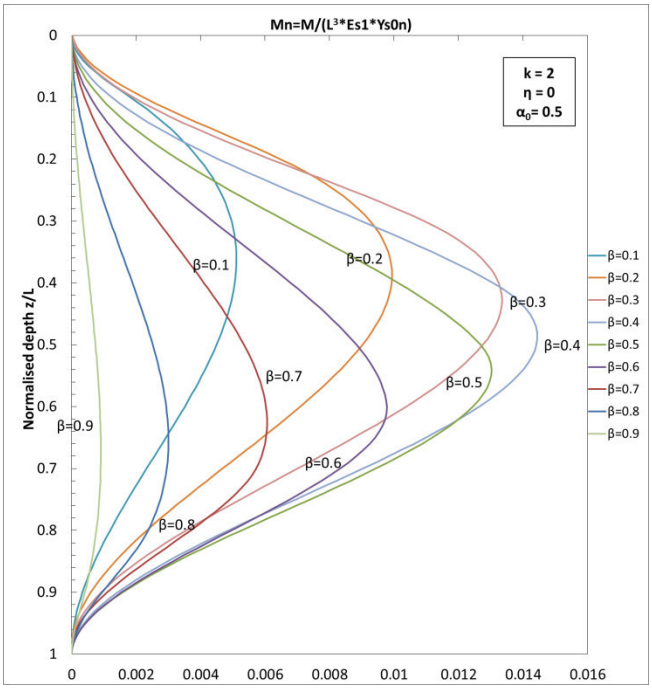

Figure 3-30: Normalised bending moment with depth for k=2, η=0 and α_0=0.5

3.5.2. Unrotated head condition

It is here investigated the case showed in Figure 3-31: a rigid unrotated-head pile is embedded in a two-layered soil where a shallow layer with a subgrade modulus varying with depth slides over a firm stratum having a constant E_s. As already explained, the fixity condition is represented by the bending moment M_0 applied on the pile head .

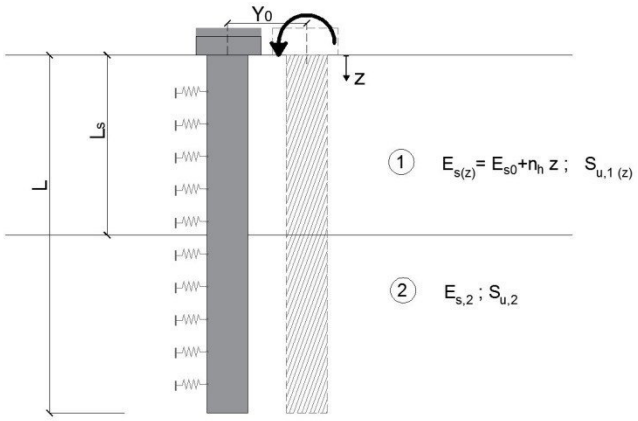

Figure 3-31:Soil profile and pile displacement geometry for a unrotated-head passive rigid pile in a normal-consolidated sliding cohesive soil over a firm layer

This assumption let adequately describe pile deflection $y_p(z)$ with depth by using the head's movement parameter y_0:

$$y_p(z) = y_0 \qquad (3\text{-}49)$$

With the above assumptions, the soil reactions along the whole length L of the pile can be expressed as:

$$p_{1(z)} = -(E_{s0} + nz)[\Delta y_0 + tan\,\theta \cdot z] \qquad [FL^{-1}] \quad 0 < z < Ls \qquad (3\text{-}50)$$

$$p_{2(z)} = -E_{s2}(y_0) \qquad [FL^{-1}] \quad Ls < z < L \qquad (3\text{-}51)$$

The horizontal force equilibrium and moment equilibrium around the head of the pile are expressed by the following normalised equations:

$$\left[-\frac{1}{2}\beta(1-\alpha_0)+\beta+k(1-\beta)\right]y_{0n} = \left[-\frac{1}{2}\beta(1-\alpha_0)+\beta\right]y_{s0n}+\left[\frac{1}{6}\beta^2(1-\alpha_0)-\frac{1}{2}\beta^2\right]\tan\theta \qquad (3\text{-}52)$$

$$\left[-\frac{1}{6}\beta^2(1-\alpha_0)+\frac{1}{2}\beta^2+\frac{1}{2}k(1-\beta^2)\right]y_{0n}-M_{0n} = \left[-\frac{1}{6}\beta^2(1-\alpha_0)+\frac{1}{2}\beta^2\right]y_{s0n}+\left[\frac{1}{12}\beta^3(1-\alpha_0)-\frac{1}{3}\beta^3\right]\tan\theta \qquad (3\text{-}53)$$

The profile of the pile deflection and the bending moment M_0 acting on its head are provided in Table 3-10 while shear forces and bending moments profiles, maximum bending moment M_{max} and its depth z_n in both unstable and stable zones are provided in Table 3-11.

	Proportionality constants
	$D = k(1-\beta)+\frac{1}{2}\beta(1+\alpha_0)$
$y_{0n} = \frac{N_y}{D} y_{s0n}$	$N_y = \frac{1}{6}\beta(1+2\eta+2\alpha_0+\alpha_0\eta)$

$M_{0n} = \frac{N_M}{D} y_{s0n}$	$N_M = \frac{1}{72}\beta^3(1-\eta)(1+4\alpha_0+\alpha_0{}^2)$ $+\frac{1}{12}k\beta(1-\beta)\{1+\eta(2-\beta)+\alpha_0(2+\eta+\beta)\}$

Table 3-10: Proportionality constants for a passive unrotated-head rigid pile in a normal-consolidated sliding cohesive soil over a firm layer

Depth (z_n)	Expressions
0 – β (loading zone)	$\frac{T}{E_{s1}L^2} = -\alpha_0 \Delta y_{0n} z_n + \frac{1}{2}\alpha_0 \Delta tan\text{-} z_n{}^2 - \frac{1}{2}\frac{(1-\alpha_0)}{\beta}\Delta y_{0n} z_n{}^2 + \frac{1}{3}\frac{(1-\alpha_0)}{\beta}\Delta tan\text{-} z_n{}^3$ $\frac{M}{E_{s1}L^3} = -\frac{1}{2}\alpha_0 \Delta y_{0n} z_n{}^2 + \frac{1}{6}\alpha_0 \Delta tan\text{-} z_n{}^3 - \frac{1-\alpha_0}{6\beta}\Delta y_{0n} z_n{}^3 + \frac{1-\alpha_0}{12\beta}\Delta tan\text{-} z_n{}^4$ $\frac{M_{max}}{E_{s1}L^3} = M_{0n}$
$z_n = \beta$ (slip surface)	$\frac{T_\beta}{E_{s1}L^2 y_{s0n}} = \left[\frac{k(1-\beta)N_y}{D}\right]$ $\frac{M_\beta}{E_{s1}L^3 y_{s0n}} = \left[\frac{k(1-\beta)^2 N_y}{2D}\right]$
β – 1 (non loading zone)	$\frac{T}{E_{s1}L^2} = -k y_{0n}(z_n - 1)$

$$\frac{M}{E_{s1}L^3} = -ky_{0n}\left(\frac{1}{2}z_n{}^2 - z_n + \frac{1}{2}\right)$$

Table 3-11: Elastic solutions for a passive unrotated-head rigid pile in a normal-consolidated sliding cohesive soil over a firm layer

The distribution profiles of the pile response can then be obtained with the new solutions, concerning the depth of the sliding surface. The normalised shear force $T_n = T/(L^2\, E_{s1} y_{s0n})$ and bending moment $M_n = M/(L^3 E_{s1} y_{s0n})$ are plotted in the following pictures, for η equal to 1 and 0 and for a fixed k = 2 and α_0=0.5.
It is evident, as for the free-head pile, that the normalised stresses shift with the normalised depth of the sliding surface β.
Shear forces and bending moments are respectively positive and negative along the whole pile length. The max T_n value, for η = 1, occurs at z_n=β, with values of T_n obtained in correspondence of β values ranging between 0.4 and 0.6 .
On the contrary, the case η = 0 presents lower values of $T_{n,max}$. M_n shows the same profile for both η = 0 and η = 1, with always negative values. Once again, the condition η = 1 results to give slightly higher values of $M_{n,ma}$.

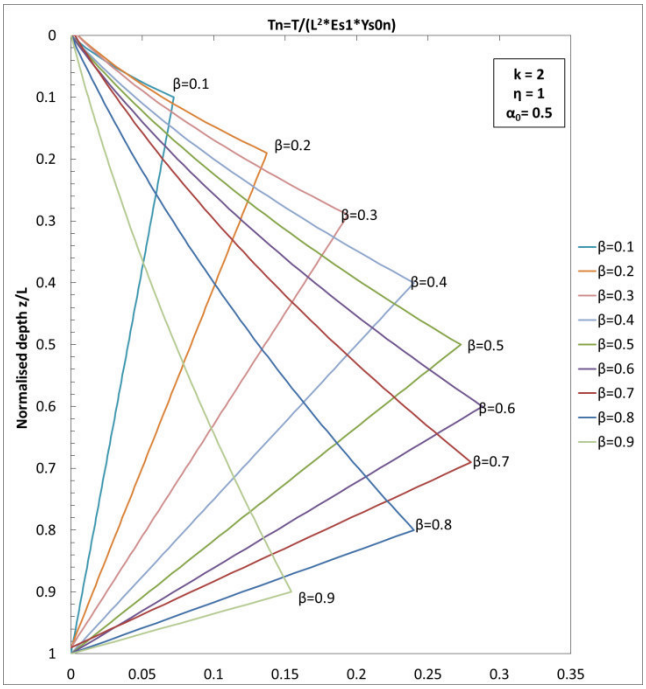

Figure 3-32: Normalised shear force with depth for an unrotated pile and for k=2, η=1 and α0=0.5

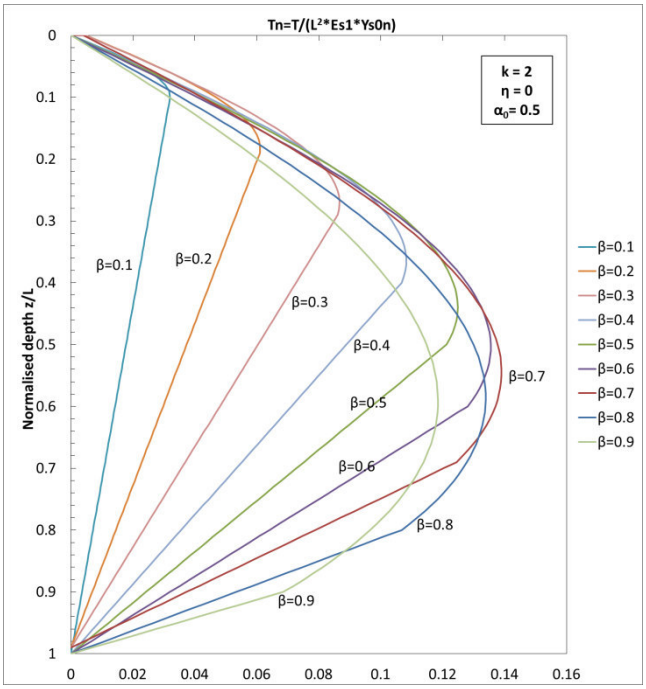

Figure 3-33: Normalised shear force with depth for an unrotated pile and for k=2, η=0 and α0=0.5

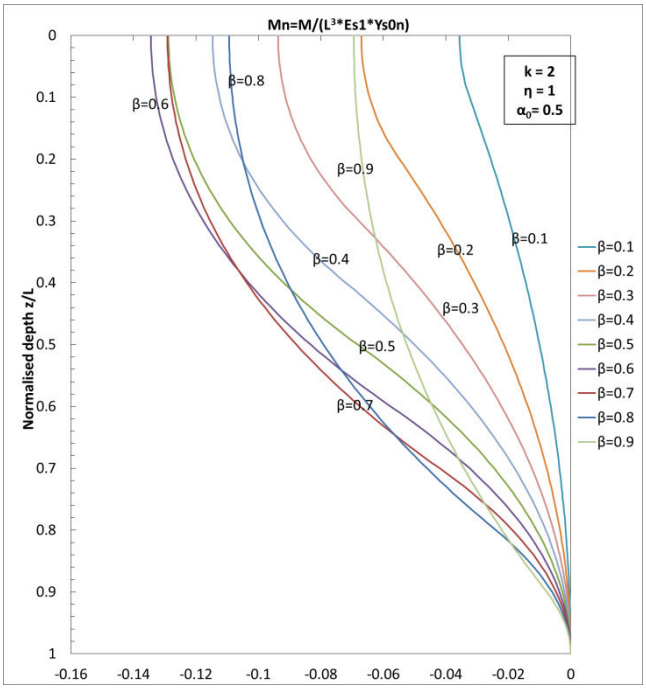

Figure 3-34: Normalised bending moment with depth for an unrotated pile and *for k=2, η=1 and α0=0.5*

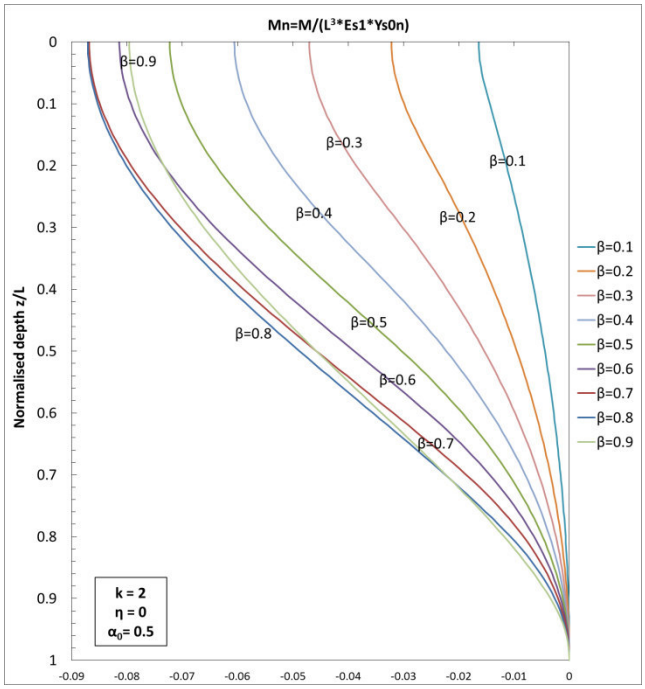

Figure 3-35: Normalised bending moment with depth for an unrotated pile and for k=2, η=0 and α0=0.5

3.5.3. Parametric analysis

The solution provided have been implemented in spreadsheets to carry out a parametric analysis of the problem.
The elastic solutions for a passive rigid pile in a two-layered soil with subgrade modulus varying with depth as the sliding cohesive mass presents an undrained shear strength increasing with depth, are governed by the parameter k that represents the ratio between E_s values E_{s2} and E_{s1} respectively of the stable and unstable soils:

$$k = \frac{E_{s2}}{E_{s1}} \qquad (3\text{-}54)$$

the parameter η that represents between soil displacement at ground level and at the sliding depth:

$$\eta = \frac{y_{s(z=Ls)}}{y_{s0}} \qquad (3\text{-}55)$$

the parameter α_0 that represents the ratio between modulus of subgrade reaction at ground level and at L_s :

$$\alpha_0 = \frac{E_{s0}}{E_{s1}} \qquad (3\text{-}56)$$

The parametric analysis focuses on their effects on the normalised pile shear resistance at $z=L_s$:

$$T_{\beta,n} = \frac{T_{(z=Ls)}}{E_{s1}L^2 y_{s0,n}} \qquad (3\text{-}57)$$

Normalised bending moment at $z=L_s$:

$$M_{\beta,n} = \frac{M_{(z=Ls)}}{E_{s1}L^3 y_{s0,n}} \qquad (3\text{-}58)$$

Normalised maximum bending moment acting on the pile:

$$M_{n,max} = \frac{M_{max}}{E_{s1}L^3 y_{s0,n}} \qquad (3\text{-}59)$$

Normalised pile head displacement:

$$\frac{y_{0n}}{y_{s0n}} = \frac{y_0}{y_{s0}} \qquad (3\text{-}60)$$

In every chart, values are plotted against the normalised depth of the sliding surface. The analysis concerns both the boundary conditions of free-head (Figure 3-36 through Figure 3-39) and unrotated-head (Figure 3-40 through Figure 3-43).

Several considerations can be done on the presented results:

- The ratio between modulus of subgrade reaction at ground level and at L_s is represented by the parameter α_0: when assumed equal to 1, the configuration coincides to the case of two-layered soil with a constant modulus. The graphs show that the higher is the value of this parameter, the higher is the stress state acting on the pile; in other words, a sliding soil subgrade modulus varying with depth ($\alpha_0<1$) leads to lower pile reactions than those relative to a constant profile ($\alpha_0=1$). It is reasonable result as a lower modulus implicates lower force per unit length available on the pile and consequently lower stress state. The only exception is the shear force on a free-head pile with $\eta=0$, where the parameter α_0 does not seem to be really effective.

- With regard to the lateral soil movement distribution, higher pile head deflection and stress states are expected for higher values of η. This result appears reasonable as, with the same maximum value at the soil surface, the rectangular profile corresponds to a higher total soil displacement and consequently higher loading on the pile. It is worth to be noticed that the

condition $\eta=0$ is the only one which corresponds to a negative shear force at the sliding surface for high values of β in the free-head condition.

- Several ratios between subgrade modulus of the stable and unstable soils have been considered, by varying k from 1 to 10. This parameter has a scale effect on the pile stress state: higher the k value, higher the value of shear forces and bending moments acting on the pile. However, a higher value of k corresponds to lower pile deflection, reasonably due to the stronger embedment given to the pile. Moreover, as k increases, the maximum value of T_n and M_n tend to occur at deeper sliding depths.

- With attention to the two boundary condition analysed, the unrotated-head condition corresponds to higher stress states on the pile, with shear forces and bending moments at the sliding depth sensibly higher than those developed by the free-head condition, at the same time associated lower pile head deflection. The free-head condition presents two local maximum values in both the shear force and the bending moment profiles. Finally, both the boundary conditions, as reasonably expected, presents a pile head deflection proportionally increasing with β.

FREE-HEAD PILE

Effect of different α_0 values (η=0):

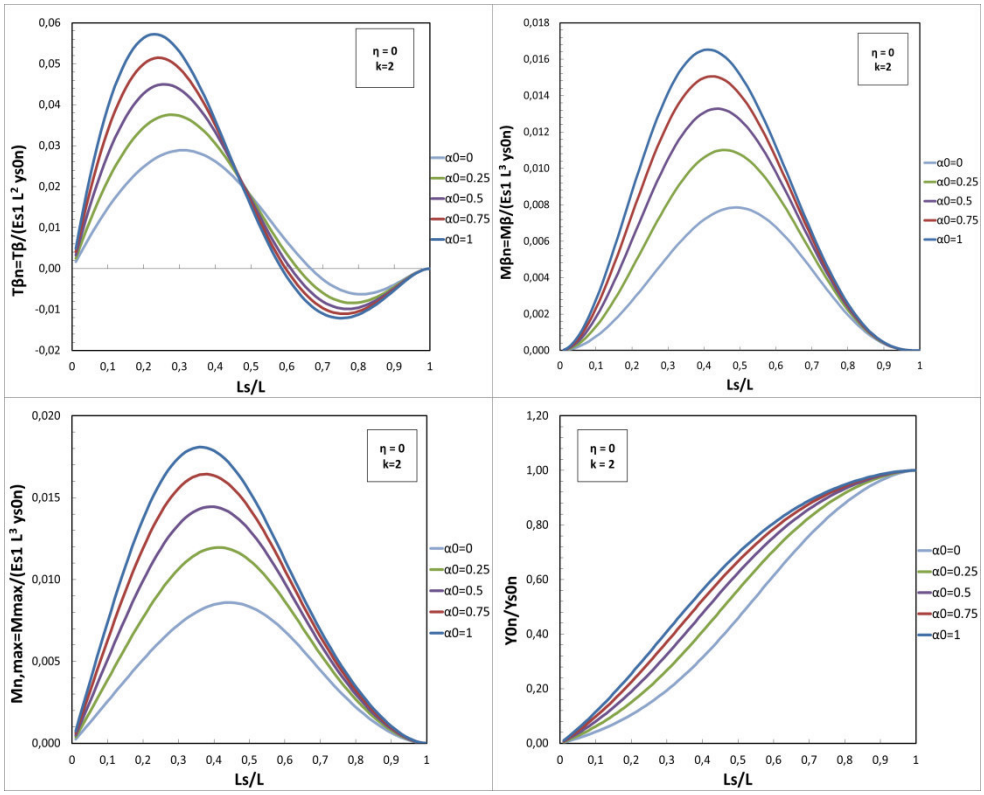

Figure 3-36: Normalised shear force at $z_n=\beta$, bending moment at $z_n=\beta$, maximum bending moment and pile head displacement versus L_s/L, for η=0,k=2 and different α_0 values. Free-head condition

Effect of different k values (η=0):

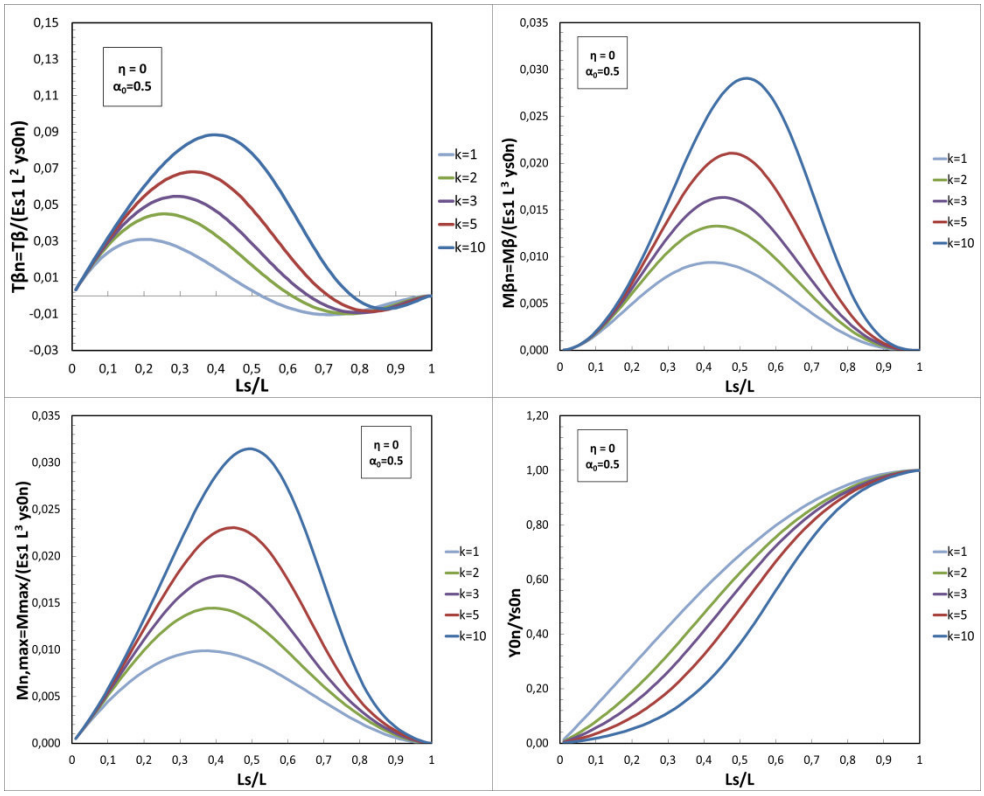

Figure 3-37: Normalised shear force at $z_n=\beta$, bending moment at $z_n=\beta$, maximum bending moment and pile head displacement versus L_s/L, for $\eta=0$, $\alpha_0=0.5$ and different k values. Free-head condition

Effect of different k values (η=1):

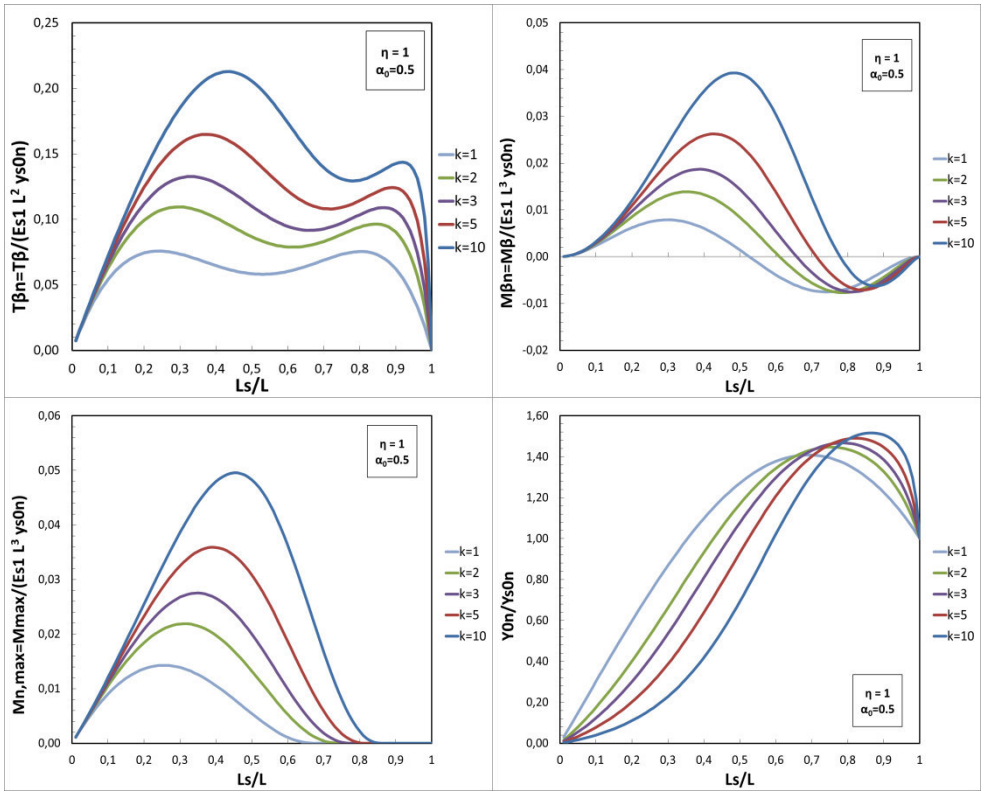

Figure 3-38: Normalised shear force at $z_n=\beta$, bending moment at $z_n=\beta$, maximum bending moment and pile head displacement versus L_s/L, for $\eta=1$, $\alpha_0=0.5$ and different k values. Free-head condition

Effect of different η values:

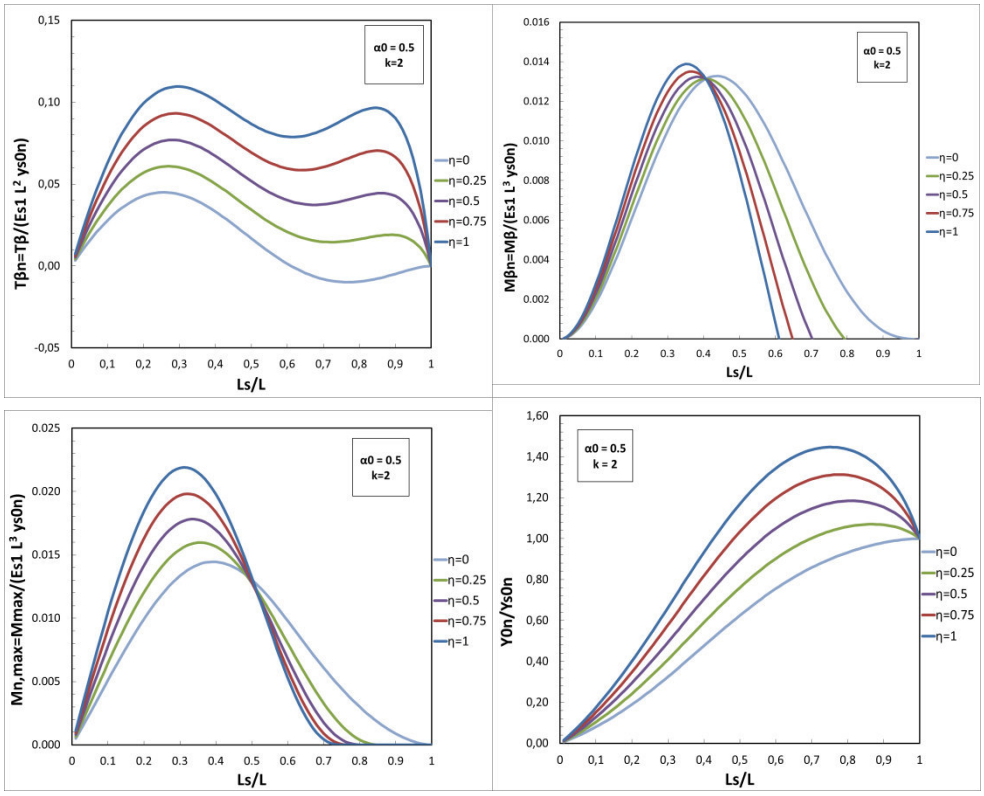

Figure 3-39: Normalised shear force at $z_n=\beta$, bending moment at $z_n=\beta$, maximum bending moment and pile head displacement versus L_s/L, for k=2, $\alpha_0=0.5$ and different η values. Free-head condition

UNROTATED-HEAD PILE

Effect of different k values (η=0):

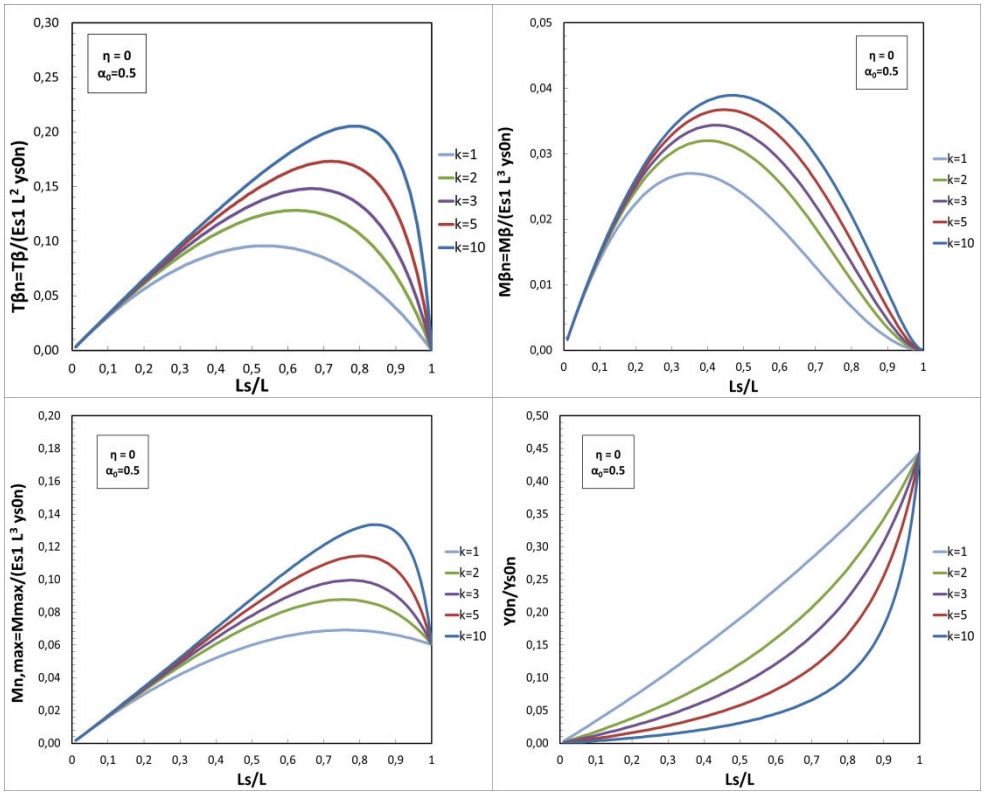

Figure 3-40: Normalised shear force at $z_n=\beta$, bending moment at $z_n=\beta$, maximum bending moment and pile head displacement versus L_s/L, for $\eta=0$, $\alpha_0=0.5$ and different k values. Unrotated-head condition

Effect of different k values (η=1):

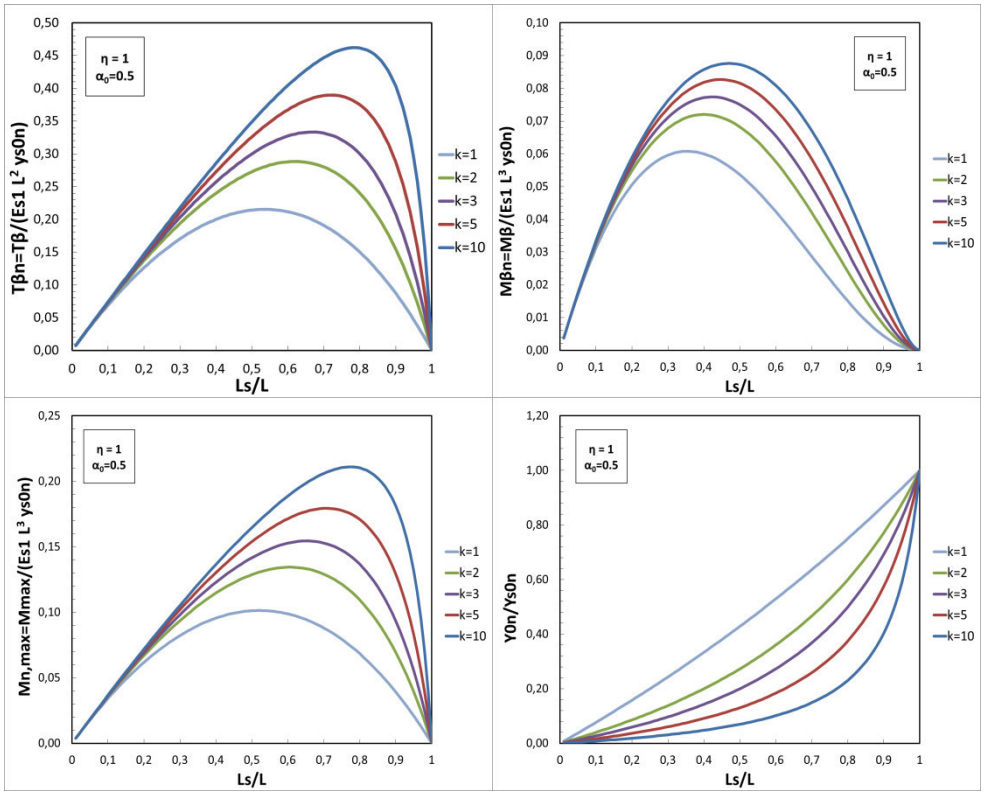

Figure 3-41: Normalised shear force at $z_n=\beta$, bending moment at $z_n=\beta$, maximum bending moment and pile head displacement versus L_s/L, for $\eta=1$, $\alpha_0=0.5$ and different k values. Unrotated-head condition

Effect of different η values:

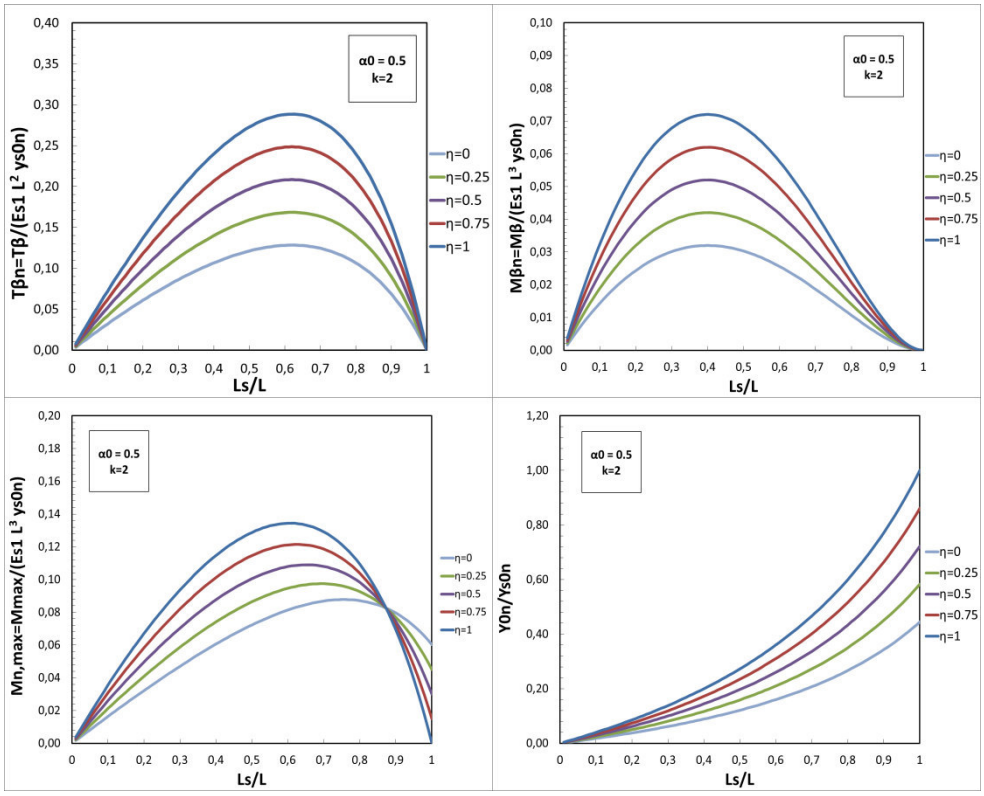

Figure 3-42: Normalised shear force at $z_n=\beta$, bending moment at $z_n=\beta$, maximum bending moment and pile head displacement versus L_s/L, for k=2, $\alpha_0=0.5$ and different η values. Unrotated-head condition

Effect of different α_0 values (η=0):

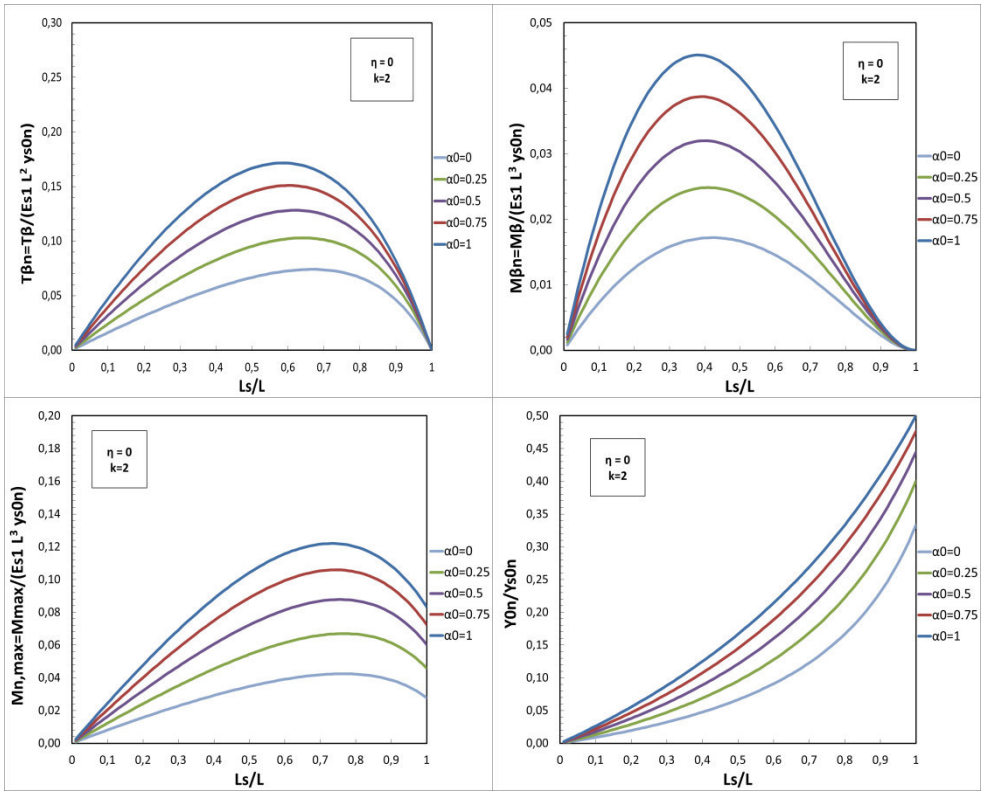

Figure 3-43: Normalised shear force at $z_n=\beta$, bending moment at $z_n=\beta$, maximum bending moment and pile head displacement versus L_s/L, for k=2, η=0 and different α_0 values. Unrotated-head condition

3.6. Elastic solutions for a passive rigid pile in a two-layered profile with subgrade modulus linearly increasing with depth

3.6.1. Free-head condition

For a non-cohesive soil, the assumption of a non-null subgrade constant at ground level may not be always appropriate. For this reason, the case of a cohesionless soil mass having a linearly increasing with depth subgrade modulus, sliding on a cohesive firm layer, is here investigated.

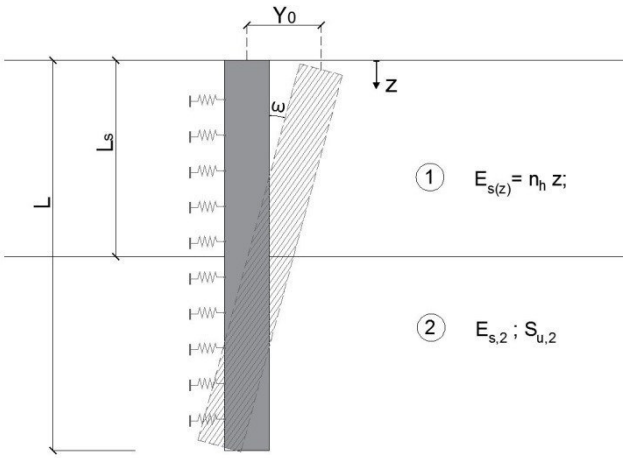

Figure 3-44: Soil profile and pile displacement geometry for a unrotated-head passive rigid pile in a cohesionless sliding soil over a cohesive firm layer

The E_s modulus of the sliding layer has a linear variation with depth, from a zero value at ground level to E_{s1} at its bottom (see paragraph 3.4 for a sandy soil). At the same time, the underlying firm layer (ideally a cohesive material with a constant undrained shear strength) has a constant modulus ($E_{s2} = k\ E_{s1}$) (Figure 3-45).

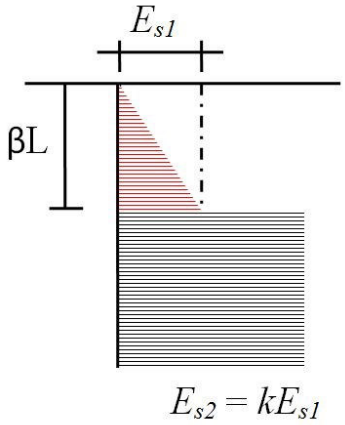

Figure 3-45: Variation of E_s with depth for a free-head passive rigid pile in a cohesionless sliding soil over a cohesive firm layer

With the above assumptions, the soil reactions acting on the pile can be expressed as:

$$p_{1(z)} = -(n_h z)[\Delta y_0 - \Delta\, tan \cdot z] \qquad [FL^{-1}] \quad 0 < z < Ls \qquad (3\text{-}61)$$

$$p_{2(z)} = -E_{s2}(y_0 - z\, tan\, \omega) \qquad [FL^{-1}] \quad Ls < z < L \qquad (3\text{-}62)$$

Where

$$n_h = \frac{E_{s1} - E_{s0}}{\beta L} = \frac{E_{s1}(1-\alpha_0)}{\beta L} \qquad (3\text{-}63)$$

Pile deflection can be obtained by imposing the horizontal force equilibrium and moment equilibrium around the head of the pile:

$$\left[\frac{1}{2}\beta + k(1-\beta)\right] y_{0n} + \left[-\frac{1}{3}\beta^2 - \frac{1}{2}k(1-\beta^2)\right] \tan\omega = \frac{1}{2}\beta y_{s0n} - \frac{1}{3}\beta^2 \tan\theta \qquad (3\text{-}64)$$

$$\left[+\frac{1}{3}\beta^2 + \frac{1}{2}k(1-\beta^2)\right] y_{0n} + \left[-\frac{1}{4}\beta^3 - \frac{1}{3}k(1-\beta^3)\right] \tan\omega = +\frac{1}{3}\beta^2 y_{s0n} - \frac{1}{4}\beta^3 \tan\theta \qquad (3\text{-}65)$$

As for the previous cases investigated, the pile deflection is found to be directly proportional to the soil free field movement through proportionally constants (expressed in Table 3-12).

Proportionality constants	
	$D = \frac{1}{6}\beta^4 + k^2(1-\beta)^4 + k\beta(1-\beta)\left[\beta^2 - 2\beta + 2\right]$
$y_{0n} = \frac{N_y}{D} y_{s0n}$	$N_y = \frac{1}{6}\beta^4 + \frac{1}{6}k\beta^2(1-\beta^2)[1-\eta] + \frac{2}{3}k\beta(1-\beta)[1+2\eta]$
$tan\omega = \frac{N_t}{D} y_{s0n}$	$N_t = \frac{1}{6}\beta^3(1-\eta) + k\beta(1-\beta)[1+\eta(2-\beta)]$

Table 3-12: Proportionality constants for a passive unrotated-head rigid pile in a cohesionless sliding soil over a cohesive firm layer

Shear forces and bending moments profiles, maximum bending moment M_{max} and its depth z_n in both loading and non-loading zones are provided in the following table.

Depth (z_n)	Expressions
0 – β (unstable zone)	$\frac{T}{E_{s1}L^2} = -\frac{1}{2\beta}\Delta y_{0n} z_n^{\ 2} + \frac{1}{3\beta}\Delta\tan\cdot z_n^{\ 3}$
	$\frac{M}{E_{s1}L^3} = -\frac{1}{6\beta}\Delta y_{0n} z_n^{\ 3} + \frac{1}{12\beta}\Delta\tan\cdot z_n^{\ 4}$
	$z_{nM} = \frac{3}{2}\frac{N_{\Delta y}}{N_{\Delta t}}$
	$\frac{M_{max}}{E_{s1}L^3 y_{s0n}} = \left[\frac{9}{64\beta}\left(\frac{N_{\Delta y}}{N_{\Delta t}}\right)^4 \frac{N_{\Delta t}}{D}\right]$
$z_n = \beta$ (slip surface)	$\frac{T_\beta}{E_{s1}L^2 y_{s0n}} = \frac{k(1-\beta)}{2D}\left[2N_y - N_t(1+\beta)\right]$
	$\frac{M_\beta}{E_{s1}L^3 y_{s0n}} = \frac{k(1-\beta)^2}{6D}\left[3N_y - N_t(2+\beta)\right]$

β – 1 (stable zone)	$\frac{T}{E_{s1}L^2} = -ky_{0n}(z_n - 1) + \frac{1}{2}k\tan\omega(z_n^2 - 1)$
	$\frac{M}{E_{s1}L^3} = -ky_{0n}\left(\frac{1}{2}z_n^2 - z_n + \frac{1}{2}\right) + \frac{1}{2}k\tan\omega\left(\frac{1}{3}z_n^3 - z_n + \frac{2}{3}\right)$
	$z_n = \frac{2y_{0n}}{\tan\omega} - 1$
	$\frac{M_{max}}{E_{s1}L^3 y_{s0n}} = \frac{2k(N_t - N_y)^3}{3DN_t^2}$

Table 3-13: Elastic solutions for a passive unrotated-head rigid pile in a cohesionless sliding soil over a cohesive firm layer

The distribution profile of the pile response can then be obtained with the new solutions, concerning the depth of the sliding surface. The normalised shear force $T_n = T/(L^2\, E_{s1} y_{s0n})$ and bending moment $M_n = M/(L^3 E_{s1} y_{s0n})$ are plotted in Figure 3-46, Figure 3-47, Figure 3-48 and Figure 3-49, for η equal to 1 and 0 and for a fixed k = 2.

It is evident that the normalised stresses shift with the normalised depth of the sliding surface β, with similar trends than those showed for the previous case of a constant E_s value in the top layer, where T_n profiles have two local extrema, a positive one close to the pile head and a negative one.

In particular, for η = 1, T_n has its maximum value in correspondence of the sliding surface, once again with a value almost identical for the different values of β. The case η = 0 presents lower values of $T_{n,max}$, with peaks which occur at z_n values closer to the pile's top and bottom (with a negative value) than the sliding depth.

M_n generally has its maximum value at depths closer to the middle of the pile, for both configurations, while for η = 0 the bending moment on the pile is always positive, for η = 1 it is negative if β ≥ 7. Anyway, if compared to the previous case

with a constant subgrade modulus, the obtained T_n and M_n values are considerably lower, due to the minor stiffness available.

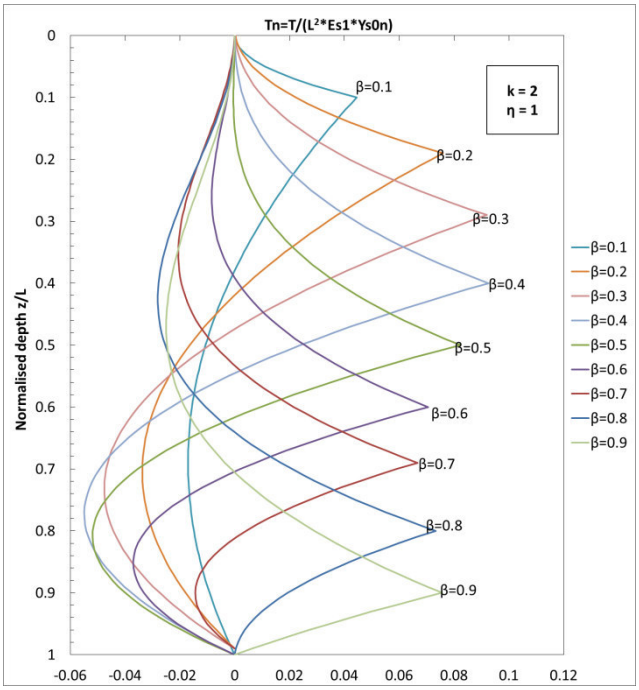

Figure 3-46: : Normalised shear force with depth for k=2, η=1

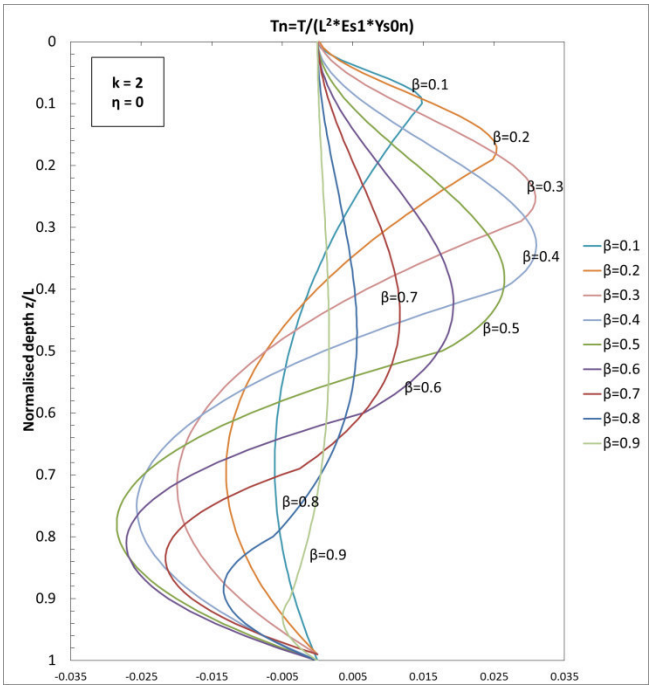

Figure 3-47: Normalised shear force with depth for k=2, η=0

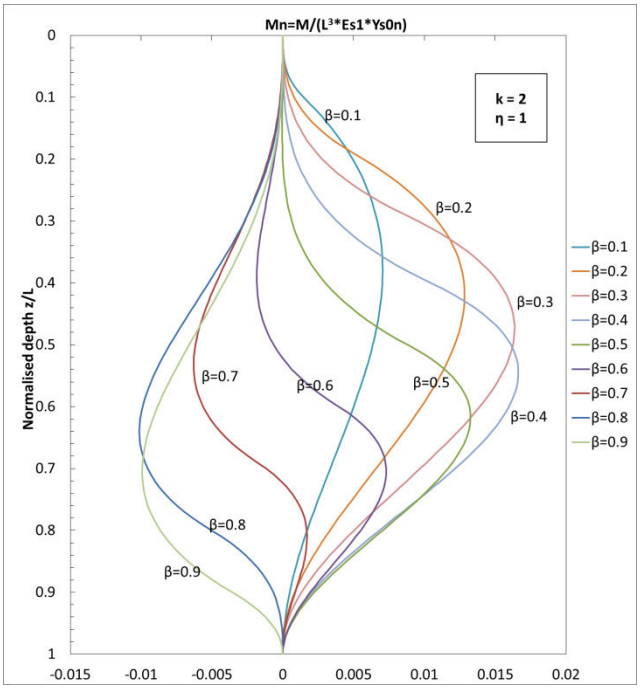

Figure 3-48: Normalised bending moment with depth for k=2, η=1

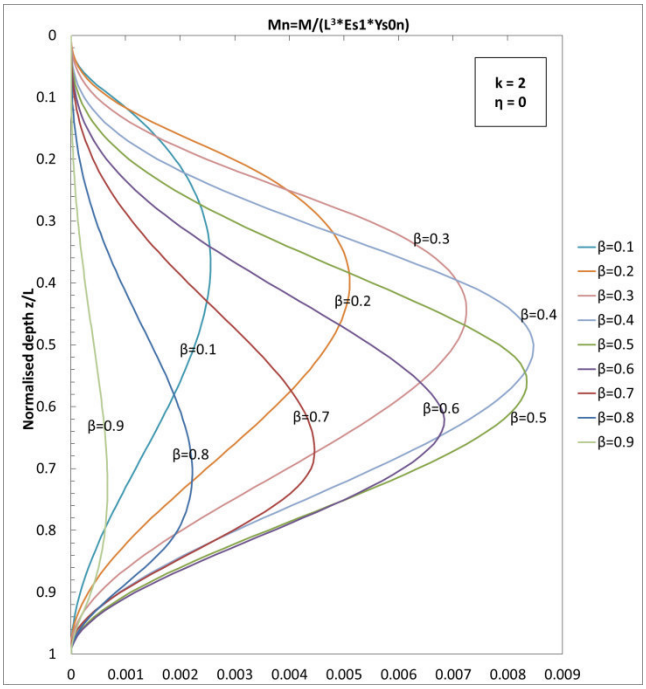

Figure 3-49: Normalised bending moment with depth for k=2, η=1

3.6.2. Unrotated head condition

It is here investigated the case showed in Figure 3-50: a rigid unrotated-head pile is embedded in a two-layered soil where a shallow layer, assumed as a cohesionless soil, with a subgrade modulus increasing with depth from a null value at ground level, slides over a firm stratum having a constant E_s. As already explained, the fixity condition is represented by the bending moment M_0 applied on the pile head.

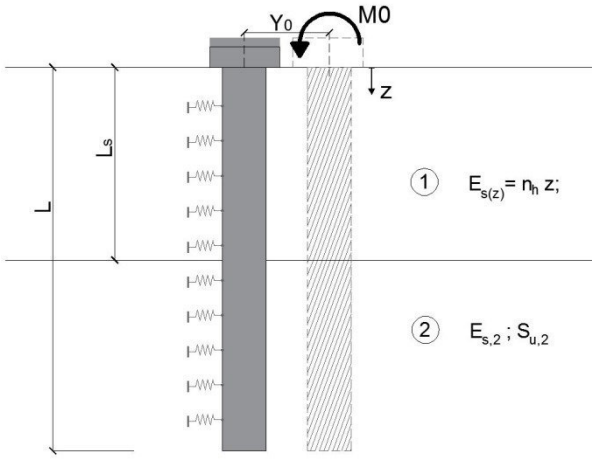

Figure 3-50: Soil profile and pile displacement geometry for a unrotated-head passive rigid pile in a cohesionless sliding soil over a cohesive firm layer

The soil reactions along the whole length L of the pile can be expressed as:

$$p_{1(z)} = -(nz)[\Delta y_0 + \tan\theta \cdot z] \qquad [FL^{-1}] \quad 0 < z < Ls \qquad (3\text{-}66)$$

$$p_{2(z)} = -E_{s2}(y_0) \qquad [FL^{-1}] \quad Ls < z < L \qquad (3\text{-}67)$$

The global equations of the problem are obtained by imposing the horizontal force equilibrium and moment equilibrium around the head of the pile; in an explicit non-dimensional form, they are expressed as:

$$\left[\frac{1}{2}\beta + k(1-\beta)\right] y_{0n} = \left[\frac{1}{2}\beta\right] y_{s0n} + \left[-\frac{1}{3}\beta^2\right] tan\,\theta \qquad (3\text{-}68)$$

$$\left[\frac{1}{3}\beta^2 + \frac{1}{2}k(1-\beta^2)\right] y_{0n} - M_{0n} = \left[+\frac{1}{3}\beta^2\right] y_{s0n} + \left[-\frac{1}{4}\beta^3\right] tan\,\theta \qquad (3\text{-}69)$$

The profile of the pile deflection and the bending moment M_0 acting on its head are provided in Table 3-14 while shear forces and bending moments profiles, maximum bending moment M_{max} and its depth z_n in both unstable and stable zones are provided in Table *3-14: Proportionality constants for* a passive unrotated-head rigid pile in a cohesionless sliding soil over a cohesive firm layer

Proportionality constants	
	$D = k(1-\beta) + \frac{1}{2}\beta$
$y_{0n} = \frac{N_y}{D} y_{s0n}$	$N_y = \frac{1}{6}\beta(2\eta + 1)$
$M_{0n} = \frac{N_M}{D} y_{s0n}$	$N_M = \frac{1}{72}\beta^3(1-\eta) + \frac{1}{12}k\beta(1-\beta)\{1 + \eta(2-\beta)\}$

Table 3-14: Proportionality constants for a passive unrotated-head rigid pile in a cohesionless sliding soil over a cohesive firm layer

Depth (z_n)	Expressions
0 – β (unstable zone)	$\frac{T}{E_{s1}L^2} = -\frac{1}{2\beta}\Delta y_{0n} z_n^{\ 2} + \frac{1}{3\beta}\Delta \tan\cdot z_n^{\ 3}$ $\frac{M}{E_{s1}L^3} = -M_{0n} - \frac{1}{6\beta}\Delta y_{0n} z_n^{\ 3} + \frac{1}{12\beta}\Delta tan\cdot z_n^{\ 4}$ $\frac{M_{max}}{E_{s1}L^3} = M_{0n}$
$z_n = \beta$ (slip surface)	$\frac{T_\beta}{E_{s1}L^2 y_{s0n}} = \left[\frac{k(1-\beta)N_y}{D}\right] y_{s0n}$ $\frac{M_\beta}{E_{s1}L^3 y_{s0n}} = \left[\frac{k(1-\beta)^2 N_y}{2D}\right] y_{s0n}$
β – 1 (stable zone)	$\frac{T}{E_{s1}L^2} = -k y_{0n}(z_n - 1)$ $\frac{M}{E_{s1}L^3} = -k y_{0n}\left(\frac{1}{2} z_n^{\ 2} - z_n + \frac{1}{2}\right)$

Table 3-15: Elastic solutions for a passive unrotated-head rigid pile in a cohesionless sliding soil over a cohesive firm layer

The distribution profiles of the pile response can then be obtained with the new solutions, concerning the depth of the sliding surface. The normalised shear force $T_n = T/(L^2\, E_{s1} y_{s0n})$ and bending moment $M_n = M/(L^3 E_{s1} y_{s0n})$ are plotted in Figure 3-51, Figure 3-52, Figure 3-53, Figure 3-54, for η equal to 1 and 0 and for a fixed k = 2.

Once again, it is evident that the normalised stresses shift with the normalised depth of the sliding surface β, with similar profiles than the previous configurations.

T_n profiles present one only global maximum value that, for η = 1, occurs in correspondence of the sliding surface, and in general for β values from 0.5 to 0.8. The case η = 0 presents lower values of $T_{n,max}$, with peaks which occur at z_n slightly upper than β.

M_n shows a similar profile for both η = 0 and η = 1, with always negative values. The condition η = 1 results to give slightly higher values of $M_{n,ma}$.

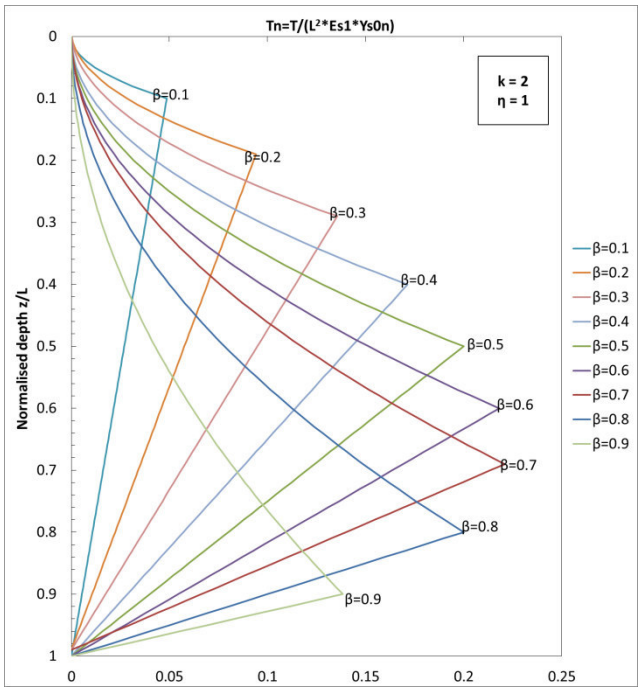

Figure 3-51: Normalised shear force with depth for k=2, η=1

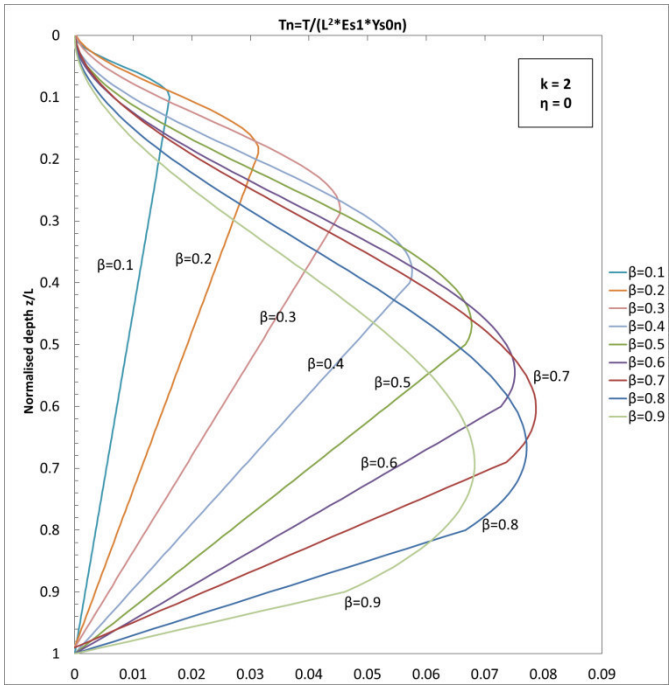

Figure 3-52: Normalised shear force with depth for k=2, η=0

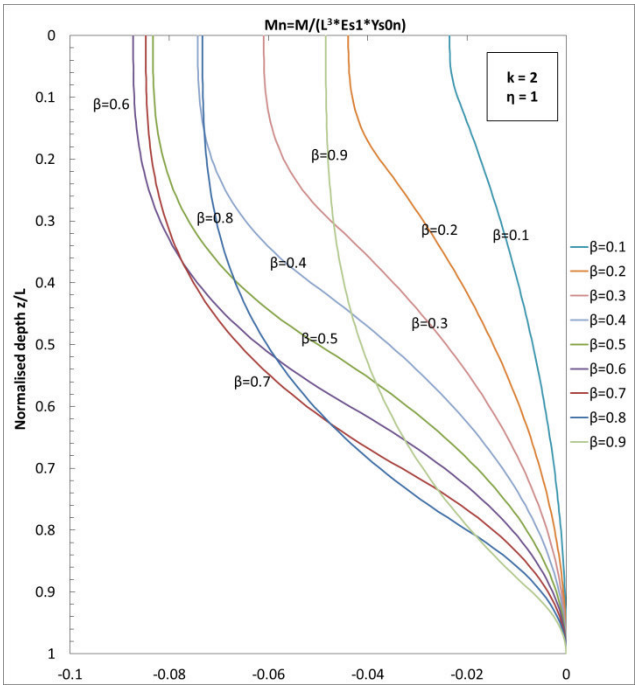

Figure 3-53: Normalised bending moment with depth for k=2, η=1

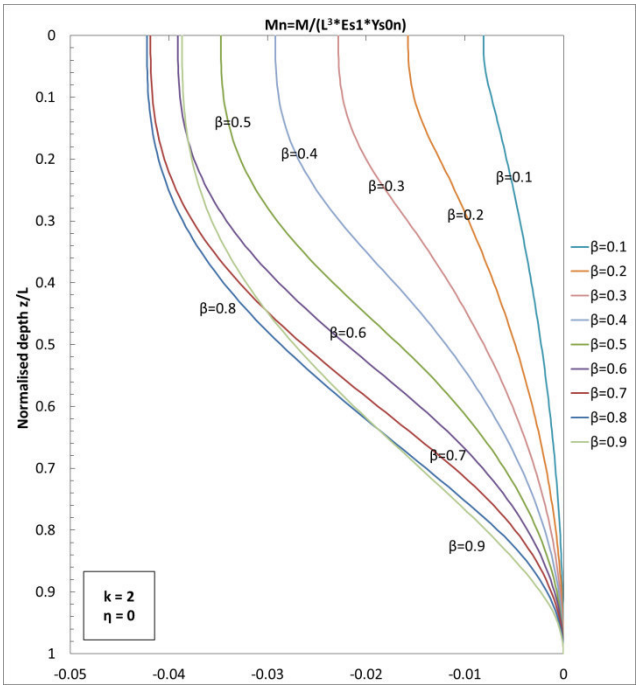

Figure 3-54: Normalised bending moment with depth for k=2, η=0

3.6.3. Parametric analysis

The solution provided have been implemented in spreadsheets to carry out a parametric analysis of the problem.
The elastic solutions for a passive rigid pile in a two-layered cohesive soil with a sliding cohesionless soil having a constant subgrade reaction modulus increasing with depth are governed by the parameter k that represents the ratio between E_s values E_{s2} and E_{s1} respectively of the stable and unstable soils:

$$k = \frac{E_{s2}}{E_{s1}} \qquad (3\text{-}70)$$

the parameter η that represents between soil displacement at ground level and at the sliding depth:

$$\eta = \frac{y_{s(z=Ls)}}{y_{s0}} \qquad (3\text{-}71)$$

The parametric analysis focuses on their effects on the normalised pile shear resistance at $z=L_s$:

$$T_{\beta,n} = \frac{T_{(z=Ls)}}{E_{s1}L^2 y_{s0,n}} \qquad (3\text{-}72)$$

Normalised bending moment at $z=L_s$:

$$M_{\beta,n} = \frac{M_{(z=Ls)}}{E_{s1}L^3 y_{s0,n}} \qquad (3\text{-}73)$$

Normalised maximum bending moment acting on the pile:

$$M_{n,max} = \frac{M_{max}}{E_{s1}L^3 y_{s0,n}} \qquad (3\text{-}74)$$

Normalised pile head displacement:

$$\frac{y_{on}}{y_{son}} = \frac{y_o}{y_{so}} \qquad (3\text{-}75)$$

In every chart, values are plotted against the normalised depth of the sliding surface. The analysis concerns both the boundary conditions of free-head (Figure 3-55 through Figure 3-57) and unrotated-head (Figure 3-58 through Figure 3-60). Several considerations can be done on the shown results:

- The parameter k that represents the ratio between E_s values E_{s2} and E_{s1} respectively of the stable and unstable soils has an important scale effect on the pile stress state as it is the only parameter ruling the distribution of E_s: it obviously results that the higher is the k value, the higher is the value of shear forces and bending moments acting on the pile.
  However, a higher value of k corresponds to lower pile deflection, reasonably due to the stronger embedment given to the pile, except for the condition η=1 where the trend is reversed at deeper sliding depths.
- Lateral soil movements have been assessed as triangular (η=0),rectangular (η=1) and trapezoidal (η=0.25,0.5,0.75) profiles. The rectangular shape results in the largest stress state on the pile, followed in order by the trapezoidal and triangular soil profiles. Similarly, higher pile head deflection has to be expected for higher values of η. This result appears reasonable as, with the same maximum value at the soil surface, the rectangular profile corresponds to a higher total soil displacement and consequently loading on the pile. It is worth to be noticed that the condition η=0 is the only one which corresponds to a negative shear force at the sliding surface for high values of β for the free-head condition.
- The pile head boundary condition considerably affects the pile response. The unrotated-head condition corresponds to higher stress states on the pile, with shear forces and bending moments at the sliding depth sensibly higher than those developed by the free-head condition. However, this comes with an associated lower pile head deflection. Both the boundary conditions, as

reasonably expected, presents a pile head deflection proportionally increasing with β.

FREE-HEAD PILE

Effect of different η values:

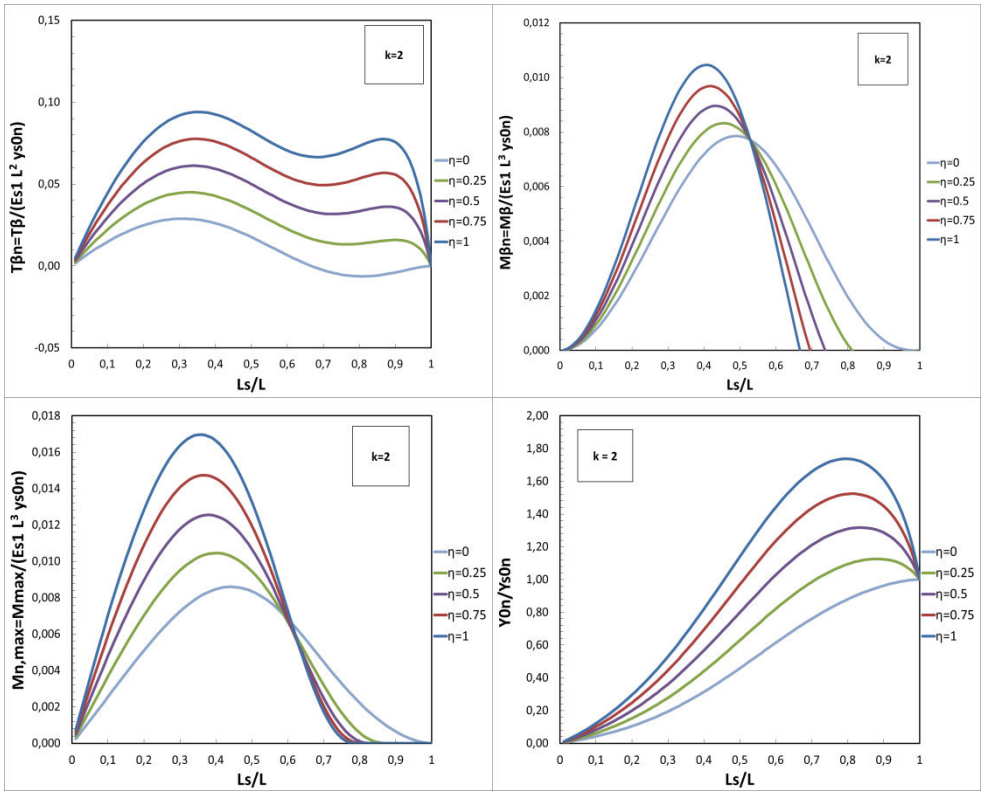

Figure 3-55: Normalised shear force at $z_n=\beta$, bending moment at $z_n=\beta$, maximum bending moment and pile head displacement versus L_s/L, for k=2 and different η values. Free-head condition

Effect of different k values (η=0):

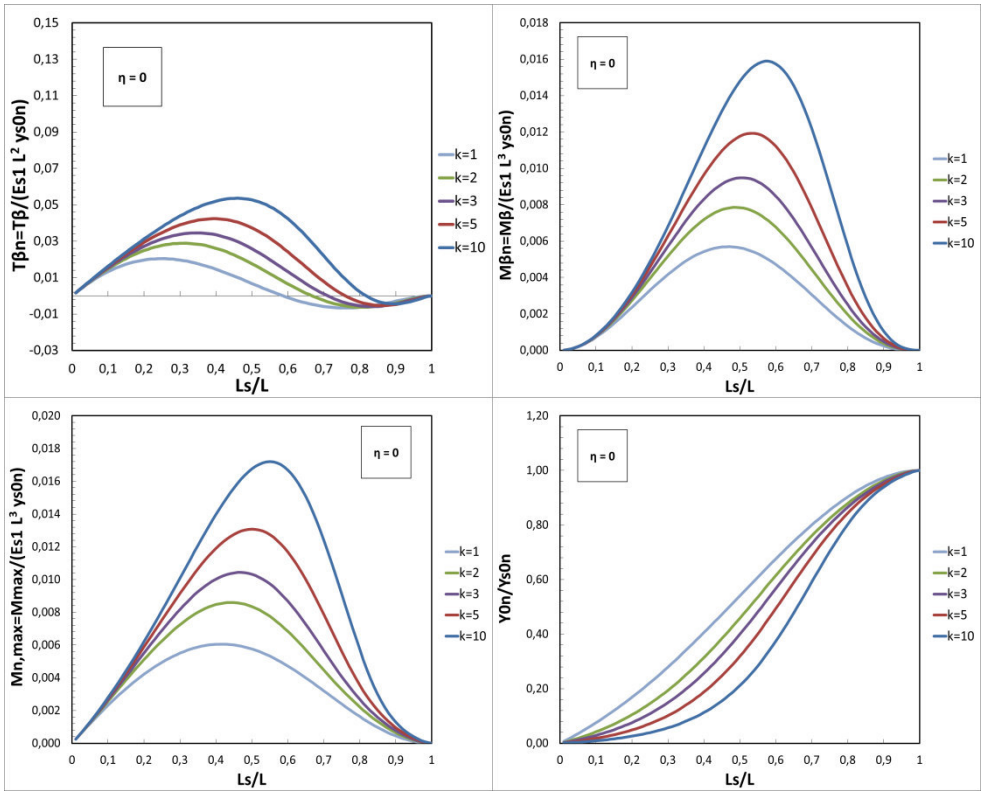

Figure 3-56: Normalised shear force at $z_n=\beta$, bending moment at $z_n=\beta$, maximum bending moment and pile head displacement versus L_s/L, for $\eta=0$ and different k values. Free-head condition

Effect of different k values (η=1):

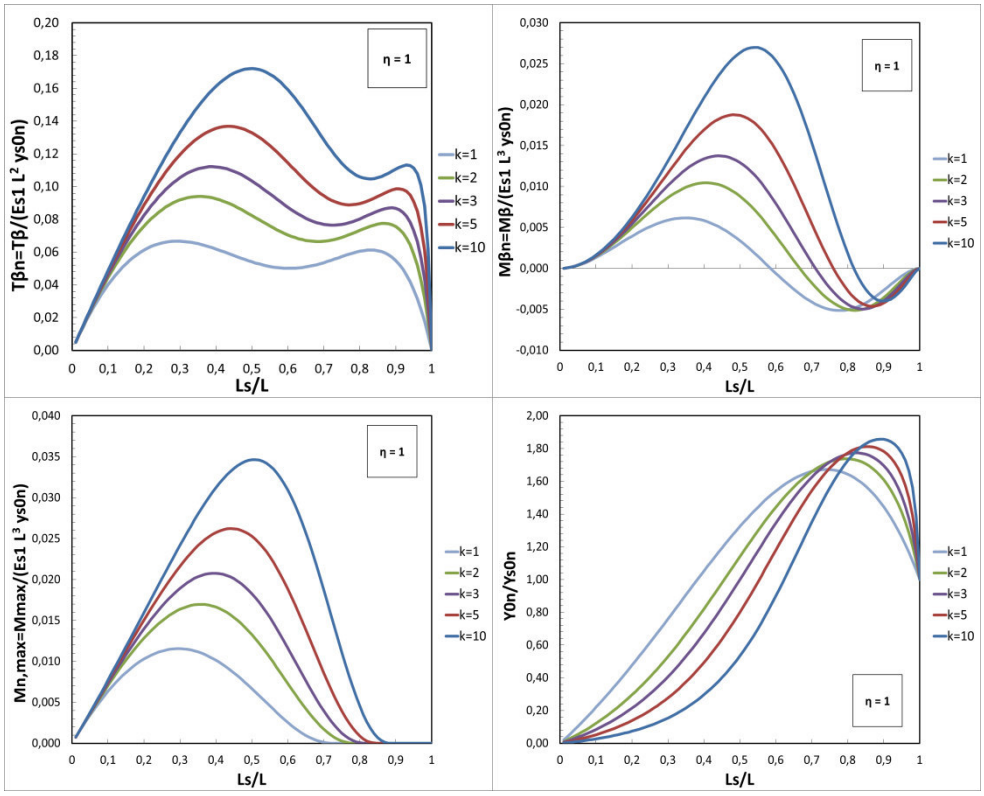

Figure 3-57: Normalised shear force at $z_n=\beta$, bending moment at $z_n=\beta$, maximum bending moment and pile head displacement versus L_s/L, for η =1 and different k values. Free-head condition

UNROTATED-HEAD PILE

Effect of different η values :

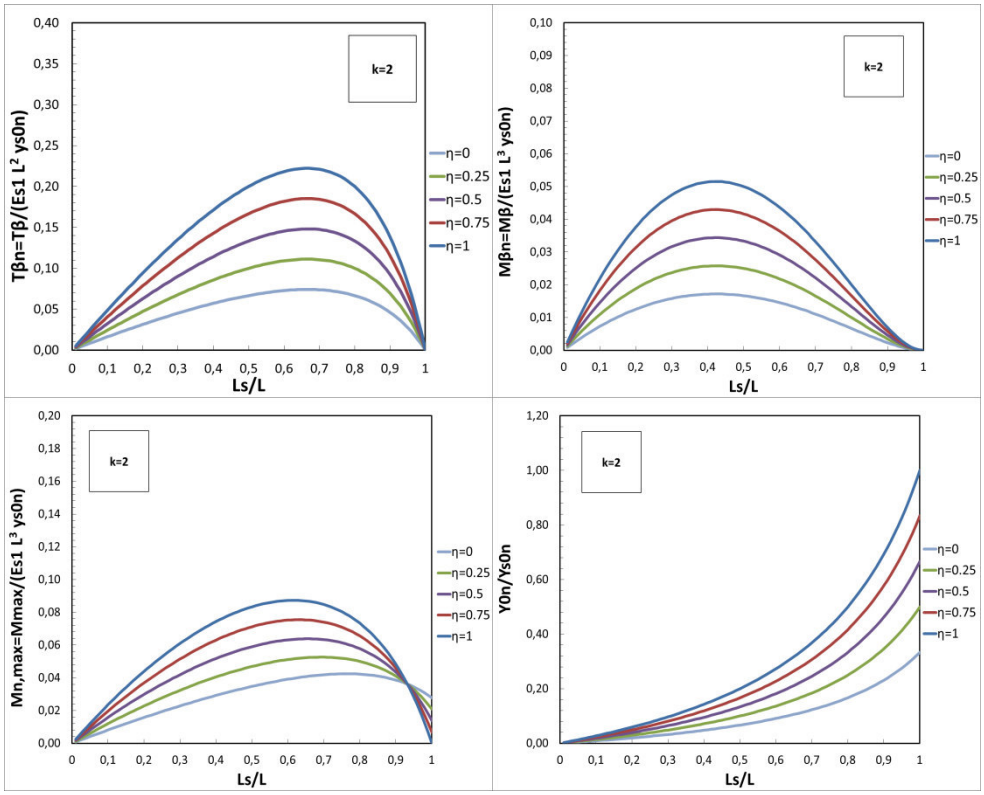

Figure 3-58: Normalised shear force at $z_n=\beta$, bending moment at $z_n=\beta$, maximum bending moment and pile head displacement versus L_s/L, for k=2 and different η values. Unrotated-head condition

Effect of different k values (η=0):

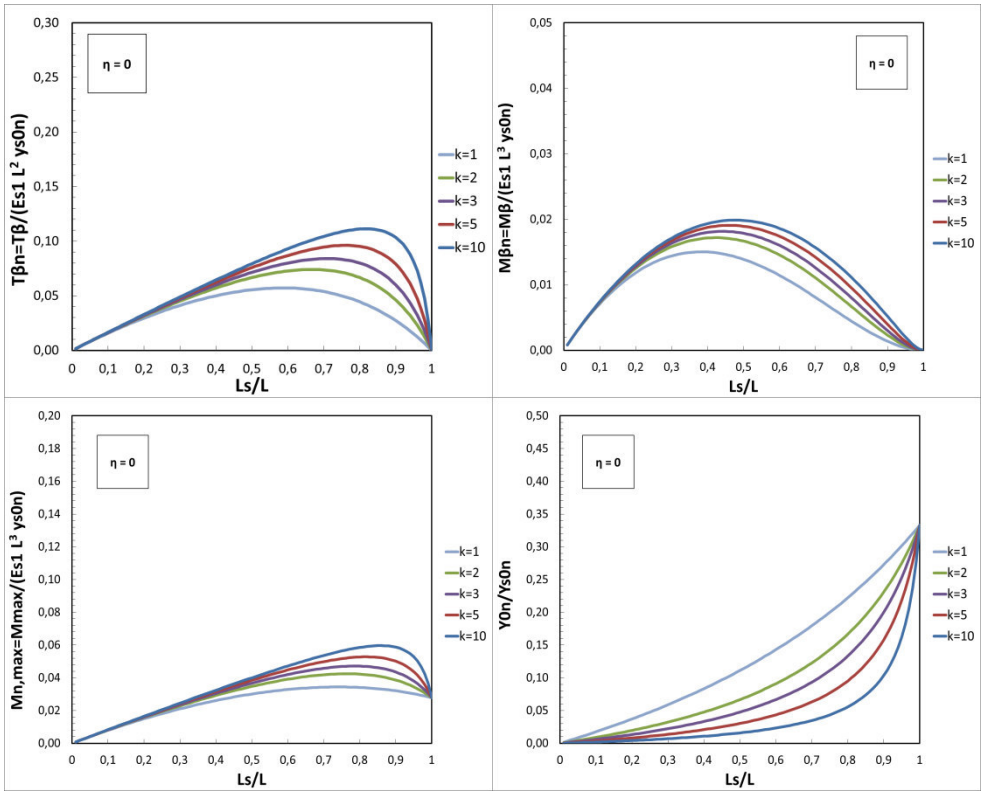

Figure 3-59: Normalised shear force at $z_n=\beta$, bending moment at $z_n=\beta$, maximum bending moment and pile head displacement versus L_s/L, for η =0 and different k values. Unrotated-head condition

Effect of different k values (η=1):

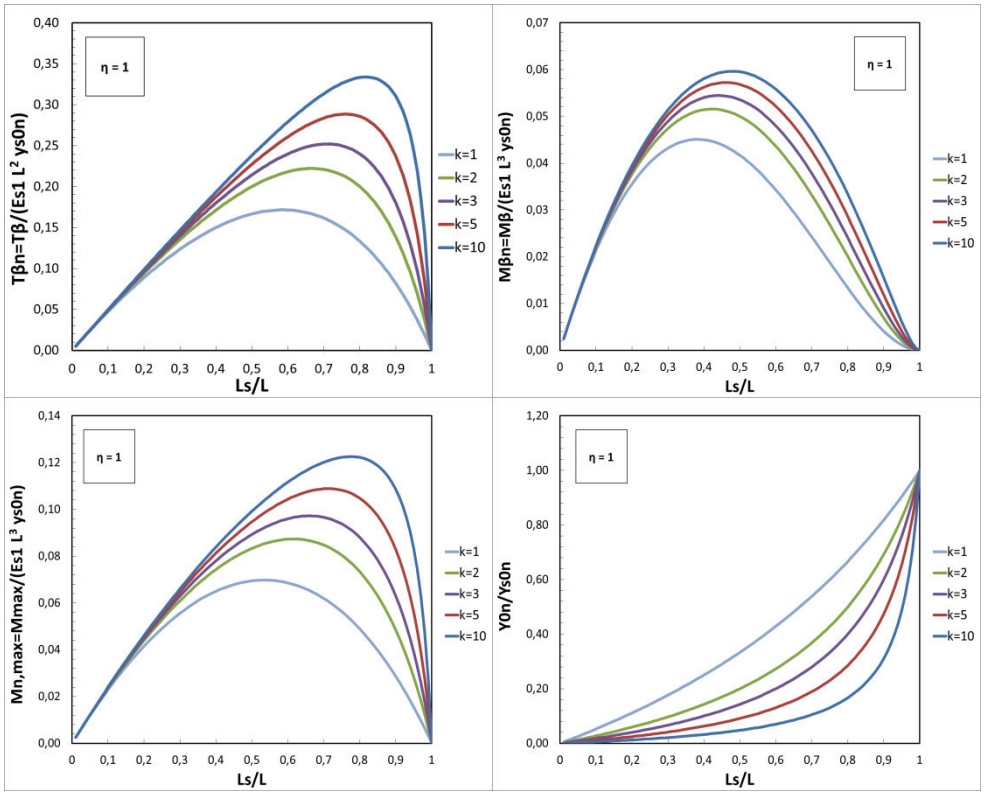

Figure 3-60: Normalised shear force at $z_n=\beta$, bending moment at $z_n=\beta$, maximum bending moment and pile head displacement versus L_s/L, for η =1 and different k values. Unrotated-head condition

3.7. Elastic solutions for a passive rigid pile in a three-layered soil

3.7.1. Free-head condition

A single free-head passive pile is embedded in a three-layered soil (Figure 3-61). It represents a more general case in which the sliding mass presents different characteristics at shallower depths or a weathered layer.

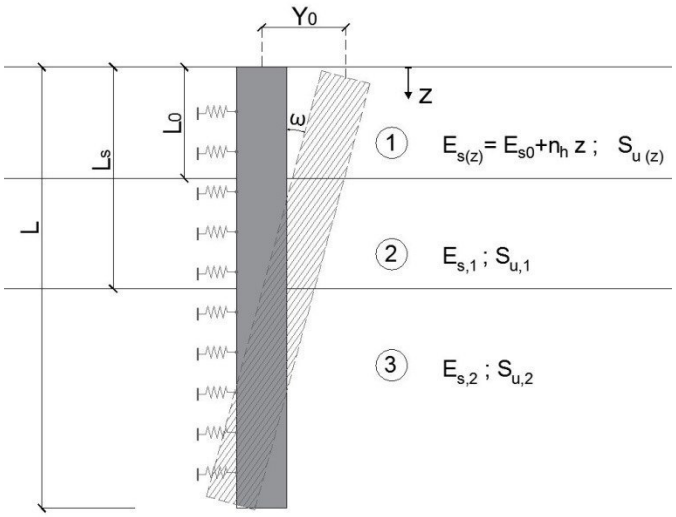

Figure 3-61: Soil profile and pile displacement geometry for a free-head passive rigid pile in a three-layered cohesive soil

A different value of the modulus of subgrade E_s is assigned to every soil layer; in particular, the values of soil stiffness assumed within the firm soil below the slip surface exceeds the values of the sliding layers, according to different schemes of the pile-soil interaction ([5], [23]). The distribution of the modulus of subgrade reaction with depth is showed in Figure 3-62. In the first layer, E_s varies linearly

between E_{s0} (= α_0 E_{s1}) and E_{s1} . In the second and third layer Es is constant with a value of E_{s1} and E_{s2}, respectively.

$E_s(z) = E_{s0} + nz = \alpha_0 E_{s1} + nz$	$[FL^{-2}]$	$0 < z < \lambda L$	(3-76 9
$E_s(z) = E_{s1}$	$[FL^{-2}]$	$\lambda L < z < \beta L$	(3-77)
$E_s(z) = E_{s2} = k \cdot Es1$	[FL-2]	$\beta L < z < L$	(3-78)

Where *k* and *n* are defined as :

$$k = \frac{E_{s2}}{E_{s1}}$$

and

$$n = \frac{E_{s1} - E_{s0}}{\lambda L} = \frac{E_{s1}(1 - \alpha_0)}{\lambda L}$$

from which:

$$\alpha_0 = \frac{E_{s0}}{E_{s1}}$$

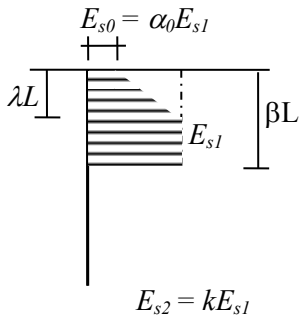

Figure 3-62: Variation of Es with depth for a free-head passive rigid pile in a three-layered soil

Interestingly, the parametric nature of the model makes it adaptable to a variety of different configurations. In particular, by varying the geometric parameters and the soil stiffness ratios, it is possible to adapt this more complex configuration regarding a three-layer to the previous ones already investigated. Specifically:

- the case of a two-layered cohesive soil if α_0=1 and/or λ=0 is imposed
- the case of a normal-consolidated cohesive soil sliding on a firm one if $\lambda=\beta$ is imposed
- the case of a cohesionless soil sliding on a cohesive firm layer if $\lambda=\beta$ and α_0=0 are imposed

The three layer configuration can be considered as a general model, which includes all the others already developed and discussed more in detail in the previous paragraphs.

According to the geometry and soil parameters distribution, the soil reactions along the whole length L of the pile can be expressed as:

$$p_{1(z)} = -(E_{s0} + nz)[\Delta y_0 + \Delta tan \cdot z] \qquad [FL^{-1}] \quad 0 < z < L0 \qquad (3\text{-}79)$$

$$p_2 = -E_{s1}[\Delta y_0 + \Delta tan \cdot z] \qquad [FL^{-1}] \quad L_0 < z < L_s \qquad (3\text{-}80)$$

$$p_3 = -E_{s2}(y_0 - z\, tan\, \omega) \qquad [FL^{-1}] \quad L_s < z < L \qquad (3\text{-}81)$$

Pile deflection of the head and the pile rotation can be obtained by imposing the horizontal force equilibrium and moment equilibrium around the head of the pile; in an explicit non-dimensional form, they are expressed as

$$\left[-\frac{1}{2}\lambda(1-\alpha_0)+\beta+k(1-\beta)\right]y_{0n}+\left[\frac{1}{6}\lambda^2(1-\alpha_0)-\frac{1}{2}\beta^2-\frac{1}{2}k(1-\beta^2)\right]\tan\omega=$$
$$\left[-\frac{1}{2}\lambda(1-\alpha_0)+\beta\right]y_{s0n}+\left[\frac{1}{6}\lambda^2(1-\alpha_0)-\frac{1}{2}\beta^2\right]\tan\theta \qquad (3\text{-}82)$$

$$\left[-\frac{1}{6}\lambda^2(1-\alpha_0)+\frac{1}{2}\beta^2+\frac{1}{2}k(1-\beta^2)\right]y_{0n}+\left[\frac{1}{12}\lambda^3(1-\alpha_0)-\frac{1}{3}\beta^3-\frac{1}{3}k(1-\beta^3)\right]\tan\omega=$$
$$\left[-\frac{1}{6}\lambda^2(1-\alpha_0)+\frac{1}{2}\beta^2\right]y_{s0n}+\left[\frac{1}{12}\lambda^3(1-\alpha_0)-\frac{1}{3}\beta^3\right]\tan\theta \qquad (3\text{-}83)$$

As for the previous cases investigated, the pile deflection is found to be directly proportional to the soil free field movement

	Proportionality constants
$y_{0n}=\dfrac{N_y}{D}y_{s0n}$	$D=\beta^4+2k\beta(1-\beta)(2-\beta+\beta^2)+k^2(1-\beta)^4$ $+\lambda(1-\alpha_0)\left\{\frac{1}{6}\lambda^3(1-\alpha_0)-k(\lambda^2-2\lambda+2)+\beta(k-1)(\lambda^2-2\beta\lambda+2\beta^2)\right\}$
	$N_y=\beta^4(1-k)-k\beta^2(1+2\eta)+2k\beta(1+\eta)+$ $\lambda(1-\alpha_0)\left\{\begin{array}{l}\frac{1}{6}\lambda^3(1-\alpha_0)-\beta(\lambda^2-2\beta\lambda+2\beta^2)+k(1-\beta)[\lambda(1+\beta)-2(1+\beta+\beta^2)]\\+\frac{1}{6}k\lambda(1-\beta)\left(\frac{1-\eta}{\beta}\right)[-3\lambda(1+\beta)+4(1+\beta+\beta^2)]\end{array}\right\}$

$tan\omega = \frac{N_t}{D} y_{s0n}$	$N_t = (1-\eta)(1-k)\beta^3 - 2k\beta^2(1+2\eta) + 3k\beta(1+\eta)$ $+ \lambda(1-\alpha_0)\left\{\begin{array}{l} \frac{1}{6}\lambda^3(1-\alpha_0)\frac{(1-\eta)}{\beta} + k\lambda(1-\beta)\frac{(1-\eta)}{\beta}(1+\beta-\lambda) \\ + k(1-\beta)(2\lambda-3-3\beta) - (1-\eta)(2\beta^2 - 2\beta\lambda + \lambda^2) \end{array}\right\}$

Table 3-16: Proportionality constants for a passive unrotated-head rigid pile in a three-layered soil

Shear forces and bending moments profiles, maximum bending moment M_{max} and its depth z_n in both loading and non-loading zones are provided in the following table.

Depth (z_n)	Expressions
0 – λ (unstable zone)	$\frac{T}{E_{s1}L^2} = -\alpha_0\Delta y_{0n} z_n + \frac{1}{2}\alpha_0\Delta tan\cdot z_n^{\,2} - \frac{1}{2}\frac{(1-\alpha_0)}{\lambda}\Delta y_{0n} z_n^{\,2} + \frac{1}{3}\frac{(1-\alpha_0)}{\lambda}\Delta tan\cdot z_n^{\,3}$
	$\frac{M}{E_{s1}L^3} = -\frac{1}{2}\alpha_0\Delta y_{0n} z_n^{\,2} + \frac{1}{6}\alpha_0\Delta tan\cdot z_n^{\,3} - \frac{1}{6}\frac{1-\alpha_0}{\lambda}\Delta y_{0n} z_n^{\,3} + \frac{1}{12}\frac{1-\alpha_0}{\lambda}\Delta tan\cdot z_n^{\,4}$
	$z_{nM} = \frac{3}{4}\left\{x - y + \sqrt{x^2 + \frac{10}{3}xy + y^2}\right\}$
	$\frac{M_{1max}}{E_{s1}L^3} = \frac{1}{12} z_{1n}^{\,2} \frac{\Delta t}{\lambda}\left\{-6\alpha_0\lambda x + 2\left[\alpha_0\lambda - (1-\alpha_0)x\right]\cdot z_{1n} + (1-\alpha_0) z_{1n}^{\,2}\right\}$

λ – β (stable zone)

$$\frac{T}{E_{s1}L^2} = -\Delta y_{0n}\left(z_n - \lambda\right) + \frac{1}{2}\Delta\tan\left(z_n{}^2 - \lambda^2\right) - \alpha_0\lambda\Delta y_{0n}$$
$$+\frac{1}{2}\alpha_0\lambda^2\Delta\tan - \frac{1}{2}\lambda\left(1-\alpha_0\right)\Delta y_0 + \frac{1}{3}\lambda^2\left(1-\alpha_0\right)\Delta\tan$$

$$\frac{M}{E_{s1}L^3} = -\Delta y_{0n}\left(\frac{1}{2}z_n{}^2 - \lambda z_n + \frac{1}{2}\lambda^2\right) + \frac{1}{2}\Delta\tan\left(\frac{1}{3}z_n{}^3 - \lambda^2 z_n + \frac{2}{3}\lambda^3\right)$$
$$-\alpha_0\lambda\Delta y_{0n}\left(z_n - \lambda\right) + \frac{1}{2}\alpha_0\lambda^2\Delta\tan\left(z_n - \lambda\right) - \frac{1}{2}\alpha_0\Delta y_{0n}\lambda^2$$
$$+\frac{1}{6}\alpha_0\Delta\tan\cdot\lambda^3 - \frac{1}{6}\lambda^2\left(1-\alpha_0\right)\Delta y_{0n} + \frac{1}{12}\lambda^3\left(1-\alpha_0\right)\Delta\tan\cdot$$

$$x = \frac{N_{\Delta y}}{N_{\Delta t}}$$

$$z_{nM} = x + \sqrt{x^2 - \lambda\left(1-\alpha_0\right)\left(x - \frac{1}{3}\lambda\right)}$$

$$\frac{M_{2\,max}}{E_{s1}L^3} = \frac{\Delta tan}{12}\left\{-4x^3 + \lambda\left(1-\alpha_0\right)\left(6x^2 - 4x\lambda + \lambda^2\right) - 4\left(z_{2n} - x\right)^{3/2}\right\}$$

$z_n = \beta$ (slip surface)

$$\frac{T_\beta}{E_{s1}L^2 y_{s0n}} = \frac{k\left(1-\beta\right)}{2D}\left[2N_y - N_t\left(1+\beta\right)\right]$$

$$\frac{M_\beta}{E_{s1}L^3 y_{s0n}} = \frac{k\left(1-\beta\right)^2}{6D}\left[3N_y - N_t\left(2+\beta\right)\right]$$

β – 1 (stable zone)

$$\frac{T}{E_{s1}L^2} = -ky_{0n}\left(\mathrm{z_n} - 1\right) + \frac{1}{2}k\,tan\,\omega\left(z_n{}^2 - 1\right)$$

$$\frac{M}{E_{s1}L^3} = -ky_{0n}\left(\frac{1}{2}z_n{}^2 - z_n + \frac{1}{2}\right) + \frac{1}{2}k\,tan\omega\left(\frac{1}{3}z_n{}^3 - z_n + \frac{2}{3}\right)$$

$$z_n = \frac{2y_{0n}}{\tan\omega} - 1$$

$$\frac{M_{\max}}{E_{s1}L^3 y_{s0n}} = \frac{2k\left(N_t - N_y\right)^3}{3DN_t^2}$$

Table 3-17: Elastic solutions for a passive unrotated-head rigid pile in a three-layered soil

The pile response is evaluated in terms of shear stress and bending moment along the pile at varying value of the sliding surface depth. The normalised shear force $T_n = T/(L^2\, E_{s1} y_{s0n})$ and bending moment $M_n = M/(L^3 E_{s1} y_{s0n})$ are plotted in Figure 3-63, Figure 3-64, Figure 3-65 and Figure 3-66, for η equal to 1 and 0 and for fixed k = 2, λ=0.3 and α_0=0.25.

Since the previous cases can be considered as particular configurations of the more complex three-layered soil model here under investigation, the same expected trends are confirmed.

For η = 1, T_n has its maximum value in correspondence of the sliding surface, with a value almost identical for the different values of β and a second negative local maximum in the opposite part of the pile. The case η = 0 shows two local extrema with opposite signs in T_n profile. An almost null T_n at sliding depth corresponds to β=0.6 while a negative value occurs in correspondence of higher β.

M_n has its maximum value at depths closer to the middle of the pile, for both configurations. The bending moment on the pile is always positive if η = 0 and it is negative if η =1 and β ≥ 7.

The weathered shallower layer has the effect of reducing the pile response if compared to the results related to a constant E_s value on the sliding soils.

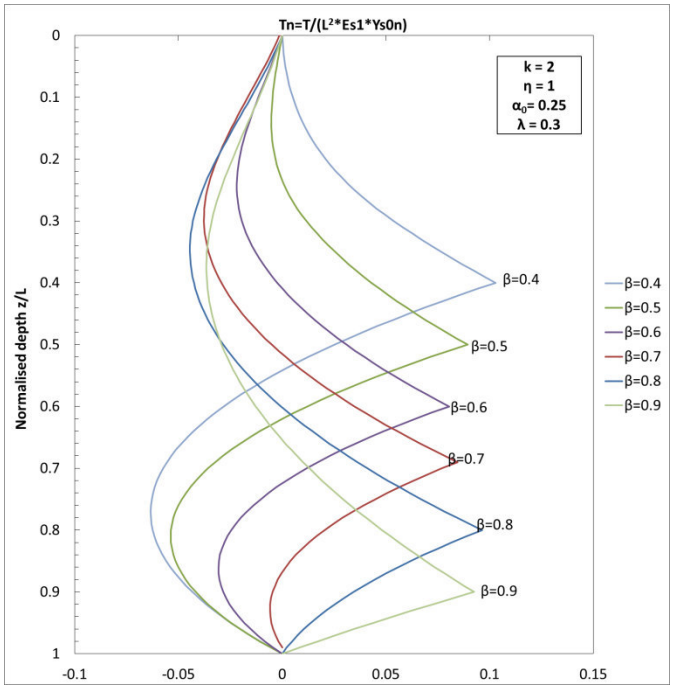

Figure 3-63: Normalised shear force with depth for k=2, η=1, λ=0.3 and α_0=0.25

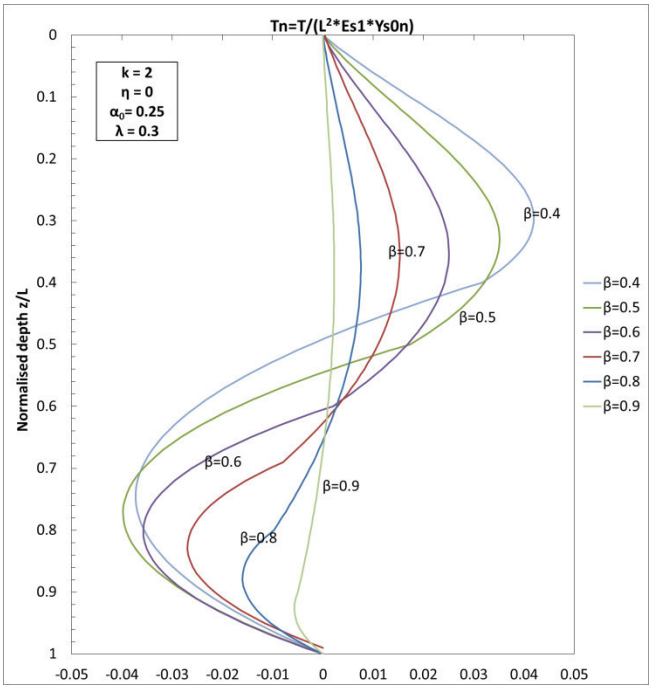

Figure 3-64: Normalised shear force with depth for k=2, η=0, λ=0.3 and α_0=0.25

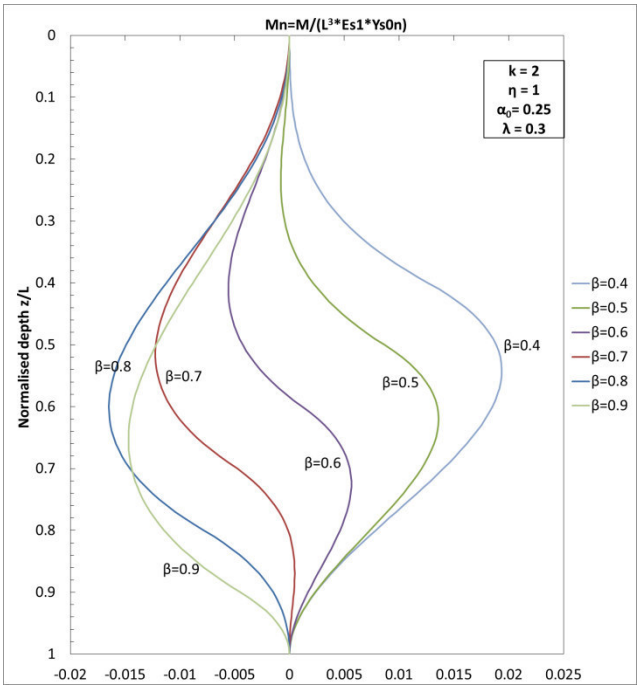

Figure 3-65: Normalised bending moment with depth for k=2, η=1, λ=0.3 and α_0=0.25

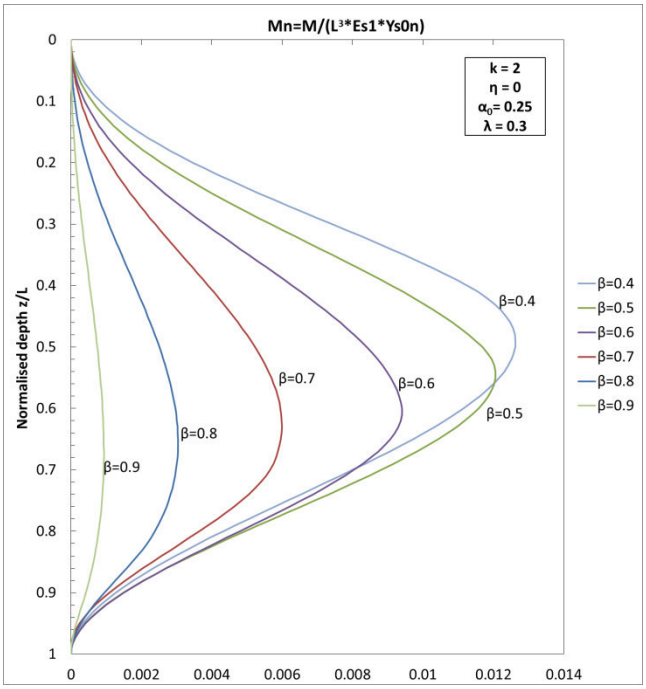

Figure 3-66: Normalised bending moment with depth for k=2, η=0, λ=0.3 and α_0=0.25

3.7.2. Elastic solutions for unrotated-head condition

In the present paragraph, it is investigated the same case of a three-layered soil, where the soil mass presents a weaker shallow layer, but for the fixity condition of unrotated head (displacement without rotation).

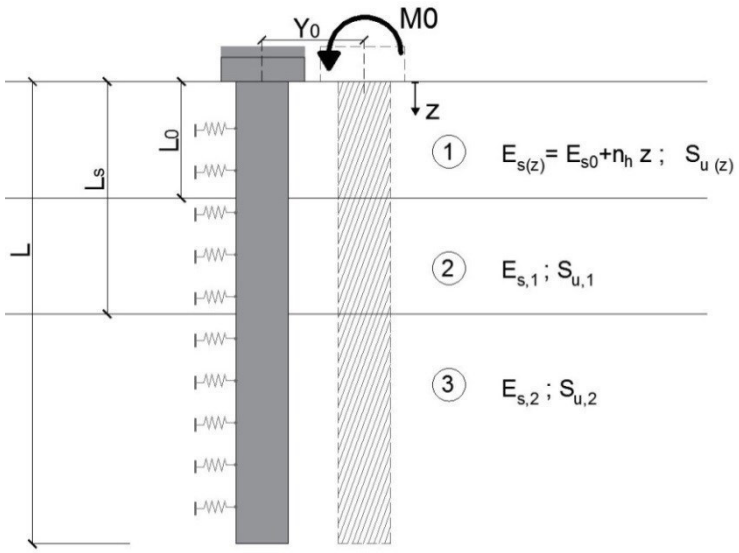

Figure 3-67: Soil profile and pile displacement geometry for a unrotated-head passive rigid pile in a cohesionless sliding soil over a cohesive firm layer

The soil reactions along the whole length L of the pile can be expressed as:

$$p_{1(z)} = -(E_{s0} + nz)[\Delta y_0 + tan\,\theta \cdot z] \qquad [FL^{-1}] \quad 0 < z < L0 \qquad (3\text{-}84)$$

$$p_{2(z)} = -E_{s1}[\Delta y_0 + tan\,\theta \cdot z] \qquad [FL^{-1}] \quad L0 < z < Ls \qquad (3\text{-}85)$$

$$p_{3(z)} = -E_{s2}(y_0) \qquad [FL^{-1}] \quad Ls < z < L \qquad (3\text{-}86)$$

Pile deflection of the head and the pile rotation can be obtained by imposing the horizontal force equilibrium and moment equilibrium around the head of the pile; in an explicit non-dimensional form, they are expressed as:

$$\left[-\frac{1}{2}\lambda(1-\alpha_0)+\beta+k(1-\beta)\right]y_{0n}= \left[-\frac{1}{2}\lambda(1-\alpha_0)+\beta\right]y_{s0n}+\left[\frac{1}{6}\lambda^2(1-\alpha_0)-\frac{1}{2}\beta^2\right]\tan\theta \quad (3\text{-}87)$$

$$\left[-\frac{1}{6}\lambda^2(1-\alpha_0)+\frac{1}{2}\beta^2+\frac{1}{2}k(1-\beta^2)\right]y_{0n}-M_{0n}= \left[-\frac{1}{6}\lambda^2(1-\alpha_0)+\frac{1}{2}\beta^2\right]y_{s0n}+\left[\frac{1}{12}\lambda^3(1-\alpha_0)-\frac{1}{3}\beta^3\right]\tan\theta \quad (3\text{-}88)$$

The profile of the pile deflection and the bending moment M_0 acting on its head are provided in Table 3-18 while shear forces and bending moments profiles, maximum bending moment M_{max} and its depth z_n in both unstable and stable zones are provided in Table 3-19.

Proportionality constants	
	$D=\beta+k(1-\beta)-\frac{1}{2}\lambda(1-\alpha_0)$
$y_{0n}=\frac{N_y}{D}y_{s0n}$	$N_y=\beta-\frac{1}{2}\beta(1-\eta)-\frac{1}{2}\lambda(1-\alpha_0)\left[1-\frac{1}{3}\frac{\lambda}{\beta}(1-\eta)\right]$

$M_{0n} = \frac{N_M}{D} y_{s0n}$	$N_M = \frac{1}{2} k\beta(1-\beta) + \frac{1}{12}\beta^3(1-\eta) - \frac{1}{12} k\beta(1-\eta)(3-4\beta+\beta^2)$ $-\frac{1}{12} k\lambda(1-\alpha_0)(1-\beta)\{3(1+\beta)-2\lambda\}$ $-\frac{1}{72}\lambda(1-\alpha_0)(1-\eta)\left\{12\beta(\beta-\lambda) - \frac{\lambda^3}{\beta}(1-\alpha_0) + 6\lambda^2 - 6k\frac{\lambda}{\beta}(1-\beta)(1+\beta-\lambda)\right\}$

Table 3-18: Proportionality constants for a unrotated-head passive rigid pile in a three-layered cohesive soil

Depth (z_n)	Expressions
0 – λ (unstable zone)	$\frac{T}{E_{s1}L^2} = -\alpha_0 \Delta y_{0n} z_n + \frac{1}{2}\alpha_0 \Delta\tan\cdot z_n{}^2 - \frac{1}{2}\frac{(1-\alpha_0)}{\lambda}\Delta y_{0n} z_n{}^2$ $+\frac{1}{3}\frac{(1-\alpha_0)}{\lambda}\Delta\tan\cdot z_n{}^3$ $\frac{M}{E_{s1}L^3} = -M_{0n} - \frac{1}{2}\alpha_0 \Delta y_{0n} z_n{}^2 + \frac{1}{6}\alpha_0 \Delta\tan\cdot z_n{}^3$ $-\frac{1}{6}\frac{1-\alpha_0}{\lambda}\Delta y_{0n} z_n{}^3 + \frac{1}{12}\frac{1-\alpha_0}{\lambda}\Delta\tan\cdot z_n{}^4$ $\frac{M_{max}}{E_{s1}L^3 y_{s0n}} = \frac{N_M}{D}$
λ – β (second unstable zone)	$\frac{T}{E_{s1}L^2} = -\Delta y_{0n}(z_n - \lambda) + \frac{1}{2}\Delta\tan(z_n{}^2 - \lambda^2) - \alpha_0\lambda\Delta y_{0n} + \frac{1}{2}\alpha_0\lambda^2\Delta\tan$ $-\frac{1}{2}\lambda(1-\alpha_0)\Delta y_0 + \frac{1}{3}\lambda^2(1-\alpha_0)\Delta\tan$

	$\frac{M}{E_{s1}L^3} = -\Delta y_{0n}\left(\frac{1}{2}z_n{}^2 - \lambda z_n + \frac{1}{2}\lambda^2\right) + \frac{1}{2}\Delta\tan\left(\frac{1}{3}z_n{}^3 - \lambda^2 z_n + \frac{2}{3}\lambda^3\right)$ $-\alpha_0\lambda\Delta y_{0n}(z_n - \lambda) + \frac{1}{2}\alpha_0\lambda^2\Delta\tan(z_n - \lambda)$ $-M_{0n} - \frac{1}{2}\alpha_0\Delta y_{0n}\lambda^2 + \frac{1}{6}\alpha_0\Delta\tan\cdot\lambda^3 - \frac{1}{6}\lambda^2(1-\alpha_0)\Delta y_{0n} + \frac{1}{12}\lambda^3(1-\alpha_0)\Delta\tan\cdot$
$z_n = \beta$ (slip surface)	$\frac{T_\beta}{E_{s1}L^2} = \left[\frac{k(1-\beta)N_y}{D}\right]y_{s0n}$ $\frac{M_\beta}{E_{s1}L^3 y_{s0n}} = \frac{k(1-\beta)^2 N_y}{2D}$
$\beta - 1$ (stable zone)	$\frac{T}{E_{s1}L^2} = -ky_{0n}(z_n - 1)$ $\frac{M}{E_{s1}L^3} = -ky_{0n}\left(\frac{1}{2}z_n{}^2 - z_n + \frac{1}{2}\right)$

Table 3-19: Elastic solutions for a passive unrotated-head rigid pile in a three-layered soil

The distribution profile of the pile response can then be obtained with the new solutions, at varying of the depth of the sliding surface. The normalised shear force $T_n = T/(L^2\, E_{s1} y_{s0n})$ and bending moment $M_n = M/(L^3 E_{s1} y_{s0n})$ are plotted in the following figures, for η equal to 1 and 0 and for fixed k=2, η=1, λ=0.3 and α_0=0.25.

The Figure 3-68 through Figure 3-71 show that the higher pile stiffness given by the unrotated-head condition corresponds to higher T_n and M_n, if compared to the free-head condition.

For $\eta = 1$, T_n has its maximum value again in correspondence of the sliding surface, while the case $\eta = 0$ presents lower values of $T_{n,max}$, with peaks which occur at z_n generally slightly upper than β.
M_n shows the same profile for both $\eta = 0$ and $\eta = 1$, with always negative values and lightly higher values of Mn if $\eta = 1$.

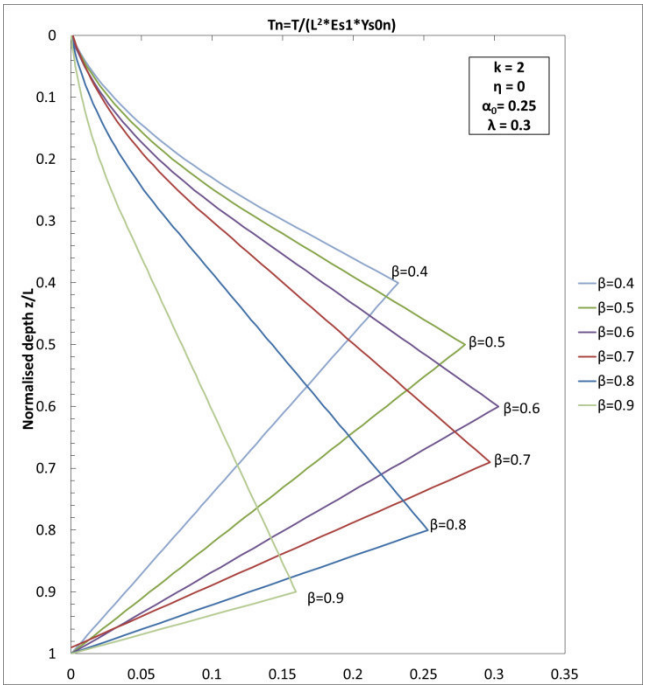

Figure 3-68: Normalised shear force with depth for k=2, η=1, λ=0.3 and α_0=0.25

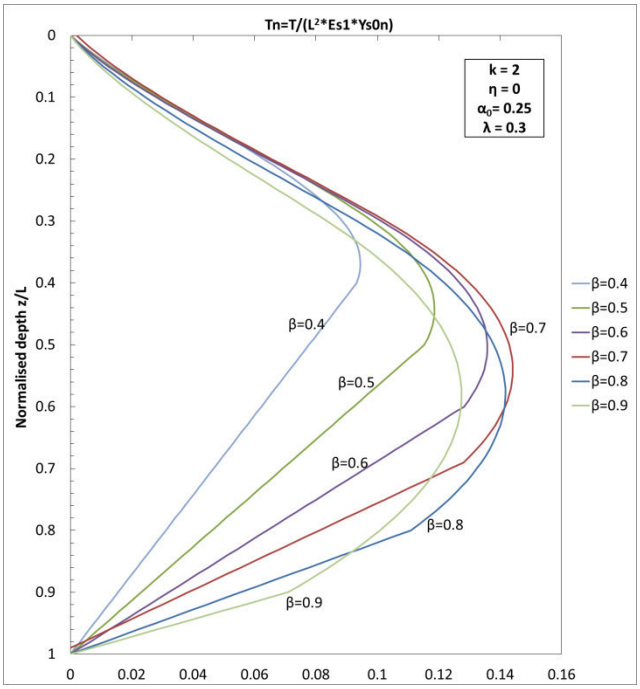

Figure 3-69: Normalised shear force with depth for k=2, η=0, λ=0.3 and α0=0.25

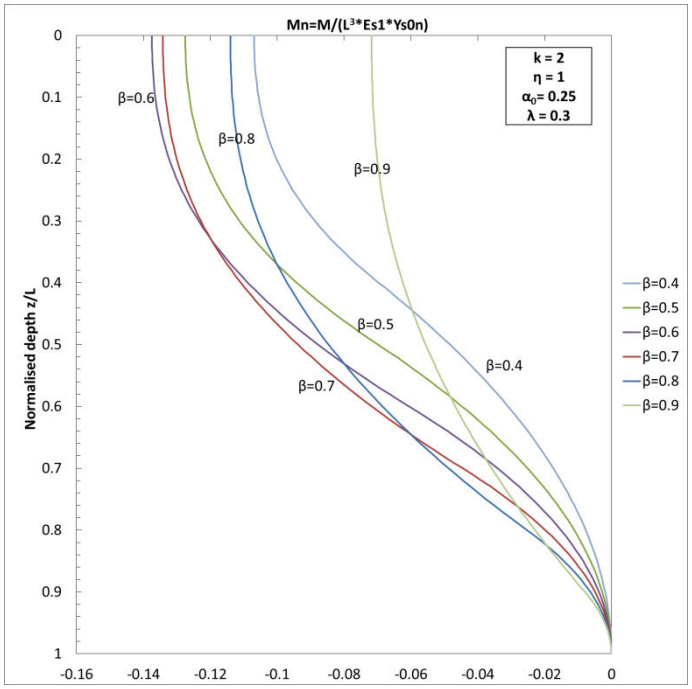

Figure 3-70: Normalised bending moment with depth for k=2, η=1, λ=0.3 and α0=0.25

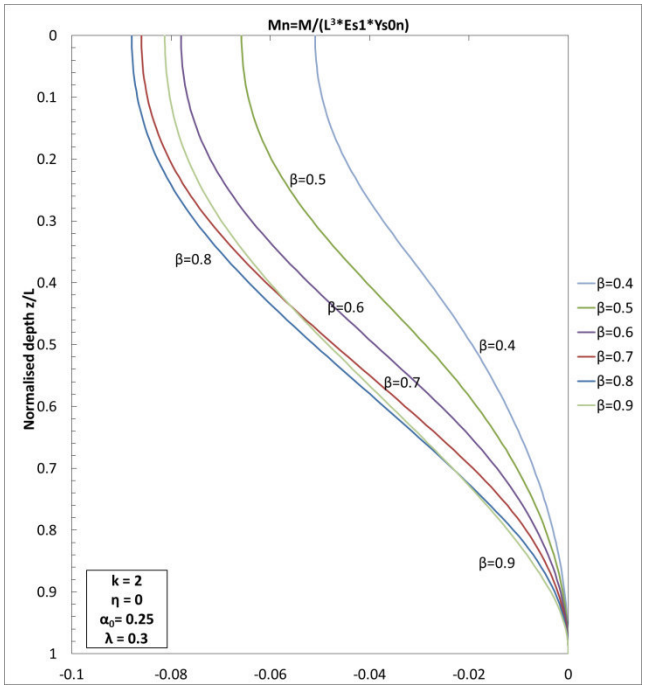

Figure 3-71: Normalised bending moment with depth for k=2, η=0, λ=0.3 and α0=0.25

3.7.3. Parametric analysis

The solution provided have been implemented in spreadsheets to carry out a parametric analysis of the problem.
The elastic solutions for a passive rigid pile in a three-layered soil are governed by the parameter k that represents the ratio between E_s values E_{s2} and E_{s1} respectively of the stable and unstable soils:

$$k = \frac{E_{s2}}{E_{s1}} \qquad (3\text{-}89)$$

the parameter η that represents between soil displacement at ground level and at the sliding depth:

$$\eta = \frac{y_{s(z=Ls)}}{y_{s0}} \qquad (3\text{-}90)$$

the parameter α_0 that represents the ratio between modulus of subgrade reaction at ground level and at L_0 :

$$\alpha_0 = \frac{E_{s0}}{E_{s2}} \qquad (3\text{-}91)$$

the parameter λ that represents the ratio between first layer thickness and pile length L_0/L

$$\lambda = \frac{L_0}{L} \qquad (3\text{-}92)$$

The parametric analysis focuses on their effects on the normalised pile shear resistance at $z=L_s$:

$$T_{\beta,n} = \frac{T_{(z=Ls)}}{E_{s1}L^2 y_{s0,n}} \qquad (3\text{-}93)$$

Normalised bending moment at $z=L_s$:

$$M_{\beta,n} = \frac{M_{(z=Ls)}}{E_{s1}L^3 y_{s0,n}} \qquad (3\text{-}94)$$

Normalised maximum bending moment acting on the pile:

$$M_{n,max} = \frac{M_{max}}{E_{s1}L^3 y_{s0,n}} \qquad (3\text{-}95)$$

Normalised pile head displacement:

$$\frac{y_{0n}}{y_{s0n}} = \frac{y_0}{y_{s0}} \qquad (3\text{-}96)$$

In every chart, values are plotted against the normalised depth of the sliding surface. The analysis concerns both the boundary conditions of free-head (Figure 3-72 through Figure 3-76) and unrotated-head (Figure 3-77 through Figure 3-81). Several considerations can be done on the showed results:

- The parameter λ represents the ratio between first layer thickness and pile length L_0/L. If λ=0 is imposed, the case of a two-layered soil with constant E_s will be reproduced, while if λ=β, the case of a modulus increasing with depth is obtained. It is more effective for the more superficial sliding depth where the shallow layer's low parameters are more effective. In fact, lower pile reactions result for higher values of the parameter λ. In other words, the presence of a weathered sliding superficial layer leads to lower stress states and deflection on the pile.
- The unrotated-head condition corresponds to stress states on the pile sensibly higher than those developed by the free-head condition and at the same time to lower pile head deflection. This lead to consider the restrained pile head condition as recommended in case low pile displacements are requested, or whenever a high pile resistance at the sliding depth is preferable, as in the case of pile used as stabilising systems, if the pile's stress state is verified.

- Lateral soil movements have been assessed as triangular (η=0),rectangular (η=1) and trapezoidal (η=0.25,0.5,0.75) profiles. The rectangular shape results in the largest stress state on the pile, followed in order by the trapezoidal and triangular soil profiles. Similarly, higher pile head deflection has to be expected for higher values of η. This result appears reasonable as, with the same maximum value at the soil surface, the rectangular profile corresponds to a higher total soil displacement and consequently loading on the pile. Moreover, the condition η=0 is the only one which corresponds to a negative shear force at the sliding surface for high values of β for the free-head condition.
- Several ratios between subgrade modulus of the stable and unstable soils have been considered, by varying k from 1 (corresponding to a uniform soil) to 10. This parameter has a scale effect on the pile stress state: higher the k value, higher the value of shear forces and bending moments acting on the pile. However, a higher value of k correspond to lower pile deflection, reasonably due to the stronger embedment given to the pile, and maximum values of T_n and M_n tend to shift to deeper depths if k is increased.

FREE-HEAD PILE

Effect of different λ values (η=0):

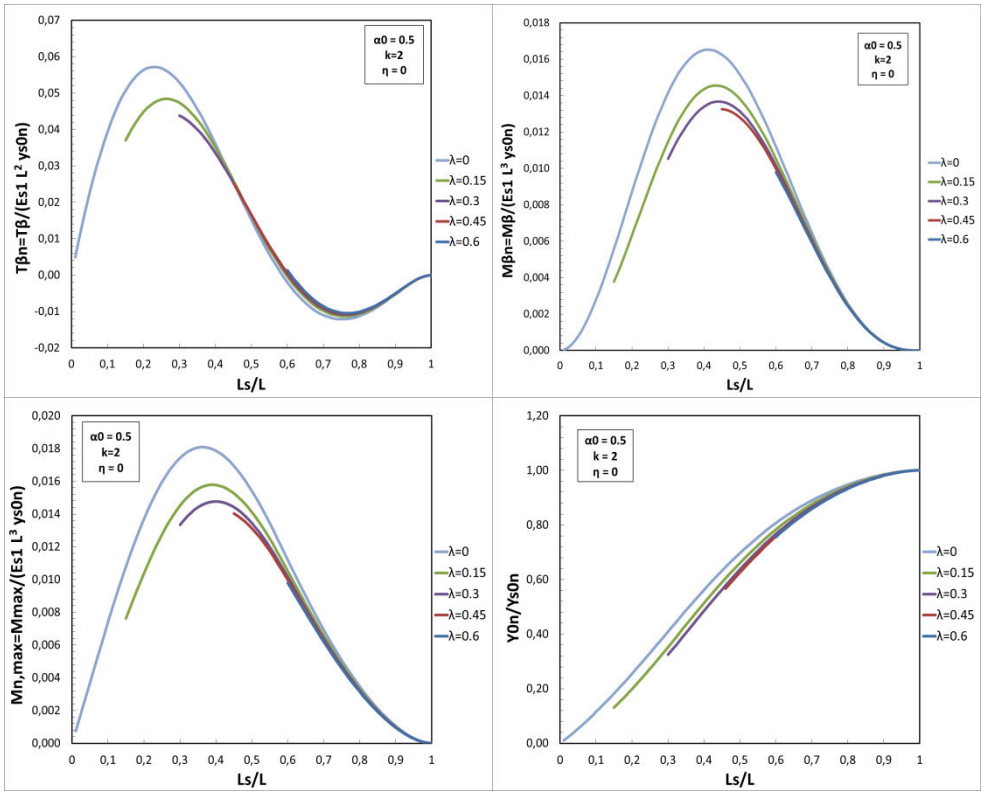

Figure 3-72: Normalised shear force at $z_n=\beta$, bending moment at $z_n=\beta$, maximum bending moment and pile head displacement versus L_s/L, for $\eta=0$, $\alpha_0=0.5$,k=2 and different λ values. Free-head condition

Effect of different η values:

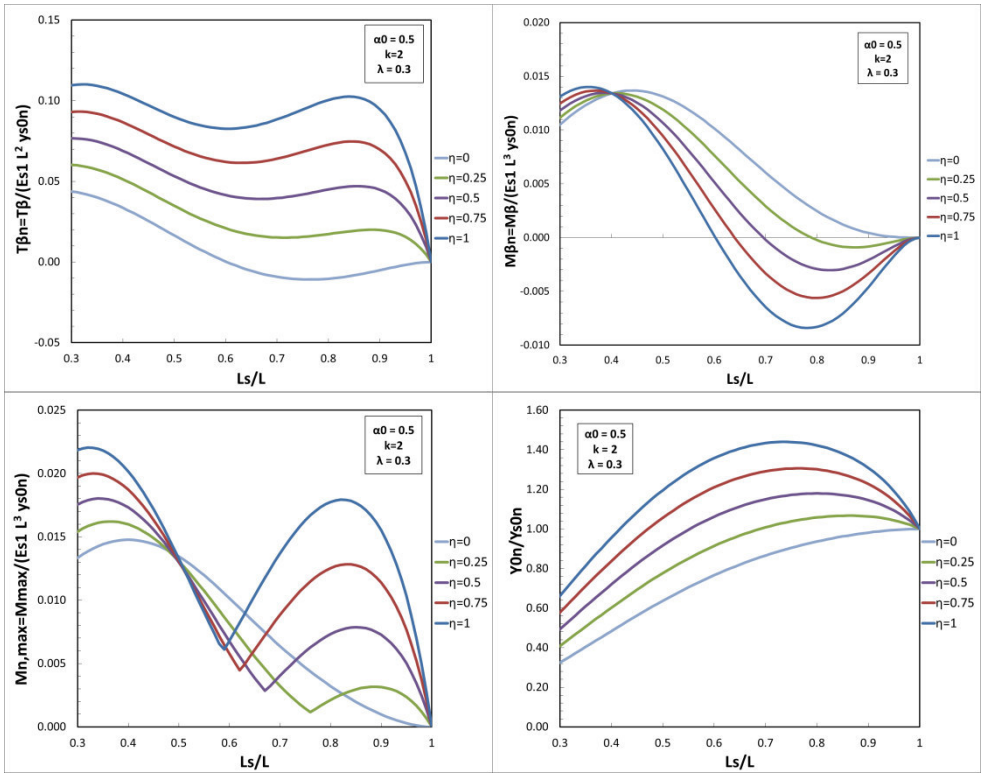

Figure 3-73: Normalised shear force at $z_n=\beta$, bending moment at $z_n=\beta$, maximum bending moment and pile head displacement versus L_s/L, for λ =0.3, α_0=0.5,k=2 and different η values. Free-head condition

Effect of different k values (η=0):

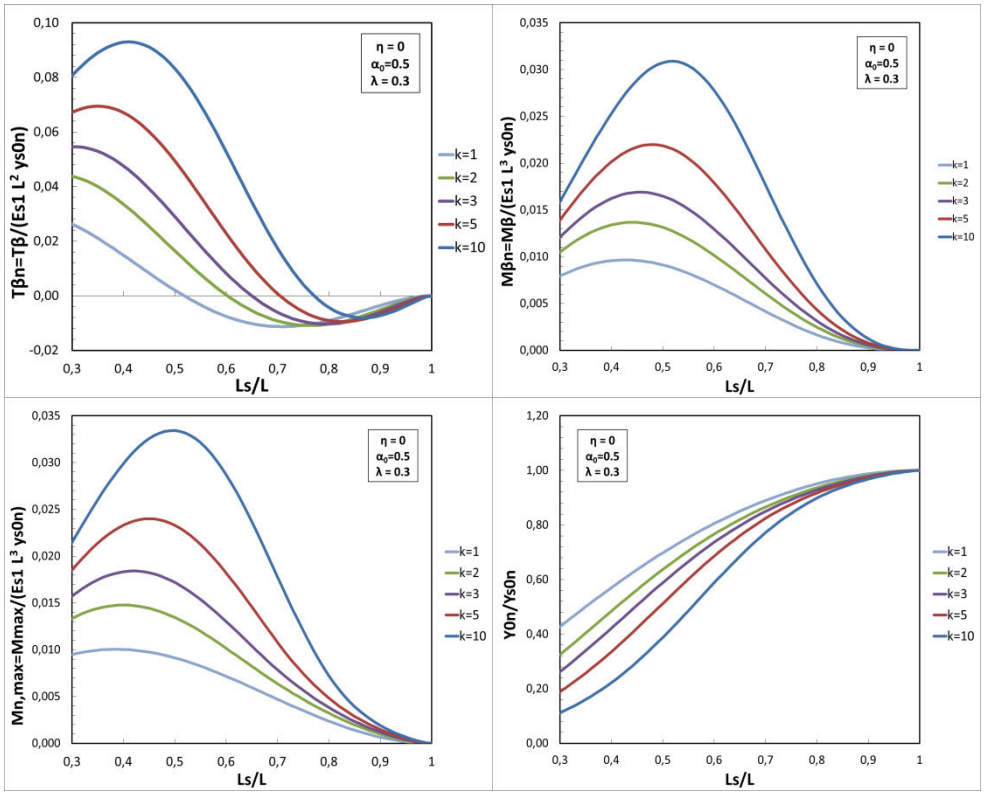

Figure 3-74: Normalised shear force at $z_n=\beta$, bending moment at $z_n=\beta$, maximum bending moment and pile head displacement versus L_s/L, for λ =0.3, α_0=0.5, η=0 and different k values. Free-head condition

Effect of different k values (η=1):

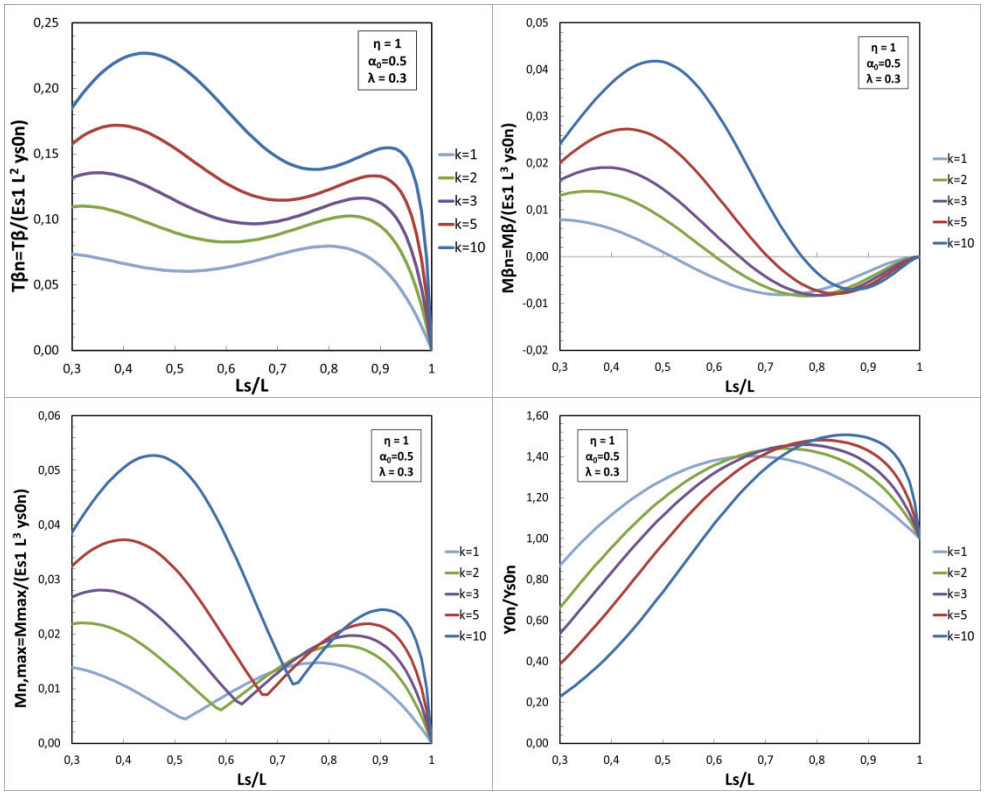

Figure 3-75: Normalised shear force at $z_n=\beta$, bending moment at $z_n=\beta$, maximum bending moment and pile head displacement versus L_s/L, for λ =0.3, α_0=0.5, η=1 and different k values. Free-head condition

Effect of different α_0 values (η=0):

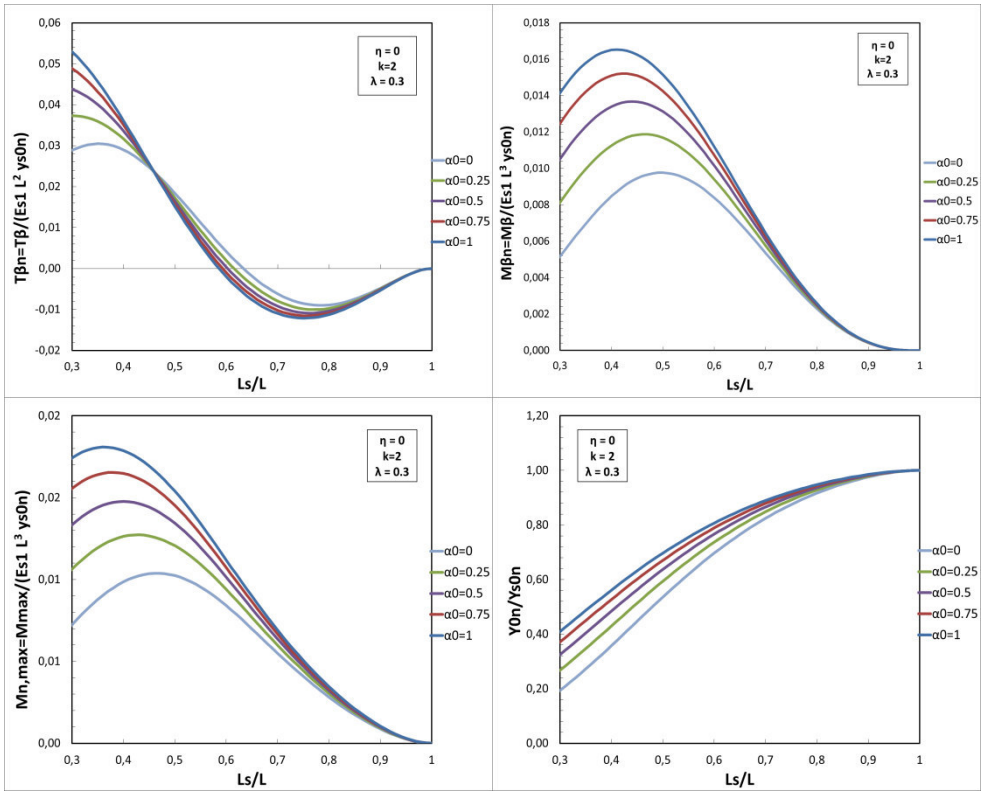

Figure 3-76: Normalised shear force at $z_n=\beta$, bending moment at $z_n=\beta$, maximum bending moment and pile head displacement versus L_s/L, for λ =0.3,k =2, η=0 and different α_0 values. Free-head condition

UNROTATED-HEAD PILE
Effect of different k values (η=0):

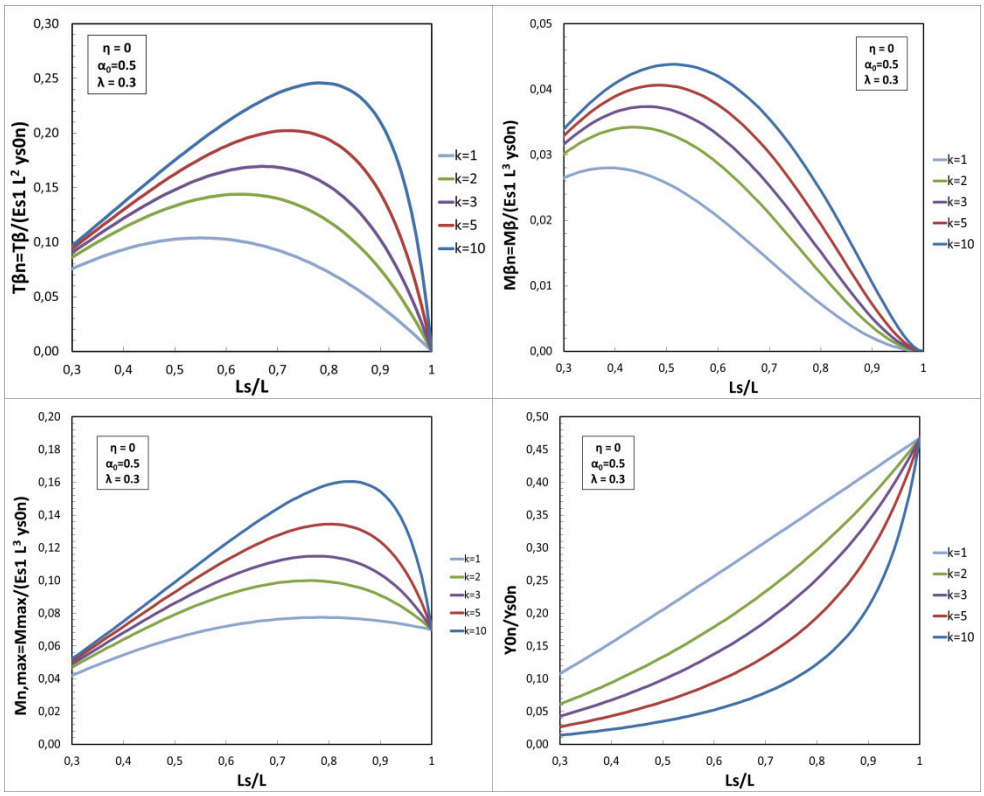

Figure 3-77: Normalised shear force at $z_n=\beta$, bending moment at $z_n=\beta$, maximum bending moment and pile head displacement versus L_s/L, for λ =0.3, α_0=0.5, η=0 and different k values. Unrotated-head condition

Effect of different k values (η=1):

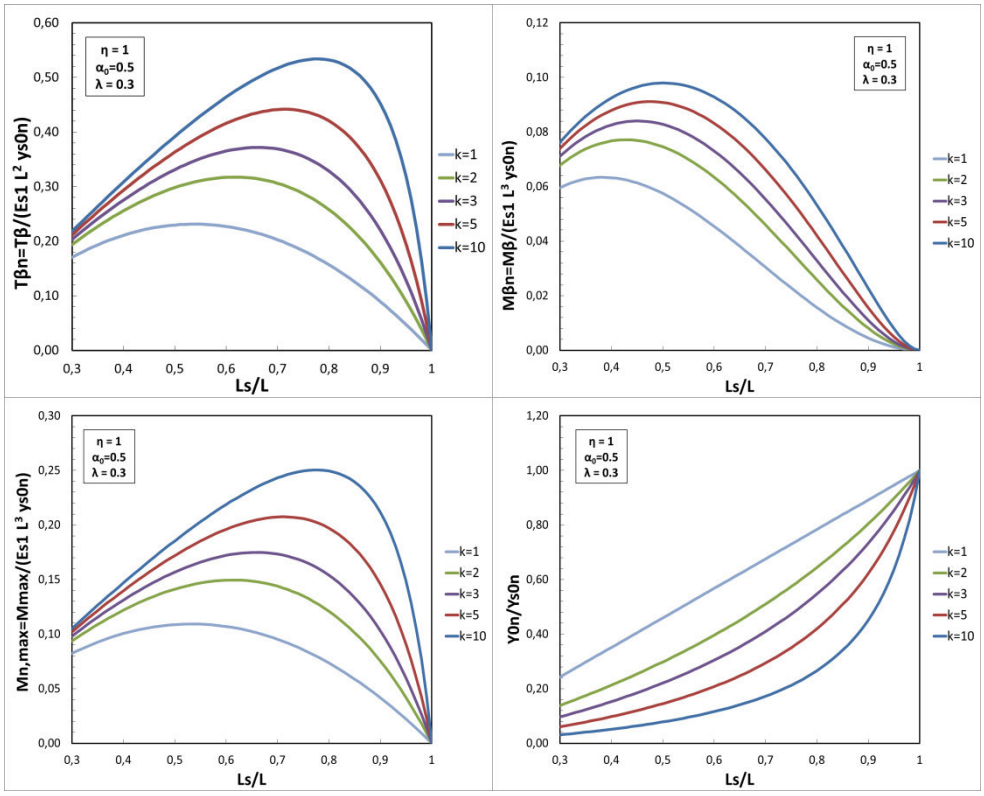

Figure 3-78: Normalised shear force at $z_n=\beta$, bending moment at $z_n=\beta$, maximum bending moment and pile head displacement versus L_s/L, for λ =0.3, α_0=0.5, η=1 and different k values. Unrotated-head condition

Effect of different η values:

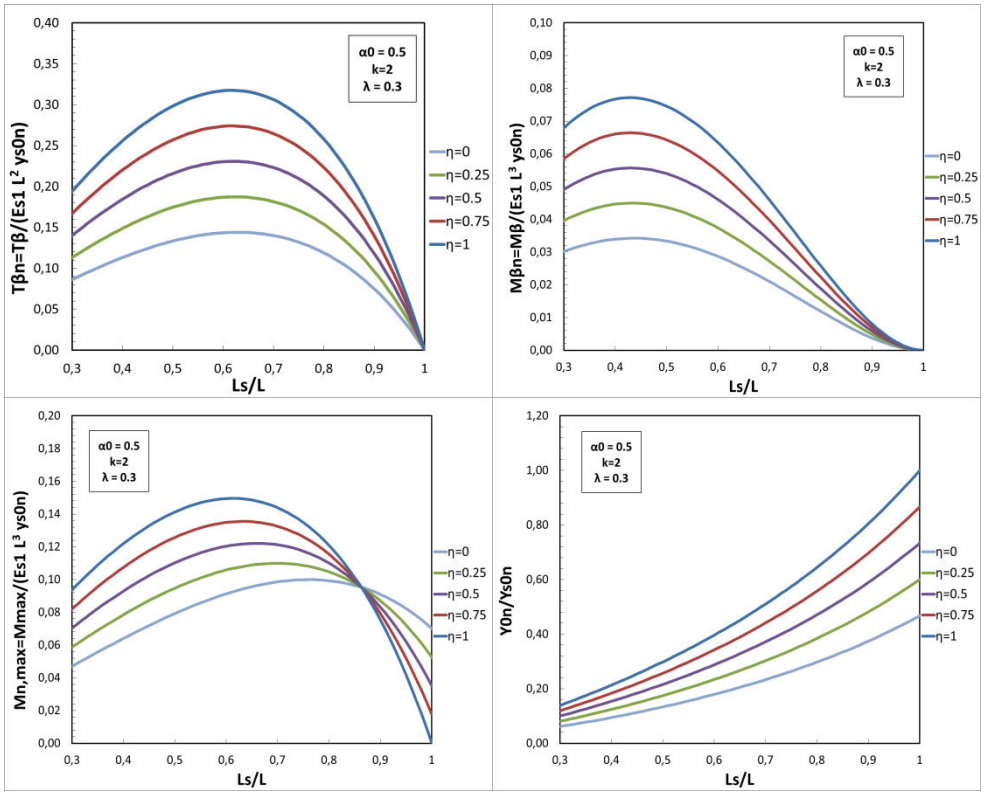

Figure 3-79: Normalised shear force at $z_n=\beta$, bending moment at $z_n=\beta$, maximum bending moment and pile head displacement versus L_s/L, for λ =0.3, α_0=0.5, k=2 and different η values. Unrotated-head condition

Effect of different λ values (η=0):

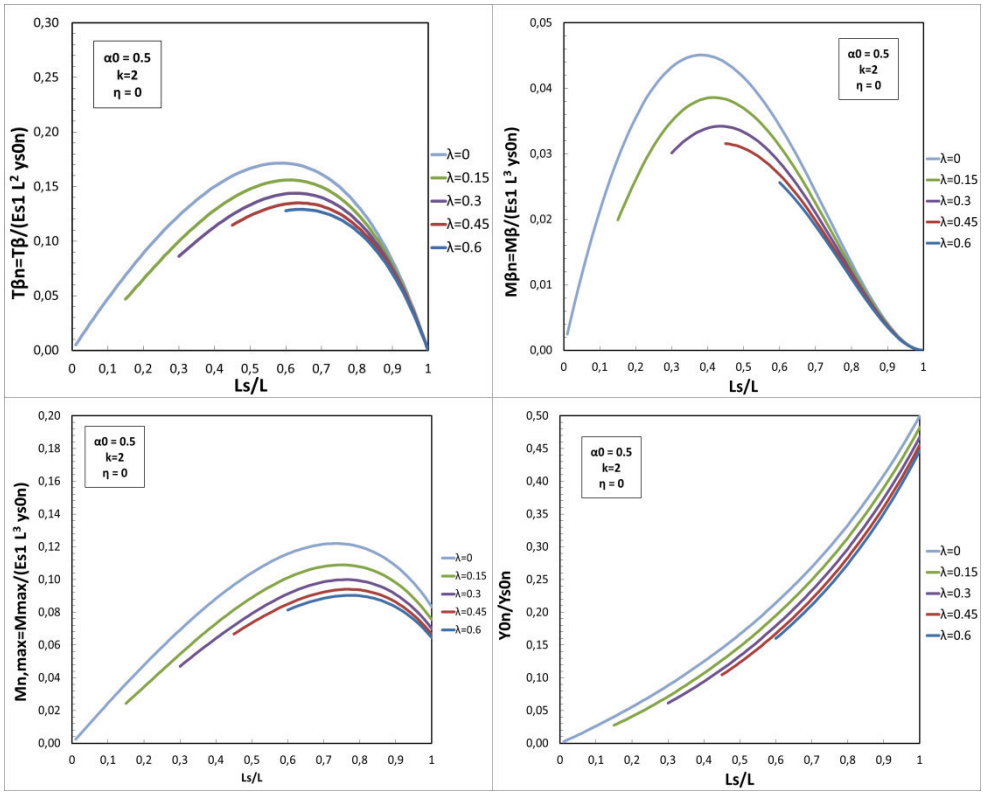

Figure 3-80: Normalised shear force at $z_n=\beta$, bending moment at $z_n=\beta$, maximum bending moment and pile head displacement versus L_s/L, for $\eta=0$, $\alpha_0=0.5$, $k=2$ and different λ values. Unrotated-head condition

Effect of different α_0 values (η=0):

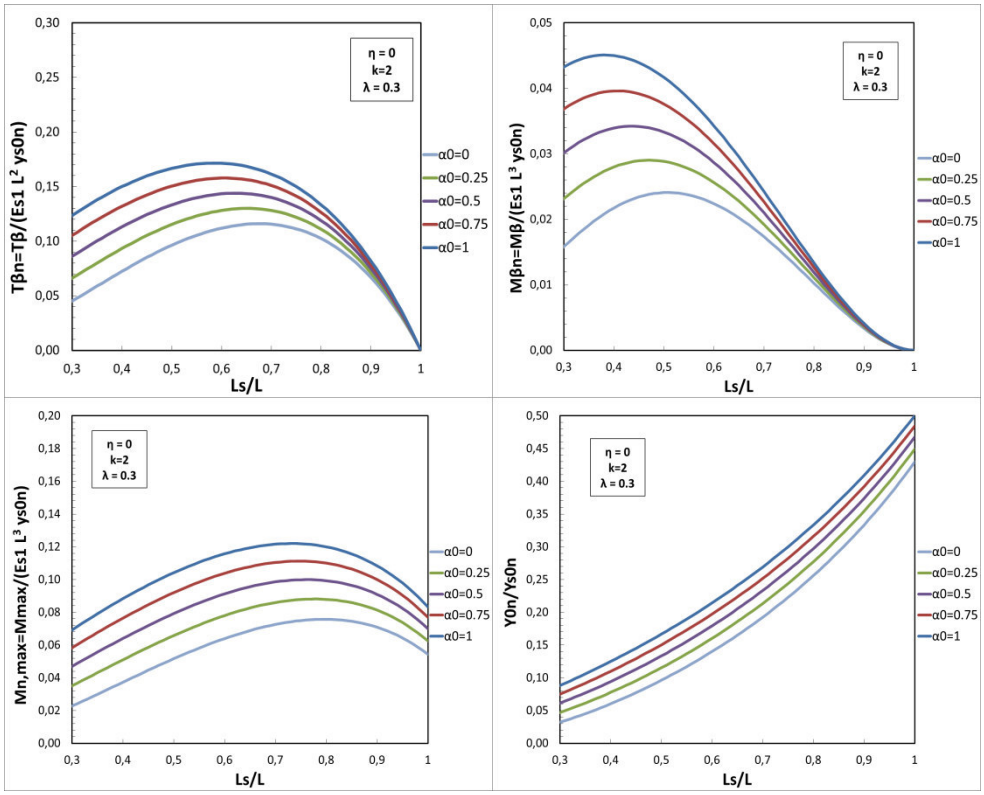

Figure 3-81: Normalised shear force at $z_n=\beta$, bending moment at $z_n=\beta$, maximum bending moment and pile head displacement versus L_s/L, for λ=0.3,k =2, η=0 and different α0 values. Unrotated-head condition

3.8. Elastic solutions for a passive rigid pile on a soil with Es linearly increasing with depth

3.8.1.Free-head condition

For sands and for normally consolidated clays under long-term loading, it is reasonable to assume that the modulus of subgrade reaction varies linearly with depth. E_s may be hence written as

$$E_s(z) = n\,z \qquad (3\text{-}97)$$

referred to as Gibson approach hereinafter and where:
n= gradient of the horizontal subgrade reaction modulus [FL^{-3}]

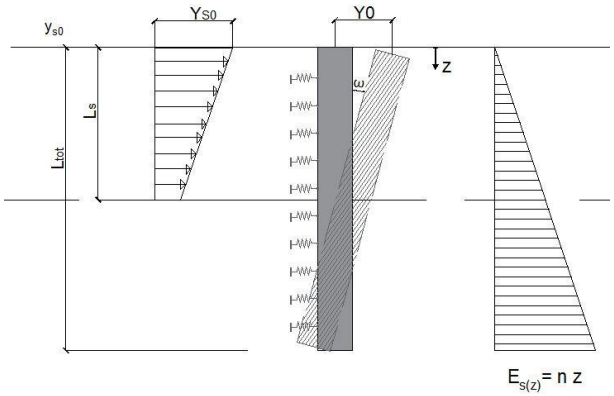

Figure 3-82: Soil profile and pile displacement geometry for a rigid pile in cohesionless soil

In particular, the problem under consideration in the present paragraph is represented in Figure 3-82; a single rigid pile of length L and diameter D is embedded in a homogeneous soil with E_s linearly increasing with depth; a sliding surface crosses the pile at depth $L_s=\beta L$. With the above assumptions and assuming there is no soil-yielding, the on-pile force (per unit length), $p_e(z)$, at any depth, is

proportional to the local displacement, Δy(z), and to the modulus of subgrade reaction, E_s [FL^{-2}] along the whole length L of the pile and can be expressed as:

$$p_{1(z)} = -\mathrm{nz}\left(Y_{0(z)} - Y_{s(z)}\right) = -nz[\Delta Y_0 - z\,\Delta tan] \qquad [FL^{-1}] \qquad 0 < z < Ls \qquad (3\text{-}98)$$

$$p_{2(z)} = -nz[Y_0 - z\,tan\,\omega] \qquad [FL^{-1}] \qquad Ls < z < L \qquad (3\text{-}99)$$

The profile of the pile deflection and the bending moment M_0 acting on its head are provided in Table 3-20 while shear forces and bending moments profiles, maximum bending moment M_{max} and its depth z_n in both loading and non-loading zones are provided in Table 3-21.

	Proportionality constants
$y_{0n} = N_y y_{s0n}$	$N_y = \beta^2\left[(3-2\beta)+6\eta(1-\beta)\right]$
$tan\omega = N_t y_{s0n}$	$N_t = \beta^2\left[(4-3\beta)+\eta(8-9\beta)\right]$

Table 3-20: Proportionality constants for a passive rigid pile on a cohesionless soil

Depth (z_n)	Expressions
0 – β (unstable zone)	$\frac{T}{nL^3} = -\frac{1}{2}\Delta y_{0n} z_n^{\ 2} + \frac{1}{3}\Delta tan \cdot z_n^{\ 3}$
	$\frac{M}{nL^4} = -\frac{1}{6}(\Delta y_{0n}) z_n^{\ 3} + \frac{1}{12}\Delta tan \cdot z_n^{\ 4}$
	$z_{n1} = 1.5\frac{\Delta y_{0n}}{\Delta tan} = 1.5x$
$\frac{\Delta y_{0n}}{\Delta \tan} = x$	$\frac{\lvert M_{n\max}\rvert}{nL^4 Y_{s0n}} = -\left(\frac{9}{64}x^4\right)\lvert N_{\Delta t}\rvert$
$z_n = \beta$ (slip surface)	$\frac{T_\beta}{nL^3} = \frac{1}{6}\beta^2(-3N_{\Delta y} + 2\beta N_{\Delta t}) y_{s0n}$
	$\frac{M_\beta}{nL^4} = \frac{1}{12}\beta^3(2N_{\Delta y} - \beta N_{\Delta t}) y_{s0n}$
β – 1 (stable zone)	$\frac{T}{nL^3} = -\frac{1}{2} y_{0n}(z_n^{\ 2} - 1) + \frac{1}{3} tan\omega \cdot (z_n^{\ 3} - 1)$
	$\frac{M}{nL^4} = -\frac{1}{6} y_{0n}(z_n^{\ 3} - 3z_n + 2) + \frac{1}{12} tan\omega \cdot (z_n^{\ 4} - 4z_n + 3)$
$a_n = y_{0n}/tan\omega$	$z_{n2} = 0.75a_n - 0.5 + 0.25\sqrt{(3a_n - 2)(3a_n + 6)}$

$$\frac{|M_{n\max}|}{nL^4 Y_{s0n}} = \frac{1}{12} N_t \left[-2a_n \left({z_{n2}}^3 - 3z_{n2} + 2 \right) + \left({z_{n2}}^4 - 4z_{n2} + 3 \right) \right]$$

Table 3-21: Elastic solutions for a passive rigid pile on a cohesionless soil

The distribution profile of the pile response can then be obtained with the new solutions, concerning the depth of the sliding surface. The normalised shear force $T_n = T/(L^2\, E_{s1} y_{s0n})$ and bending moment $M_n = M/(L^3 E_{s1} y_{s0n})$ are plotted in Figure 3-83 through Figure 3-86.

In agreement with the solution presented by Poulos [26], for η = 1 the shear force profile has its maximum value in correspondence of the sliding depth, with a value slightly higher for higher values of β.

The case η = 0 instead presents lower values of $T_{n,max}$, with two local extrema having opposite signs in the upper and lower part of the pile.

M_n generally has its maximum value for depths close to the middle of the pile in both the considered free-field soil movement rate. It has to be noticed that, while for η = 0 the bending moment on the pile is always positive, for η = 1 it is negative for β ≥ 6.

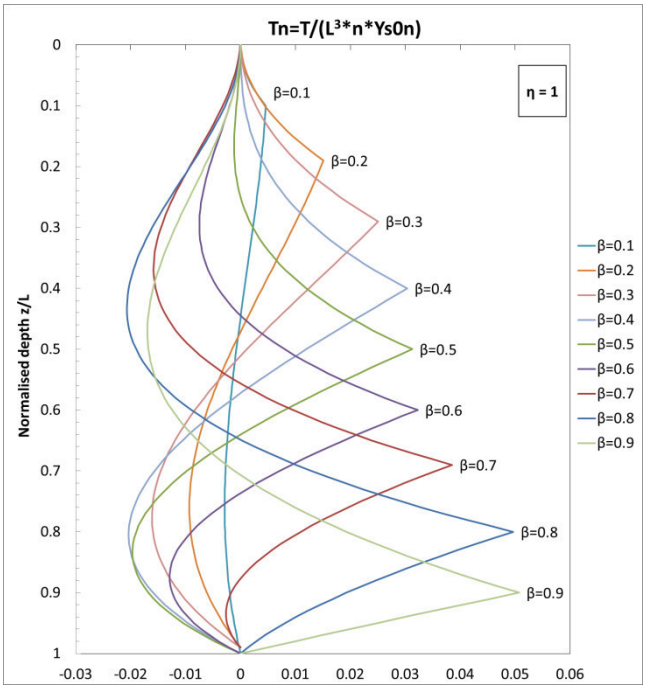

Figure 3-83: Normalised shear force with depth for η=1

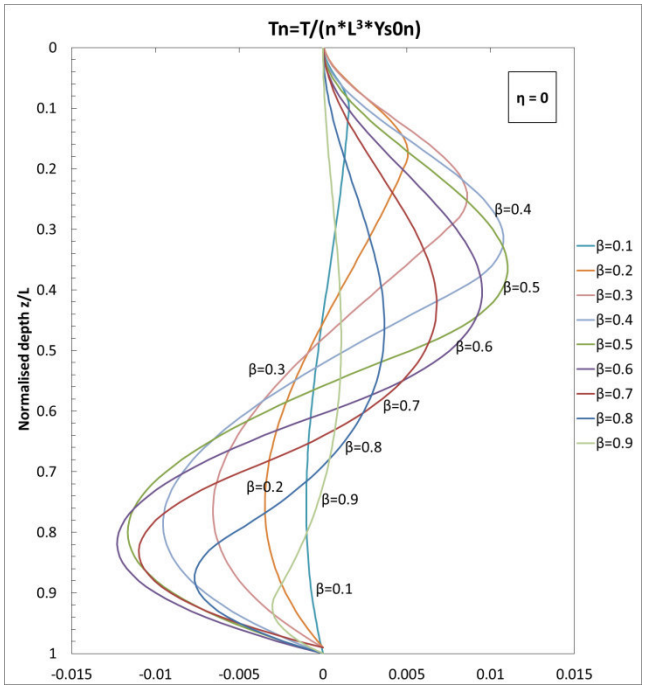

Figure 3-84: Normalised shear force with depth for η=0

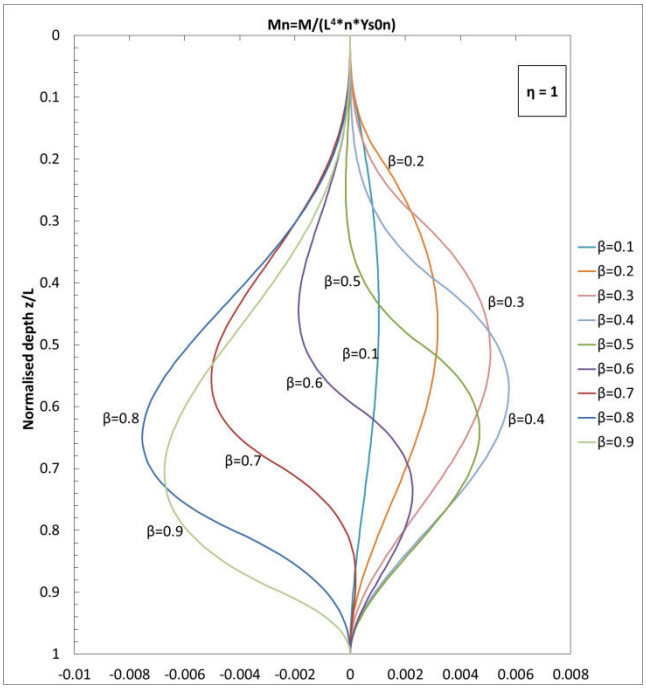

Figure 3-85: Normalised bending moment with depth for η=1

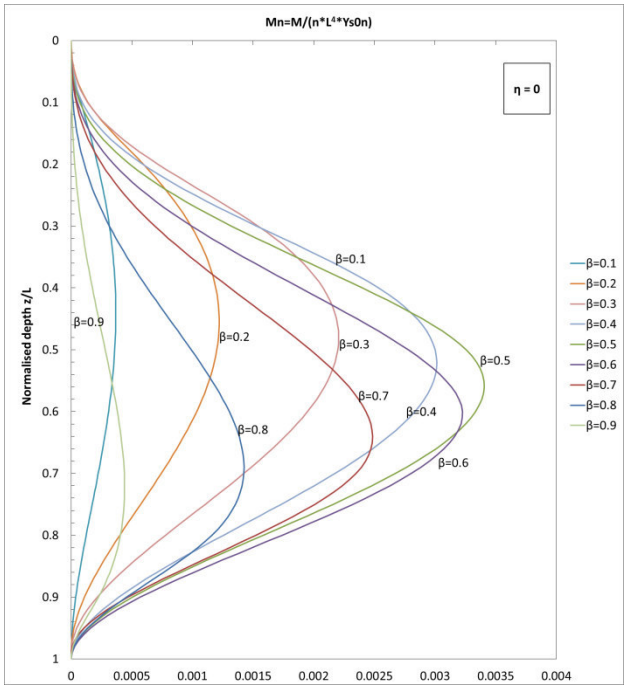

Figure 3-86: Normalised bending moment with depth for η=0

3.8.2. Elastic solutions for an unrotated-head passive rigid pile on a cohesionless soil

The problem shown in Figure 3-87 regards the same soil stratigraphy and properties than the previous case of a free-head pile in a cohesionless soil, but as consequence of an applied constrain the rigid pile is assumed not to rotate and the angle ω is equal to zero, i.e. Nt = 0.

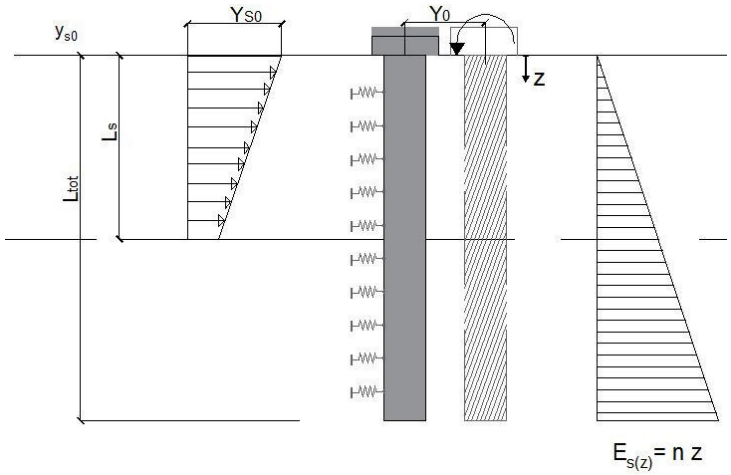

Figure 3-87: Soil profile and pile displacement geometry for a unrotated-head rigid pile in a cohesionless soil

While the ground is assumed to have the same stratigraphy and properties than the previous case of free-head pile, as consequence of the applied constrain the rigid pile cannot rotate .
This assumption let adequately describe pile deflection $y_p(z)$ with depth by using the head's movement parameter y0

$$y_p(z) = y_0 \qquad (3\text{-}100)$$

With the above assumptions, the soil reactions along the whole length L of the pile can be expressed as:

$$p_{1(z)} = -nz\left(y_{0(z)} - y_{s(z)}\right)$$
$$= -nz[\Delta y_0 + z(tan\,\theta)] \qquad [FL\text{-}1] \quad 0 < z < Ls \qquad (3\text{-}101)$$

$$p_{2(z)} = -nz\, y_0 \qquad [FL^{-1}] \quad Ls < z < L \qquad (3\text{-}102)$$

The expression to calculate pile deflection and bending moment M_0 are provided in Table 3-22 while shear forces and bending moments profiles, maximum bending moment M_{max} and its depth z_n in both stable and non-stable zones are provided in Table 3-23.

	Proportionality constants
$y_{0n} = N_y y_{s0n}$	$N_y = \frac{\beta^2}{3}(1+2\eta)$
$M_{0n} = N_M y_{s0n}$	$N_M = \frac{\beta^2}{36}\left[4(1+2\eta) - 3\beta(1+3\eta)\right]$

Table 3-22: Proportionality constants for a unrotated-head passive rigid pile on a cohesionless soil

Depth (z_n)	Expressions
0 – β (unstable zone)	$\frac{T}{nL^3} = -\frac{1}{2}\Delta y_{0n} z_n^{\ 2} + \frac{1}{3}\Delta tan\cdot z_n^{\ 3}$
	$\frac{M}{nL^4} = -M_{0n} - \frac{1}{6}\Delta y_{0n} z_n^{\ 3} + \frac{1}{12}\Delta tan\cdot z_n^{\ 4}$
	$\frac{M_{max}}{nL^4} = M_{0n}$
$z_n = \beta$ (slip surface)	$\frac{T_\beta}{nL^3} = -\frac{1}{2} y_{0n}\left(\beta^2 - 1\right)$
	$\frac{M_\beta}{nL^4 y_{s0n}} = \frac{1}{6} N_y (1-\beta)^2 (\beta + 2)$
β – 1 (stable zone)	$\frac{T}{nL^3} = -\frac{1}{2} y_{0n}\left(z_n^{\ 2} - 1\right)$
	$\frac{M}{nL^4} = -\frac{1}{6} y_{0n}\left(z_n^{\ 3} - 3z_n + 2\right)$

Table 3-23: Elastic solutions for a unrotated-head passive rigid pile on a cohesionless soil

The distribution profile of the shear stresses and bending moments along the pile length can then be obtained with the developed, at varying of the depth of the sliding surface. The normalised shear force $T_n = T/(L^2\, E_{s1} y_{s0n})$ and bending moment $M_n = M/(L^3 E_{s1} y_{s0n})$ are plotted in the Figure 3-88 through Figure 3-91,

for η equal to 1 and 0. It is evident also in case of an homogeneous soil that the normalised stresses shift with the normalised depth of the sliding surface β.
For η = 1, T_n has its maximum value again in correspondence of the sliding surface; β values from 0.6 to 0.8 are the ones obtaining the higher response of the pile in terms of shear force. The case η = 0 presents lower values of $T_{n,max}$, with peaks occurring at z_n generally upper than β.
Even the case of homogeneous soil shows the same M_n profile for both η = 0 and η = 1, always occurring with a negative value. The inverse triangular free-field soil displacement confirms slightly lower values of $M_{n,max}$, reasonably because lower total load affects the pile.

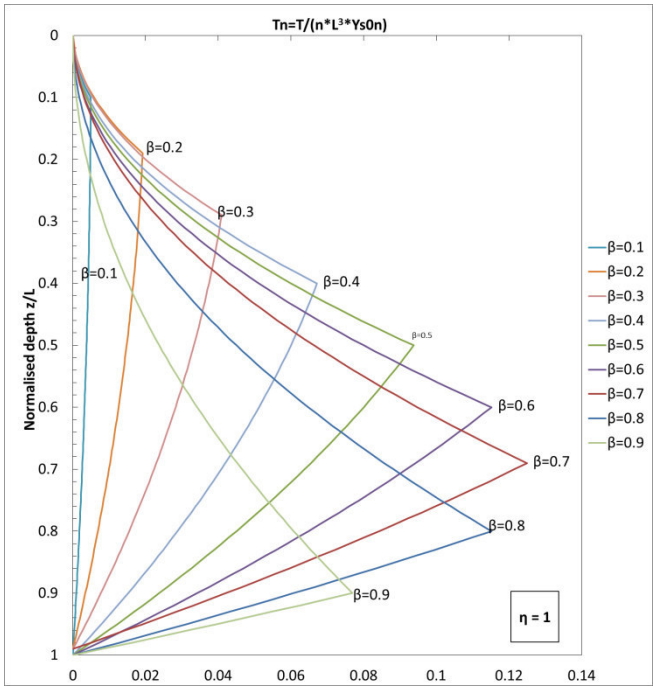

Figure 3-88: Normalised shear force with depth for η=1

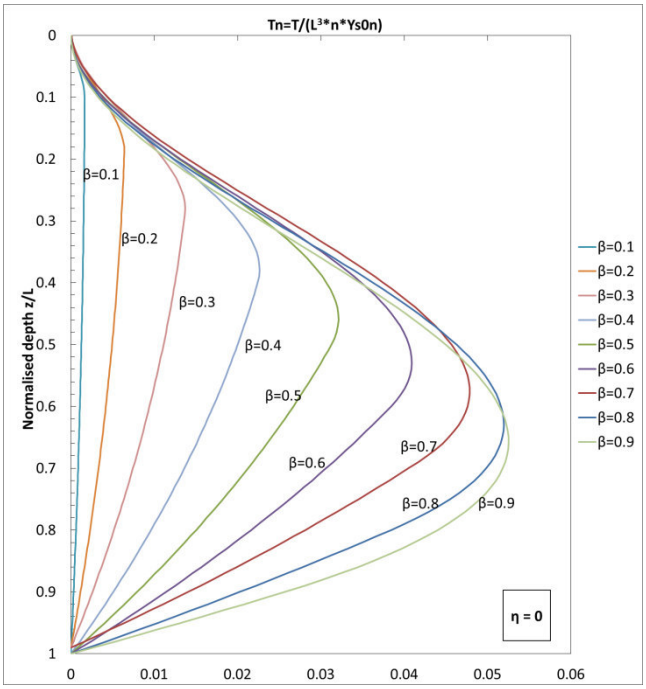

Figure 3-89: Normalised shear force with depth for η=0

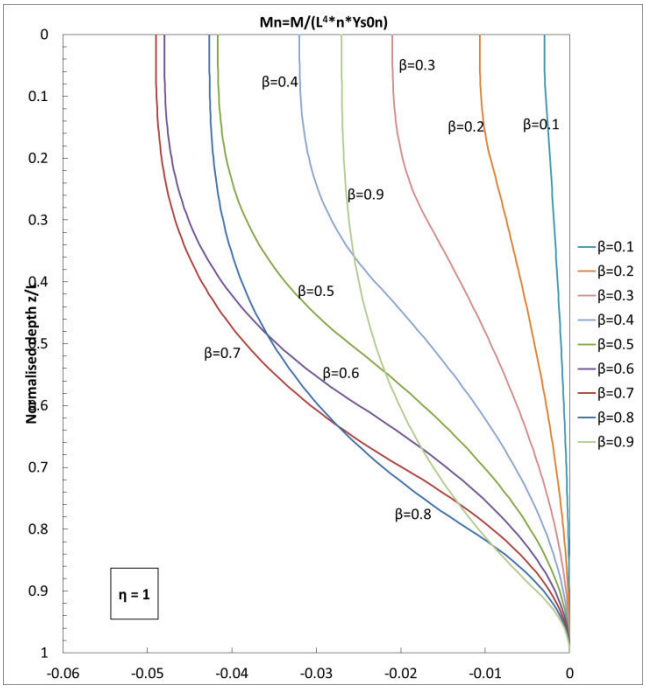

Figure 3-90: Normalised bending moment with depth for η=1

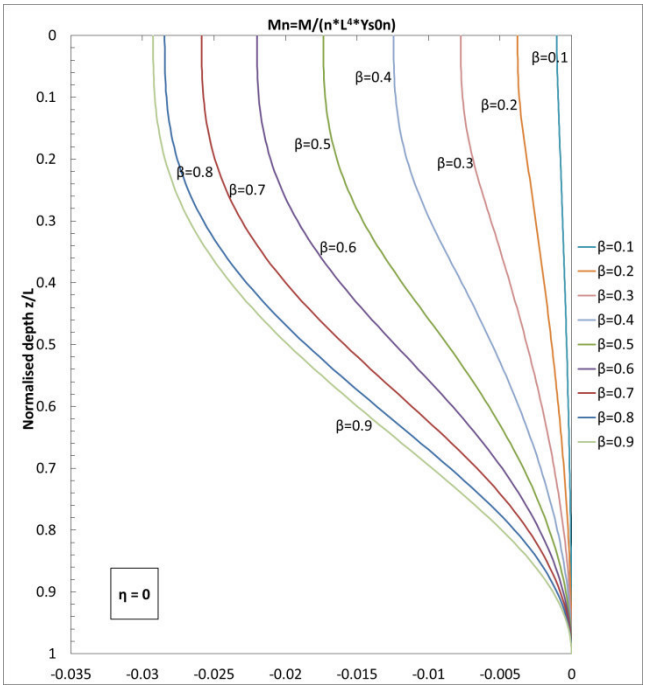

Figure 3-91: Normalised bending moment with depth for η=0

3.8.3. Parametric analysis

The solution provided have been implemented in spreadsheets to carry out a parametric analysis of the problem.
The normalised elastic solutions for a passive rigid pile on a soil with Es linearly increasing with depth are only governed by the parameter η that represents between soil displacement at ground level and at the sliding depth:

$$\eta = \frac{y_{s(z=Ls)}}{y_{s0}} \qquad (3\text{-}103)$$

The parametric analysis focuses on their effects on the normalised pile shear resistance at $z=L_s$:

$$T_{\beta,n} = \frac{T_{(z=Ls)}}{E_{s1}L^2 y_{s0,n}} \qquad (3\text{-}104)$$

Normalised bending moment at $z=L_s$:

$$M_{\beta,n} = \frac{M_{(z=Ls)}}{E_{s1}L^3 y_{s0,n}} \qquad (3\text{-}105)$$

Normalised maximum bending moment acting on the pile:

$$M_{n,max} = \frac{M_{max}}{E_{s1}L^3 y_{s0,n}} \qquad (3\text{-}106)$$

Normalised pile head displacement:

$$\frac{y_{0n}}{y_{s0n}} = \frac{y_0}{y_{s0}} \qquad (3\text{-}107)$$

In every chart, values are plotted against the normalised depth of the sliding surface. The analysis concerns both the boundary conditions of free-head (Figure 3-92) and unrotated-head (Figure 3-93).

Several considerations can be done on the showed results:

- Lateral soil movements have been assessed as triangular (η=0),rectangular (η=1) and trapezoidal (η=0.25,0.5,0.75) profiles. The rectangular shape results in the largest stress state on the pile and higher pile head deflection, followed in order by the trapezoidal and triangular soil profiles. This result appears reasonable as, with the same maximum value at the soil surface, the rectangular profile corresponds to a higher total soil displacement and consequently loading on the pile. It is worth to be noticed also that the condition η=0 is the only one which corresponds to a negative shear force at the sliding surface for high values of β for the free-head condition.
- The free-head pile boundary condition leads to shear force and bending moment profiles having two local maximum values, higher in correspondence of deeper sliding depths. The unrotated-head condition corresponds to higher stress states on the pile, with shear forces and bending moments at the sliding depth sensibly higher than those developed by the free-head condition. However, this comes with an associated lower pile head deflection. This lead to consider the restrained pile head condition as recommended in case low pile displacements are requested, or whenever a high pile resistance at the sliding depth is preferable, as in the case of pile used as stabilising systems, if the pile's stress state is verified.

FREE-HEAD PILE

Effect of different η values:

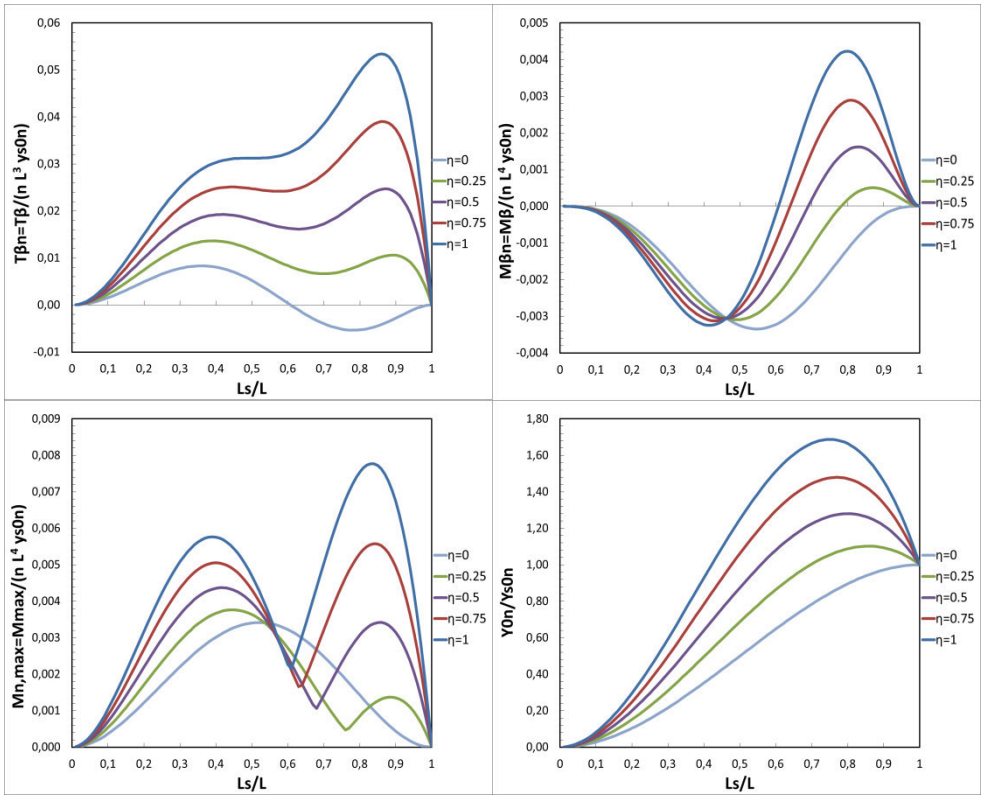

Figure 3-92: Normalised shear force at $z_n=\beta$, bending moment at $z_n=\beta$, maximum bending moment and pile head displacement versus L_s/L, for different η values and free-head condition

UNROTATED-HEAD PILE

Effect of different η values:

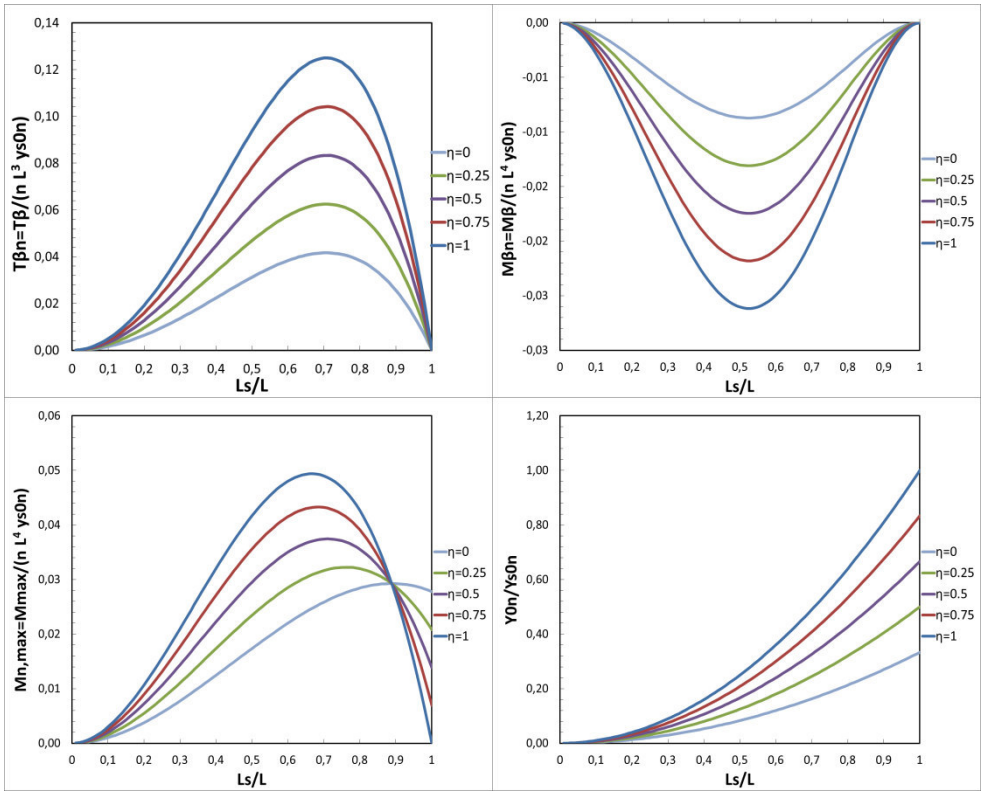

Figure 3-93: Normalised shear force at $z_n=\beta$, bending moment at $z_n=\beta$, maximum bending moment and pile head displacement versus L_s/L, for different η values and unrotated-head condition

4. Elasto-plastic analysis of passive rigid piles in cohesive soils

The relation between soil reaction and pile displacement is non-linear and presents an upper value represented by the ultimate force per unit pile length p_u [FL^{-1}]; as the pile movement increases, the pressure on the soil grows until the limit yielding value is reached. After a fully elastic condition associated with small free-field soil movements (and therefore with small pile deflections), the soil-pile pressure profile starts developing one or more regions in which the yield has been reached. Although to the detriment of high soil and pile displacement, the soil-pile system achieves its limit reaction value as soon as the on-pile force (per unit length) p(z) attains the ultimate plastic pressure p_u all along the yielded regions and a failure mode is activated. The upper limit of the pile reactions is represented by the solutions that Viggiani [23] developed for a double layered cohesive soil, where it is assumed that the pile-soil displacement is such to fully mobilize the yield value p_u all along the whole pile length, ideally for a complete rotation of the pile to the horizontal.

While the elastic solutions provided in the previous chapter only regard a full elastic behaviour of the soil-pile system and do not consider the occurring of the yielding state on the soil, the elasto-plastic method aims to consider the development of soil resistance with shaft deflection, developing complete solutions for the intermediate states between the elastic and the ultimate ones, as they are determined in function of the external free-field soil displacement and of the associated pile deflection. For this reason, the previous model only concerning an elastic behaviour of the soil has been modified and enhanced in order to account for the soil reaction distribution with yielding in one or more regions.

In particular, two of the elastic cases already investigated have been implemented into the elasto-plastic method: the one concerning a two-layered soil with constant values of the subgrade reaction modulus and the homogeneous soil with E_s linearly increasing with depth.

The same hypotheses expressed for the elastic model in paragraph 3.2 are still valid; anyway, in order to simplify the problem, in here the soil non-linearity is schematized by a linear elastic-perfectly plastic constitutive law [34]. The mobilised soil strain varies along the pile length due to the increasing soil-pile relative displacement and to the distribution of the modulus of reaction (E_s), until the limiting soil pressure p_u is reached.
An iterative process has been implemented in a computer program written in FORTRAN, in order to numerically solve the system and to track all the different configurations reached as the soil movement is increased or the sliding depth varies.
The developing of the soil-pile system's failure modes is investigated and finally, examples of non-dimensional design charts have been developed.

4.1. Limiting soil resistance p_u

4.1.1. Limiting soil resistance a single passive pile

Upon reaching plastic state, the interaction force between pile and soil interface attains a maximum. But the pile-soil-pile interaction is quite complicated due to the non-linear soil properties and the group effects interesting the piles in a row.
On the basis of observations in the field and in the laboratory, it is well established that soil failure around a laterally loaded pile can be distinguished into two failure conditions. A passive wedge-failure occurs near the ground surface and a wedge of soil is moved up and away from the pile. In addition, failure surfaces are generated by the pile several diameters below the ground surface. Here the soils are limited to plane-strain behaviour and are forced to move in a flow-around manner. As a consequence, for a homogeneous soil, the limit force per unit length of the soil p_u is assumed to increase with depth in the upper part of the pile up to a maximum value and remains constant in the lower part.
Anyway, as noteworthy uncertainties still exist around this topic and given its importance, a basic understanding of p_u dependencies is essential in order to allow a complete and proper fruition of the charts by evaluating the most suitable parameters for piles in cohesive soils.

By assuming a three-dimensional wedge-type soil-pile failure modes for small z/D ratios and a two-dimensional one for higher depths, Broms [1] suggested the following equations to calculate the ultimate soil-pile pressure p_u in sand, for a single pile:

$$p_u = 3 \cdot D \cdot K_p \cdot \sigma'_{v0} \qquad [FL^{-1}] \qquad (4\text{-}1)$$

where K_p is the Rankine passive pressure coefficient,

$$K_p = tan^2\left(45 + \frac{\varphi\prime}{2}\right) \qquad (4\text{-}2)$$

and φ' is the internal friction angle of the soil, σ'_{v0} is the initial vertical effective stress.

For cohesive soils, Broms suggested to consider the ultimate value of soil-pile lateral force per unit length p_u for a saturated clay as proportional to its undrained shear strength S_u and given by the nowadays usual expression:

$$p_u = N_p \cdot S_u \cdot D \qquad (4\text{-}3)$$

where S_u is the undrained shear strength, D is the pile diameter. N_p is the ultimate undrained lateral bearing capacity factor varying with depth, for a single pile regardless of the pile spacing and the group effect.
With these assumptions, Poulos suggested that N_p can be assumed to increase linearly from 2 at the ground surface to the limiting value of N_p=9 at a depth of 3.5 pile diameters or width D and beyond [42],[26]:

$$N_p = 2\,(1 + z/D) \leq 9 \qquad (4\text{-}4)$$

4.1.2. Limiting soil resistance for a row of piles

Aiming to improve the methods based on the analysis of an isolated pile, Ito et al. [43] calculated the lateral force acting on a row of piles due to soil movement using the theoretical equations, derived previously by Ito and Matsui [25] and based on the theory of plastic deformation as well as a consideration of the plastic flow of the soil through the piles. This model was developed for rigid piles with infinite lengths, and it is assumed that only the soil around the piles is in a state of plastic equilibrium, satisfying the Mohr–Coulomb yield criterion. The ultimate soil pressure on the pile segment, which is induced by flowing soil, depends on the strength properties of the soil, diameters and spacing between the piles.
For a cohesive soil in undrained conditions and shear strength S_u, Ito and Matsui derived the relation:

$$p_u(z) = S_u \left\{ s\left(3log\frac{s}{d} + \frac{s-d}{d}tan\frac{\pi}{8}\right) - 2(s-d)\right\} + \gamma z(s-d) \qquad (4\text{-}5)$$

Where s is the centre-to-centre pile spacing in a row; d is the clear spacing between the piles, γ is the unit weight of the soil; z is an arbitrary depth from the ground surface, K_p is the Rankine passive pressure coefficient.
For cohesionless soils, authors derived the relation:

$$p_u(z) = \frac{\gamma z}{K_p}\left\{ \begin{array}{c} s\left(\frac{s}{d}\right)\left(K_p{}^{\frac{1}{2}}tan\,\varphi' + K_p - 1\right) \\ \cdot exp\left(\frac{s-d}{d}K_p\,tan\,\varphi\,tan\left(\frac{\pi}{8}+\frac{\varphi}{4}\right)\right) - d \end{array} \right\} \qquad (4\text{-}6)$$

where s is the centre-to-centre pile spacing in a row; d is the clear spacing between the piles.

The method is only valid over a limited range of spacing since, at large or at very close spacing, the mechanism of soil flow through the piles postulated by Ito and Matsui (1975) is not the critical mode (Poulos, 1995). Finally, it has to be noticed

that a significant increase in the value of the soil-pile pressure can be observed by reducing the clear spacing between piles.

A general formulation has been suggested by Wang and Reese [44] for a pile in clay soil, computing the ultimate soil resistance both for the wedge-type failure and the flow-around failure. In particular, for a drilled shaft wall, they suggest a critical spacing to evaluate if a group effect has to be considered. In particular, to calculate the ultimate soil resistance for a wedge-type failure per unit length of the drilled shaft in clay from the equations:

$$p_u = 2\,S_u D + \gamma L D + 2.83 S_u L \qquad d > d_{cr} \qquad (4\text{-}7)$$

and to use the following formulation to take into account the shadowing effect if the clear spacing is smaller than the critical:

$$p_u = 2\,S_u (D + d) + \gamma L (D + d) + S_u d \qquad d < d_{cr} \qquad (4\text{-}8)$$

Where d_{cr} is the critical clear spacing calculated as:

$$d_{cr} = 2.828\,S_u L / [\gamma L + 6 S_u] \qquad (4\text{-}9)$$

The ultimate soil resistance of flow-around failure is instead

$$p_u = 11 D S_u \qquad (4\text{-}10)$$

Developed for a single pile and modified with a factor taking account of group effect which increases as pile spacing decreases. The global ultimate soil resistance is selected as the smaller value between the wedge-type failure and flow-around failure. It has to be noticed that, in opposition to what suggested by Ito et al. [43], the soil-pile pressure p_u increases as the pile clear spacing in increased.

More recently, Georgiadis et al. [45] combined a displacement finite element (FEM), lower and upper bound finite element limit analysis (LE) and an analytical upper bound plasticity methods to investigate the undrained limiting lateral

resistance of piles in a pile row, for various pile spacing and pile-soil adhesion factors (=limiting interface shear stress/undrained shear strength). The obtained results by FEM and LE show an excellent agreement and have been used as the basis for developing an empirical equation for the determination of a single-pile ultimate undrained lateral bearing capacity factor N_p. In particular, they observed that the effect of the pile-soil adhesion factor μ is more significant than the pile spacing over the practical range of s/D values (i.e. $\frac{s}{D} \geq 1.5$). For pile spacing beyond the critical spacing s1

$$\frac{S_1}{D} = 3.1 + 1.4\mu \qquad (4\text{-}11)$$

They suggest the formulation of N_{p1} proposed by Randolph and Houlsby [24]

$$N_{p1} = \frac{p_u}{S_u D} = \pi + 2\sin^{-1}\mu + 2\cos\left(\sin^{-1}\mu\right) + 4\left[\cos\left(\frac{\sin^{-1}\mu}{2}\right) + \sin\left(\frac{\sin^{-1}\mu}{2}\right)\right] \qquad (4\text{-}12)$$

where Su is the undrained shear strength, p_u the ultimate force per unit length of the pile, D is the pile diameter and μ is the pile-soil adhesion factor, while for normalised pile spacing greater than s1/D:

$$N_p = N_{p1}\left[1 + \left(0.13\, ln\frac{\frac{s}{D}-1}{\frac{S_1}{D}-1} + 0.24 - 0.02\mu\right) ln\frac{\frac{s}{D}-1}{\frac{S_1}{D}-1}\right] \qquad (4\text{-}13)$$

Figure 4-1 shows the variation of the undrained lateral bearing capacity factor with the normalised pile spacing for adhesion factors μ = 0, 0.25, 0.5, 0.75 and 1, demonstrating that the adhesion factor significantly affects the value of Np. As a result, the ultimate soil pressure increases as both pile centre-to-centre spacing or μ are increased.

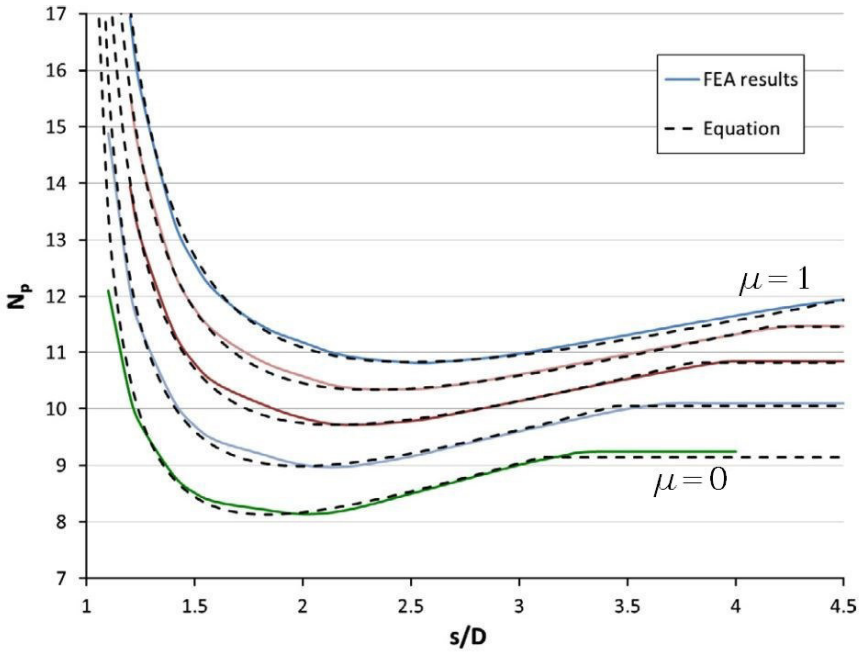

Figure 4-1: Variation of Np with s/D for a = 0, 0.25, 0.5, 0.75 and 1 as proposed by Georgiadis K. et al. [45]

Kourkoulis et al. [22] suggested that a centre to centre pile spacing of 3-4 diameter can be considered reasonable to both neglect the group effect in terms of p_u and to allow the development of soil arching between the piles.
Finally, as pointed out by Poulos [27], it is important to reaffirm that the selection of an appropriate value of p_u for passive pile is a crucial step for realistic elasto-plastic analysis.

4.2. Modes of failure for a passive pile

The limit lateral resistance a passive pile can develop depends on which failure mechanism is reached by the soil-pile system. In other words, depending on the soil-pile geometry and materials properties, the system can go to different failure modes, which consequently affects the limit lateral resistance it can furnish.
By developing a limit equilibrium method for evaluating the ultimate lateral resistance of piles used to stabilise landslides in a two-layer purely cohesive soil, Viggiani [23] identified six modes of failure for a single passive pile in undrained conditions, either within the soil or in pile; the mechanism that occurs have been found to depend on the length and diameter of the pile together with the yield moment of its section, the strengths of the stable and sliding soil layers and the depth of the sliding soil mass. Dimensionless solutions for the ultimate lateral resistance exerted by the pile on the sliding plane and the maximum bending moment on the pile for each failure mode have been developed, by assuming that:

- the ground has only two layers of soil, with the top layer of thickness βL moving uniformly over the underlying material;
- the shear strength of the soil remains constant with depth, but not necessarily equal, in the sliding and stable layers, and it is evaluated according to the formulation presented by Broms [1] for cohesive soil

$$p_u = N_p \cdot S_u \cdot D \qquad (4\text{-}14)$$

- the ultimate lateral force per unit length p_u is uniform with depth in each layer, except eventually for a reduction to zero over the top 1.5D (where D is the pile diameter) in the sliding layer to account for ground surface effects.
- the pile is unrestrained, i.e. the pile head is not fixed, connected to or restrained against a structure or piles.
- pile-soil interaction along the pile attains the ultimate state so that the limiting force between the pile and soil is achieved.

The solutions were subsequently amended by Chmoulian [28] and are summarised in Table 4-1. Kanagasabai et al. [46] also identified the same failure modes by using a finite-difference method to study a single pile embedded in stable strata to stabilise the slipping mass of the soil. Poulos [26] also, by developing a method of analysis of a row of passive piles basically as improvement of the solutions already provided by Viggiani [23], revealed the same failure modes (cf. paragraph 2.3.4).

In particular, three main modes of failure within the soil have been identified as possible for a rigid pile, as shown in Figure 4-2, with full mobilisation of the soil resistance either in the sliding layer, or in the stable layer, or in both layers simultaneously. They are:

- Mechanism A, “translational” failure mode or “short pile mode”: it occurs when the pile length embedded in the stable soil is shallow and the pile will experience excessive displacement due to soil failure in the stable layer; the firm layer fails and is ripped by the pile that translates together with the sliding mass

- Mechanism B, “rotational” failure mode or “intermediate mode”: it occurs when the depth of the slip surface is relatively deep and the soil strength along the pile length in both unstable and stable layers is fully mobilised. According to the models presented by Viggiani [23] (and later by Poulos [26] and Kanagasabai et al. [46]), in this mode, the pile deflection at the upper portion exceeds the soil movement.

- Mechanism C, or “flow mode”: it occurs when the depth of the slip surface is shallow and the soil strength of the sliding mass is fully mobilised; the pile results to be fixed in the stable layer while the sliding soil mass becomes plastic and flows around the pile. The pile deflection is considerably less than the soil movement. It is also the same failure mode analysed by Kourkoulis et al. ([22],[21])

Similar generalised failure mechanisms are expected to be revealed by the implemented analysis method.

Anyway, it is worth to highlight that within the 'rotational' failure mode, Viggiani identified three additional sub-failure modes of pile itself by developing plastic hinges in correspondence of the local largest bending moments. These correspond to the "long-pile" failure mode where the pile itself yields and could be associated with the previous three modes of soil failure.

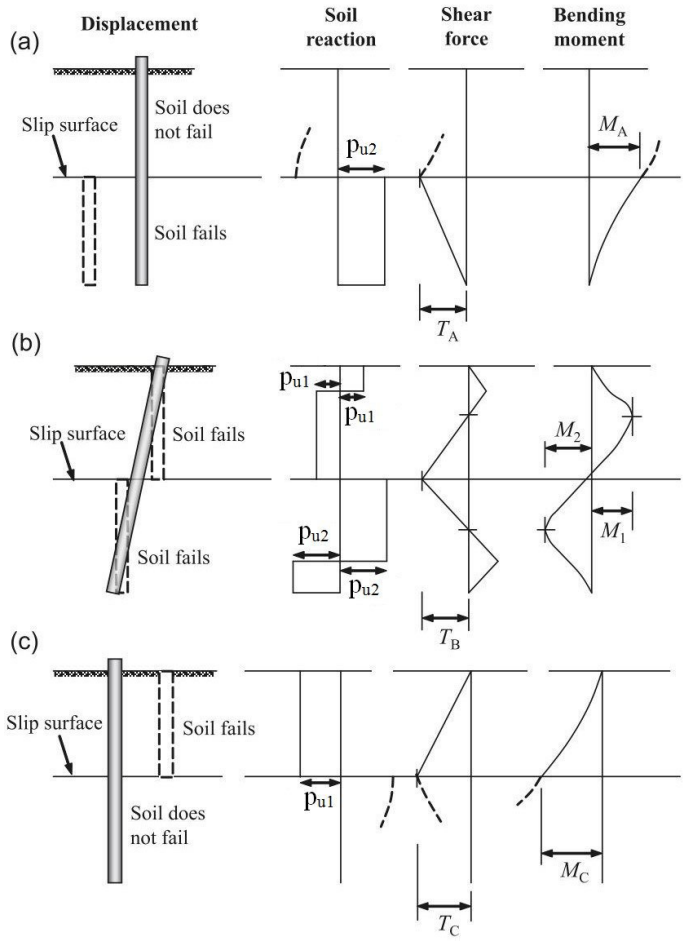

Figure 4-2: Pile failure modes: (a) failure mechanism A; (b) failure mechanism B; (c) failure mechanism C [23], [28], [46]

Failure Mode	Ultimate lateral load and Maximum bending moment
Mode A	$\frac{T_A}{p_{u1}L} = k(1-\beta)$
Mode B	$\frac{T_B}{p_{u1}L} = \beta\left[\sqrt{\frac{\left(\frac{1-\beta}{\beta}\right)^2+\frac{1}{k}}{\frac{1}{k}(1+\frac{1}{k})}+\left(\frac{1+\left(\frac{1-\beta}{\beta}\right)}{1+\frac{1}{k}}\right)^2}-\frac{1+\frac{1-\beta}{\beta}}{1+\frac{1}{k}}\right]$ $\frac{M_1}{p_{u1}L^2} = \frac{\beta^2}{4}\left[1-\frac{T_B}{p_{u1}\beta L}\right]^2$ $\frac{M_2}{p_{u1}L^2} = \frac{k\beta^2}{4}\left[\left(\frac{1-\beta}{\beta}\right)-\frac{T_B}{kp_{u1}\beta L}\right]^2$
Mode C	$\frac{T_C}{p_{u1}L} = \beta$

Table 4-1: Equations for calculating ultimate lateral load for piles in a two-layer cohesive soil (after Viggiani [23] and Chmoulian [28]) for a pile of length L; p_{u2} and p_{u1} are the limit soil resistance in the stable and sliding layers, $k=p_{u2}/p_{u1}$, βL is the pile length in the sliding layer

4.3. Elasto-plastic analysis of passive rigid piles in cohesive soils

4.3.1.Soil profile and geometry of the problem

The presence of a sliding cohesive mass over a stiffer stratum is a typical slope instability condition. The corresponding problem under consideration is represented in Figure 4-3 and presents the same soil stratigraphy already investigated in the case of the elastic solutions for a free-head passive rigid pile in a two-layered cohesive soil (Paragraph 3.4); moreover, it corresponds to that analysed by Viggiani.

A soil mass of thickness $L_s=\beta \cdot L$ slides on a stable underlying soil along a defined slip surface. Each layer is assumed to be a saturated cohesive soil in undrained conditions, each one with a constant shear strength S_u (the case of a cohesionless soil presents some peculiarity and is analysed in the next chapter).

A free-head rigid pile of length L and diameter D crosses the slip surface and penetrates the firm soil layer. For simplicity, the ground and the slip surface are assumed to be horizontal.

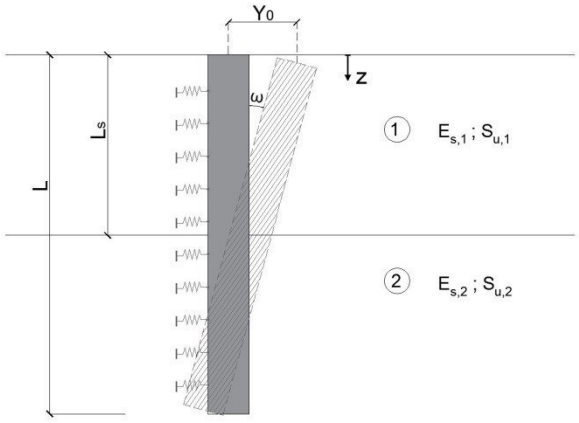

Figure 4-3: Soil profile and pile displacement geometry

Once again, the distribution of the soil movement along L_s is assumed to be linear with depth and defined through the soil top displacement parameters y_{s0} and the ratio η, varying from a triangular variation with depth when no displacement occurs in correspondence of the slip surface (η=0) to a uniform distribution, when the unstable soil layer slides down as a unique mass block (η=1). Intermediate values of η describe a generic trapezoidal profile of the soil movement.

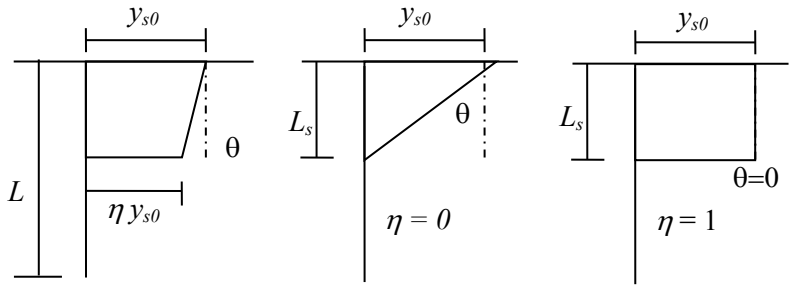

Figure 4-4:Distribution of the soil movement: a) generic distribution; b) inverse triangular variation with depth η=0; c)uniform distribution with depth η=1

4.3.2.Constitutive model and ultimate soil resistance p_u

The soil is modelled according to a Winkler approach [32] in which the ground is modelled as a set of elastic springs distributed along the pile shaft. Despite the assumption of a linear elastic soil made in the previous models, the problem is more complex because soils in real field situations behave nonlinearly. In order to simplify the problem, the soil is assumed to be linear elastic up to the yielding point and perfectly plastic beyond it [34]; the pile–soil interaction is characterised by a series of springs which operates within the elastic state. In the elastic-plastic model, the soil pressure is limited by its ultimate value. If less than the limiting value p_u, the on-pile force per unit length p, at any depth, is proportional to the local pile displacement through the modulus of subgrade reaction E_s [FL^{-2}].

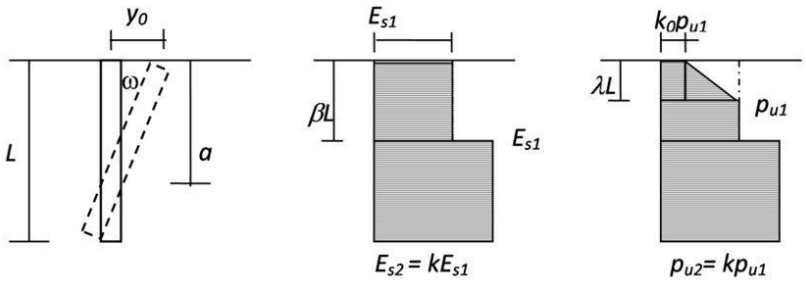

Figure 4-5:(a) Rigid pile deflection; (b) Variation of E_s with depth; (c) Variation of p_u with depth

As shown in Figure 4-5b, a different value of the modulus of subgrade E_s is assigned to every soil layer. The springs of each layer have a constant modulus of subgrade reaction, regardless of depth: Es_1 for the first sliding layer and Es_2 =k*Es_1 for the stable layer:

$$E_s(z) = E_{s1} \qquad [FL^{-2}] \qquad 0 < z < \beta L \qquad (4\text{-}15)$$

$$E_s(z) = E_{s2} = k \cdot E_{s1} \qquad [FL\text{-}2] \qquad \beta L < z < L \qquad (4\text{-}16)$$

Where *k* is defined as :

$$k = \frac{E_{s2}}{E_{s1}} \qquad (4\text{-}17)$$

The method implements a generalised linear relationship between the ultimate value of lateral pressure p_u acting on the pile and depth; p_u in assumed to increase linearly from ground level to a depth of 3D, where D is the diameter of the pile, and to assume a constant value at depths below, ideally proportional to their S_u value. This assumption let account for ground surface effects on p_u values close to pile head.
The profile of p_u is then showed in Figure 4-5c, and schematized by the following expressions:

$$p_u(z) = p_{u0} + mz \qquad 0 < z < \lambda L \qquad (4\text{-}18)$$

$$p_u(z) = p_{u1} \qquad \lambda L < z < \beta L \qquad (4\text{-}19)$$

$$p_u(z) = p_{u2} = k \cdot p_{u1} \qquad \beta L < z < L \qquad (4\text{-}20)$$

Where

$$m = \frac{p_{u1} - p_{u0}}{\lambda L} = \frac{p_{u1}(1 - k_0)}{\lambda L} \qquad (4\text{-}21)$$

$$k_0 = \frac{p_{u1}}{p_{u0}} \qquad (4\text{-}22)$$

and

$$k = \frac{p_{u2}}{p_{u1}} \qquad (4\text{-}23)$$

The use of parametric ratios between stiffness and resistance parameters of each soil layer allow adapting the model to several different real situations which can be similarly modelled. At the same time, it is important to notice that, as the method

gives normalised solution, the values attributed to p_u and E_s do not enter into the developed solutions, and their evaluation is not directly considered inside the proposed method.

4.3.3. Method of analysis

Similarly to the solutions developed for the elastic case, the non-linear analysis method solves the equation of the soil-pile system with the soil represented as linear springs providing resisting forces that increase with the relative lateral deflection. Once again, by considering horizontal force and moment equilibrium along the pile length, a system of two equations in two variables y_0 and $\tan\omega$ is derived.

The program considers the external soil movement as an input for the definition of the soil-pile pressure profile and the building of the equation system. This is made in order to follow the progressive pile deflection which occurs at the same time with the progression of the external soil sliding: as y_s increases, the pile rotates and pressures $p_e(z)$ along it develops. In a first step, soil reaction all along the pile length is small enough not to reach the ultimate resistance p_u. In this case, the whole system soil-pile is in an elastic condition and no yielding affects the soil. Such a configuration represents the elastic case, the starting point for the iterating process and corresponds to the configuration presented in paragraph 3.4. Explicit solutions are available.

From the elastic field, the progressive increment of soil and pile movements lead the soil-pile system to enter the plastic fields and the pressures to reach a first yielding point at a certain depth or region of the soil-pile interface.

Due to different geometries, stiffness and resistances that the model can consider, different first yielding regions may be reached. In particular, for the soil model under investigation it has been found ten singular first yielding regions, equivalent likewise to the same number of cases. Moreover, by imposing proper boundary conditions for each configuration, it is possible to calculate the soil threshold displacement y_{s0} that, if reached, leads to the respective first yielding cases.

Based on the different zone where plasticization occurs first and progressively with the increasing of soil external movement y_s, different configurations or cases may occur next. In fact, after the first case encountered, other configurations follow in cascade as soon as new yielding points are reached by the pressures along the pile, while the already yielded regions expand. The new successive configurations can be considered as made of the combination of several singular yielded regions.

The equilibrium equations system for a soil reaction distribution with yielding in one or more regions generally needs to be numerically solved: an iterative process has been implemented in a computer program written in FORTRAN, in order to numerically solve the system and track all the different configurations coming in succession as the soil movement is increased. The implemented procedure applies the bisection root-finding method for numerically solving the equations of the shear forces and bending moments equilibrium for the real variable y_0 and $\tan\omega$. Moreover, the iterative procedure implements a control over the pressures to check if new yielding regions had developed. In that case, it moves to the next soil reaction configuration subroutine.

Although all the different cases are linked each other by the increasing value of y_s and y_0, they have been implemented singularly in the FORTRAN code as singular subroutines in order to solve singularly every corresponding equilibrium equations system. The program stops when a failure mode is reached. With regard to the mode B, the soil-pile interaction tends only asymptotically toward it; for this reason, in the software, these limit states have been implemented separately from the others, as a final step the process tends to.

4.3.4. First yielding cases and threshold soil displacements

The particular distribution of Es and of the ultimate soil pressure lead to several different first yielding cases: due to the assumed geometry (in particular η, λ and β parameters) and of the stiffness and resistance ratios (k, k_0), a different first yielding case is expected.
In particular, ten different singular yielding regions have been identified and developed, occurring in correspondence of likewise points in the ultimate soil pressure profile: they are located at depth $z_n = z/L = 0$ (cases P1 and P5), $z_n = \lambda$ (cases P6), $z_n = \beta$ (cases P2, P3 and P32=P2$^-$), $z_n = 1$ (case P4) and at a depth into the interval $0 < z_n < \lambda$ (case P8). A scheme is stated in the Figure 4-6.

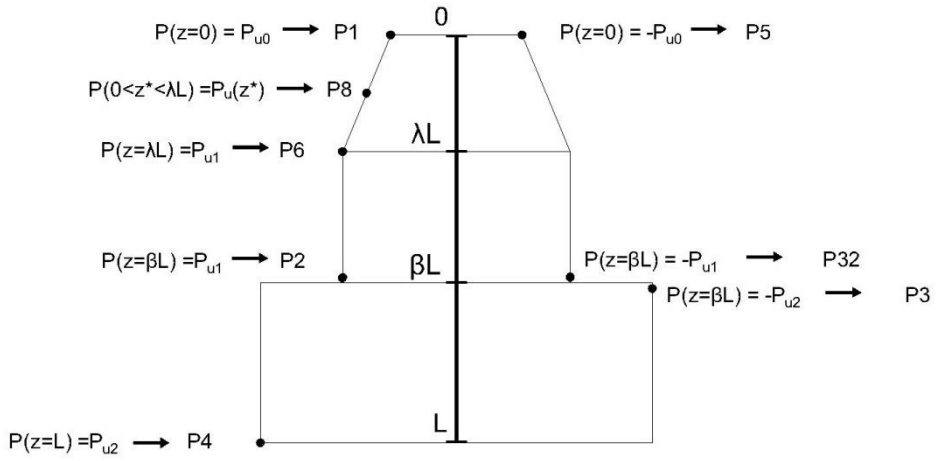

Figure 4-6: First yielding points and corresponding first yielding case

Every case is also associated to a characteristic threshold soil displacement y_{s0} that, if passed, drive the elastic system to one of the first yielding cases.

They are estimated by imposing the proper boundary condition into the elastic solutions developed for the case of a two-layered soil analysed in the paragraph 3.4:

$$p_{1(z)} = -E_{s1}\left(y_{0(z)} - y_{s(z)}\right) = -E_{s1}[(yY_0 - y_{s0}) - (\tan\omega - \tan\alpha)z] \quad [FL^{-1}] \quad 0 < z < Ls \quad (4\text{-}24)$$

$$p_{2(z)} = -E_{s2}[y_0 - \tan\omega\, z] \quad [FL^{-1}] \quad Ls < z < L \quad (4\text{-}25)$$

Table 4-2 presents the so evaluated threshold soil displacements as a function of the elastic proportionality constants D, N_y, N_t, $N_{\Delta y}$ and $N_{\Delta t}$ for a passive free-head rigid pile in a two-layered soil with constant values of the subgrade reaction modulus presented in Table 3-5.
It has to be noticed as pile-soil pressures on the pile are assumed positive if acting in the same direction of the soil displacement. Otherwise, they are considered negative.

First yielding case	Threshold soil displacement
Case P1 (positive yielding at z = 0)	$\left(\frac{y_{s0}E_{s1}}{p_{u1}}\right)_{lim1} = -k_0\frac{D}{N_{\Delta y}}$
Case P5 (negative yielding at z=0)	$\left(\frac{y_{s0}E_{s1}}{p_{u1}}\right)_{lim5} = k_0\frac{D}{N_{\Delta y}}$
Case P2 (yielding at $z=Ls^-$)	$\left(\frac{y_{s0}E_{s1}}{p_{u1}}\right)_{lim2+} = \frac{D}{\beta N_{\Delta t} - N_{\Delta y}}$
Case P3 (negative yielding at $z=Ls^+$)	$\left(\frac{y_{s0}E_{s1}}{p_{u1}}\right)_{lim3} = \frac{D}{N_y - \beta N_t}$

Case P2-	$\left(\frac{y_{s0}E_{s1}}{p_{u1}}\right)_{\lim 2-} = -\left(\frac{y_{s0}E_{s1}}{p_{u1}}\right)_{\lim 2+} = \frac{-D}{N_y - \beta N_t}$
CASE P4 (yielding at z=L)	$\left(\frac{y_{s0}E_{s1}}{p_{u1}}\right)_{lim\,4} = \frac{D}{N_t - N_y}$
Case P6 (yielding at z=λL)	$\left(\frac{y_{s0}E_{s1}}{p_{u1}}\right)_{lim\,6} = \frac{D}{\lambda N_{\Delta t} - N_{\Delta y}}$
Case P8 (yielding at z_n=c, with 0<c<L_0)	$\left(\frac{y_{s0}E_{s1}}{p_{u1}}\right)_{lim\,8} = -\frac{(1-k_0)}{\lambda}\frac{D}{N_{\Delta t}}$

Table 4-2: Threshold soil displacements for all the first yielding cases

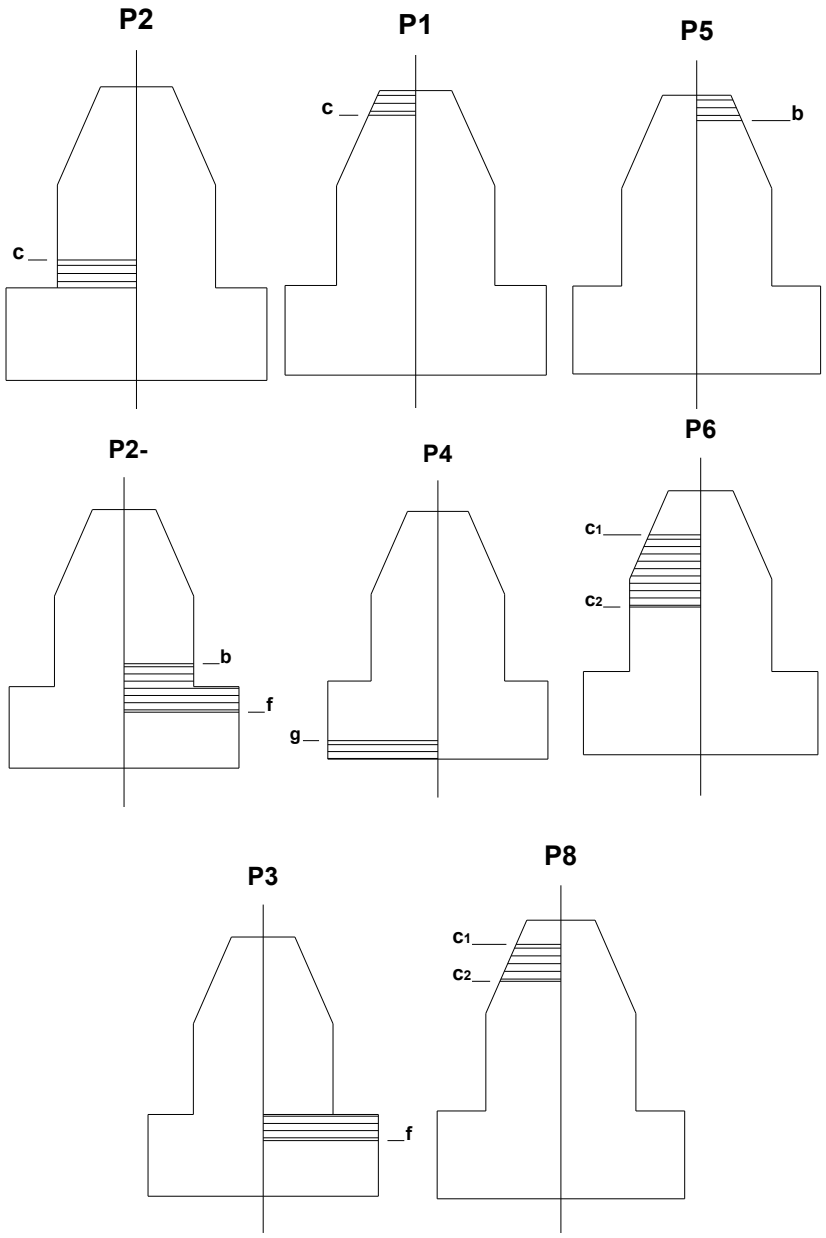

Table 4-3: Yielded regions for the first yielding cases

The yielding regions so identified (Figure 4-7) can be considered as basic components of a more complex cases that occur with the increasing of the imposed free-field soil displacement. For this reason, hereafter their nomenclature is used to describe and mention the successive complex cases. In example, case P23 indicates that both region 2 and 3 are yielded, while the rest of the pressure profile is still elastic.

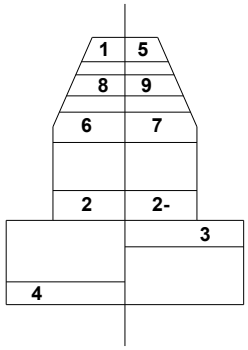

Figure 4-7: Identified yielded region and their nomenclature

As mentioned, the minimum of all threshold displacements identifies which case is the first occurring for that particular geometry and soil properties configuration.

$$y_{s0,lim} = \min\{y_{s0,lim1}, y_{s0,lim2}, y_{s0,lim2^-}, y_{s0,lim3}, y_{s0,lim4}, y_{s0,lim5}, y_{s0,lim6}, y_{s0,lim7},\}$$

Nevertheless, all the described threshold soil displacements y_{s0lim} can be plotted over $L_s=\beta L$ in order to understand which is the case that has to be expected to occur and approximately which ones will follow even later as y_s increases (Figure 4-8). For example, considering a $\beta=Ls/L$ value of 0.5, the pile is in the elastic field since the soil displacement is less than the yielding threshold value. As this value is reached, the pile-soil limit pressure extends along the negative region 5 and the pile-soil system enters into the cases P5.

As y_{s0n} increases more, soil pressure will reach the yield also in the region 3, and the system the configuration P53. Similarly, the pile is expected to arrive, in the end, to the configuration P56234, corresponding to a failure mode B1

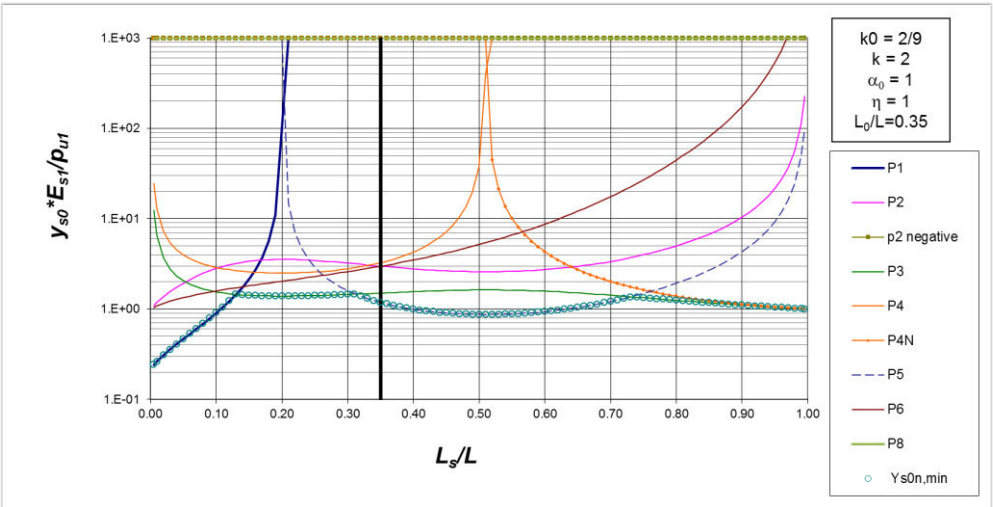

Figure 4-8: Example of first yielding non-dimensional displacement Ys0n diagram over L_s/L

All the listed simple configurations are followed by more complex cases in which soil reaction distribution has reached the ultimate resistance p_u in more than one region. According to all possible combinations of the different ten regions, more than sixty different cases have been identified. For each one, similarly to what showed for the elastic case, the equilibrium equations have to be solved in order to obtain pile deflection and strain state. Since those equations are nonlinear, a numerical procedure has been developed to solve the systems; moreover, to follow the cases path by checking soil reaction distribution to find if yielding has been reached until one of the possible limit states is achieved.

4.3.5.Iterative numerical procedure and cases

The first step in the analysis of a given configuration is to calculate all the yielding threshold displacement y_{s0}; lately, the procedures tracks and controls the whole soil reaction profile in order to control if new yield regions have been developed and to follow the cases succession path.
As equations systems are nonlinear, an iterative numerical procedure has been developed to solve them and a computer program in FORTRAN code has been written to implement and run the procedure.
The transition from a case to another is ruled by the check of the pressure value at the specific depth of the yielding regions:

$$r_i = \frac{p_{(z=zi)}}{p_u} \qquad (4\text{-}26)$$

for each one of the five identified first yielding depth:

$$r_1 = \frac{p_{(z=0)}}{p_{u(z=0)}} = -r_5 \qquad (4\text{-}27)$$

$$r_2 = \frac{p_{(z=Ls^-)}}{p_{u(z=Ls^-)}} \qquad (4\text{-}28)$$

$$r_3 = \frac{p_{(z=Ls^+)}}{p_{u(z=Ls^+)}} \qquad (4\text{-}29)$$

$$r_4 = \frac{p_{(z=L)}}{p_{u(z=L)}} \qquad (4\text{-}30)$$

$$r_6 = \frac{p_{(z=L0)}}{p_{u(z=L0)}} = -r_7 \qquad (4\text{-}31)$$

Similarly, it has been defined the parameter IP which is regulated by a subroutine that checks if the p_u value is reached at depth ranging between 0 and L_0 (cases P9 and P8).
Whenever one of the above exceeds the unity, it means a new region of the pressure profile has reached the yield. The pressure is then fixed as equal to p_u and the iteration process make the transition to the new successive case.
As an example, considering the case P1, a ratio r2 reaching the unity implicates the transition to the case P12, where the ultimate pressure is mobilized, positively, in the region 1 close to the pile's head (P1 case) and above the slip surface at z=Ls (proper of the case P2).

In order to reduce the analysed cases, all analysed and implemented cases can be derived from 8 more complex cases, all named following the nomenclature used for the single configurations. Their formulation is presented in Appendix A.
The several combinations of yield in the different zones include over 60 possible cases (showed in Appendix A). In order to optimise the FORTRAN code, the possible cases are all analysed by 8 generalised cases.

4.3.6.Failure modes

The analysis carried out by applying the developed soil-pile interaction model revealed three main failure modes, basically the same found by Viggiani [23]. Anyway, the particular hypothesis of the p_u profile along the pile length taking care of ground surface effects by varying linearly with depth instead of being assumed as zero, have implicated some differences in the resulting failure modes.
These cases here considered are involved when the pile is assumed not to reach its limiting tension (i.e. the bending moment acting on the pile is lower than its yield moment M_y); it is so assumed that failure occurs only in the soil:

- For low values of β, the Mechanism C, or "flow mode", governs the problem: when the depth of the slip surface is shallow and the soil strength of the sliding mass is fully mobilised, the pile results to be fixed in the stable layer while the sliding soil mass becomes plastic and flows around the pile. The pile deflection is considerably less than the soil movement. The shear stress at the sliding surface is available in explicit form:

$$\frac{T_C}{p_{u1}L} = \beta - \frac{1}{2}\lambda(1 - k_0) \qquad (4\text{-}32)$$

It is worth to be noticed that the value of T_C takes care of the assumed p_u distribution close to the pile head. The same values suggested by Viggiani for a two-layered cohesive soil with constants p_u values are obtained if k_0 is imposed equal to 1.
Moreover, the so described Mode C refers to three sub-configurations, named C1(also named 16200), C2 (16230) and C3 (16234), different each-other for the pile-soil pressure distribution below the sliding surface: C1 refers to a fully elastic pressure distribution, while C2 occurs when the limit soil resistance has been reached into the zone 3 and finally C3 where p_u is reached into both 3 and 4 zones (Figure 4-9).

Should be noted also that, as the mode C is reached, for higher value of the free-field soil the pile does not deflect anymore while the soil flows around it and the stress state on the pile does not change either.

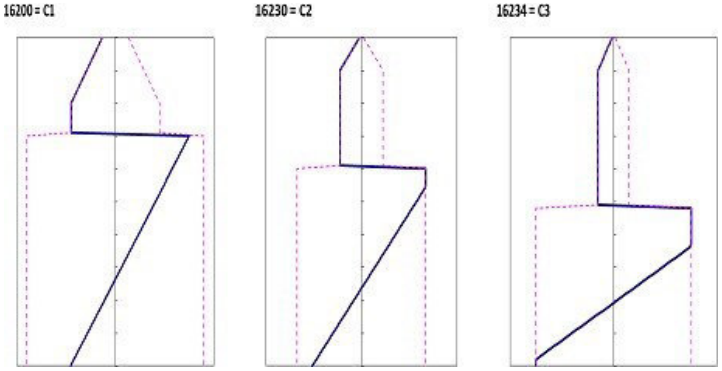

Figure 4-9: Soil pressure distribution for the different cases C1, C2 and C3. The dashed line represents the limit soil resistance distribution while the blue line the pile-soil reaction

- The mechanism A, or "short pile mode" occurs when the pile length embedded in the stable soil is shallow and the pile experiences excessive displacement due to soil failure in the stable layer; the firm layer fails and is ripped by the pile that translates together with the sliding mass: its rotation and the relative soil-pile displacement remain constant (together with its stress state) while the pile translates as a block together with the soil.
  In analogy with the previous Mode C, several different configurations have been found to be related to the mode A, and divided in groups A1 (when the soil pressure is fully elastic above the sliding surface), A2 (when p_u is reached in only one zone above the slip surface) and A3 (when p_u is reached in two different zones above the slip surface).
  Finally, the value of the shear force at the depth of the sliding surface coincides with the value found by Viggiani:

$$\frac{T_A}{p_{u1}L} = k(1-\beta) \qquad (4\text{-}33)$$

- The Mechanism B, or “intermediate mode”, becomes the most critical when the depth of the slip surface is relatively deep and the soil strength along the pile length in both unstable and stable layers is fully mobilised. According to the models presented by Viggiani [23] and Poulos [26], in this mode, the pile deflection at the upper portion exceeds the soil movement. Thanks to the soil-pile relative displacement evaluated in the model and the displacement approach used, the presented model can also take into account two groups of sub-modes, named as B1 and B2, respectively when the pile head displacement is greater or smaller than the soil one. This implicates that all the configurations B1 will include the plasticised zone 5, while for B1 is considered the zone 1. This is an improvement with regards to the solutions provided by Viggiani as they considered only the corresponding mechanism B1.

  Contrary to the mechanism A and C that are reached by the pile-soil system for a finite (and computable) free-field soil displacement, the limit states corresponding to the modes B1 and B2 are reached only asymptotically as it is considered that the pile-soil interaction along the full length of the pile attains the limiting force between the pile and soil. This ultimate state corresponds to an infinite pile deflection (the pile reclines horizontally). Four limit states are so defined and called B1-L1 and B2-L1, B1-L2 and B2-L2, respectively when the change between positive and negative pressure is above or below $z=\lambda L$. They are solved numerically.

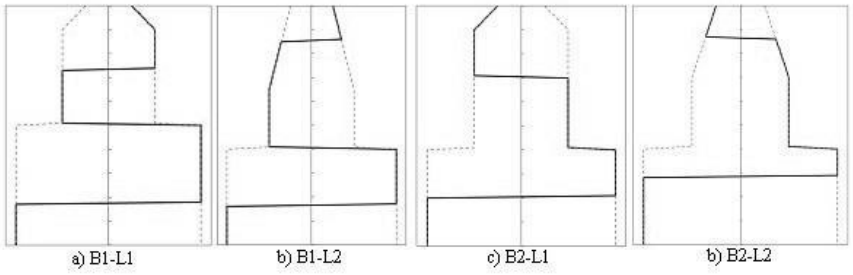

Figure 4-10: Soil pressure distribution for the different cases B1-L1, B1-L2, B2-L1 and B2-L2. The dashed line represents the limit soil resistance distribution while the continue line the pile-soil reaction

The complete formulation of the several failure modes is presented in Appendix A, where for each configuration the equations of shear forces and bending moments along the pile are expressed.

Since all the different mechanisms are defined, the lateral resistance of passive pile in a two-layered cohesive soil corresponds to the smaller of the three associated shear forces at the depth of the slip surface:

$$T_\beta = min(T_{A,}T_{B,}T_C) \qquad (4\text{-}34)$$

Figure 4-11 shows the dimensionless shear force offered by a pile in a two-layered cohesive soil at the depth of sliding, for different configurations.
In particular, it is noticeable that the results presented by Viggiani are the same obtained by considering a constant limit soil resistance within the first layer. Moreover, it is worth to highlight the influence of the ground surface effects on p_u: the relative values of the shear force are noticeable lower than those obtained for a constant value as a lower resistance is offered by the soil. The solutions provided by Viggiani also concern a larger range for the failure mode B.
Finally, in case the soil slides with a triangular distribution over depth (corresponding to η=0), for sliding depth deeper than about 0.65L, the shear force values becomes negative: it is an important result as, if the pile is used as a slope stabilising system, its contribution has to be considered null.

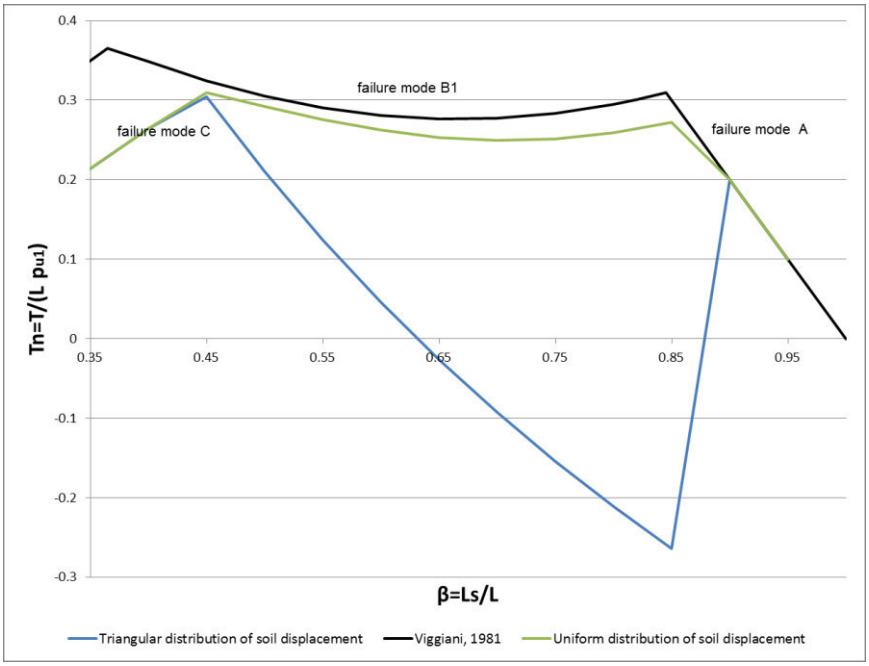

Figure 4-11: Dimensionless shear force induced in a two-layered cohesive soil at sliding depth as a function of the normalized sliding depth at the ultimate state for soil sliding with both a triangular and uniform distribution over depth (fixed $L_0/L=0.35$, $k_0=2/9$, $k=2.0$, eta=1. Only values for $L_s>L_0$ are shown)and the solutions as presented by Viggiani [23].

4.3.7.Design charts

As a design expedient, when it is not possible to carry out a complete site-specific analysis, useful design charts can be derived not only for the ultimate pile response to lateral movements (as suggested by Viggiani in 1981) but also for the maximum shear force the pile can provide in correspondence of different soil movements. Moreover, the maximum shear force given by the pile can be related to its head displacement or to the maximum bending moment.
A series of design charts are presented as example of the available output the code can develop. They give dimensionless curves for the normalised shear resistance T_n occurring at the depth of the slip surface for two cases, different each other only for the soil movement distribution shape: the first case considers a uniform distribution of the displacement, corresponding to η=1, while the second refers to η=0.
In each case, the following dimensionless quantities are indicated:

Dimensionless pile shear resistance at $z=L_s$:

$$T_n = \frac{T_{(z=Ls)}}{p_{u1}L} \qquad (4\text{-}35)$$

Dimensionless depth of the sliding surface:

$$\beta = \frac{Ls}{L} \qquad (4\text{-}36)$$

Dimensionless maximum bending moment:

$$M_n = \frac{M_{max}}{p_{u1}L^2} \qquad (4\text{-}37)$$

Dimensionless pile head displacement:

$$Y_{0n} = \frac{Y_0 E_{s1}}{p_{u1}} \qquad (4\text{-}38)$$

Dimensionless soil movement:

$$Y_{s0n} = \frac{Y_{s0} E_{s1}}{p_{u1}} \qquad (4\text{-}39)$$

Other assumed parameters are:

$$\lambda = L_0/L \ = \ 0.35 \qquad (4\text{-}40)$$

$$k = \frac{E_{s2}}{E_{s1}} = \frac{p_{u2}}{p_{u1}} = \ 2 \qquad (4\text{-}41)$$

$$k_0 = \frac{p_{u0}}{p_{u1}} = \ 2/9 \qquad (4\text{-}42)$$

The normalised shear force and moment for non-yielding piles are plotted against the normalised depth of the sliding surface for η=1 and η=0. For an assigned value of β, normalised shear force is calculated by the implemented code and is plotted in the graphs showed from the Figure 4-12 to the Figure 4-17. T_n is plotted also with reference to the relative external soil displacement y_s, the maximum normalised bending moment acting on the pile or the pile head deflection y_{0n}.

In all the charts, the dashed line represents the boundary of the elastic zone, corresponding to an external soil displacement equal to the threshold value. Within it, the relationships between shear forces, bending moments, pile and free-field soil displacements are linear. The equations correspond to those presented in the elastic method (and reported in Table 4-4).
The upper boundaries in all the charts represent the limit values of the shear force at the depth of the sliding surface. It is obtained by considering the minimum value among those obtained by implementing the different failure modes A, B and C at varying of β.

$$T_{n,limit} = min(T_A, T_B, T_C) \qquad (4\text{-}43)$$

Negative T_n values are not plotted as their contribution, in case the pile is used as a slope stabilising system, hast to be considered null.

Proportionality constants	
	$D = \beta^4 + 2k\beta(1-\beta)\{2-\beta+\beta^2\} + k^2(1-\beta)^4$
$y_{0n} = \frac{N_y}{D} y_{s0n}$	$N_y = \beta^4(1-k) + 2k\beta(1+\eta) - k\beta^2(1+2\eta)$
$tan\omega = \frac{N_t}{D} y_{s0n}$	$N_t = \beta^3(1-k)(1-\eta) + 3k\beta(1+\eta) - 2k\beta^2(1+2\eta)$
Shear force at sliding depth	$\frac{T_\beta}{p_{u1}L} = \frac{k(1-\beta)}{2D}\left[2N_y - N_t(1+\beta)\right] y_{s0n}$
Shear forces at sliding depth in function of maximum bending moment	$\frac{T_\beta}{p_{u1}L} = \frac{3(1-\beta)\left[2N_y - N_t(1+\beta)\right]}{4} \frac{{N_{\Delta t}}^2}{\left\lvert N_{\Delta y}\right\rvert^3} M_{1\max,n}$
	$\frac{T_\beta}{p_{u1}L} = \frac{3(1-\beta)\left[2N_y - N_t(1+\beta)\right]}{4} \frac{{N_t}^2}{\left\lvert N_t - N_y\right\rvert^3} M_{2\max,n}$

Table 4-4: Proportionality constants and elastic solutions for shear forces and bending moments for a passive free-head rigid pile in a two-layered cohesive soil

Results for η=1 case:

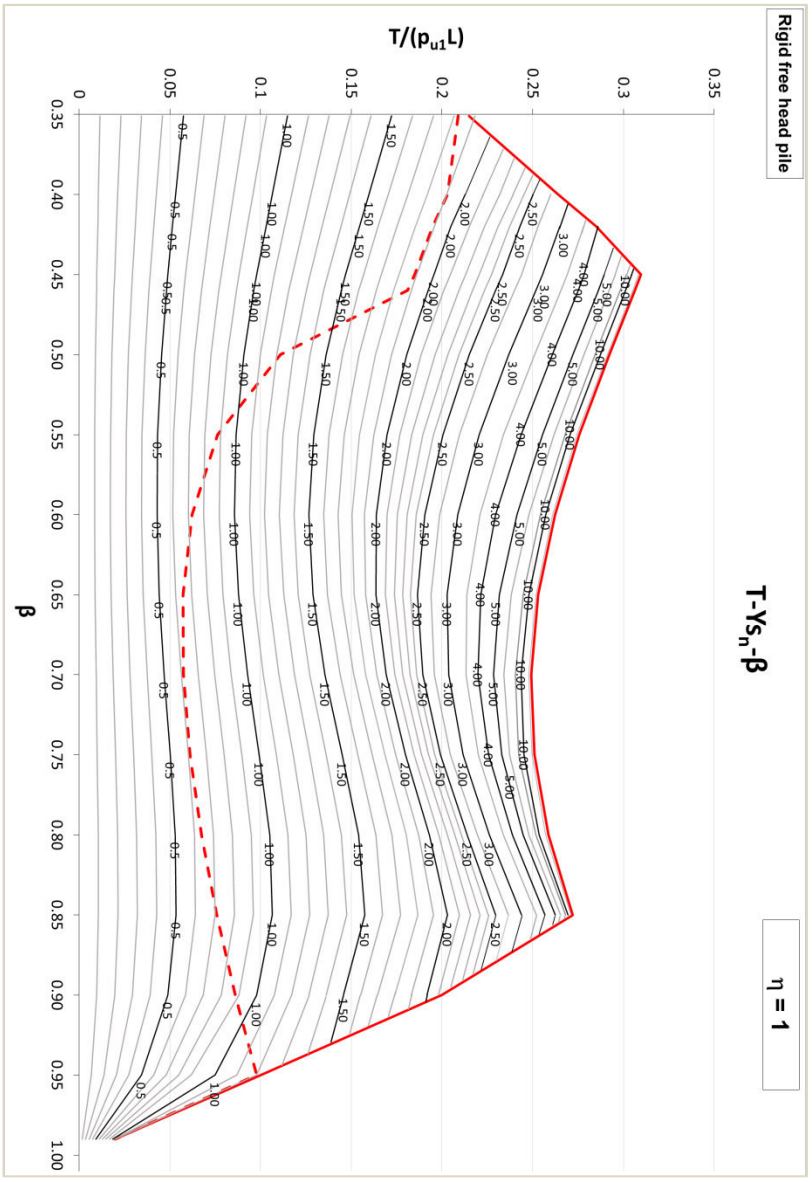

Figure 4-12: Design curves for piles in two layered cohesive soil; L_0/L=0.35, k_0=2/9, k=2.0, eta=1; non-dimensional shear force T_n over β and y_{sn}. Dotted line represents the limit elastic solutions and the red one the ultimate pile resistance

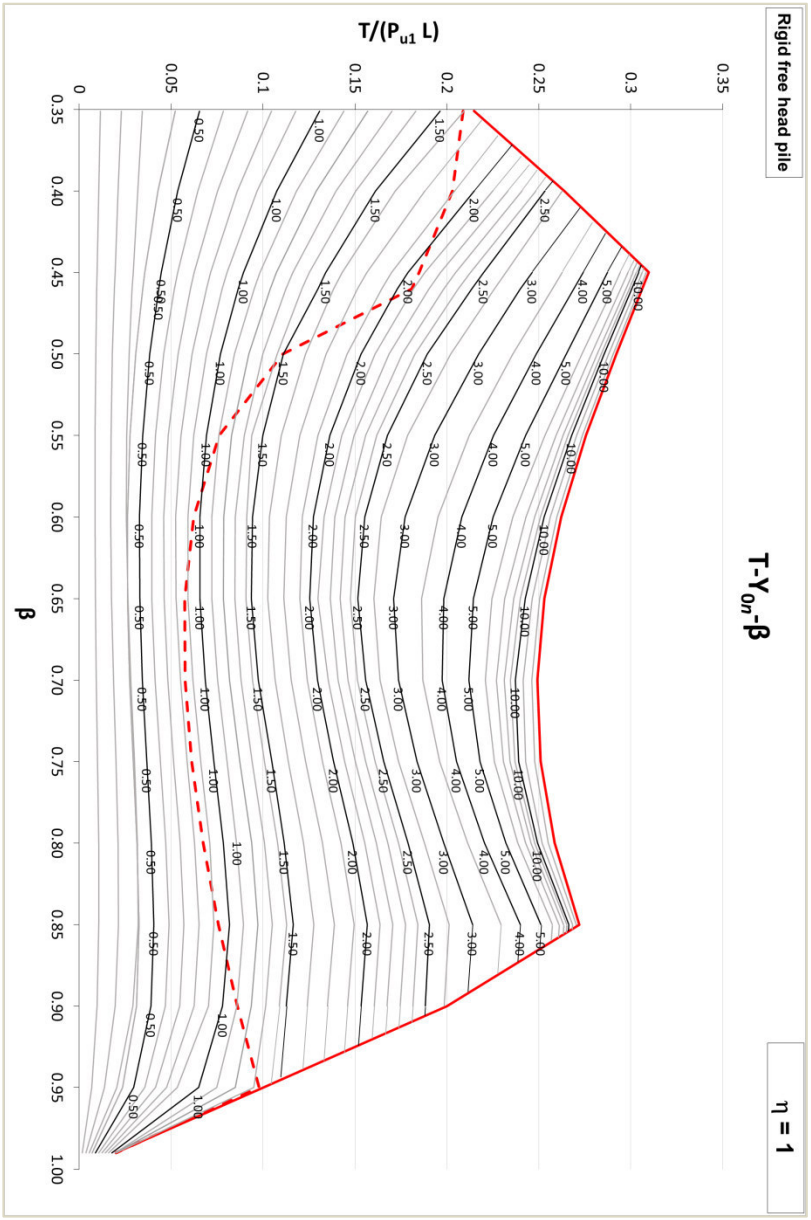

Figure 4-13: Design curves for piles in two layered cohesive soil; L_0/L=0.35, k_0=2/9, k=2.0, eta=1; non-dimensional shear force T_n over β and y_{0n}. Dot line represents the limit elastic solutions and the red one the ultimate pile resistance

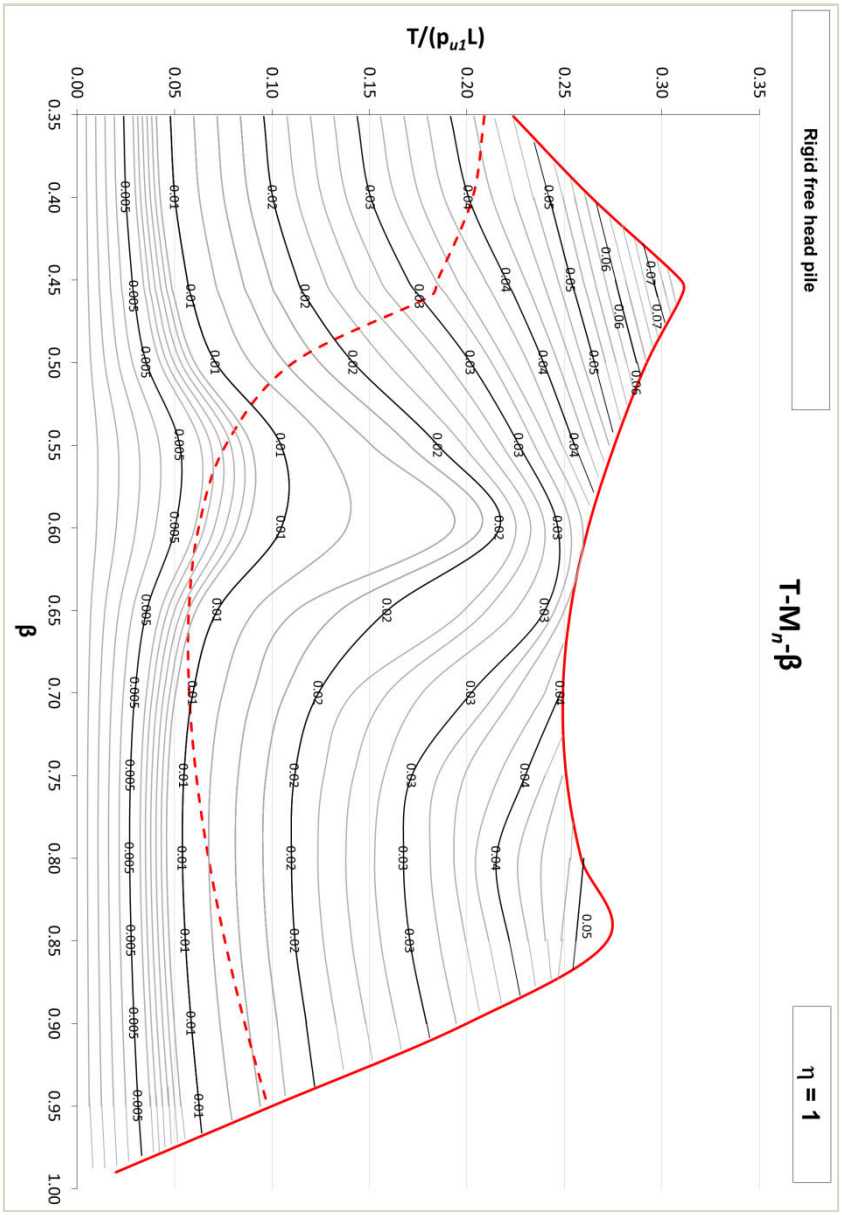

Figure 4-14: Design curves for piles in two layered cohesive soil; L_0/L=0.35, k_0=2/9, k=2.0, eta=1; non-dimensional shear force T_n over β and M_n. Dot line represents the limit elastic solutions and the red one the ultimate pile resistance

Results for η=0 case

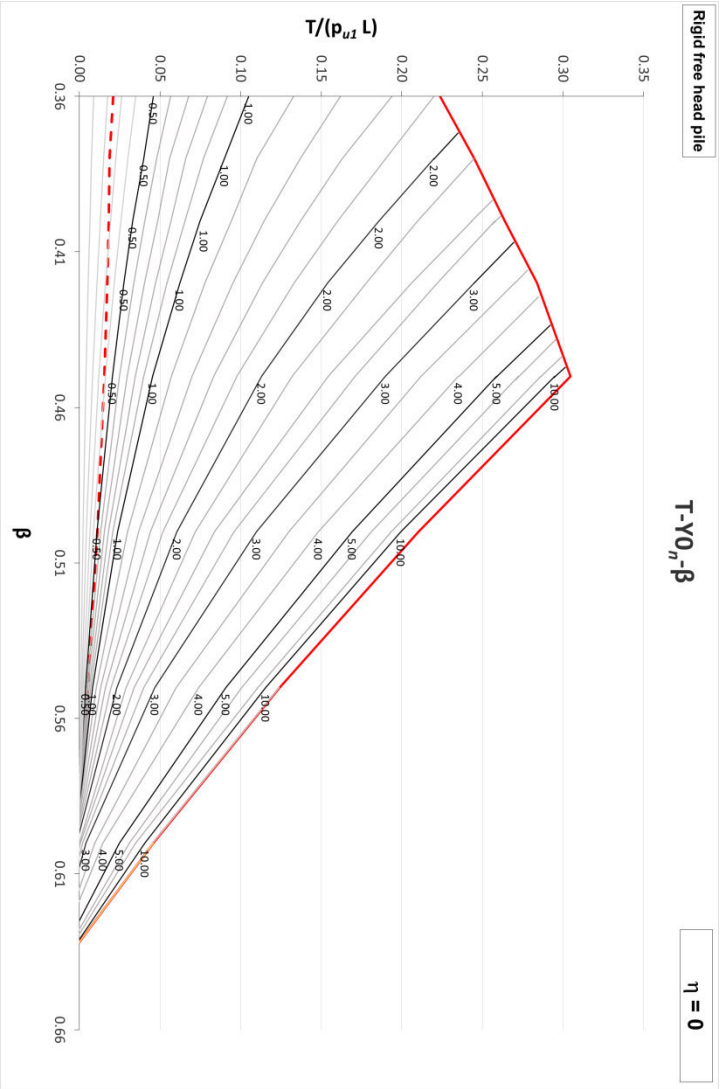

Figure 4-15: Design curves for piles in two layered cohesive soil; L_0/L=0.35, k_0=2/9, k=2.0, eta=0; non-dimensional shear force T_n over β and Y_{0n}. To be noticed the negative values of T_n for y_s>0.57. Dot line represents the limit elastic solutions and the red one the ultimate pile resistance

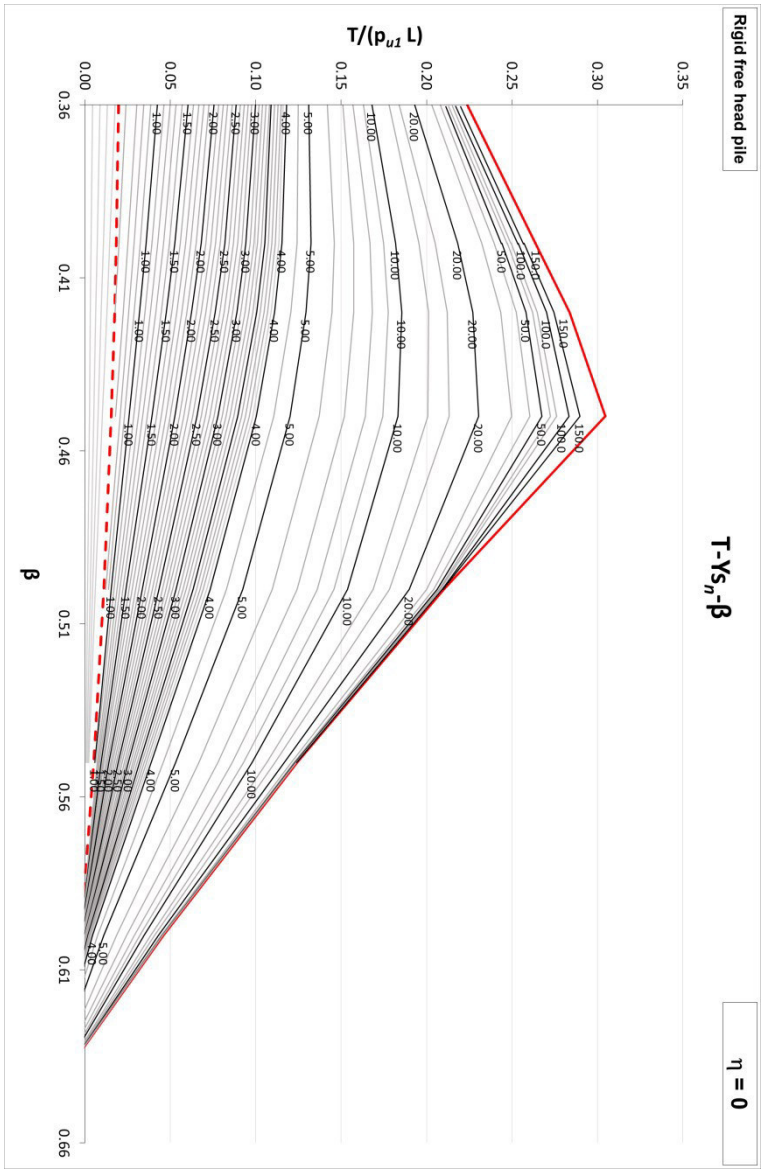

Figure 4-16: Design curves for piles in two layered cohesive soil; $L_0/L=0.35$, $k_0=2/9$, $k=2.0$, eta=0; non-dimensional shear force T_n over β and y_{sn}. Dot line represents the limit elastic solutions and the red one the ultimate pile resistance

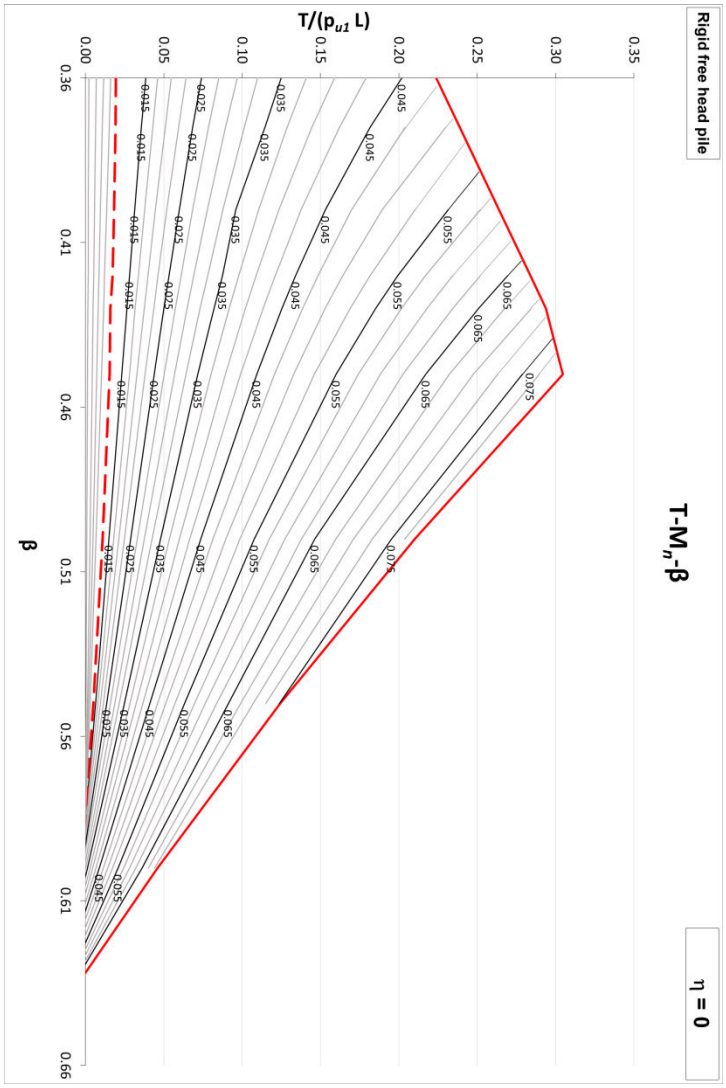

Figure 4-17: Design curves for piles in three layered cohesive soil; $L_0/L=0.35$, $k_0=2/9$, $k=2.0$, eta=0; non-dimensional shear force T_n over β and M_n. Dot line represents the limit elastic solutions and the red one the ultimate pile resistance

4.3.8. Results and discussion

Depending on both the geometry of the problem , the stiffness and strength of the stable and sliding soils, the result presented in the confirm the three main failure mechanisms. This is in agreement with results obtained by Viggiani [23] and Poulos [26] in their analysis of pile-stabilized slopes:

- For low values of β, the Mechanism C, or "flow mode", governs the problem: in this case the pile deflection is considerably less than the soil movement. For practical uses, Poulos endorsed the flow mode that creates the least damage from soil movement on the pile. It is also the same failure mode analysed by Kourkoulis et al. ([22][21]) .
- At increasing β, there is a first threshold value of β above which the Mechanism B, or "intermediate mode", becomes the most critical. According to the models presented by Viggiani [23] and Poulos [26], in this mode, the pile deflection at the upper portion exceeds the soil movement. Thanks to the soil-pile relative displacement evaluated in the model and the displacement approach used, the presented model can also take into account two sub-modes B1 and B2, respectively when the pile head displacement is greater or smaller than the soil one.

- Finally, there is the Mechanism A, or "short pile mode": when the pile length embedded in the stable soil is shallow and the pile will experience excessive displacement due to soil failure in the stable layer; the firm layer fails and is ripped by the pile that translates together with the sliding mass

Over these three modes of soil failure, there is the hypothesis of the finite strength of the pile. The "long pile failure" occurs when, in one or more point along the pile length, the maximum bending moment of the pile reaches the yields moment (the yielding moment M_y) of the pile section and the pile structural failure takes place ($M_{max} = M_y$), developing plastic hinges, generally even without fully mobilising the soil resistance. It is left to singular case to check that the stress state acting on the pile is compatible with the structural resistance of the pile: as the normalised shear force is presented in function of the maximum bending moment (Figure 4-14 and

Figure 4-17), it is possible to compare it with the plastic moment M_y and verify the compatibility of the stresses on the designed pile.

What is interesting about the data showed in the charts is that the ultimate lateral pile load is associated with the relative soil free-pile external displacement y_{s0} necessary to mobilise it and to the pile head deflection y_0, in order to verify if specific service requirements are satisfied.
In particular, for the mechanism A and C the model can evaluate the exact values of both y_{s0} and y_0. This is an improvement in the results suggested in the literature, where these failure mechanisms are derived from the assumption of full mobilisation of the soil resistance without any information about the pile and soil displacements.
For what concerns the B mechanism, the relative ultimate lateral pile load is, by definition, associated with an infinite displacement of the pile and is reached only asymptotically by the soil-pile system. Nevertheless, the model is able to furnish an esteem of real y_{s0} and y_0 values, associated to pile reactions close in magnitude to the limit ones.

Analysing more in particular the results presented from the Figure 4-12 to the Figure 4-17, it is noticeable how the case of a soil sliding as a block mass (η=1), all the three failure mechanism are activated at varying of the sliding surface depth (the mechanism B becomes predominant for β higher than 0.45 while the mechanism A is activated when β passes 0.85). In the case of a triangular inverse distribution of the soil free-field displacement, the mechanism A does not occur and the pile is not able to furnish a positive reaction in term of shear force for values of β higher than about 0.65.

For both the configurations, the maximum contribute in terms of shear force in correspondence of the limit state is provided for β values close to 0.45 (i.e. when the pile is embedded for almost half of its length in the firm layer), in correspondence to the transition from the mechanism C to the mechanism B.

In both cases, the maximum normalised shear force is close to 0.3, associated with a maximum normalised bending moment of about 0.06-0.075 and to a normalised pile head deflection equal to 10.
Instead, the relative soil displacement at ground level is different in size between the two cases: y_{0n} is equal to 10 in case of $\eta=1$ and it increases to 150 for $\eta=0$, where, due to the soil distribution shape, a higher top value is necessary to deflect the pile and mobilise its resistance.

4.4. Elasto-plastic analysis of passive rigid piles in a homogeneous non-cohesive soil

Similarly to the nonlinear method developed for a two-layered soil with a constant modulus of subgrade reaction, the present chapter shows a nonlinear method concerning a homogeneous soil modelled according to a Gibson model, having then both the modulus of subgrade reaction and the ultimate lateral pressure increasing with depth. It is the case of sands and normally consolidated clays under long-term loading, for which it is reasonable to assume that the modulus of subgrade reaction varies linearly with depth.
Solutions for an active pile embedded in an analogue soil stratigraphy are already been found by Zhang [3] who developed a computational method for predicting the displacement of an active laterally loaded rigid pile in cohesionless soil that, for small displacements, were assumed to rotate about a single point.

The soil stratigraphy here investigated also coincides with the one analysed in paragraph 3.8. As improvement of the elastic solutions there presented, this method aims to consider the development of soil resistance with the shaft deflection, elaborating complete solutions for the intermediate states between the elastic and the ultimate ones, as they are determined in function of the external free-field soil displacement and of the associated pile deflection.
For this reason, the previous model only concerning an elastic behaviour of the soil has been modified and enhanced in order to account for the soil reaction distribution with yielding in one or more regions.

4.4.1.Geometry, constitutive model and ultimate soil resistance p_u

The investigated problem concern a single rigid pile of length L and diameter D is embedded in a homogeneous soil, moving along a slip surface located at a depth of $L_s=\beta L$. The Figure 4-18 shows the problem under consideration in the present paragraph.

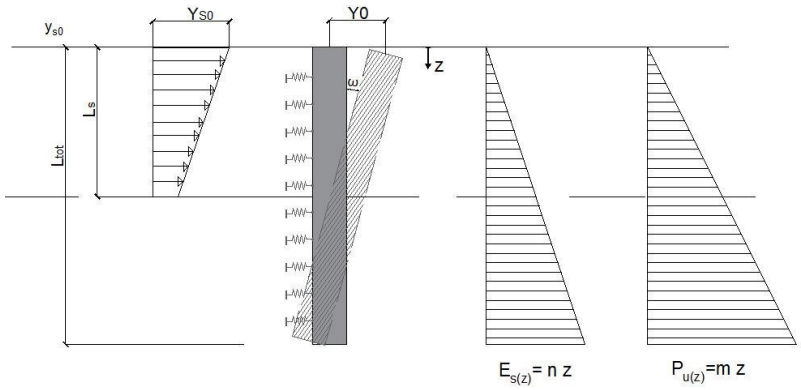

Figure 4-18: Soil displacement distribution, pile displacement geometry, distributions of the subgrade reaction modulus and of the ultimate soil pressure for a rigid pile in cohesionless soil

Once again, the distribution of the soil movement along L_s is assumed to be linear with depth and defined through the soil top displacement parameters y_{s0} and the ratio η, varying from a triangular variation with depth when no displacement occurs in correspondence of the slip surface (η=0) to a uniform distribution, when the unstable soil layer slides down as a unique mass block (η=1). Intermediate values of η describe a generic trapezoidal profile of the soil movement.

The on-pile force (per unit length), $p_e(z)$, at any depth is proportional to the local displacement of the soil-pile interface, $\Delta y_{(z)}$, and to the modulus of subgrade reaction. For sands and for normally consolidated clays under long-term loading, it is reasonable to assume that the modulus of subgrade reaction varies linearly with depth, so that E_s [FL^{-2}] can be expressed as

$$Es(z) = n\,z \qquad (4\text{-}44)$$

where:
n= gradient of the horizontal subgrade reaction modulus (FL^{-3})

With the above assumptions and assuming there is no soil-yielding, the elastic soil reactions along the whole length L of the pile can be expressed as:

$$p_{e(z)} = -nz\left(y_{0(z)} - y_{s(z)}\right) = -nz[(y_0 - y_{s0}) - (tan\,\omega - tan\,\alpha)z]$$
$$= -nz(\Delta y_0 - z\Delta t) \qquad [FL\text{-}1] \quad 0<z<Ls \qquad (4\text{-}45)$$

$$p_{e(z)} = -nz[y_0 - z\,tan\,\omega] \qquad [FL\text{-}1] \quad Ls<z<L \qquad (4\text{-}46)$$

Several expressions have been proposed in the literature to describe the variation of limiting soil pressure p_u with depth (Brinch Hansen [47], Reese et al [48]) for a cohesionless soil.
As shown in Figure 4-18, in the present model it is assumed that soil resistance p_u varies proportionally with depth [42]:

$$p_u = mz \qquad [FL^{-1}] \qquad (4\text{-}47)$$

No complete agreement has been reached yet on the analytical expression of *m* (cf. paragraph 4.1); even if a deeper investigation is left to what already mentioned, for a good fruition of the results, it can be considered what suggested by Broms [1] who expressed the gradient of the average ultimate pressure across the width of a pile as:

$$m = 3 \cdot D \cdot K_p \cdot \gamma' \qquad [FL^{-1}] \qquad (4\text{-}48)$$

where K_p is the Rankine passive pressure coefficient,

$$K_p = tan^2\left(45 + \frac{\varphi\prime}{2}\right) \qquad (4\text{-}49)$$

γ' the effective soil unit weight and D the pile diameter. As the formulation presented resulted in giving underestimated values when compared to field test, other authors [42] found that the data from lateral pile tests could be matched sufficiently by the simple variation given by

$$m = D \cdot {K_p}^2 \cdot \gamma' \qquad [FL^{-1}] \qquad (4\text{-}50)$$

It has to be noticed that for almost all naturally occurring sand, K_p^2 will be greater than 3.

4.4.2.Method of analysis, first yielding cases and threshold soil displacements

Similarly to the solutions developed for the elastic case, the non-linear analysis method solves the equations of the soil-pile system with the soil represented as linear springs providing resisting forces that increase with lateral deflection. Once again, by considering horizontal force and moment equilibrium along the pile length, a system of two equations in two variables y_0 and tanω is derived.
From the elastic field, the progressive increment of soil and pile movements lead the soil-pile system to enter the plastic fields and the pressures to reach a first yielding point at a certain depth or region of the soil-pile interface. The non-linear system of the relative to soil reaction distribution with yielding in one or more regions are numerically solved by an implemented FORTRAN code, similar to the one presented for the case of a two-layered cohesive soil, which applies the bisection method for solving the equilibrium equations until the variables y_0 and tanω are obtained.

Due to the assumed geometry (in particular η and β parameters), the stiffness and resistance ratios (n,m), a different first yielding case is expected.In particular, five different singular yielding regions have been identified and developed, occurring in correspondence of likewise points in the ultimate soil pressure profile: they are located at depth z_n=0 (cases P1 and P5), z_n=β (cases P2, P3), z_n=1 (case P4).
Starting from the elastic solution and imposing the yielding criterion at the relative depth, the threshold soil displacement can be found.
In example, for the zone 1 (located at depth z_n=0 and with a positive yielding pressure at pile head) and introducing the elastic proportionality constants:

$$y_{0n} = \frac{y_0}{L} = N_y \frac{y_{s0}}{L} \qquad (4\text{-}51)$$

$$\Delta y_{0n} = \frac{\Delta y_0}{L} = N_{\Delta y} \frac{y_{s0}}{L} \qquad (4\text{-}52)$$

the threshold soil displacement is calculated as follow ($c<L_s$):

$$p_{e(z=c)} = p_{u(z=c)} \qquad (4\text{-}53)$$

$$-nc(\Delta y_0 - c\Delta t) = mc \qquad (4\text{-}54)$$

$$-n(\Delta y_0 - c\Delta t) = m \qquad (4\text{-}55)$$

$$(\Delta y_0 - c\Delta t) = -\frac{m}{n} \qquad (4\text{-}56)$$

By imposing z=0:

$$\Delta y_0 = -\frac{m}{n} \qquad (4\text{-}57)$$

$$N_{\Delta y} y_{s0} = -\frac{m}{n} \qquad (4\text{-}58)$$

$$y_{s0} = -\frac{m}{nN_{\Delta y}} \qquad (4\text{-}59)$$

$$\left(y_{s0}\frac{n}{m}\right)_{lim1} = -\frac{1}{N_{\Delta y}} \qquad (4\text{-}60)$$

The Table 4-5 presents the characteristic normalised threshold soil displacement, expressed as function of the elastic proportionality constants D, N_y, N_t, $N_{\Delta y}$ and $N_{\Delta t}$ for a free-head rigid pile in a Gibson soil model as presented in Table 3-20.
As already mentioned, the pile-soil pressures on the pile are assumed positive if acting in the same direction of the soil displacement.

CASE	Threshold soil displacement
CASE P1 (positive yielding at z = 0)	$\left(y_{s0}\frac{n}{m}\right)_{lim1} = -\frac{1}{N_{\Delta y}} = \frac{1}{1-N_y}$
CASE P5 (negative yielding at z = 0)	$\left(y_{s0}\frac{n}{m}\right)_{lim1} = \frac{1}{N_{\Delta y}} = \frac{1}{N_y - 1}$
CASE P2 (positive yielding at z = β)	$\left(y_{s0}\frac{n}{m}\right)_{lim2} = \frac{1}{\beta N_{\Delta t} - N_{\Delta y}} = \frac{1}{\eta + \beta N_t - N_y}$

CASE P3 (negative yielding at z = β)	$\left(y_{s0}\frac{n}{m}\right)_{lim3} = \frac{1}{N_y - \beta N_t}$
CASE P4 (positive yielding at z =1)	$\left(y_{s0}\frac{n}{m}\right)_{lim4} = \frac{1}{N_t - N_y}$

Table 4-5: Threshold soil displacements for a homogeneous Gibson soil

The yielding regions so identified can be considered as basic components of the more complex cases that occur with the increasing of the imposed free-field soil displacement and their nomenclature is used to describe and mention the successive complex cases (Figure 4-19).

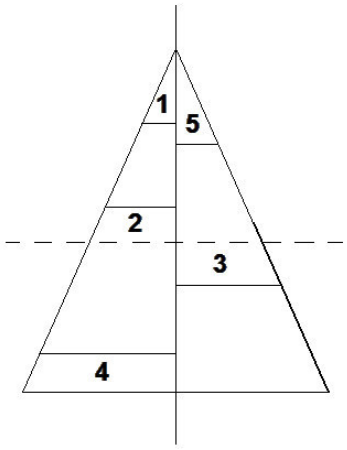

Figure 4-19: Identified yielded region and their nomenclature

For the purpose of calculation and presentation, all analysed and implemented cases can be derived from two more complex cases, all named following the nomenclature used for the single configurations.
The formulation of the 24 identified cases is presented in Appendix B.

4.4.3.Failure modes

The analysis carried out by applying the developed soil-pile interaction model to a homogeneous soil revealed the same three main failure modes presented for a two-layered cohesive soil:

- For low values of β, the Mechanism C, or "flow mode", governs the problem: when the depth of the slip surface is shallow and the soil strength of the sliding mass is fully mobilised, the pile results to be fixed in the stable layer while the sliding soil mass becomes plastic and flows around the pile. The pile deflection is considerably less than the soil movement. The shear stress at the sliding surface can be expressed in explicit form:

$$T_{C,m} = \frac{T_C}{mL^2} = \frac{1}{2}\beta^2 \qquad (4\text{-}61)$$

The so described Mode C refers to three sub-configurations, named C1, C2 and C3 different each-other for the pile-soil reaction distribution below the sliding surface: C1 refers to a fully elastic pressure distribution, while C2 considers that the limit soil resistance has been reached into the zone 3 and finally C3 where p_u is reached into both 3 and 4 zones (Figure 4-9).
Should be noted also that, as the mode C is reached, for higher value of the free-field soil the pile does not deflect anymore while the soil flows around it and the stress state on the pile does not change either.

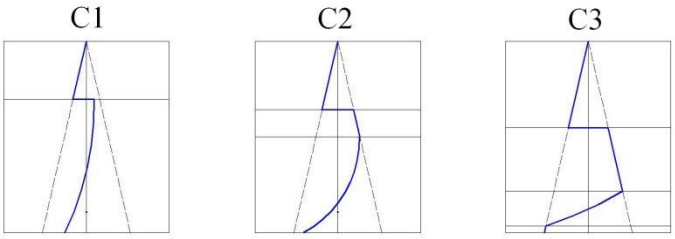

Figure 4-20: Soil pressure distribution for the different cases C1, C2 and C3. The dashed line represents the limit soil resistance distribution while the continue one the pile-soil profile

- The mechanism A, or "short pile mode" is involved when the pile has a shallow embedment in the stable soil and experiences excessive displacement due to soil failure in the stable layer; the firm layer fails and is ripped by the pile that translates together with the sliding mass: the pile maintains constant rotation and relative soil-pile displacement (together with its stress state) while it translates as a block together with the soil.
  In analogy with the previous Mode C, several different configurations have been found to be related to the mode A, and divided in groups A1 (when the soil pressure is fully elastic above the sliding surface), A2 (when p_u is reached in also in the zone 5 above the slip surface) and A3 (when p_u is reached in zones 5 and 2 above the slip surface).

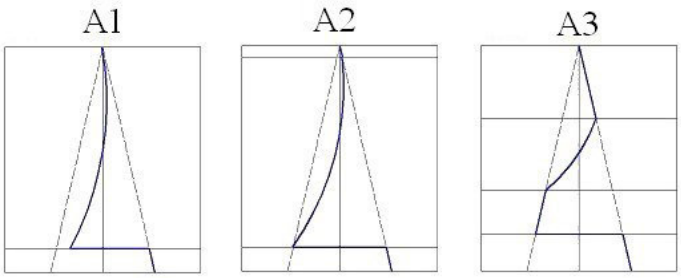

Figure 4-21: Soil pressure distribution for the different cases A1, A2 and A3. The dashed line represents the limit soil resistance distribution while the continue one the pile-soil reaction

For the mode A, the value of the shear force at the depth of the sliding surface coincides with the value found by Viggiani:

$$T_{A,m} = \frac{T_A}{mL^2} = \frac{1}{2}(1-\beta^2) \qquad (4\text{-}62)$$

- The Mechanism B, or "intermediate mode", becomes the most critical when the depth of the slip surface is relatively deep and the soil strength along the pile length in both unstable and stable layers is fully mobilised. The solutions presented by Viggiani [23] and Poulos [26] for cohesive soils recognise that

the pile deflection at the upper portion exceeds the soil movement. The presented model can also take into account two groups of sub-modes, named as B1 and B2, respectively when the pile head displacement is greater or smaller than the soil one. This implicates that all the configurations B1 will include the plasticised zone 5, while for B1 is considered the zone 1.

Contrary to the mechanism A and C that are reached by the pile-soil system for a finite (and computable) free-field soil displacements value, the limit states corresponding to the modes B1 and B2 are reached only asymptotically as it is considered that the pile-soil interaction along the full length of the pile attains the limiting force between the pile and soil. This ultimate state corresponds to infinite pile deflection (the pile reclines horizontally). Two limit states are so associated with the modes B1 and B2.

For the limit case B1 the normalised shear force is:

$$\frac{T_{B1}}{mL^2} = \frac{1}{2}\beta^2 - x_n^2 \qquad (4\text{-}63)$$

where x_n and y_n depend on β and their solution is admissible if

$$0 < x_n < \beta \qquad (4\text{-}64)$$

and

$$\beta < y_n < 1 \qquad (4\text{-}65)$$

In the appendix B, values of x_n and y_n are listed for different values of β. Similarly, for the limit case B2 :

$$\frac{T_{B2}}{mL^2} = x_n^2 - \frac{1}{2}\beta^2 \qquad (4\text{-}66)$$

where x_n and y_n do not depend on β and are:
$x_n \approx 0.4545$
$y_n \approx 0.84$

their solution is admissible if

$$x_n < \beta < y_n \qquad (4\text{-}67)$$

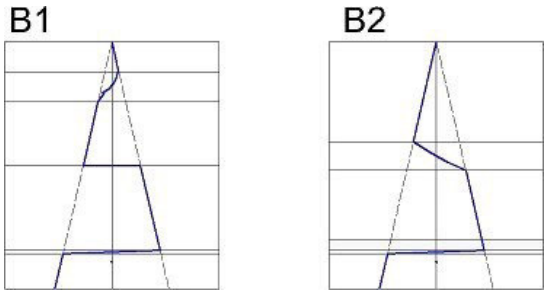

Figure 4-22: Soil pressure distribution for the different cases B1 B2-L2. The dashed line represents the limit soil resistance distribution while the continue line the pile-soil reaction

The complete formulation of the several failure modes is presented in Appendix B, where for each configuration the equations of shear forces and bending moments along the pile are expressed.

Lateral resistance of passive pile in a two-layered cohesive soil corresponds to the smaller of the three shear forces associated with the respectively defined mechanism, evaluated at the depth of the slip surface:

$$T_\beta = min(T_A, T_B, T_C) \qquad (4\text{-}68)$$

Figure 4-23 shows the dimensionless shear force offered by a pile in a non-cohesive soil at the depth of sliding, for different configurations. In case the soil slides with a triangular distribution over depth (corresponding to η=0), for sliding

depth deeper than about 0.65L, the shear force values becomes negative: it is an important result as, if the pile is used as a slope stabilising system, its contribution has to be considered null.

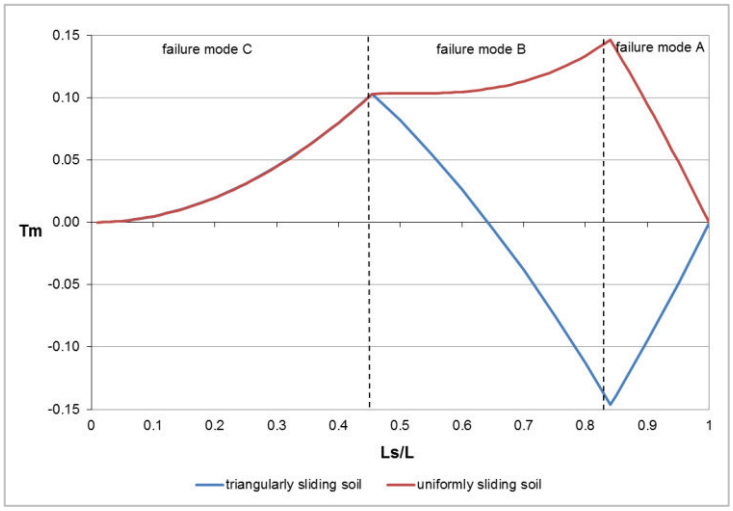

Figure 4-23: Dimensionless shear force $T_m=T/(mL^2)$ offered by a pile in a non-cohesive soil at the sliding depth for different configurations: soil sliding with a triangular distribution over depth, soil sliding with a uniform distribution over depth

4.4.4.Design charts

A series of design charts is presented as result of the analysis.
They give dimensionless curves for the normalised shear resistance T_m occurring at the depth of the slip surface for two distinct cases, different each other only for the soil movement distribution shape: the first case considers a uniform distribution of the soil displacement, corresponding to η=1, while the second refers to η=0.
In each case, the following dimensionless quantities are indicated:
Dimensionless pile shear resistance at z=Ls:

$$T_m = \frac{T_{(z=Ls)}}{mL^2} \qquad (4\text{-}69)$$

Dimensionless depth of the sliding surface:

$$\beta = \frac{Ls}{L} \qquad (4\text{-}70)$$

Dimensionless maximum bending moment:

$$M_{max,m} = \frac{M_{max}}{mL^3} \qquad (4\text{-}71)$$

Dimensionless pile head displacement:

$$Y_{0n} = \frac{Y_0\, n}{m} \qquad (4\text{-}72)$$

Dimensionless soil movement:

$$Y_{s0n} = \frac{Y_{s0} n}{m} \qquad (4\text{-}73)$$

The normalised shear force and moment for non-yielding piles are plotted against the normalised depth of the sliding surface for η=1 and η=0. For an assigned value of β, normalised shear force is calculated by the implemented code and is plotted in the charts. T_n is plotted also with reference to the relative external soil displacement y_s, the maximum normalised bending moment acting on the pile or the pile head deflection y_{0n}.

In all the charts, the dashed line represents the boundary of the elastic zone, corresponding to an external soil displacement equal to the threshold value. Within

it, the relationships between shear forces, bending moments, pile and free-field soil displacements are linear. The equations correspond to those presented in the elastic method (and reported in Table 4-6).
The upper boundaries in all the charts represent the limit values of the shear force at the depth of the sliding surface. It is obtained by considering the minimum value among those obtained by implementing the different failure modes A, B and C at varying of β.

$$T_{m,limit} = min(T_{A,}T_{B,}T_{C}) \qquad (4\text{-}74)$$

Negative T_n values are not plotted as their contribution, in case the pile is used as a slope stabilising system, hast to be considered null.
It is worth to be noticed that due to the normalisation made on the parameters, they result to be applicable to every case that corresponds to the assumed geometry and in which the soil can be modelled according to the Gibson model.

	Proportionality constants
$y_{0n} = N_y y_{s0n}$	$N_y = \frac{\beta^2}{3}(1+2\eta)$
	$N_t = \beta^2[(4-3\beta)+\eta(8-9\beta)]$
Shear force at sliding depth	$\frac{T_\beta}{mL^2} = \frac{1}{6}\beta^2\left(-3N_{\Delta y} + 2\beta N_{\Delta t}\right)y_{s0n}$

Table 4-6: Proportionality constants and elastic solutions for shear forces and bending moments for a passive free-head rigid pile in a non-cohesive soil

CHARTS FOR T_m OVER β AND Y_{s0n}

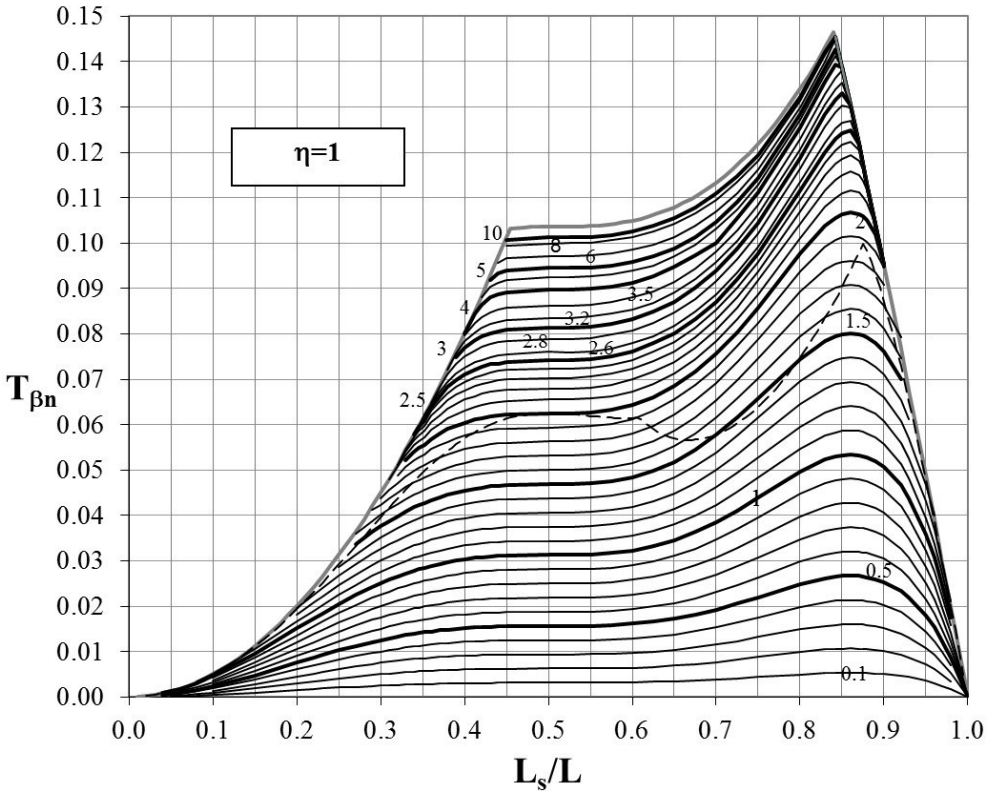

*Figure 4-24: Curves of normalised shear force T_m over L_s/L for η=1. Numbers indicates the external normalised soil displacement y_{s0}*m/n. Dashed line represents the limit elastic solutions*

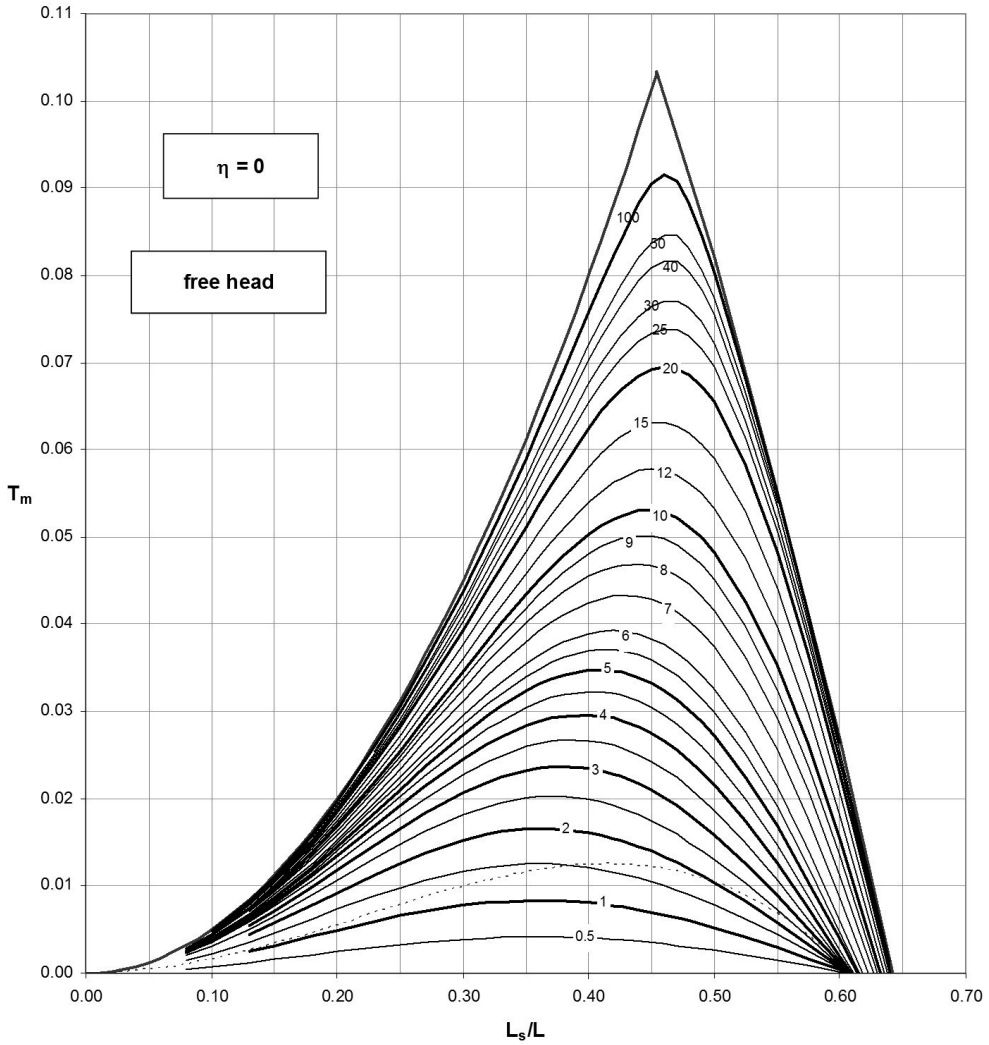

*Figure 4-25: Curves of normalised shear force T_m over Ls/L for η= 0. Numbers indicates the external normalised soil displacement y_{s0}*m/n. Dashed line represents the limit elastic solutions*

CHARTS FOR T_m OVER β AND Y_{0n}

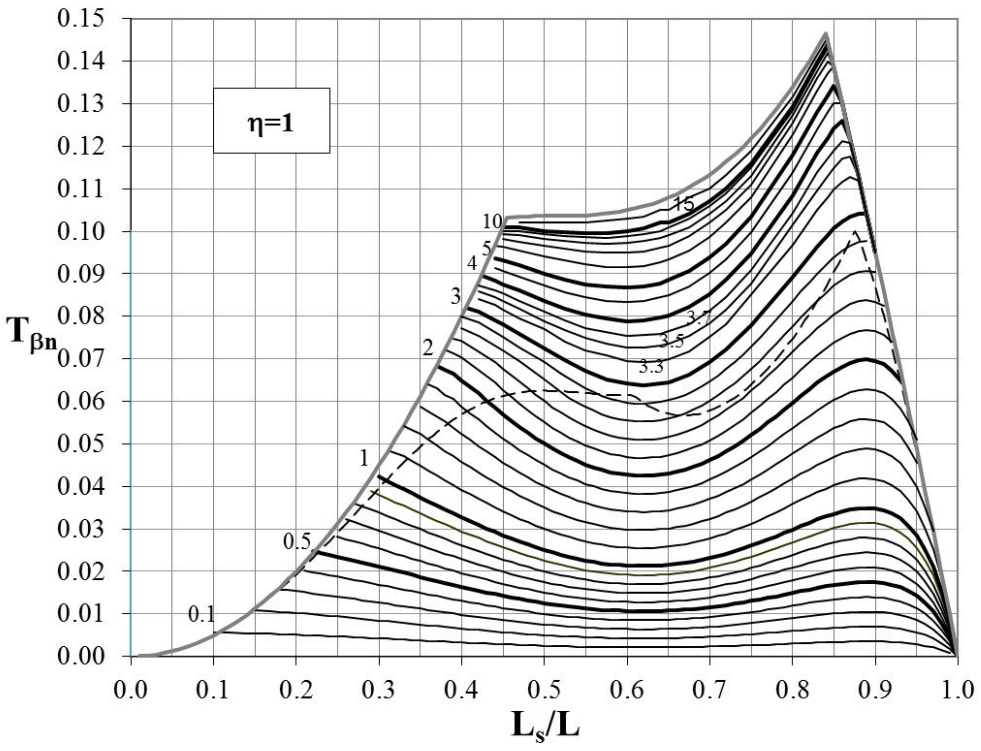

*Figure 4-26: Curves of normalised shear force T_m over Ls/L for η=1. Numbers indicates the external normalised pile head displacement y0*m/n. Dashed line represents the limit elastic solutions*

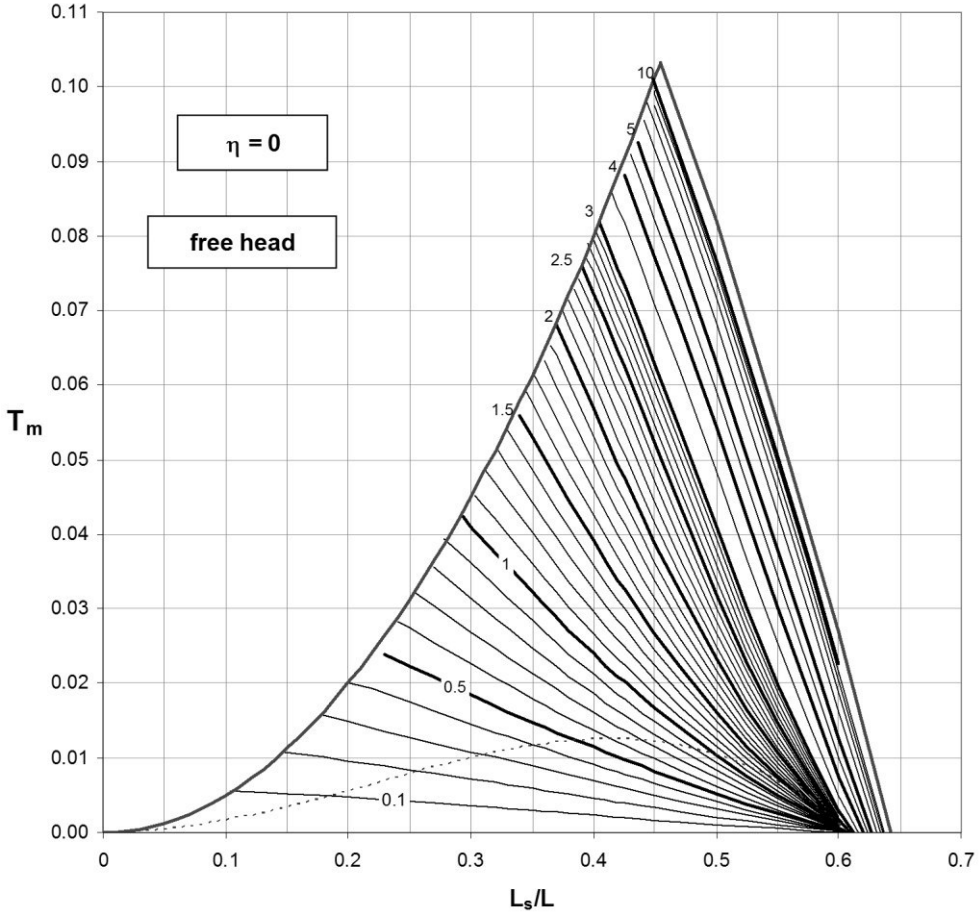

*Figure 4-27: Curves of normalised shear force T_m over Ls/L for η=0. Numbers indicates the external normalised pile head displacement y0*m/n. Dashed line represents the limit elastic solutions*

CHARTS FOR T_m OVER β AND $M_{max,m}$

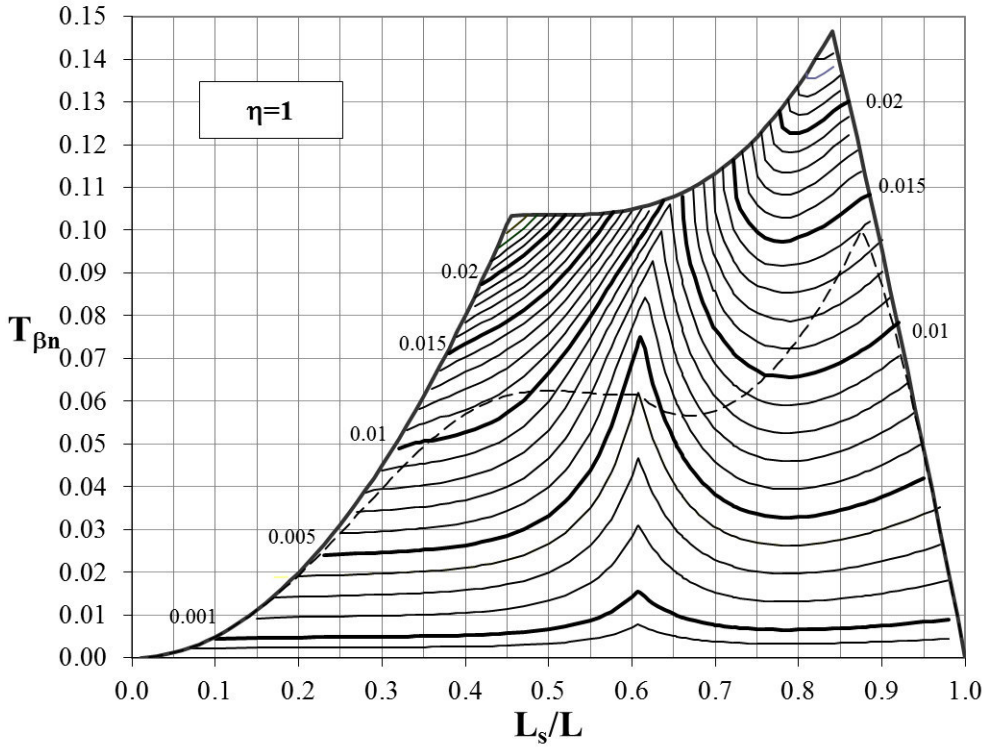

Figure 4-28: Curves of normalised shear force T_m over Ls/L for η=1. Numbers indicates the normalised maximum bending moment $M_{max}/(mL^3)$. Dashed line represents the limit elastic solutions

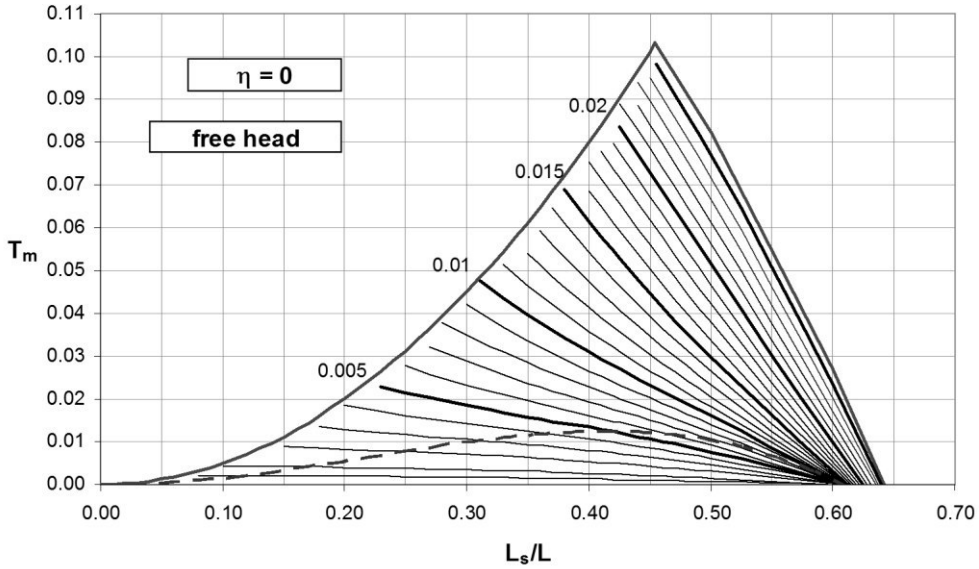

Figure 4-29: Curves of normalised shear force T_m over Ls/L for η=0. Numbers indicates the normalised maximum bending moment $M_{max}/(mL^3)$. Dashed line represents the limit elastic solutions

4.4.5.Results and discussion

The analysis of a passive pile embedded in a homogeneous soil modelled according to a Gibson model shows similar results to those obtained for a two-layered soil with constant values of strength and resistance.
In particular, the same failure mechanism A,B and C have been identified (cf. paragraph 4.3.8).
Once again, the peculiarity of the model is that the ultimate lateral pile load is associated with the relative soil free-pile external displacement y_{s0} necessary to mobilise it and to the pile head deflection y_0; it is then possible to verify if specific service requirements are satisfied if a certain resistance contribute is requested to the pile.

With regard to the case of a soil sliding as a block mass (η=1), all the three failure mechanism are activated at varying of the sliding surface depth (the mechanism B becomes predominant for β higher than 0.45 while the mechanism A is activated when β passes 0.85). In the case of a triangular inverse distribution of the soil free-field displacement, the mechanism A does not occur and the pile is not able to furnish a positive reaction in term of shear force for values of β higher than about 0.65.

Similarly to the results for a two-layered soil, for the case of a triangular inverse distribution of the soil free-field displacement (η=0), the maximum contribute in terms of shear force is provided for β values close to 0.45 (i.e. when the pile is embedded for almost half of its length in the firm layer), in correspondence to the transition from the mechanism C to the mechanism B. Instead, the case of a soil sliding as a block mass (η=1) shows a maximum value of T_m.
In both cases, the maximum normalised shear force is close to 0.3, associated with a maximum normalised bending moment of about 0.06-0.075 and to a normalised pile head deflection equal to 10.
Instead, the relative soil displacement at ground level is different in size between the two cases: y_{0n} is equal to 10 in case of η=1 and it increases to 150 for η=0, where, due to the soil distribution shape, a higher top value is necessary to deflect the pile and mobilise its resistance.

5. Lateral resistance of passive piles in a double-layered non-cohesive soil

Viggiani [23] suggested the results of his evaluation of the ultimate resistance of passive piles in cohesive soils.
In the present chapter, a similar approach is developed for a two-layered non-cohesive soil in which both the modulus of subgrade reaction and the ultimate lateral pressure are expected to increase with depth.

5.1. Geometry

The geometry of the problem is represented in Figure 5-1. A pile of length L and diameter D is embedded in a two-layered soil made by a sliding layer of thickness $L_s=L_1$ with a limiting soil pressure $p_{u1}=m_1 z$ and a stable layer of thickness L_2 with $p_{u2}=m_2 z$. For simplicity, the ground surface and the slip surface are assumed horizontal.

In the following analysis dimensionless expressions for shear and moment at $z = L_1$ are derived as a function of two dimensionless parameters:

$$\beta = L_s/L \qquad (5\text{-}1)$$

$$X = m_1/m_2 \qquad (5\text{-}2)$$

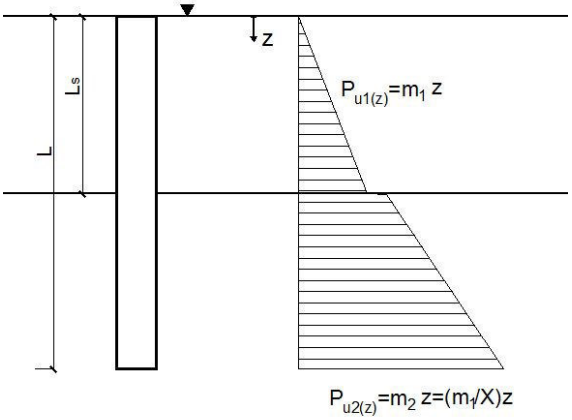

Figure 5-1: Soil profile used in the analysis

5.2. Limiting soil pressure

Similarly to Viggiani (1981) the force and moment provided by pile at the depth of sliding surface are obtained assuming that the soil has reached its ultimate state. In this study refers to a p_u linearly varying with depth (Fleming et al. [42]):

$$p_u = mz \qquad [FL^{-1}] \qquad (5\text{-}3)$$

The gradient m depends on Rankine coefficient of passive resistance K_p and effective soil unit weight γ', as well as the pile diameter. Some studies (e.g. Poulos [26]; Kourkoulis et al. [22]) follow the recommendation of Broms [1] assuming

$$m = (3 \div 5)K_p\gamma' D \qquad (5\text{-}4)$$

elsewhere it is assumed (e.g. Zhang, [3]; Ellis et al [49]; Fleming et al. [42]):

$$m = K_p^{\,2}\gamma' D \qquad (5\text{-}5)$$

It can be observed that the above expressions are valid for an isolated pile, whereas for a row of pile p_u is expected to vary with pile spacing (Georgiadis et al. [45]; Rollins et al. [50]) .

A centre to centre pile spacing of 3-4 diameter can be considered reasonable to both neglect the group effect in terms of p_u and to allow the development of soil arching between the piles (Kourkoulis et al. [22])

A deeper analysis regarding the evaluation of the gradient m has also been made in paragraph 4.1 .

5.3. Failure modes for non-yielding piles

Similarly to the case of cohesive soils presented by Viggiani, six different failure modes can be found. Three cases are involved when the pile is assumed not to reach its limiting tension (i.e. the bending moment acting on the pile is lower than its yield moment M_y); it is so assumed that failure occurs only in the soil:

Mode A – short pile mode

In this case, the ultimate lateral pressure is achieved in the stable layer (Figure 5-2a). The shear force T and the bending moment M at depth $z = L_1$ can be easily obtained as:

$$T_{An} = \frac{T_A}{m_1 L^2} = \frac{1-\beta^2}{2X} \qquad (5\text{-}6)$$

$$M_{An} = \frac{M_A}{m_1 L^3} = \frac{(1-\beta)^2(2+\beta)}{6X} \qquad (5\text{-}7)$$

Mode B – intermediate mode

Soil failure occurs both above and below the slip surface (Figure 5-2b). The sign of the ultimate soil pressure change along the pile at depth z_1, $L_1=L_s$ and z_2.

The horizontal force equilibrium and bending moment equilibrium about pile head, can be written as:

$$\frac{1}{2} m_1 \left(L_1^{\,2} - 2z_1^{\,2}\right) - \frac{1}{2} m_2 \left(2z_2^{\,2} - L_1^{\,2} - L^2\right) = 0 \qquad (5\text{-}8)$$

$$\frac{1}{3} m_1 \left(L_1^{\,3} - 2z_1^{\,3}\right) - \frac{1}{3} m_2 \left(2z_2^{\,3} - L_1^{\,3} - L^3\right) = 0 \qquad (5\text{-}9)$$

The value of z_{1n} is calculated by solving a six order equation:

$$z_{1n}{}^6 + a_{4B} z_{1n}{}^4 + a_{3B} z_{1n}{}^3 + a_{2B} z_{1n}{}^2 + a_{0B} = 0 \qquad (5\text{-}10)$$

whose expressions of coefficients *a* are listed in Table 5-1.

Shear and moment at the depth L_1 can be expressed as a function of z_{1n}, i.e. the normalized depth z_1/L at which the first pressure inversion occurs.

$$T_{Bn} = \frac{T_B}{m_1 L^2} = 0.5\beta^2 - z_{1n}{}^2 \qquad (5\text{-}11)$$

$$M_{Bn} = \frac{M_B}{m_1 L^3} = -\frac{1}{6}\beta^3 + z_{1n}{}^2\left(\beta - \frac{2}{3} z_{1n}\right) \qquad (5\text{-}12)$$

The maximum moment in the unstable and stable layer are respectively:

$$M_{1n} = \frac{M_1}{m_1 L^3} = \frac{2}{3} z_{1n}{}^3\left(\sqrt{2} - 1\right) \qquad (5\text{-}13)$$

$$M_{2n} = \frac{M_2}{m_1 L^3} = \frac{1}{3X}\left\{\sqrt{\left(2 z_{2n}{}^2 - 1\right)^3} + 1 - 2 z_{2n}{}^3\right\} \qquad (5\text{-}14)$$

Where

$$z_{2n} = \sqrt{0.5\left(1 + \beta^2\right) + X\left(0.5\beta^2 - z_{1n}{}^2\right)} \qquad (5\text{-}15)$$

Mode C – flow mode

In this case, the ultimate lateral pressure is fully mobilised only in the unstable layer (Figure 5-2c). The shear force and the bending moment at depth L_1 can be easily obtained as:

$$T_{Cn} = \frac{T_C}{m_1 L^2} = 0.5\beta^2 \qquad (5\text{-}16)$$

$$M_{Cn} = \frac{M_C}{m_1 L^3} = -\frac{1}{6}\beta^3 \qquad (5\text{-}17)$$

mode	$x^6 + a_4 x^4 + a_3 x^3 + a_2 x^2 + a_0 = 0$			
	a_4	a_3	a_2	a_0
B	$-\frac{3\left(1+\beta^2(1+X)\right)}{2(1+X)}$	$-\frac{1+\beta^3(1+X)}{X(1+X)}$	$\frac{3\left\{1+\beta^2(1+X)\right\}^2}{4X(1+X)}$	$\frac{2\left\{1+\beta^3(1+X)\right\}^2-\left\{1+\beta^2(1+X)\right\}^3}{8X^2(1+X)}$
B1	$-\frac{3\left(\beta^2(1+X)+1\right)}{2+X}$	$-\frac{4\left\{\beta^3(1+X)+1+3XM_{yn}\right\}}{X(2+X)}$	$\frac{3\left(\beta^2(1+X)+1\right)^2}{X(2+X)}$	$\frac{2\left[\beta^3(1+X)+1+3XM_{yn}\right]^2-\left[\beta^2(1+X)+1\right]^3}{X^2(X+2)}$
BY	$-3\beta^2$	$-\frac{2\left\{\beta^3(1+X)+6XM_{yn}\right\}}{X(1+X)}$	$\frac{3\beta^4(1+X)}{X}$	$\frac{1}{X^2(1+X)}\left\{\beta^3(1+X)+6XM_{yn}\right\}^2-\beta^6\frac{(1+X)^2}{X^2}$
B2	$-\frac{3\beta^2(1+X)}{(1+2X)}$	$-\frac{3XM_{yn}+\beta^3(1+X)}{X(1+2X)}$	$\frac{1.5\beta^4(1+X)^2}{X(1+2X)}$	$\frac{9XM_{yn}{}^2+6M_{yn}\beta^3(1+X)-\beta^6(1+X)^2}{4X(1+2X)}$

Table 5-1: Expressions for the coefficients of governing equations for failure mode B, B1, BY and B2

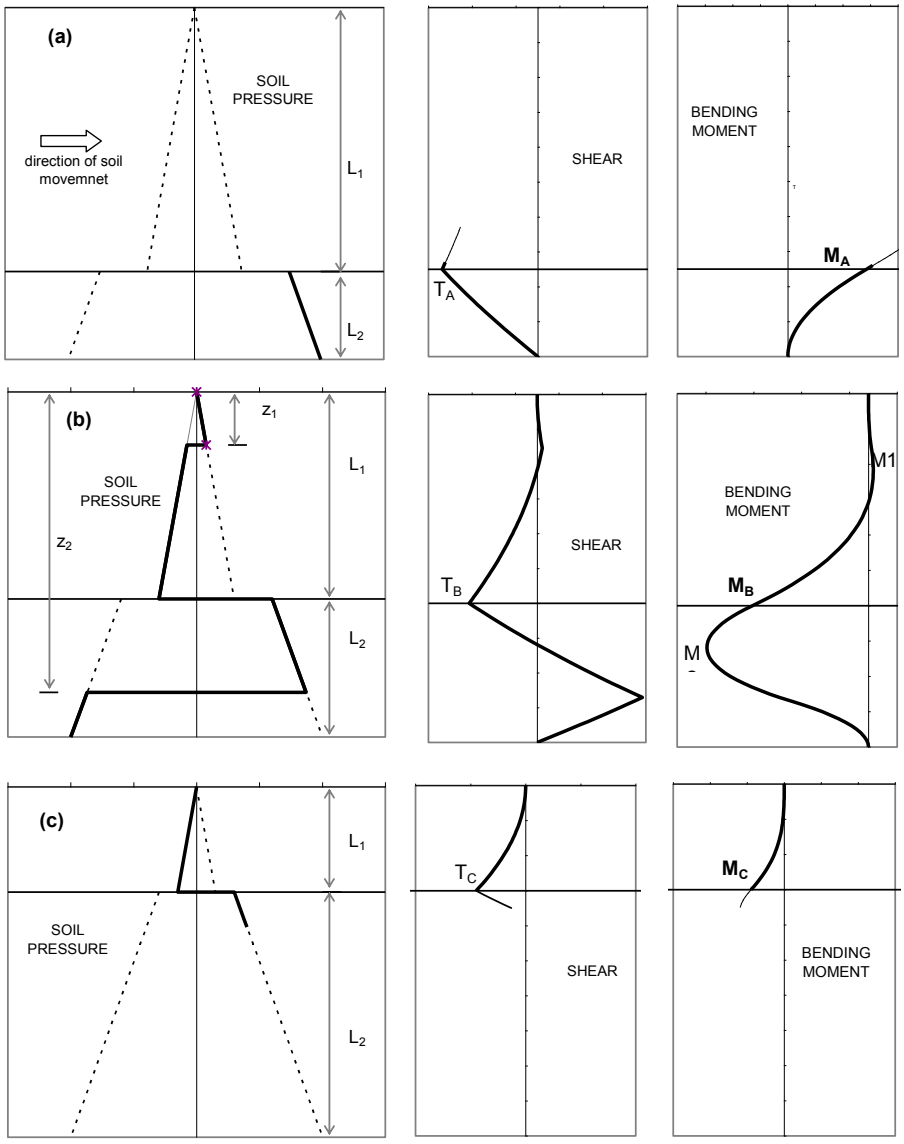

Figure 5-2: Failure mechanisms for non-yielding piles: (a) failure mechanism A; (b) failure mechanism B; (c) failure mechanism C

5.4. Failure modes for yielding piles

When pile failure is considered in the analysis, one or two plastic hinges are assumed to develop along pile shaft in which bending moment is equal to yield moment. The yield moment of the pile can be conveniently expressed in dimensionless form:

$$M_{yn} = M_y/(m_1 L^3) \qquad (5\text{-}18)$$

Mode B1

A plastic hinge develops at depth p1 in the unstable layer (Figure 5-3a).
The shear force and bending moment at depth L1 are given by:

$$T_{B1n} = \frac{T_{B1}}{m_1 L^2} = 0.5\,(\beta^2 - p_1^2) \qquad (5\text{-}19)$$

$$M_{B1n} = \frac{M_{B1}}{m_1 L^3} = \frac{1}{6}(\beta^3 - 3\beta p_1^2 + 2p_1^3) \qquad (5\text{-}20)$$

The maximum moment in the stable zone can be calculated by (5-6) with:

$$z_{2n} = \sqrt{0.5\left(1+\beta^2\right) + 0.5X\left(\beta^2 - {p_{1n}}^2\right)} \qquad (5\text{-}21)$$

The horizontal force equilibrium and bending moment equilibrium about pile head, of the part of pile below the plastic hinge can be written as:

$$\frac{1}{2}m_1\left({L_1}^2 - {p_1}^2\right) - \frac{1}{2}m_2\left({z_2}^2 - {L_1}^2\right) + \frac{1}{2}m_2\left(L^2 - {z_2}^2\right) = 0 \qquad (5\text{-}22)$$

$$\frac{1}{3}m_1\left({L_1}^3 - {p_1}^3\right) - \frac{1}{3}m_2\left({z_2}^3 - {L_1}^3\right) + \frac{1}{3}m_2\left(L^3 - {z_2}^3\right) + M_y = 0 \qquad (5\text{-}23)$$

The value of p_{1n} (= p_1/L) , obtained by imposing horizontal and rotational equilibrium, is the solution of the following six order equation:

$$p_{1n}^{\ 6} + a_{4B1} p_{1n}^{\ 4} + a_{3B1} p_{1n}^{\ 3} + a_{2B1} p_{1n}^{\ 2} + a_{0B1} = 0 \qquad (5\text{-}24)$$

Expressions for coefficients of (5-19) are in Table 5-1.

Mode BY

This failure mode includes two plastic hinges at depth p1 and p2 (Figure 5-3b).
The shear and moment at the sliding surface can be calculated by (5-18) and (5-19), respectively. The horizontal force equilibrium and bending moment equilibrium about pile head, of the part of pile between the plastic hinges can be written as:

$$\frac{1}{2} m_1 \left(L_1^{\ 2} - p_1^{\ 2} \right) - \frac{1}{2} m_2 \left(p_2^{\ 2} - L_1^{\ 2} \right) = 0 \qquad (5\text{-}25)$$

$$\frac{1}{3} m_1 \left(L_1^{\ 3} - p_1^{\ 3} \right) - \frac{1}{3} m_2 \left(p_2^{\ 3} - L_1^{\ 3} \right) + 2M_y = 0 \qquad (5\text{-}26)$$

The value of p_{1n} (= p_1/L), obtained by combining equilibrium conditions, is the solution of the following equation:

$$p_{1n}^{\ 6} + a_{4BY} p_{1n}^{\ 4} + a_{3BY} p_{1n}^{\ 3} + a_{2BY} p_{1n}^{\ 2} + a_{0BY} = 0 \qquad (5\text{-}27)$$

Details of the coefficients a are provided in Table 1.

Mode B2

A plastic hinge is developed at depth p2 in the stable layer (Figure 5-3c). Shear and moment at the depth of sliding surface can be calculated by (5-10) and (5-11) whereas the maximum moment in the unstable layer is calculated by (5-12,5-13). The horizontal force equilibrium and bending moment equilibrium about pile head of the part of pile above the plastic hinge can be written as:

$$\frac{1}{2}m_1\left(L_1^{\,2}-z_1^{\,2}\right)-\frac{1}{2}m_1 z_1^{\,2}-\frac{1}{2}m_2\left(p_2^{\,2}-L_1^{\,2}\right)=0 \qquad (5\text{-}28)$$

$$\frac{1}{3}m_1\left(L_1^{\,3}-z_1^{\,3}\right)-\frac{1}{3}m_1 z_1^{\,3}-\frac{1}{3}m_2\left(p_2^{\,3}-L_1^{\,3}\right)+M_y=0 \qquad (5\text{-}29)$$

The value of z_{1n} ($=z_1/L$), obtained by imposing horizontal and rotational, is the solution of the following six order equation:

$$z_{1n}^{\,6}+a_{4B2}z_{1n}^{\,4}+a_{3B2}z_{1n}^{\,3}+a_{2B2}z_{1n}^{\,2}+a_{0B2}=0 \qquad (5\text{-}30)$$

The coefficients a are listed in Table 5-1.

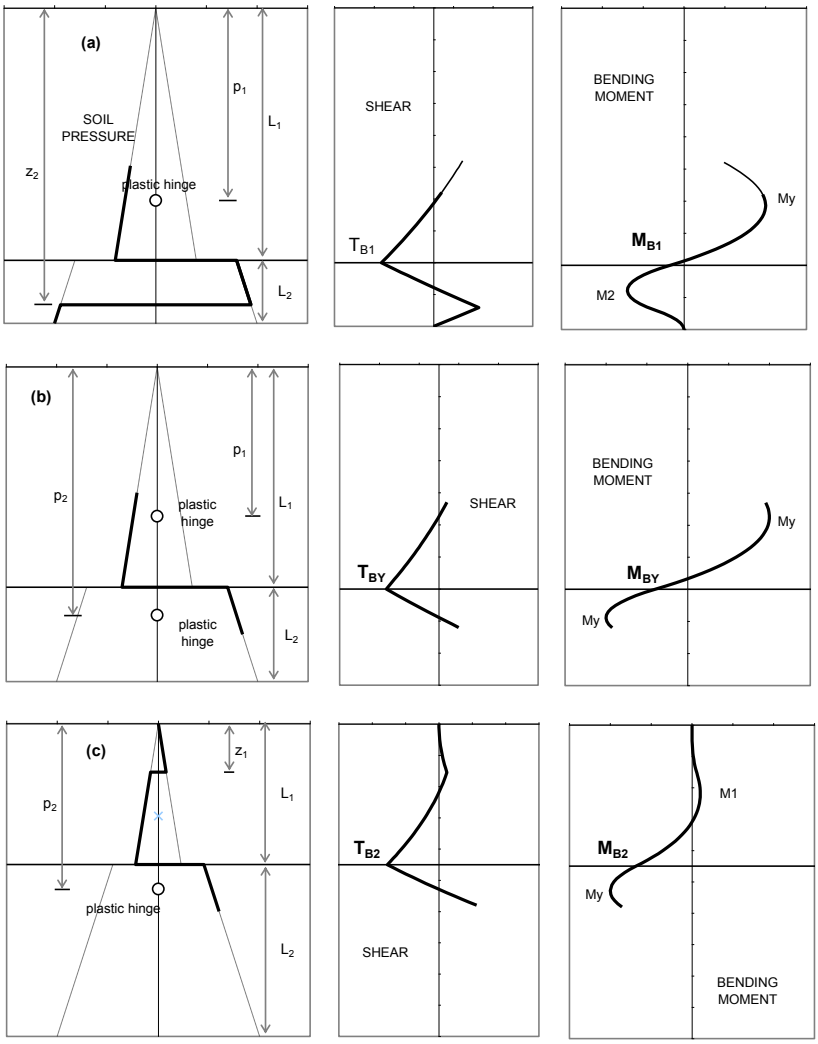

Figure 5-3: Failure mechanisms for yielding piles: (a) failure mechanism B1; (b) failure mechanism BY; (c) failure mechanism B2

5.5. Results and discussion

In Figure 5-4 the normalised shear force and moment for non-yielding piles are plotted against the normalised depth of the sliding surface for X=1 and X=0.5. For an assigned value of β, normalised shear force is calculated by (5-5), (5-10) and (5-15) and the minimum value is plotted in the graph.

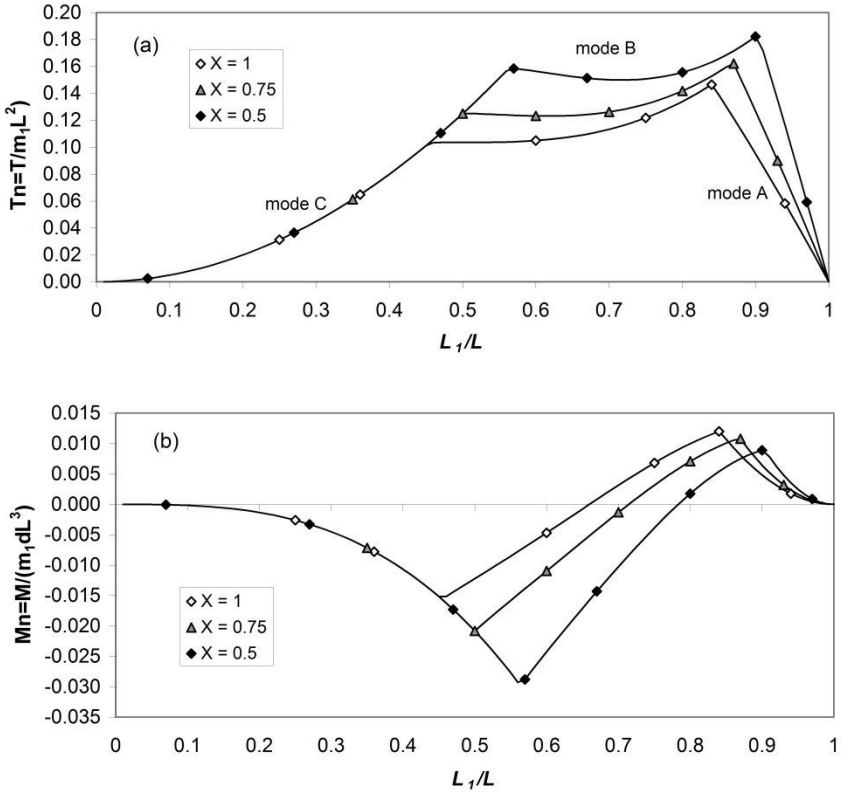

Figure 5-4: Dimensionless resistance offered by non-yielding piles at the depth of sliding (a) shear (b) bending moment

Three different zones can be distinguished. For low values of β the mode C governs the problem. In this range the curve is unique regardless of the value of X. At increasing β there is a first threshold value of β (β_1) above which the mode B

becomes the most critical. Finally there is a second threshold value (β_2) over which the critical mode becomes the mode A. The threshold values are found to increase at decreasing the ratio X.

The maximum contribute in terms of shear is provided for $\beta > 0.8$, (i.e. when a relatively little embedment in the stable layer). However, this solution is of doubt efficacy in designing piles for stabilise an active landslide when a greater embedment is requested (Kourkoulis et al. 2011 [21], [22]). As far as the bending moment is concerned, the contribute is generally negative for LEM analysis, as the sign is opposite to that of soil shear stresses along the sliding surface. Only for high values of β the contribute is positive.

Figure 5-5 and Figure 5-6 show normalised shear force and moment for yielding piles. For assigned values of β, X and M_{yn} shear force is calculated according to all six failure modes and then the minimum value is plotted in the graph as a function of β.

For M_{yn} greater than 0.04 the trend of T_n coincides with that of nonyielding piles. As expected, the normalised shear force is found to generally decrease at decreasing M_{yn}. Regardless of the value of M_{yn} the mode C is more critical for low values of β, whereas the mode A is the more critical for high value of β. Threshold values β_1 and β_2 depend on both M_{yn} and X.

In the intermediate range of β shear force is governed by mode B2 and B1. For M_{yn}=0.02 a very narrow range of β is found where the mode B is the more critical. For $M_{yn} \leq 0.01$ the mode B disappears and a range of β exists in which mode BY becomes more critical.

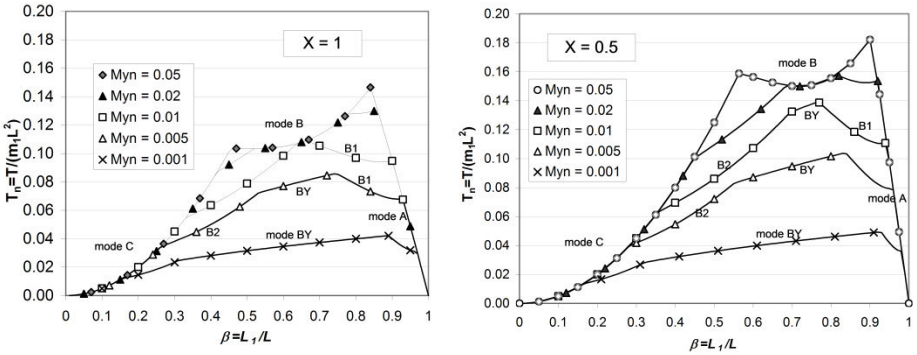

Figure 5-5:Dimensionless shear offered by yielding piles at the depth of sliding; (a) X=1; (b) X= 0.5

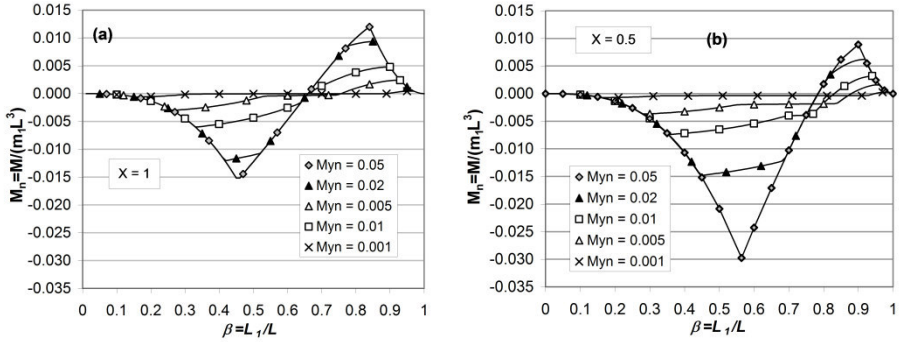

Figure 5-6: Dimensionless bending moment offered by yielding piles at the depth of sliding; (a) X=1; (b) X= 0.5

5.6. Final considerations

This chapter has examined the behaviour of pile in a sliding cohesionless soils. Assuming a linear distribution of the limiting soil pressure with depth in both stable and unstable layer, shear force and bending moment at the depth of the sliding surface are obtained in non-dimensional form. Six failure modes have been analysed, the occurrence of which depend on the depth of sliding surface, yield moment of the pile section and strength gradient ratio (m_2/m_1).

The proposed solution can be useful in stability analyses made by Limit Equilibrium Methods in which the contribute of pile is considered as an additional resistance. Similarly to the original solution proposed by Viggiani for cohesive soils, the proposed approach refers only to ultimate state of soil and pile and no information on pile and soil displacements are provided. For these reasons this approach seems to be more applicable for a stable slope than for a slope with an active landslide. In such a case, a suitable constitutive model is necessary as pile stability and displacement should be checked on the basis of the actual soil pressure distribution instead of an idealised distribution relevant to soil ultimate state.

6. Stability analysis of slopes reinforced with piles

6.1. Stability analysis of a pile-reinforced slope

Among all the different situations where a pile acts as passive, one of the most common and at the same time studied in literature is the case of passive piles for slope stabilization: the use of piles is nowadays one of the most important and innovative slope reinforcement technique used to stabilise active landslides or to forestall instability in stable slopes.

This is carried out by installing piles in one or more rows crossing the slope declivity. Experimental tests demonstrated that an arching effect between piles and soil underlies the interaction soil-pile, and through that the pile row works as a continuum retaining system absorbing soil strains [51]. However, the arching effect is established only after a sufficient soil movement around the piles, necessary to mobilise their reaction; Figure 6-1 shows a common scheme of a pile-reinforced slope in which the pile transfers the loading due to unstable mass in the stable underlying bed and that can be represented as generalised forces (T, M, N) provided by the lower part of the pile embedded in the stable soil (Figure 6-2).

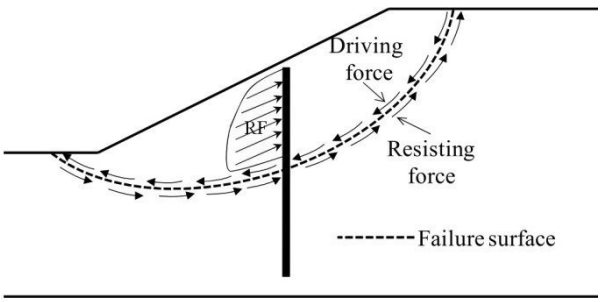

Figure 6-1: Schematic cross section of a pile reinforced slope

For these reasons, the study of a pile-reinforced slope must take into account the pile stabilising contribution and at the same time compute the stability analysis of the pile-slope system.

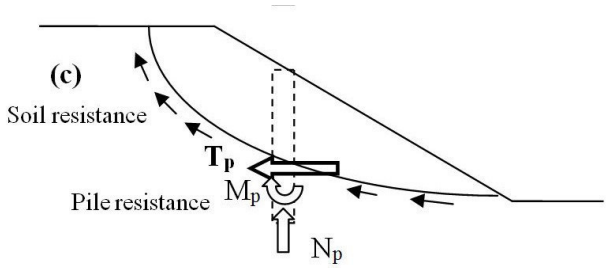

Figure 6-2: Theoretical forces due to a pile row to include in slope stability analyses

In practical applications, the study of pile reinforced slopes is usually carried out by applying the same methods commonly used in the stability analysis of natural slopes [52], in which it has been incorporated the stabilising contributions provided by the piles. The available approaches can traditionally be divided into limit analysis methods, numerical methods (finite-element FEM or the finite-difference methods FDM) and limit equilibrium methods. However, depending on how the pile reaction is evaluated and implemented, these methods can be further divided into two categories: coupled and uncoupled.

Numerical methods allow analysing the whole piles-slope system in a coupled approach, in which the contribution of the piles and the global stability analysis are implemented in the same calculation. In a decoupled approach, instead, the contribution of pile rows is calculated separately than the global safety factor of the reinforced slope. While being used also in the limit analyses, to date, the limit equilibrium method is the most widely used into decoupled slope stability analysis due to its simplicity of use and to its formulation that can be easily modified to include piles effect [21], [27], [43], [53], [54].

Moreover, the different approach used affects the evaluation of the slope stability. Slope stability is in fact generally assessed by determining the safety factor SF, in

both numerical and decoupled methods. The most general definition of this factor can be written :

$$SF = \frac{available\ resistance}{applied\ loading} \qquad (6\text{-}1)$$

For slopes, SF is also traditionally defined as the ratio of the actual soil shear strength to the minimum shear strength required to prevent failure [55]. SF is then the factor by which the soil shear strength must be divided to bring the slope to the verge of failure. In other words, when the factor of safety is 1.0, the slope is in a state of limiting equilibrium. This definition of the global safety factor is identical for both numerical and limit equilibrium methods.

6.1.1.Numerical methods

Numerical methods allow to model the pile–slope system as a continuous elastic or elasto-plastic medium and provide coupled solutions in which the pile response and slope stability are considered simultaneously and, consequently, the pile or the slope failures do not request any assumptions to be determined.
Since SF is defined as a shear strength reduction factor, a clear way of computing it with a finite element or finite difference program is simply to reduce the soil shear strength until collapse occurs. The resulting factor of safety is the ratio of the soil's actual shear strength to the reduced shear strength at failure [18], [19]. The reduced shear strength parameters c_R and φ_R are defined as

$$\varphi_R = tan^{-1}\left(\frac{tan\,\varphi}{SF}\right) \qquad (6\text{-}2)$$

$$c_R = \frac{c}{SF} \qquad (6\text{-}3)$$

The reduced shear strength parameters replace those of Mohr-Coulomb's failure criterion in the elasto-plastic analysis of the soil-pile system. The factor SF is initially selected to be so small that materials of the slope are under elastic conditions. It is then increased incrementally until the global failure is achieved and the calculation diverges. For a slope with piles, the slope completely consists

of the soil when the shear strength reduction SF is less than unit and the material of the solid elements within the extent of the pile is changed from soil into the pile material only when SF reaches unity (the stresses in the pile are assumed to be zero when the material is changed). Then, the factor increases once again, step by step until failure occurs.

One of the main advantages of the shear strength reduction numerical method is that the safety factor emerges naturally from the analysis without the user having to commit any particular assumption a priori on the slope failure geometry or pile contribution.

Ugai [18] and Won et al. [19] gave interesting examples of the application of numerical methods: Cai and Ugai [18] in particular have considered the effects of a row of piles on the stability of a slope by a three-dimensional finite-element analysis using the SRM and analysing the effects of pile spacings, pile head conditions, bending stiffness and pile positions on the SF. Won et al. [19] and Wei and Cheng [20] have also analysed the same slope as by Cai and Ugai using a three-dimensional finite-difference code by the SRM. Their results together give important information on the shape of the critical surface as identified automatically by the numerical method: it is claimed that, when the pile spacing is small, the critical slip surface is shallow and is nearly divided into two parts. With the increase in the pile spacing, the critical slip surface becomes deeper and the two parts of the critical slip surface more connected. When the pile spacing is large enough, the two parts of the critical slip surface gradually turn into a clear single critical slip surface which is nearly the same as the critical slip surface with no pile. This means that the critical slip surface of a piled slope is usually shallower than that of a slope with no pile. With the placement of a pile, the two smaller slip surfaces will control the slope failure while the original overall critical slip surface will no longer control the failure as there is an obstruction to the failure by the pile. Moreover, the location for the maximum shear force in the pile seems not to correspond to the location of the maximum shear strain in soil.

Wei and Cheng [20] finally conclude that a detailed 3D piled slope analysis is extremely time-consuming to carry out; they suggests a practical analysis and design, stating that the upper and lower bounds of the factor of safety can be

determined easily by a 2D analysis (either SRM or limit equilibrium analysis) and they are useful for the preliminary design before conducting a detailed 3D analysis. This proves how the applications of numerical methods in three dimensions may result unattractive for practitioners as they are complex, computationally expensive and time-consuming. For this reason, several decoupled approaches have been proposed and nowadays accepted in the practice [20]–[22].

6.1.2. Limit analysis

A similar iterative procedure in which the resistance parameters of the soil are progressively changed according to equations (6-2) and (6-3), is applied in the methods using the kinematic approach of limit analysis. It states that a slope will collapse if the rate of work done by external loads as well as body forces exceeds the energy dissipation rate for any assumed kinematically admissible failure mechanism. The pile resistance contribution is taken into account as an additional energy dissipation along the potential sliding surface.
The value of the FS is reached as soon as the critical height evaluated with the reduced parameters is equal to the actual height of the slope. When piles are installed on the slope, their contributions is taken into account in terms of energy dissipation. The method considers that, when the retaining structure is inserted in the slope, the slope safety factor and/or the potential failure mechanism, with respect to the case without piles, may change. The new most critical surface is that for which the highest value of the stabilising contribution provided by the piles RF is required to increase the safety factor to the desired value. This lets automatically identify the range of positions where the piles have to be placed for increasing effectively the slope stability.
An example of application of the method can be found in the work of Ausilio et al. [56]: it is first considered the case of a slope without piles (where the sliding surface is described by a log-spiral equation) and therefore a solution is proposed to determine the safety factor of the slope, which is defined as a reduction coefficient for the strength parameters of the soil. Then, the stability of a slope containing piles is analysed. In order to account for the presence of the piles, a lateral force and a moment are applied at the depth of the potential sliding surface.

To evaluate the resisting actions which must be provided by the piles in a row to achieve the desired value of the safety factor of the slope, an iterative procedure is used to solve the equation obtained by equating the rate of external work due to soil weight and surcharge boundary loads to the rate of energy dissipation along the potential sliding surface.
Nian et al. [57] developed a similar approach, to analyse the stability of a slope with reinforcing piles in nonhomogeneous and anisotropic soils.

6.1.3. Limit Equilibrium methods

Being valid the same definition for numerical and limit analysis methods, for limit equilibrium methods SF is usually expressed as the ratio between the resisting F_r and the driving F_d actions along the slip surface (Figure 6-1), calculated using one of the widely accepted limit equilibrium based techniques (the friction circle method [58], [59] or the more common and applied methods of slices [55], [60]–[62]):

$$SF = F_r/F_d \qquad (6\text{-}4)$$

If the actual safety factor, SF, is smaller than the requested value, the piles (if intersected by the considered slip surface) have to furnish a contribution in order to obtain a higher SF_T for the piled slope, which is evaluated separately using or a numerical or an analytical method.
It is a critical aspect of the approach as an incorrect evaluation of the pile contribution has different effects on the stability and on the structural local analysis: while an overestimation of the stabilising contribute offered by the pile leads to a structural analysis which errs on the side of safety, in the stability analysis also the factor of safety is going to be overestimated.
It is worth to be noted that when the factor of safety is defined in terms of moments along the potential failure surface it is reasonable to consider not only the shear force but also the bending moment provided by a pile at the depth of the sliding surface (Lee et al. [27] ; Jeong et al. [54]). For a single row of passive piles, the influence of axial force can be considered negligible, but it becomes crucial for two

parallel rows of piles connected by a rigid cap (Kourkoulis et al. [22]). Finally, it should be stressed that in engineering practice LEM are generally 2D; therefore the contribute of the pile in terms of shear, expressed for example in kN, must be transformed into a force per unit length (kN/m), as a function of the pile spacing.

Past studies of several authors, and among all Wright et al. [63] and Tavenas et al. [64], have proved that, whereas in most equilibrium analyses the factor of safety is assumed to be constant, it actually varies from place to place along the slip surface: it is reasonably expected a lower SF value on the upper part of the surface and a higher close to the toe. However, it is interesting to note that the average value of SF is the same for all practical purposes, even if its local value is assumed to vary along the slip surface [65]. This leads to consider the average value of the factor of safety as insensitive to the assumption of being constant, or not, for every slice.
The conventional limit-equilibrium calculation of the driving and resisting forces, of course, does not consider the three-dimensional nature of the problem. In addition, major criticism of the limit equilibrium method is that it is generally based on simplified assumptions and the results obtained from this method are, in the light of limit analysis, neither upper bounds nor lower bounds on the true solution (Ausilio et al., [56]). Otherwise, the adoption of the conventional limit-equilibrium methods is, of course, leading to a conservative estimation of the required pile resistance force as the safety factor so calculated is generally lower than that evaluated by using numerical methods.
Moreover, it does not consider that the slip surface after the installation of the piles may differ from the one characterising the unreinforced slope. It may happen that a new deeper slip surface takes origin from the effects of piles which, rotating, modify the sliding surface locally. In addition, the new surface may be so deep not to involve piles. In a different situation, shallower new sliding surfaces may take place behind or down the retaining system. For all these cases, new stability analyses are requested in order to investigate the new geometries.

Anyway a critical aspect in the use of the limit equilibrium methods for reinforced slopes is the effect of the piles on the evaluation of the factor of safety.
No agreement has even been reached on how pile stabilising contribution has to be considered in the method for the definition of the slope factor of safety as it can be

considered as a reduction of driving forces so that the factory of safety can be formulated as:

$$SF_T = F_r/(F_d - RF) \qquad (6\text{-}5)$$

or as an additional resistance:

$$SF_T = (\mathrm{F_r} + RF)/F_d \qquad (6\text{-}6)$$

When the passive piles are assumed to decrease the global driving forces, a reduction factor is generally determined and applied to the interslice forces transferred across the pile. According to this approach, Zeng and Liang [66] proposed a mathematical formulation based on interslice force equilibrium allowing for not only the determination of the safety factor of the reinforced slope, but also the forces acting on the piles. As the soil mass moves through the piles, the driving force transmitted to the soil mass behind the piles is reduced by a reduction factor (R), obtained by a two-dimensional finite element analysis by the same authors [67], leading to a higher stability of the slope as a result of soil arching. The cross-section of piled slope is illustrated in Figure 6-3.

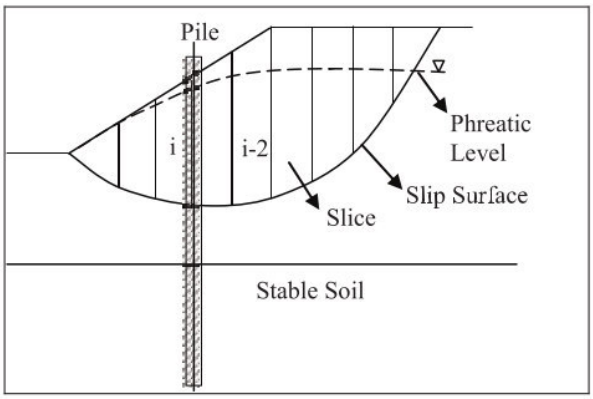

Figure 6-3:Cross section of slope stabilizing pile [66]

The forces acting on the slice are W_i, the weight of the slice; P_{i-1}, P_i, the resultant interslice forces on the (i-1)th and ith interfaces, respectively; N_i, the normal force

reaction on the base of the slice; and T_i, the shear force reaction on the base of the slices. Also, α_{i-1} and α_i are the average slopes of the bases of the slices i-1 and i, respectively. The resultant interslice force is assumed to be parallel to the base of the previous up-slope slice, with the point of application located at one third from the bottom of the interface (Figure 6-4).

$$P_i = W_i \sin\alpha_i - \left[\frac{c_i l_i}{SF_T} + (W_i \cos\alpha_i - u_i l_i)\frac{\tan\varphi_i}{SF_T}\right] + k_i R P_{i-1} \qquad (6\text{-}7)$$

Where,

$$k_i = \cos(\alpha_{i-1} - \alpha_i) - \sin(\alpha_{i-1} - \alpha_i)\frac{\tan\varphi_i}{SF_T} \qquad (6\text{-}8)$$

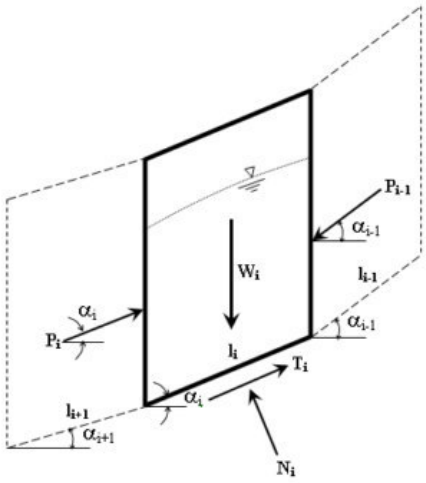

Figure 6-4: Forces acting on a typical slice [66]

P_i depends on the safety factor (SF_T), thus an iterative computational scheme is required: convergence is reached when the calculated P_n at the toe slice matches zero. The development of soil arching was assessed by the degree to which the driving force was transferred to the piles. The soil pressure acting on the soil mass between the piles due to soil arching was calculated and normalized with respect to the initial pressure to obtain a percentage factor (R_p) and given in Figure 6-5.

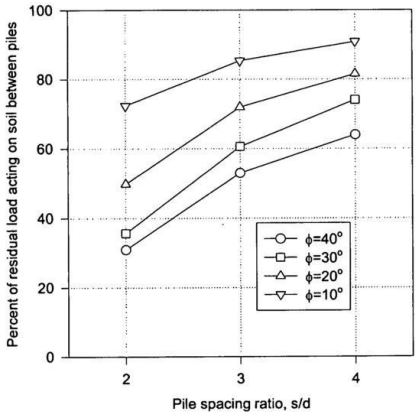

Figure 6-5: Effect of variation in internal friction angle on Rp[67]

If the value of Rp is 100%, it means that no arching effect develops and the total of the soil pressure would be fully transmitted to the soil mass downslope. The stronger the soil arching effects (the smaller R_p), the more net force would act on the pile. Reduction factor (R) is given below in the expression with pile spacing (s) and R_p.

$$R = \frac{1}{s/d} + \left(1 - \frac{1}{s/d}\right) R_p \qquad (6\text{-}9)$$

The net load acting on one pile is:

$$P_{pile} = \frac{(1-R_p)P_{i-1}}{s/d} \qquad (6\text{-}10)$$

What it is interesting is that, if there is no relative movement between soil mass and the piles, then there would be no arching effect and no net force acting on the piles. In addition, through the analysis of several case histories, the authors investigated the influence of pile rows location and spacing into unstable slopes (Figure 6-6)

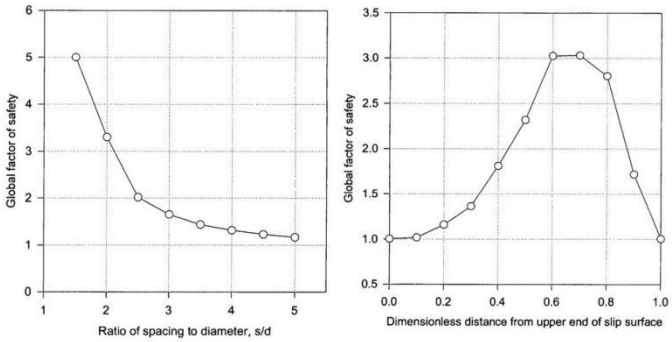

Figure 6-6: Optimisation of pile spacing and pile row location[66]

The contribution of the retaining system finds a maximum value, in terms of factor of safety, when the pile row is located at about 2/3 from the upper end of the slip surface. At the same time, as expected, the contribution of the retaining pile wall increases as the ratio of spacing to diameter decreases.

A similar approach presented by Yamin and Liang [68] uses a limit equilibrium method of slices in which an interrelationship among the drilled shaft location along the slope, the load transfer factor and the global security factor of the slope-shaft system are derived based on a numerical solution. Furthermore, design charts developed on the basis of a three-dimensional finite element analysis carried out by the same authors [69] are used to get the required configurations of a single row of drilled shafts to achieve the necessary reduction in the driving forces.

More recently, Li et Liang [70] developed an analysis and design approach based on limit equilibrium method of slices for the use of multiple rows of drilled shafts to stabilise an unstable slope. As for the method previously presented, it considers the soil arching effect to reduction the driving force between shafts and slides through a semi-empirical load transfer factor h, function of the soil properties and of the geometry of the problem and computed using a regression analysis technique on several three-dimensional finite element simulation results (Figure 6-7).

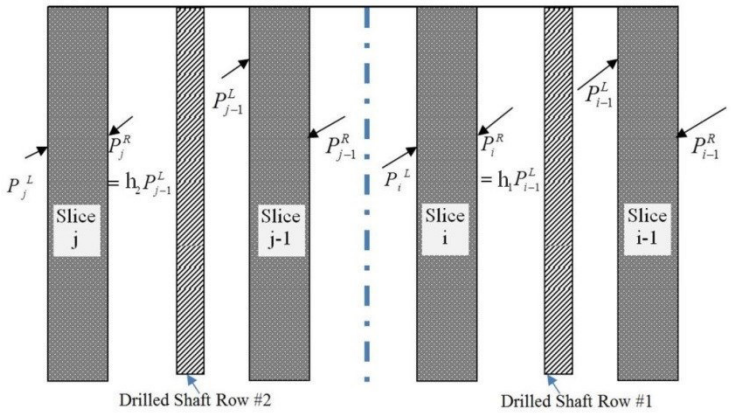

Figure 6-7: Method of slices using two rows of drilled shafts [70]

A parametric study on shaft location, diameters, spacings over the global factor of safety and shaft net force, using one or more row of drilled shafts (Figure 6-8). Results show that, as compared to one row of drilled shafts, multiple rows are effective at increasing the global factor of safety of unstable slopes and reducing the net force on the shafts. In addition, they make the reinforcement design more constructible and meeting the service limit.

Moreover, authors suggest that, regardless of shaft diameter, shaft spacing, and shaft location effects on the global factor of safety, the final design recommendation should follow the principle of using the least amount of reinforcement, as well as minimising the amount of total concrete volume.

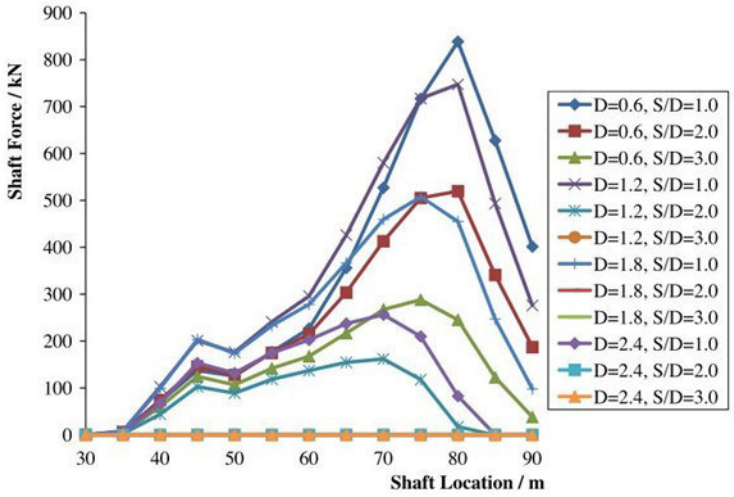

Figure 6-8: Shaft force versus shaft location for different (S, D) combinations using one row of drilled shafts [70]

When the passive piles are assumed to increase the global resistance, Viggiani [23] suggested a design approach (later adopted also by Poulos, [26]; Kourkoulis et al. [21]) requiring three steps (Figure 6-9):

1. Evaluation of the additional resistance needed to increase the safety factor to the desired value, based on analysis of the unreinforced slope carried out by using one of the widely accepted limit equilibrium methods (e.g., Spencer, Bishop, or Janbu). The possible failure slip surface is divided by vertical or inclined planes into a series of slices (Figure 6-9a); integrating the forces along all the slices the slope is divided into, it is possible to obtain the total of the disturbing F_d and resisting forces F_r along the slip surface acting on the unreinforced slope and, consequently, the additional resistance force RF the piles have to furnish so that the target factory of safety can be reached
2. Evaluation of the bending moment and the normal and shear forces, that a single pile can provide in correspondence of an admissible displacement (T,M,N) and satisfying the requested value RF in order to obtain the target factor of safety for the slope

3. Selection of the optimal spacing and location of piles in the slope

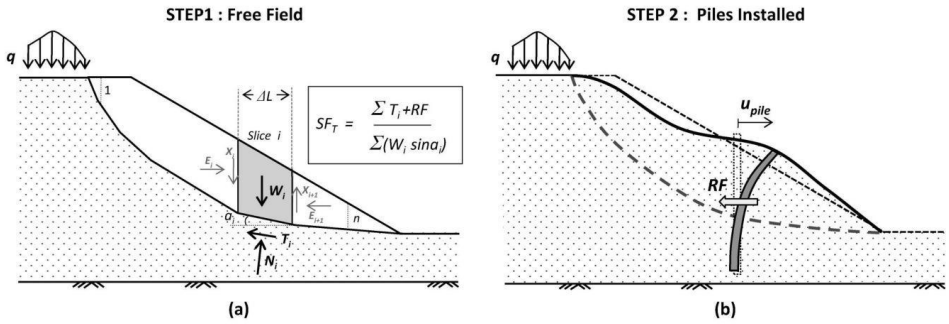

Figure 6-9: Schematic illustration of the two steps of the decoupled methodology: (a) limit equilibrium slope stability analysis to compute the additional required resistance force RF; (b) estimate pile configuration capable of providing the required RF at prescribed displacement [21]

Consequently, stability analysis by LEM must include the generalised forces (T, M, N) provided by the part of the pile embedded in the stable soil.

The dimensionless solutions for the ultimate lateral resistance of a pile in a two-layer purely cohesive soil profile derived by Viggiani [23] are an attempt to solve the second step of the decoupled design approach proposed by himself. These solutions provide the pile shear force at the slip surface and the maximum pile bending moment as a function of the pile length and the ultimate soil-pile pressure in stable and unstable soil layers, assuming that soil movements are great enough to fully mobilise the limiting soil pressure above and/or below the sliding surface. The solution of Viggiani is applicable only to soil in undrained condition with an ultimate lateral pressure constant with depth in the stable and unstable layer, and no mention is made on if new slip surfaces have to be considered after the installation of the piles.

Poulos [26] followed the same approach proposed by Viggiani, but improved his solution by introducing a displacement-based method for the evaluation of the pile resistance by implementing a finite-difference model of a pile embedded in an elastic continuum material. The author also suggests that, in case the SF of the

unreinforced slope is lower than the target, the requested pile resistance contribution RF along the slip surface can be evaluated as:

$$\Delta R = RF = \left(SF_{target} - SF\right) F_d \qquad (6\text{-}11)$$

even if it is not specified if RF should be considered in terms of bending moment or only shear forces and if it should be divided for any factor of safety either.
Poulos also faced the problem of considering that the slip surface after the installation of the piles may differ from the one characterising the unreinforced slope. To avoid this kind of situations, Poulos [26] suggested:

- To realise piles rigid enough to prevent structural failure and the consequent formation of plastic hinges around which the pile may rotate and establish new sliding surfaces
- In case of a well defined slip surface, to design the pile with a sufficient embedment on the firm layer, approximately equal to the thickness of the sliding mass, in order to avoid surfaces deeper than the pile length
- To install the piles at the centre of the sliding surface, to avoid the establishing of new surfaces behind or down the pile row

Ito et al. [43], [53] proposed a limit equilibrium method to deal with the problem of the stability of slopes containing one or multi rows of piles. The lateral force acting on a row of piles due to soil movement is evaluated using the theoretical equations derived previously by Ito and Matsui [25] based on the theory of plastic deformation and considering plastic flow of the soil through the piles. The ultimate soil pressure on the pile segment which is induced by flowing soil depends on the strength properties of the soil, overburden pressure, and spacing between the piles and is independent of pile stiffness as a rigid pile with infinite length. It has to be noticed how the authors suggest a factor of safety for the pile equal to one and defined as the ratio between the allowable bending stress and the maximum induced one, while expressing the SF target for the slope as 1.2. The authors also endorse that F_r and F_d can be obtained by any traditional slice method and that no large error is involved by considering the shearing resistance along the sliding surface located down the pile AD (Figure 6-10) as part of the resisting forces F_r, since the soil masses at the both sides of the position of pile's row will deform as

one body in the region between piles, while only the soil just around the piles in arrow will reach a plastic state. Moreover, they suggest that in case the shear failure of pile occurs, RF should be obtained by the shearing resistance of piles at the sliding surface and used in the SF evaluation.

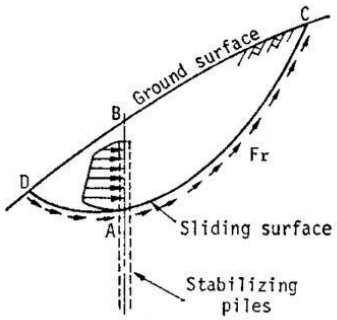

Figure 6-10: Geometry of a pile-reinforced slope [43]

Hassiotis et al. [59] have extended the friction circle method by defining new expressions for the stability factor incorporating the pile resistance. The ultimate soil– pile pressure is calculated based on the equations proposed by Ito and Matsui [25] assuming a rigid pile. However, the safety factor of the slope after inserting the piles is obtained based on the new critical failure surface, which is not necessarily the one before pile installation.

As an overestimation of RF may lead to relevant error on the evaluation of SF, The authors suggest to consider, in their formulation, only the mobilised part of the pile total contribution, by dividing the RF by the factor of safety of the unreinforced slope calculated by considering only the cohesive resistance of the soil, until the target SF is gained. This means that the mobilised RF reaches its total value only when the slope is in a limiting equilibrium, and decreases for higher SF. in addition, the authors highlight that the stability of the reinforced slope involves also the verifying of the single piles: the structural design of the pile has to be carried out by considering the total stress RF and not only the mobilised one. For this purpose, the finite difference method is used to analyse the pile section below the critical surface as a beam on elastic foundations.

Jeong et al. [54] report an uncoupled analysis in which the conventional Bishop simplified method is employed to determine the critical circular sliding surface, resisting moment M_R and disturbing moment M_d. The resisting moment generated by the pile is then obtained from the pile shear force and bending moment developed at the depth of the sliding surface analysed, evaluated separately by using a load transfer approach. Based on this, the safety factor of the reinforced slope with respect to circular sliding is calculated as:

$$SF_T = \frac{M_r}{M_d} + V_{cr} R \cos\theta - M_{cr} + V_{head} y_{head} \qquad (6\text{-}12)$$

where M_{cr} is bending moment developed at critical surface; V_{cr} is shear force developed at critical surface; V_{head} is shear force at pile head; R is radius of the sliding surface; and θ is the angle between a line perpendicular to the pile and the failure surface. It is not explained if V_{head} can be always inserted or only when the pile's head is anchored in the stable soil.

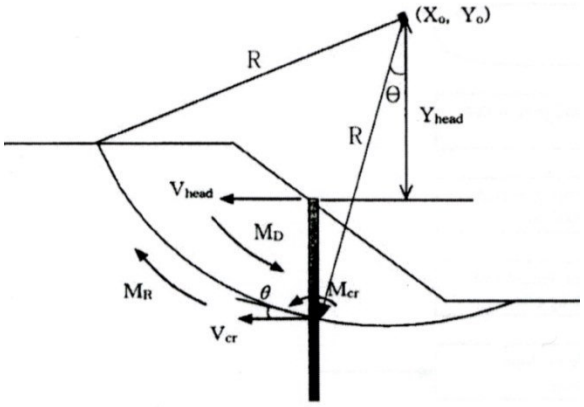

Figure 6-11: Slope geometry and pile contribution according to Jeong et al.[54]

More recently, Kourkoulis et al. [21], [22] developed a hybrid methodology for the design of slope-stabilizing piles aimed at reducing the amount of computational effort usually associated with 3D soil-structure interaction analyses. This method involves all the steps for evaluating the required lateral resisting force per unit length of the slope, needed to increase the safety factor to the desired value by

using the results of a conventional slope stability analysis, and for estimating the pile configuration that offers the required RF for a prescribed deformation level using a 3D finite element analysis. This approach computes the lateral capacity of the piles by numerically three-dimensionally simulating only a limited region of soil around the piles and imposing a uniform displacement profile into the model boundary. It is interesting to notice that the authors suggest a target SF_T equal to the unity to be used for the evaluation of the RF, and do not apply any additional reducing factor to the pile resistance.

Ashour and Ardalan [71] proposed an interesting hybrid approach in which the pile contribution is considered both as an additional resistance for the upper (or supported) part of the slope and as a reduction of the driving actions for the lower (or unsupported). On the basis of a previous work [72], they firstly proposed the assessment of the response of a laterally loaded pile group based on soil-pile interaction (Strain Wedge Model Approach), suggesting that the interaction among the piles grows with the increase in lateral loading, and the increasing depth and angle of the developing wedge. The authors also recommend to calculate the safety factor of the whole pile-stabilised slope by including the total resistance provided by piles for one unit length of the slope RF as follows:

$$SF_T = (\sum F_r + RF)/F_d \quad (6\text{-}13)$$

In addition, they introduce two different factor of safety for the supported and unsupported portions of the stabilised slope, as follows:

$$SF_{T(\text{supported})} = \frac{\sum F_{r(\text{supported})} + RF}{F_{d(supported)}} \quad (6\text{-}14)$$

$$\text{SF}_{\text{T(unsupported)}} = \frac{\sum \text{Fr(unsupported)}}{F_{d(unsupported)} + [(F_{d(supported)} - F_{r(supported)}) - RF]} \quad (6\text{-}15)$$

where F_r (supported) is the resisting force and F_d (supported) is the driving force of the soil mass along the supported portion of the critical failure surface. The resisting and driving forces of the soil mass along the unsupported portion of the

critical failure surface, Fr(unsupported) and Fd(unsupported), respectively, are also calculated using a slope stability method of slices. In Equations (6-13) and (6-15), RF is calculated from Equation (6-14) after the desired safety factor of the supported portion of the slope $SF_{T(supported)}$ is identified. By calculating RF, the targeted load carried by each pile in the pile row can be evaluated based on the assumed pile spacing.

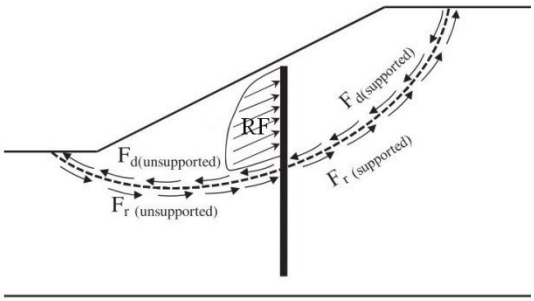

Figure 6-12: Forces acting on a pile-stabilised slope[71]

Moreover, the authors claim that $SF_{T(supported)}$ needs to be identified with a minimum value of unity. Achieving the minimum safety factor ($SF_{T(supported)} = 1$) indicates that the stabilizing pile is able to provide enough interaction with the sliding mass of soil to take a force equal to the difference between the driving and resisting forces along the slip surface of the supported portion of the slope. As a result, the second term of the denominator in Equation (6-15) would be zero. At this point, the authors have considered that, if the minimum SF indicated is not achieved by reaching the ultimate soil-pile interaction, the rest of the driving force will be delivered to the lower unsupported part of the slope. At the same time, the safety factor of the unsupported portion of the slope should not be less than the desired safety factor of the whole slope. Such a scenario could take place when the stabilizing pile is installed close to the crest of the slope. Finally, to reach the ultimate safety factor of the reinforced slope, an increasing value of the safety factor of the supported portion of the slope should be used (it means to transfer more soil pressure through the piles) until maximum interaction between the piles and surrounding soil is reached.

6.2. Discussion and application of the proposed method

As above explained, in a decoupled approach the soil-pile interaction is modelled and carried out separately to the global stability analysis which is generally made by using the more traditional limit equilibrium methods. For this reason, the developed method of analysis for a passive pile subjected to the surrounding soil displacement along a defined slip surface, results to be suitable for being implemented in a decoupled approach for the evaluation of the factor of safety of a pile reinforced slope.
Taking into account this hypothesis of a decoupled approach, after the stability analysis of the un-reinforced slope has been carried out, the developed methods can be seen as a simplified methodology for the calculation of pile lateral capacity (i.e., the ultimate pile resistance) assuming the same slope geometry (the effect of which has already been included in the calculation of the demand; i.e., the sought lateral resisting force) and analysing the pile as subjected to lateral soil movement simulating the movement of the sliding mass. The pile load evaluation at this stage depends primarily on the depth of the interface and the mechanical properties of the soil.
Since the requested pile stabilising contribution (i.e. in terms of shear force at the sliding surface) is known, as well as the position of the slip surface along the slope and the soil mechanical properties, the developed design charts or even the explicit formulations expressing the shear forces and bending moments on the pile can be used to derive the design of the stabilizing pile, by evaluating also its deflection.

Anyway, the loading on a stabilising passive pile supposes a movement of the surrounding soil along a sliding surface crossing the pile length. This happens whenever the piles have already been installed in the slope when the soil movement occurs or when they are installed properly to block a failure mechanism already ongoing. If piles are placed in stable slopes, actually not presenting any failure mechanism due to instability, they will not be undergoing any loading (eventually due only to occasional local phenomena if the stress state of the soil changes locally) and will not act as passive piles. It is this relationship between the pile stabilising contribution and the soil movement that makes it necessary to

identify two different cases of stability evaluation for stable and unstable slopes, as this affects also how the contribution of the piles is evaluated and considered in the estimation of the factor of safety SF.

6.2.1.Stable slopes

In case of a stable slope, the factor of safety of the unreinforced configuration is already higher than unity. Inclinometers eventually located in the slope would not indicate any soil sliding phenomena as no free-field soil movements are even expected to occur. Generally, in this situation, piles are only used to reach an even higher target safety factor in order to satisfy regulatory requirements.

Without any loading from the sliding soil, the supposed row of piles would not be subjected to load for the entire life, and their virtual contribution difficult to evaluate as depending on the lack of input parameters. Anyway, it's reasonable to expect an higher slope SF after their realisation and at the same time to consider the piles contribution as an additional potential resistance. As consequence, the piles have to furnish an additional resistance force RF:

$$RF = (SF_T - SF)\, F_d \qquad (6\text{-}16)$$

where SF_T is the target safety factor of the reinforced slope, SF the safety factor of the un-reinforced slope and F_d the total of the disturbing actions along the whole considered slip surface.
the application of the methods requests come considerations:

- Since no failure mechanism are already ongoing in the slope, no slip surfaces can be identified and assumed a priori. This makes necessary to identify all the “critical” surfaces from the initial stability analyses on the un-reinforced slope and analyse them singularly
- As consequence of having several possible sliding geometries, the piles can be crossed at different depth by the slip surfaces. This affects both the design of the single pile and the choice of their position. It is worth here to remember that it is more advisable to install the piles close to the crest or

the centre of the sliding surface, to guarantee a sufficient embedment on the stable layer in order to avoid surfaces deeper than the pile length (and eventually to lead the piles into failure mechanisms type C as it creates the least damage from soil movement on the pile), and to avoid the establishing of new surfaces behind or down the pile row

- No data are available regarding the sliding rate and shape, which has to be virtually assumed then in the application of the analysis. For this purpose, Poulos [73] proposed a reasonable validity of uniformity of the displacement distribution as an appealing simplification so that the displacement imposed on the piles by the sliding mass can be assumed to be uniformly distributed with depth within the sliding block (corresponding to the case of $\eta=1$; cf. paragraph 3.2).

Having the above mentioned guidelines been accomplished, the value of RF can be evaluated for every identified sliding surface and used, in the model, for the design of the pile.
In particular, for a stable slope, as no loading is expected on the pile, the contribute of passive piles can be considered on the basis of the limiting force, in analogy to the approach proposed by Viggiani (and here extended also to a two-layered cohesionless soil).
In case the only horizontal force equilibrium is imposed (i.e. applying the Janbu's simplified analysis method [61]), RF corresponds to the shear force at the depth of the sliding surface. Its value can then be evaluated by applying one of the developed formulations of the limit states as presented in paragraph 4.3 for a two-layered cohesive soil, in paragraph 4.4for a homogeneous cohesion-less soil and in paragraph 5.3 for a two-layered cohesionless soil, or in addition by using one of the corresponding design charts presented.

In example, let consider that a stability analysis on the two-layered slope presented in Figure 6-13a (the soil properties are summarised in the Table 6-1) gave a safety factor higher than unity but still lower than the target value which can be reached by applying an additional resistance contribution RF of 240 kN/m.

By assuming a centre-to-centre pile spacing of 3D (supposed to be enough to establish a soil arching effect between the piles [22]), it corresponds to a shear force on each pile of 720 kN at the depth of the sliding surface, by designing a pile diameter D=1m. Even if actually stable, for the purpose of calculation it is possible to assume the pile as subjected to soil displacements along a potential surface and uniformly distributed with depth (Figure 6-13b).
At this point, let consider a pile of length L=10m, embedded in the stable two-layered slope. The normalised shear force requested to the pile is:

$$T_{\beta,n} = \frac{T_\beta}{p_{u1}L} = \frac{720}{360*10} = 0.20$$

Depending on the position of the pile on the slope, a different depth of the slip surface can be assumed. It is then necessary to evaluated the pile response for every different β. The design chart presented in Figure 4-12 (valid for the considered case in which $k_0=p_{u0}/p_{u1}=2/9$ and $k=p_{u2}/p_{u1}=2$) shows the shear force induced at sliding depth as a function of the normalized sliding depth by the pile length. The design of the pile can be then carried out by choosing a β value corresponding to a normalised shear force higher than the requested value 0.20.
The chart in Figure 4-12 shows that this is possible for any β lying within the interval 0.35-0.9.
In example, let chose a sliding depth $L_s=\beta L=4$m that, according to the formulation presented for mechanism C which prevails for β=0.4, corresponds to the value of limit shear stress on the pile:

$$\frac{T_\beta}{p_{u1}L} = \beta - \frac{1}{2}\lambda(1-k_0) = 0.264$$

Which, in dimensional form, corresponds to

$$T_\beta = [\beta - \frac{1}{2}\lambda(1-k_0)](p_{u1}L) = 0.264 * 3600 = 950.4 \text{ kN}$$

The so evaluated value of shear stress result in fact higher than the requested value to obtain the target safety factor.

Once the pile position is fixed, it is possible to assess the dimensionless maximum bending moment corresponding to the considered limit state by mean of the design charts presented in Figure 4-14,:

$M_n = \frac{M_{max}}{p_{u1} L^2} = 0.040$

so that:

$M_{max} = 0.055\ (p_{u1} L^2) = 1980\ kNm$

Anyway, as no load is expected to act on the pile, no stress state or deflection along the pile are expected to be developed either, so that a structural analysis could not be necessary. It is nevertheless reasonable to design the pile in order to be compatible with the evaluated shear force and the relative maximum bending moment associated to the limit state considered.

Parameters	Sliding layer	Firm layer
S_u [kPa]	40	80
E_s [kPa]	9000	18000
p_{u0} [kN/m]	80	-
p_{u1} [kN/m]	360	-
p_{u2} [kN/m]	-	720

Table 6-1: Soil properties as assumed in the example

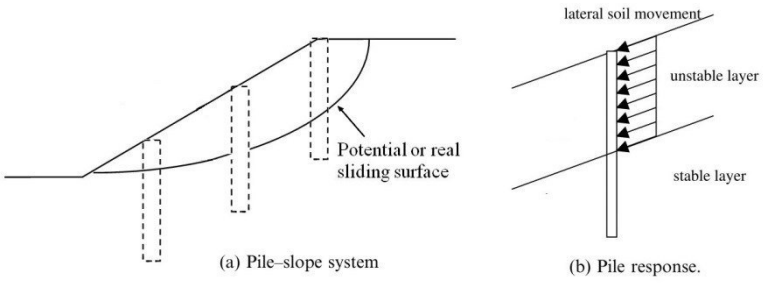

Figure 6-13: Slope geometry as considered in the example

6.2.2. Unstable slope

In case of an unstable slope, the factor of safety of the unreinforced configuration is lower than unity. Also for soils with a residual shear strength lower than the peak strength, the factor of safety can be even less than unity.
In this case, inclinometers eventually located in the slope would indicate the presence of sliding phenomena inside the ground. A surveying campaign on the unstable slope carried out by the use of inclinometers may result to be important as it can lead to a better understanding of the sliding mechanism, its magnitude and overall the shape of the soil displacement distribution, in order to better model the gravitational phenomena in the method. Moreover, the so identified sliding surface may result to be characterised by lower mechanical soil parameters with respect to the adjacent soil and so to be considered as the critical one also after the pile's installation.

Contrary to what expected for the previous case of stable slope, if a gravitational phenomenon is already ongoing or is incipient, the pile can be subjected to the surrounding soil movement and therefore be loaded and deflected until a new equilibrium is reached. The factor of safety of the slope, in such a situation, is essentially equal to 1 (as assumed also by Kourkulis et al. [21]), while that of the pile corresponds to the ratio between its flexural and shear strength and its actual stress state.
In other words, it is reasonable to consider a maximum factor of safety equal to 1 while the pile stabilising contribution is put at the denominator into the SF evaluation as the pile contrasts and absorb the driving forces until a new equilibrium is reached:

$$SF_T = 1 = \frac{F_r}{F_d - RF} \qquad (6\text{-}17)$$

and therefore

$$RF = F_d - F_r \qquad (6\text{-}18)$$

This particular condition should be considered in order to evaluate the effective and real pile stress state and to verify its serviceability by evaluating its deflection

and the associated free-field soil displacement by means of the developed analysis method for passive piles. Being valid the same general consideration made for a stable slope, the lateral capacity of the stabilization piles to soil movements in fact may be assessed using the developed method, which provides the ability to identified the corresponding surrounding soil displacement together which pile deflection and bending moments.

In example, let assume that the equilibrium on the slope is reached by developing a pile contribution RF of 265 kN/m, which assuming a centre-to-centre pile spacing of 3D corresponds to a shear force on each pile of 795 kN at the depth of the sliding surface. By considering the same soil stratigraphy of the previous example, the normalised shear force is:

$$T_n = \frac{T_\beta}{p_{u1} L} = \frac{795}{360 * 10} = 0.2208$$

According to the design chart presented in Figure 4-12 through Figure 4-14, it is possible to assess the dimensionless maximum bending moment:

$M_n = \frac{M_{max}}{p_{u1} L^2} = 0.043$

so that:

$M_{max} = 0.043\ (p_{u1} L^2) = 1540\ kNm$

The dimensionless pile head displacement:

$Y_{0n} = \frac{Y_0 E_{s1}}{p_{u1}} = 2.01$

and pile head displacement:

$Y_0 = 2.01 \frac{p_{u1}}{E_{s1}} = 0.0804\ m$

The correspondent dimensionless soil movement:

$Y_{s0n} = \frac{Y_{s0} E_{s1}}{p_{u1}} = 2.07$

which in meters is:

$Y_{s0} = 2.07 \frac{p_{u1}}{E_{s1}} = 0.0828\text{m}$

This is reasonably the right procedure to analyse the pile stress state and deflection, and so a procedure to carry its structural analysis.

Anyway, an higher FS than unity is usually demanded by guideline requirements: it can be reached only by considering the further increase in potential resistance the pile gives to the slope. At this point, not an agreement is easy to be reached and basically two different scenarios can be formulated:

For the purpose of the stability of the whole slope system, the pile acts only as an additional resistance and only its limit lateral load has to be considered in the assessment of the factor of safety:

$$SF_T = \frac{F_r + RF}{F_d} \qquad (6\text{-}19)$$

in analogy to what expressed in the case of a stable slope. This is essentially in accordance with the assumptions of the most part of authors (i.e. [21], [23], [27], [54]).

Nevertheless, in case the reduction carried by the pile to the driving actions cannot be neglected, both the contributions could be considered:

$$SF_T = \frac{\sum F_r}{\sum F_d} = \frac{F_r + RF_{limit}}{F_d - RF_{effective}} \qquad (6\text{-}20)$$

This assumption seems consistent since, at numerator the additional resistance of the pile (here named as RF_{limit} as represented by the limit lateral load on the pile) contributes to the total amount of resistance available along the slip surface. At the same time, pile's reductive contribution at denominator takes into account the reduced amount of driving actions as a lower mobilisation of soil strength due to the pile presence until the equilibrium is reached is expected.

7. Conclusion and Recommendations

7.1. Summary

The presented displacement- based methods allow for the prediction of passive piles behaviour, based on the interaction between the piles and the surrounding soils.
The mobilised lateral soil-pile pressure acting on the pile segment above the slip surface is determined as a function of the relative soil and pile displacements (i.e., the soil-pile interaction) used as an input.

As recent studies suggest that the response of rigid passive piles is dominated by elastic pile–soil interaction, linear elastic solutions for five different soil stratigraphy conditions have been developed according to a Winkler soil model used to describe the soil behaviour. These solutions result to be suitable to the analysis of passive piles in general conditions whenever small displacement are expected as pile-supported embankments or piles adjacent to excavations.

Moreover, solutions for linear elastic-perfectly plastic models have been presented for the cases of a two-layered soil with a constant distribution of the subgrade reaction modulus and of a homogeneous soil modelled as a Gibson soil type. In addition, the lateral resistance of a passive pile in a double-layered non-cohesive soil has been derived.
A computer software was written in FORTRAN and developed to implement the presented technique and numerically solve the soil-pile interaction problem.
As a design expedient, when it is not possible to carry out a complete site-specific analysis, useful design charts have been derived not only for the ultimate pile response to lateral movements (as suggested by Viggiani) but also for the maximum shear force the pile can furnish in correspondence of different soil movements. Moreover, the maximum shear force given by the pile can be related to its head displacement or to the maximum bending moment.

Finally, the presented methods result adequate to be used in a decoupled approach for the stability analysis of a pile-reinforced slopes, especially for unstable slopes in which, on the basis of the required stabilising force, the method allows to calculate pile deflection and maximum bending moment.
For stable slope, the contribute of passive piles can be considered on the basis of the limiting force evaluated similarity to the approach proposed by Viggiani (and here extended also to a two-layered cohesionless soil).
The following conclusions were obtained as a result of the work of this dissertation:

- ✓ The technique presented has the ability to predict the relative soil-pile displacement: it reflects the true mechanism of the soil-pile interaction and gives the proposed method the capacity to predict different modes of failure in pile-stabilized slopes.

- ✓ The study also shows that the depth of the failure surface at the pile position, the soil type, the pile diameter, and the pile spacings have a combined effect on the driving force that the pile can transfer to the stable soil. It provides the deflection, moment, shear force, and soil- pile reaction along the length of the installed piles. It makes possible to design the piles on the basis of the maximum shear force they must provide in order to stabilise the slope, in according to the results obtained in a previous stability analysis. In addition, the proposed model allow designing the pile also on the basis of the soil or pile head displacements in order to satisfy also specific service requirements.

- ✓ The current method detects how the external soil displacement distribution shape and the pile boundary conditions may effect the different failure modes that can occur.

- ✓ The presented method allows for the calculation of the post-pile installation safety factor (i.e., the stability improvement) for the whole stabilised slope if implemented in a decoupled approach for the evaluation of the factor of safety.

7.2. Future Researches

The presented research work on the passive pile concerned the analysis of rigid piles and suggested the use of the results in a decouples slope stability analysis method. Within these perspectives, further studies on the following areas are planned:

- Development of a program implementing both the FORTRAN code already implemented for the analysis of a single pile and a slope stability analysis for the reinforced and unreinforced slope in order to implement a complete stability analysis tool

- To extend the elasto-plastic analysis to different boundary condition of the pile, in particular the unrotated-head condition

- Development of a new analysis method for flexible passive piles based on a finite-differences model of the pile

REFERENCES

[1] B. Broms, “Lateral resistance of piles in cohesive soils,” *J. Soil Mech. Found. Div.*, vol. 90, no. 2, pp. 27–64, 1964.

[2] H. Matlock and L. C. Reese, “Generalized solutions for laterally loaded piles,” *J. Soil Mech. Found. Div. ASCE*, vol. 86, no. 5, pp. 63–91, 1960.

[3] L. Zhang, “Nonlinear analysis of laterally loaded rigid piles in cohesionless soil,” *Comput. Geotech.*, vol. 36, no. 5, pp. 718–724, Jun. 2009.

[4] E. A. Ellis and S. M. Springman, “Modelling of soil–structure interaction for a piled bridge abutment in plane strain FEM analyses,” *Comput. Geotech.*, vol. 28, no. 2, pp. 79–98, 2001.

[5] E. E. De Beer, “Piles subjected to static lateral loads: State of the Art Report,” in *Proceedings of the 9th ICSMFE Speciality Session-10 Tokyo, pp 1–14*, 1977.

[6] E. A. Ellis, “Soil-structure interaction for full-height piled bridge abutments constructed on soft clay.” University of Cambridge, 1997.

[7] K. Terzaghi, R. B. Peck, and G. Mesri, *Soil mechanics in engineering practice*. John Wiley & Sons, 1996.

[8] H. G. Poulos, “A comparison of some methods for the design of piles through embankments,” *Res. REPORT-UNIVERSITY SYDNEY Sch. Civ. Min. Eng. R*, 1996.

[9] E. E. Beer and M. Wallays, “Forces induced in piles by unsymmetrical surcharges on the soil around the piles,” in *Fifth Eur Conf On Soil Proc/Sp/*, 1972, no. Conf Paper, pp. 325–332.

[10] R. J. Finno, S. A. Lawrence, N. F. Allawh, and I. S. Harahap, “Analysis of performance of pile groups adjacent to deep excavation,” *J. Geotech. Eng.*, vol. 117, no. 6, pp. 934–955, 1991.

[11] H. G. Poulos and L. T. Chen, “Pile response due to unsupported excavation-induced lateral soil movement,” *Can. Geotech. J.*, vol. 33, no. 4, pp. 670–677, 1996.

[12] A. T. C. Goh, K. S. Wong, C. I. Teh, and D. Wen, “Pile response adjacent to braced excavation,” *J. Geotech. Geoenvironmental Eng.*, vol. 129, no. 4, pp. 383–386, 2003.

[13] C. F. Leung, Y. K. Chow, and R. F. Shen, “Behavior of pile subject to excavation-induced soil movement,” *J. Geotech. Geoenvironmental Eng.*, vol. 126, no. 11, pp. 947–954, 2000.

[14] C. F. Leung, J. K. Lim, R. F. Shen, and Y. K. Chow, “Behavior of pile groups subject to excavation-induced soil movement,” *J. Geotech. Geoenvironmental Eng.*, vol. 129, no. 1, pp. 58–65, 2003.

[15] D. E. Ong, C. E. Leung, and Y. K. Chow, “Pile behavior due to excavation-induced soil movement in clay. I: Stable wall,” *J. Geotech. Geoenvironmental Eng.*, vol. 132, no. 1, pp. 36–44, 2006.

[16] C. F. Leung, D. E. Ong, and Y. K. Chow, “Pile behavior due to excavation-induced soil movement in clay. II: Collapsed wall,” *J. Geotech. geoenvironmental Eng.*, vol. 132, no. 1, pp. 45–53, 2006.

[17] Y. K. Chow, “Analysis of piles used for slope stabilization,” *Int. J. Numer. Anal. Methods Geomech.*, vol. 20, no. 9, pp. 635–646, 1996.

[18] F. CAI and K. UGAI, “Numerical analysis of the stability of a slope reinforced with piles,” *Soils Found.*, vol. 40, no. 1, pp. 73–84, 2000.

[19] J. Won, K. You, S. Jeong, and S. Kim, “Coupled effects in stability analysis of pile–slope systems,” *Comput. Geotech.*, vol. 32, no. 4, pp. 304–315, 2005.

[20] W. B. Wei and Y. M. Cheng, “Strength reduction analysis for slope reinforced with one row of piles,” *Comput. Geotech.*, vol. 36, no. 7, pp. 1176–1185, 2009.

[21] R. Kourkoulis, F. Gelagoti, I. Anastasopoulos, and G. Gazetas, “Hybrid method for analysis and design of slope stabilizing piles,” *J. Geotech. Geoenvironmental Eng.*, vol. 138, no. 1, pp. 1–14, 2011.

[22] R. Kourkoulis, F. Gelagoti, I. Anastasopoulos, and G. Gazetas, “Slope Stabilizing Piles and Pile-Groups: Parametric Study and Design Insights,” *J. Geotech. Geoenvironmental Eng.*, vol. 137, no. 7, pp. 663–677, 2011.

[23] C. Viggiani, “Ultimate Lateral Load on Piles used to Stabilize Landslides,” in *Proceedings of the 10th International Conference on Soil Mechanics and Foundation Engineering Stockholm*, 1981, vol. 3, pp. 555–560.

[24] M. F. Randolph and G. T. Houlsby, “The limiting pressure on a circular pile loaded laterally in cohesive soil,” *Geotechnique*, vol. 34, no. 4, pp. 613–623, 1984.

[25] T. Ito and T. Matsui, “Methods to estimate lateral force acting on stabilizing piles,” *Soils Found.*, vol. 15, no. 4, pp. 43–59, 1975.

[26] H. G. Poulos, “Design of reinforcing piles to increase slope stability,” *Can. Geotech. J.*, vol. 32, no. 5, pp. 808–818, Oct. 1995.

[27] C. Y. Lee, T. S. Hull, and H. G. Poulos, “Simplified pile-slope stability analysis,” *Comput. Geotech.*, vol. 17, no. 1, pp. 1–16, 1995.

[28] A. Y. Chmoulian, “Briefing: Analysis of piled stabilisation of landslides,” *Proc. Inst. Civ. Eng. Eng.*, vol. 157, no. 2, pp. 55–56, 2004.

[29] W. D. Guo, “Elastic models for nonlinear response of rigid passive piles,” *Int. J. Numer. Anal. Methods Geomech.*, vol. 38, no. 18, pp. 1969–1989, 2014.

[30] W. D. Guo and H. Y. Qin, “Thrust and bending moment of rigid piles subjected to moving soil,” *Can. Geotech. J.*, vol. 47, no. 2, pp. 180–196, 2010.

[31] L. T. Chen and H. G. Poulos, “Piles subjected to lateral soil movements,” *J.*

Geotech. Geoenvironmental Eng., vol. 123, no. 9, pp. 802–811, 1997.

[32] E. Winkler, "Die lehre von der elastizität und festigkeit (The Theory of Elasticity and Stiffness)," *H. Dominicus Prague, Czechoslov.*, 1867.

[33] K. Terzaghi, "Evalution of coefficients of subgrade reaction," *Geotechnique*, vol. 5, no. 4, pp. 297–326, 1955.

[34] Y. Hsiung and Y. Chen, "Simplified method for analyzing laterally loaded single piles in clays," *J. Geotech. geoenvironmental Eng.*, vol. 123, no. 11, pp. 1018–1029, 1997.

[35] C. Viggiani, *Fondazioni*. Cooperativa Universitaria Editrice Napoletana, 1993.

[36] M. T. Davisson and H. L. Gill, "Laterally Loaded Piles in a Layered Soil System, ASCE," *Proc. ASCE SM3*, 1963.

[37] L. A. Palmer and J. B. Thompson, "The earth pressure and deflection along the embedded lengths of piles subjected to lateral thrusts," in *Proc, 2nd Int. Conf. Soil Mech. and Found. Eng., GEBR Kesmat, Haarlem, The Netherlands*, 1948, vol. 5, pp. 156–161.

[38] H. G. Poulos and E. H. Davis, *Pile foundation analysis and design*, no. Monograph. 1980.

[39] M. T. Davisson, "Lateral load capacity of piles," in *49th Annual Meeting of the Highway Research Board*, 1970, no. 333, pp. 104–112.

[40] L. Decourt, "Load-deflection prediction for laterally loaded piles based on N-SPT values," in *Proceedings of 9th Pan-American Conference on Soil Mechanics and Foundation Engineering*, 1991.

[41] K. Bhushan, L. J. Lee, and D. B. Grime, "Lateral load tests on drilled piers in sand," in *Drilled Piers and Caissons*, 1981, pp. 114–131.

[42] K. Fleming, A. Weltman, M. Randolph, and K. Elson, *Piling engineering*. CRC press, 2008.

[43] T. Ito, T. Matsui, and W. P. Hong, “Design method for stabilizing piles against landslide-one row of piles,” *Soils Found.*, vol. 21, no. 1, pp. 21–37, 1981.

[44] S.-T. Wang and L. C. Reese, “Study of design method for vertical drilled shaft retaining walls,” 1986.

[45] K. Georgiadis, S. W. Sloan, and A. V Lyamin, “Undrained limiting lateral soil pressure on a row of piles,” *Comput. Geotech.*, vol. 54, pp. 175–184, 2013.

[46] S. Kanagasabai, J. A. Smethurst, and W. Powrie, “Three-dimensional numerical modelling of discrete piles used to stabilize landslides,” *Can. Geotech. J.*, vol. 48, no. 9, pp. 1393–1411, 2011.

[47] J. Brinch-Hansen, *The ultimate resistance of rigid piles against transversal forces*. 1961.

[48] L. C. Reese, W. R. Cox, and F. D. Koop, “Analysis of laterally loaded piles in sand,” *Offshore Technol. Civ. Eng. Hall Fame Pap. from Early Years*, pp. 95–105, 1974.

[49] E. A. Ellis, I. K. Durrani, and D. J. Reddish, “Numerical modelling of discrete pile rows for slope stability and generic guidance for design,” *Geotechnique*, vol. 60, no. 3, pp. 185–195, 2010.

[50] K. M. Rollins, K. G. Olsen, D. H. Jensen, B. H. Garrett, R. J. Olsen, and J. J. Egbert, “Pile spacing effects on lateral pile group behavior: Analysis,” *J. Geotech. geoenvironmental Eng.*, vol. 132, no. 10, pp. 1272–1283, 2006.

[51] P. J. Bosscher and D. H. Gray, “Soil arching in sandy slopes,” *J. Geotech. Eng.*, vol. 112, no. 6, pp. 626–645, 1986.

[52] J. M. Duncan, “State of the art: limit equilibrium and finite-element analysis of slopes,” *J. Geotech. Eng.*, vol. 122, no. 7, pp. 577–596, 1996.

[53] T. Ito, T. Matsui, and W. P. Hong, “Extended design method for multi-row stabilizing piles against landslide,” *SOILS Found.*, vol. 22, no. 1, pp. 1–13,

1982.

[54] S. Jeong, B. Kim, J. Won, and J. Lee, “Uncoupled analysis of stabilizing piles in weathered slopes,” *Comput. Geotech.*, vol. 30, no. 8, pp. 671–682, 2003.

[55] A. W. Bishop, “The use of the slip circle in the stability analysis of slopes,” *Geotechnique*, vol. 5, no. 1, pp. 7–17, 1955.

[56] E. Ausilio, E. Conte, and G. Dente, “Stability analysis of slopes reinforced with piles,” *Comput. Geotech.*, vol. 28, no. 8, pp. 591–611, 2001.

[57] T. K. Nian, G. Q. Chen, M. T. Luan, Q. Yang, and D. F. Zheng, “Limit analysis of the stability of slopes reinforced with piles against landslide in nonhomogeneous and anisotropic soils,” *Can. Geotech. J.*, vol. 45, no. 8, pp. 1092–1103, 2008.

[58] D. W. Taylor, *Stability of earth slopes*. Boston Society of Civil Engineers, 1937.

[59] S. Hassiotis, J. L. Chameau, and M. Gunaratne, “Design method for stabilization of slopes with piles,” *J. Geotech. Geoenvironmental Eng.*, vol. 123, no. 4, pp. 314–323, 1997.

[60] E. Spencer, “A method of analysis of the stability of embankments assuming parallel inter-slice forces,” *Geotechnique*, vol. 17, no. 1, pp. 11–26, 1967.

[61] N. Janbu, “Application of composite slip surfaces for stability analysis,” in *Proc. European Conf. on Stability of Earth Slopes, Stockholm, 1954*, 1954, vol. 3, pp. 43–49.

[62] N. R. Morgenstern and V. E. Price, “The analysis of the stability of general slip surfaces,” *Geotechnique*, vol. 15, no. 1, pp. 79–93, 1965.

[63] S. G. Wright, F. G. Kulhawy, and J. M. Duncan, “Accuracy of equilibrium slope stability analysis,” *J. Soil Mech. Found. Div*, vol. 99, no. Proc Paper 10097, 1973.

[64] F. Tavenas, B. Trak, and S. Leroueil, “Remarks on the validity of stability analyses,” *Can. Geotech. J.*, vol. 17, no. 1, pp. 61–73, 1980.

[65] A. K. Chugh, “Variable factor of safety in slope stability analysis,” *Geotechnique*, vol. 36, no. 1, pp. 57–64, 1986.

[66] S. Zeng and R. Y. Liang, “Stability analysis of drilled shafts reinforced slope,” *Soils Found.*, vol. 42, no. 2, pp. 93–102, 2002.

[67] R. Y. Liang and S. Zeng, “Numerical study of soil arching mechanism in drilled shafts for slope stabilization,” *Soils Found.*, vol. 42, no. 2, pp. 83–92, 2002.

[68] M. Yamin and R. Y. Liang, “Limiting equilibrium method for slope/drilled shaft system,” *Int. J. Numer. Anal. Methods Geomech.*, vol. 34, no. 10, pp. 1063–1075, 2010.

[69] R. Y. Liang and M. Yamin, “Three-dimensional finite element study of arching behavior in slope/drilled shafts system,” *Int. J. Numer. Anal. Methods Geomech.*, vol. 34, no. 11, pp. 1157–1168, 2010.

[70] L. Li and R. Y. Liang, “Limit equilibrium based design approach for slope stabilization using multiple rows of drilled shafts,” *Comput. Geotech.*, vol. 59, pp. 67–74, 2014.

[71] M. Ashour and H. Ardalan, “Analysis of pile stabilized slopes based on soil–pile interaction,” *Comput. Geotech.*, vol. 39, pp. 85–97, 2012.

[72] M. Ashour, P. Pilling, and G. Norris, “Lateral behavior of pile groups in layered soils,” *J. Geotech. Geoenvironmental Eng.*, vol. 130, no. 6, pp. 580–592, 2004.

[73] H. G. Poulos, “Design of slope stabilizing piles,” *Res. REPORT-UNIVERSITY SYDNEY Dep. Civ. Eng. R*, 1999.

APPENDICES

APPENDIX A
Cases for the elasto-plastic analysis of passive rigid piles in cohesive soils

Since there exist several possible cases for given geometry and pile-soil properties, all analysed and implemented cases concerning the nonlinear analysis method for passive rigid piles in cohesive soils are presented as derived from eight more complex cases, all named following the nomenclature used for the single configurations. Limit cases B1 and B2 are also presented.

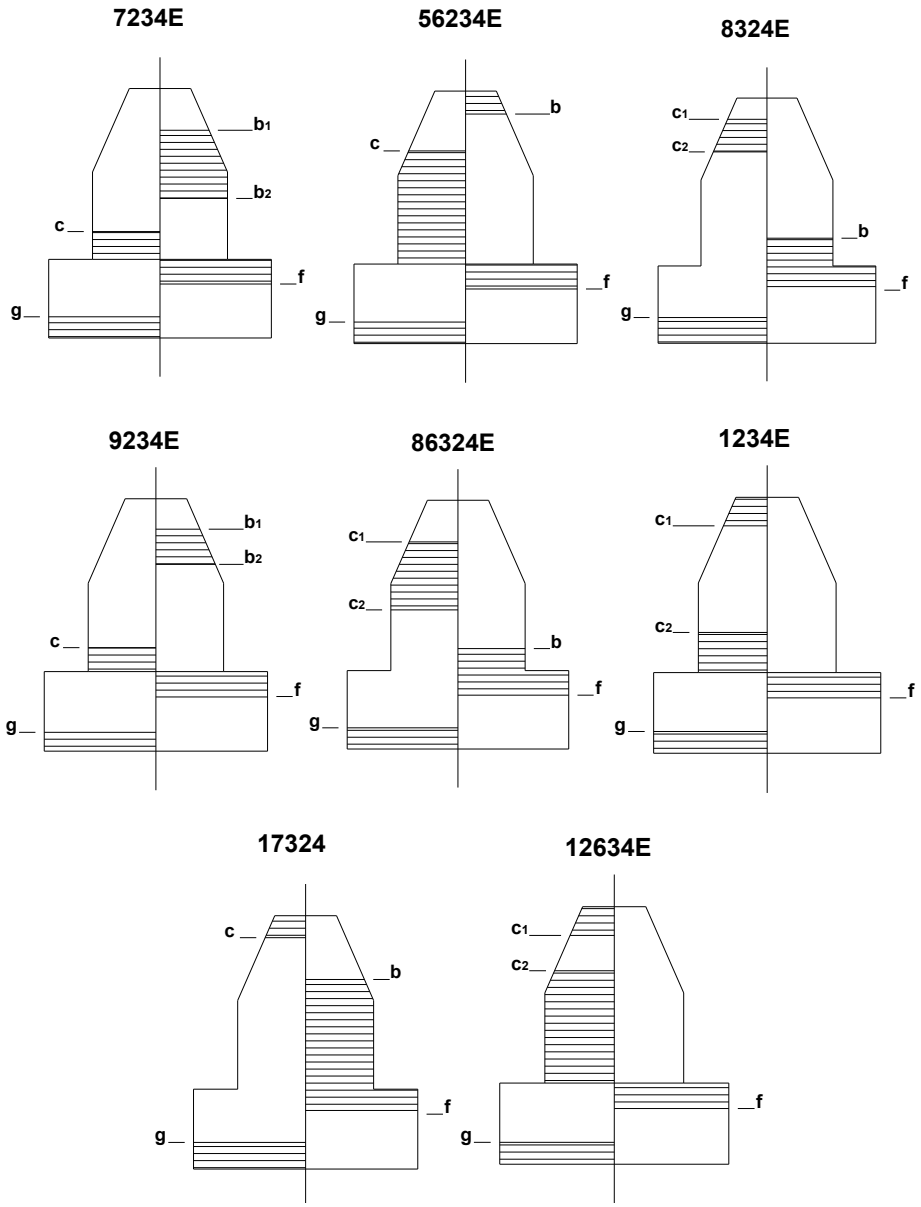

Figure A-1: Basic cases used to derive all others configurations and their yielding zone with regards to the ultimate soil pressure distribution assumed in the model

The following tables describes the main cases dependencies and the values to assign to the parameters of the system in order to obtain every particular case. (Case 17324 does not have any dependencies).

Case	b_1	b_2	c	f	g
7234	b_1	b_2	c	f	g
57234	0	b	c	f	g
5723	0	b	c	f	L
723	b_1	b_2	c	f	L
572	0	b	c	L_S	L
57	0	b	L_S	L_S	L
30570	0	b	L_S	L	L
30572	0	b	c	L	L
30072	b_1	b_2	c	L	L

Table A-1: Cases derived from the case 7234E

Case	c_1	c_2	b	f	g
8324	c_1	c_2	b	f	g
10324	0	c	b	f	g
324	0	0	b	f	g
832	c_1	c_2	b	f	L
132	0	c	b	f	L
32	0	0	b	f	L
134	0	c	L_S	f	g
13	0	c	L_S	f	L
14	0	c	L_S	L_S	g
83	c_1	c_2	L_S	f	L
8	c_1	c_2	L_S	L_S	L
1	0	c	L_S	L_S	L
834	c_1	c_2	L_S	f	g

Table A-2: Cases derived from the case 8324E

Case	b	c	f	g
56234	b	c	f	g
5623	b	c	f	L
562	b	c	L_S	L
2634	0	c	f	g
263	0	c	f	L
26	0	c	L_S	L
30260	0	c	L	L
30562	b	c	L	L

Table A-3: Cases derived from the case 56234E

Case	c_1	c_2	b	f	g
86324	c_1	c_2	b	f	g
16324	0	c	b	f	g
1632	0	c	b	f	L
1634	0	c	L_S	f	g
863	c_1	c_2	L_S	f	L
86	c_1	c_2	L_S	L_S	L
8634	c_1	c_2	L_S	f	g
8632	c_1	c_2	b	f	L
163	0	c	L_S	f	L
16	0	c	L_S	L_S	L

Table A-4: Cases derived from the case 86324E

Case	c_1	c_2	f	g
12634	c_1	c_2	f	g
1263	c_1	c_2	f	L
126	c_1	c_2	L_S	L

Table A-5: Cases derived from the case 12634E

Case	b_1	b_2	c	f	g
9234	b_1	b_2	c	f	g
50234	0	b	c	f	g
923	b_1	b_2	c	f	L
523	0	b	c	f	L
53	0	b	L_S	f	L
52	0	b	c	L_S	L
5	0	b	L_S	L_S	L
234	0	0	c	f	g
23	0	0	c	f	L
34	0	0	L_S	f	g
2	0	0	c	L_S	L
3	0	0	L_S	f	L
4	0	0	L_S	L_S	g
30000	0	0	L_S	L	L
30200	0	0	c	L	L
30500	0	b	L_S	L	L
30502	0	b	c	L	L
30092	b_1	b_2	c	L	L

Table A-6: Cases derived from the case 9234E

Case	c_1	c_2	f	g
16200 (C1)	L_0	L_0	L_S	L
16230 (C2)	L_0	L_0	f	L
16234 (C3)	L_0	L_0	f	g
1234	c_1	c_2	f	g
123	c_1	c_2	f	L
12	c_1	c_2	L_S	L
1	c	L_S	L_S	L
2	0	c	L_S	L
3	0	L_S	L_S	L
4	0	L_S		

Table A-7: Cases derived from the case 1234E

The eight generalised cases are described as follow:

CASE 8324E

Soil pressure distribution:

$p = -(E_{s0} + nz)(\Delta y_0 - z \cdot \Delta t)$ $\quad 0 < z < c_1$

$p = p_{u0} + mz$ $\quad c_1 < z < c_2$

$p = -(E_{s0} + nz)(\Delta y_0 - z \cdot \Delta t)$ $\quad c_2 < z < \lambda L$

$p = -(E_{s1})(\Delta y_0 - z \cdot \Delta t)$ $\quad \lambda L < z < b$

$p = -p_{u1}$ $\quad b < z < \beta L$

$p = -p_{u2}$ $\quad \beta L < z < f$

$p = -(E_{s2})(y_0 - z \cdot tan\omega)$ $\quad f < z < g$

$p = p_{u2}$ $\quad g < z < L$

Shear force equilibrium:

$$-E_{s0}\Delta y_0(c_1) + \frac{1}{2}E_{s0}\Delta t(c_1^2) - \frac{1}{2}n\Delta y_0(c_1^2) + \frac{1}{3}n\Delta t(c_1^3) + p_{u0}(c_2 - c_1) + \frac{1}{2}m(c_2^2 - c_1^2)$$

$$-E_{s0}\Delta y_0(\lambda L - c_2) + \frac{1}{2}E_{s0}\Delta t(\lambda^2 L^2 - c_2^2) - \frac{1}{2}n\Delta y_0(\lambda^2 L^2 - c_2^2) + \frac{1}{3}n\Delta t(\lambda^3 L^3 - c_2^3)$$

$$-E_{s1}\Delta y_0(b - \lambda L) + \frac{1}{2}E_{s1}\Delta t(b^2 - \lambda^2 L^2) - p_{u1}(\beta L - b) - p_{u2}(f - \beta L)$$

$$-E_{s2}y_0(g - f) + \frac{1}{2}E_{s2}\tan\omega(g^2 - f^2) + p_{u2}(L - g) = 0$$

Bending moment equilibrium:

$$-\frac{1}{2}E_{s0}\Delta y_0(c_1^2) + \frac{1}{3}E_{s0}\Delta t(c_1^3) - \frac{1}{3}n\Delta y_0(c_1^3) + \frac{1}{4}n\Delta t(c_1^4) + \frac{1}{2}p_{u0}(c_2^2 - c_1^2) + \frac{1}{3}m(c_2^3 - c_1^3)$$

$$-\frac{1}{2}E_{s0}\Delta y_0(\lambda^2 L^2 - c_2^2) + \frac{1}{3}E_{s0}\Delta t(\lambda^3 L^3 - c_2^3) - \frac{1}{3}n\Delta y_0(\lambda^3 L^3 - c_2^3) + \frac{1}{4}n\Delta t(\lambda^4 L^4 - c_2^4)$$

$$-\frac{1}{2}E_{s1}\Delta y_0(b^2 - \lambda^2 L^2) + \frac{1}{3}E_{s1}\Delta t(b^3 - \lambda^3 L^3) - \frac{1}{2}p_{u1}(\beta^2 L^2 - b^2) - \frac{1}{2}p_{u2}(f^2 - \beta^2 L^2)$$

$$-\frac{1}{2}E_{s2}y_0(g^2 - f^2) + \frac{1}{3}E_{s2}\tan\omega(g^3 - f^3) + \frac{1}{2}p_{u2}(L^2 - g^2) = 0$$

Congruence:

$$b = \frac{\Delta y_0 - p_{u1}/E_{s1}}{\Delta t} \qquad f = \frac{y_0 - p_{u2}/E_{s2}}{tan\omega} \qquad g = \frac{y_0 + p_{u2}/E_{s2}}{tan\omega}$$

$$c_{1,2} = \frac{-E_{s0}\Delta t + n\Delta y_0 + m \pm \sqrt{(-E_{s0}\Delta t + n\Delta y_0 + m)^2 + 4n\Delta t(E_{s0}\Delta y_0 + p_{u0})}}{2n\Delta t}$$

Shear force:

$$T_1 = -E_{s0}\Delta y_0(z) + \frac{1}{2}E_{s0}\Delta t(z^2) - \frac{1}{2}n\Delta y_0(z^2) + \frac{1}{3}n\Delta t(z^3) \qquad 0 < z < c_1$$

$$T_2 = p_{u0}(z - c_1) + \frac{1}{2}m(z^2 - c_1^2) - E_{s0}\Delta y_0(c_1) + \frac{1}{2}E_{s0}\Delta t(c_1^2) - \frac{1}{2}n\Delta y_0(c_1^2) + \frac{1}{3}n\Delta t(c_1^3) \qquad c_1 < z < c_2$$

$$T_3 = -E_{s0}\Delta y_0(z - c_2) + \frac{1}{2}E_{s0}\Delta t(z^2 - c_2^2) - \frac{1}{2}n\Delta y_0(z^2 - c_2^2) + \frac{1}{3}n\Delta t(z^3 - c_2^3)$$

$$+ p_{u0}(c_2 - c_1) + \frac{1}{2}m(c_2^2 - c_1^2) - E_{s0}\Delta y_0(c_1) + \frac{1}{2}E_{s0}\Delta t(c_1^2) - \frac{1}{2}n\Delta y_0(c_1^2) + \frac{1}{3}n\Delta t(c_1^3) \qquad c_2 < z < \lambda L$$

$$T_4 = -E_{s1}\Delta y_0(z - b) + \frac{1}{2}E_{s1}\Delta t \cdot (z^2 - b^2) - pu1(b - \beta L)$$

$$- p_{u2}(\beta L - f) - E_{s2}y_0(f - g) + \frac{1}{2}E_{s2}\tan\omega(f^2 - g^2) + p_{u2}(g - L) \qquad \lambda L < z < b$$

$$T_5 = -p_{u1}(z - \beta L) - p_{u2}(\beta L - f) - E_{s2}y_0(f - g) + \frac{1}{2}E_{s2}\tan\omega(f^2 - g^2) + p_{u2}(g - L) \qquad b < z < \beta L$$

$$T_6 = -p_{u2}(z-f) - E_{s2}y_0(f-g) + \frac{1}{2}E_{s2}\tan\omega\left(f^2-g^2\right) + p_{u2}(g-L) \qquad \beta L < z < f$$

$$T_7 = -E_{s2}y_0(z-g) + \frac{1}{2}E_{s2}\tan\omega\left(z^2-g^2\right) + p_{u2}(g-L) \qquad f < z < g$$

$$T_8 = p_{u2}(z-L) \qquad g < z < L$$

Bending moment:

$$M_1 = -\frac{1}{2}E_{s0}\Delta y_0\left(z^2\right) + \frac{1}{6}E_{s0}\Delta t\left(z^3\right) - \frac{1}{6}n\Delta y_0\left(z^3\right) + \frac{1}{12}n\Delta t\left(z^4\right) \qquad 0 < z < c_1$$

$$M_2 = p_{u0}\left(\frac{1}{2}z^2 - c_1 z + \frac{1}{2}c_1^{\,2}\right) + \frac{1}{2}m\left(\frac{1}{3}z^3 - c_1^{\,2}z + \frac{2}{3}c_1^{\,3}\right) - E_{s0}\Delta y_0(c_1)(z-c_1) + \frac{1}{2}E_{s0}\Delta t\left(c_1^{\,2}\right)(z-c_1)$$
$$-\frac{1}{2}n\Delta y_0\left(c_1^{\,2}\right)(z-c_1) + \frac{1}{3}n\Delta t\left(c_1^{\,3}\right)(z-c_1) - \frac{1}{2}E_{s0}\Delta y_0\left(c_1^{\,2}\right) + \frac{1}{6}E_{s0}\Delta t\left(c_1^{\,3}\right) - \frac{1}{6}n\Delta y_0\left(c_1^{\,3}\right) + \frac{1}{12}n\Delta t\left(c_1^{\,4}\right) \qquad c_1 < z < c_2$$

$$M_3 = -E_{s0}\Delta y_0\left(\frac{1}{2}z^2 - c_2 z + \frac{1}{2}c_2^{\,2}\right) + \frac{1}{2}E_{s0}\Delta t\left(\frac{1}{3}z^3 - c_2^{\,2}z + \frac{2}{3}c_2^{\,3}\right) - \frac{1}{2}n\Delta y_0\left(\frac{1}{3}z^3 - c_2^{\,2}z + \frac{2}{3}c_2^{\,3}\right)$$
$$+\frac{1}{3}n\Delta t\left(\frac{1}{4}z^4 - c_2^{\,3}z + \frac{3}{4}c_2^{\,4}\right) + p_{u0}(c_2-c_1)(z-c_2) + \frac{1}{2}m\left(c_2^{\,2}-c_1^{\,2}\right)(z-c_2)$$
$$-E_{s0}\Delta y_0(c_1)(z-c_2) + \frac{1}{2}E_{s0}\Delta t\left(c_1^{\,2}\right)(z-c_2) - \frac{1}{2}n\Delta y_0\left(c_1^{\,2}\right)(z-c_2) + \frac{1}{3}n\Delta t\left(c_1^{\,3}\right)(z-c_2) \qquad c_2 < z < \lambda L$$
$$+p_{u0}\left(\frac{1}{2}c_2^{\,2} - c_1 c_2 + \frac{1}{2}c_1^{\,2}\right) + \frac{1}{2}m\left(\frac{1}{3}c_2^{\,3} - c_1^{\,2}c_2 + \frac{2}{3}c_1^{\,3}\right) - E_{s0}\Delta y_0(c_1)(c_2-c_1) + \frac{1}{2}E_{s0}\Delta t\left(c_1^{\,2}\right)(c_2-c_1)$$
$$-\frac{1}{2}n\Delta y_0\left(c_1^{\,2}\right)(c_2-c_1) + \frac{1}{3}n\Delta t\left(c_1^{\,3}\right)(c_2-c_1) - \frac{1}{2}E_{s0}\Delta y_0\left(c_1^{\,2}\right) + \frac{1}{6}E_{s0}\Delta t\left(c_1^{\,3}\right) - \frac{1}{6}n\Delta y_0\left(c_1^{\,3}\right) + \frac{1}{12}n\Delta t\left(c_1^{\,4}\right)$$

$$M_4 = -E_{s1}\Delta y_0\left(\frac{1}{2}z^2 - bz + \frac{1}{2}b^2\right) + \frac{1}{2}E_{s1}\Delta t\cdot\left(\frac{1}{3}z^3 - b^2 z + \frac{2}{3}b^3\right)$$
$$-pul(b-\beta L)(z-b) - p_{u2}(\beta L - f)(z-b) - E_{s2}y_0(f-g)(z-b) + \frac{1}{2}E_{s2}\tan\omega\left(f^2-g^2\right)(z-b)$$
$$-p_{u2}(g-L)(z-b) - pul\left(\frac{1}{2}b^2 - \beta L b + \frac{1}{2}\beta^2 L^2\right) - p_{u2}(\beta L - f)(b-\beta L) - E_{s2}y_0(f-g)(b-\beta L) \qquad \lambda L < z < b$$
$$+\frac{1}{2}E_{s2}\tan\omega\left(f^2-g^2\right)(b-\beta L) - p_{u2}(g-L)(b-\beta L)$$
$$-p_{u2}\left(\frac{1}{2}\beta^2 L^2 - f\beta L + \frac{1}{2}f^2\right) - E_{s2}y_0(f-g)(\beta L - f) + \frac{1}{2}E_{s2}\tan\omega\left(f^2-g^2\right)(\beta L - f) - p_{u2}(g-L)(\beta L - f)$$
$$-E_{s2}y_0\left(\frac{1}{2}f^2 - gf + \frac{1}{2}g^2\right) - \frac{1}{2}E_{s2}\tan\omega\left(\frac{1}{3}f^3 - g^2 f + \frac{2}{3}g^3\right) + p_{u2}(g-L)(f-g) + p_{u2}\left(\frac{1}{2}g^2 - Lg + \frac{1}{2}L^2\right)$$

$$M_5 = -pul\left(\frac{1}{2}z^2 - \beta L z + \frac{1}{2}\beta^2 L^2\right) - p_{u2}(\beta L - f)(z-\beta L) - E_{s2}y_0(f-g)(z-\beta L)$$
$$+\frac{1}{2}E_{s2}\tan\omega\left(f^2-g^2\right)(z-\beta L) + p_{u2}(g-L)(z-\beta L) - p_{u2}\left(\frac{1}{2}\beta^2 L^2 - f\beta L + \frac{1}{2}f^2\right) \qquad b < z < \beta L$$
$$-E_{s2}y_0(f-g)(\beta L - f) + \frac{1}{2}E_{s2}\tan\omega\left(f^2-g^2\right)(\beta L - f) + p_{u2}(g-L)(\beta L - f)$$
$$-E_{s2}y_0\left(\frac{1}{2}f^2 - gf + \frac{1}{2}g^2\right) + \frac{1}{2}E_{s2}\tan\omega\left(\frac{1}{3}f^3 - g^2 f + \frac{2}{3}g^3\right)$$
$$+p_{u2}(g-L)(f-g) + p_{u2}\left(\frac{1}{2}g^2 - Lg + \frac{1}{2}L^2\right)$$

$$M_6 = -p_{u2}\left(\frac{1}{2}z^2 - fz + \frac{1}{2}f^2\right) - E_{s2}y_0(f-g)(z-f) + \frac{1}{2}E_{s2}\tan\omega\left(f^2 - g^2\right)(z-f)$$
$$+ p_{u2}(g-L)(z-f) - E_{s2}y_0\left(\frac{1}{2}f^2 - gf + \frac{1}{2}g^2\right)$$
$$+ \frac{1}{2}E_{s2}\tan\omega\left(\frac{1}{3}f^3 - g^2 f + \frac{2}{3}g^3\right) + p_{u2}(g-L)(f-g) + p_{u2}\left(\frac{1}{2}g^2 - Lg + \frac{1}{2}L^2\right)$$

βL < z < f

$$M_7 = -E_{s2}y_0\left(\frac{1}{2}z^2 - gz + \frac{1}{2}g^2\right) + \frac{1}{2}E_{s2}\tan\omega\left(\frac{1}{3}z^3 - g^2 z + \frac{2}{3}g^3\right)$$
$$+ p_{u2}(g-L)(z-g) + p_{u2}\left(\frac{1}{2}g^2 - Lg + \frac{1}{2}L^2\right)$$

f < z < g

$$M_8 = p_{u2}\left(\frac{1}{2}z^2 - Lz + \frac{1}{2}L^2\right)$$

g < z < L

CASE 86324E

Soil pressure distribution:

$p = -(E_{s0} + nz)(\Delta y_0 - z \cdot \Delta t)$ $\quad 0 < z < c_1$

$p = p_{u0} + mz$ $\quad c_1 < z < \lambda L$

$p = p_{u1}$ $\quad \lambda L < z < c_2$

$p = -(E_{s1})(\Delta y_0 - z \cdot \Delta t)$ $\quad c_2 < z < b$

$p = -p_{u1}$ $\quad b < z < \beta L$

$p = -p_{u2}$ $\quad \beta L < z < f$

$p = -(E_{s2})(y_0 - z \cdot tan\omega)$ $\quad f < z < g$

$p = p_{u2}$ $\quad g < z < L$

Shear force equilibrium

$$-E_{s0}\Delta y_0(c_1) + \frac{1}{2}E_{s0}\Delta t(c_1^2) - \frac{1}{2}n\Delta y_0(c_1^2) + \frac{1}{3}n\Delta t(c_1^3) + p_{u0}(\lambda L - c_1)$$
$$+\frac{1}{2}m(\lambda^2 L^2 - c_1^2) + p_{u1}(c_2 - \lambda L) - E_{s1}\Delta y_0(b - c_2) + \frac{1}{2}E_{s1}\Delta t(b^2 - c_2^2)$$
$$-p_{u1}(\beta L - b) - p_{u2}(f - \beta L) - E_{s2}y_0(g - f) + \frac{1}{2}E_{s2}\tan\omega(g^2 - f^2) + p_{u2}(g - L) = 0$$

Bending moment equilibrium

$$-\frac{1}{2}E_{s0}\Delta y_0(c_1^2) + \frac{1}{3}E_{s0}\Delta t(c_1^3) - \frac{1}{3}n\Delta y_0(c_1^3) + \frac{1}{4}n\Delta t(c_1^4) + \frac{1}{2}p_{u0}(\lambda^2 L^2 - c_1^2) + \frac{1}{3}m(\lambda^3 L^3 - c_1^3)$$
$$+\frac{1}{2}p_{u1}(c_2^2 - \lambda^2 L^2) - \frac{1}{2}E_{s1}\Delta y_0(b^2 - c_2^2) + \frac{1}{3}E_{s1}\Delta t(b^3 - c_2^3) - \frac{1}{2}p_{u1}(\beta^2 L^2 - b^2)$$
$$-p_{u2}\frac{1}{2}(f^2 - \beta^2 L^2) - \frac{1}{2}E_{s2}y_0(g^2 - f^2) + \frac{1}{3}E_{s2}\tan\omega(g^3 - f^3) + p_{u2}\frac{1}{2}(g^2 - L^2) = 0$$

Congruence in z = c_1 e in z = c_2

$$c_1 = \frac{-E_{s0}\Delta t + n\Delta y_0 + m \pm \sqrt{(-E_{s0}\Delta t + n\Delta y_0 + m)^2 + 4n\Delta t(E_{s0}\Delta y_0 + p_{u0})}}{2n\Delta t}$$

$$c_2 = \frac{\Delta y_0 + p_{u1}/E_{s1}}{\Delta t}$$

Shear force

$T_1 = -E_{s0}\Delta y_0(z) + \frac{1}{2}E_{s0}\Delta t(z^2) - \frac{1}{2}n\Delta y_0(z^2) + \frac{1}{3}n\Delta t(z^3)$ $\quad 0 < z < c_1$

$T_2 = p_{u0}(z - c_1) + \frac{1}{2}m(z^2 - c_1^2) - E_{s0}\Delta y_0(c_1) + \frac{1}{2}E_{s0}\Delta t(c_1^2) - \frac{1}{2}n\Delta y_0(c_1^2) + \frac{1}{3}n\Delta t(c_1^3)$ $\quad c_1 < z < \lambda L$

$T_3 = +p_{u1}(z - \lambda L) + p_{u0}(\lambda L - c_1) + \frac{1}{2}m(\lambda^2 L^2 - c_1^2) - E_{s0}\Delta y_0(c_1)$
$+\frac{1}{2}E_{s0}\Delta t(c_1^2) - \frac{1}{2}n\Delta y_0(c_1^2) + \frac{1}{3}n\Delta t(c_1^3)$ $\quad \lambda L < z < c_2$

$$T_4 = -E_{s1}\Delta y_0(z-b)+\frac{1}{2}E_{s1}\Delta t\cdot(z^2-b^2)-pu1(b-\beta L)$$
$$-p_{u2}(\beta L-f)-E_{s2}y_0(f-g)+\frac{1}{2}E_{s2}\tan\omega(f^2-g^2)+p_{u2}(g-L) \qquad c_2 < z < b$$

$$T_5 = -p_{u1}(z-\beta L)-p_{u2}(\beta L-f)-E_{s2}y_0(f-g)+\frac{1}{2}E_{s2}\tan\omega(f^2-g^2)+p_{u2}(g-L) \qquad b < z < \beta L$$

$$T_6 = -p_{u2}(z-f)-E_{s2}y_0(f-g)+\frac{1}{2}E_{s2}\tan\omega(f^2-g^2)+p_{u2}(g-L) \qquad \beta L < z < f$$

$$T_7 = -E_{s2}y_0(z-g)+\frac{1}{2}E_{s2}\tan\omega(z^2-g^2)+p_{u2}(g-L) \qquad f < z < g$$

$$T_8 = +p_{u2}(z-L) \qquad g < z < L$$

$$T_\beta = -E_{s2}y_0(\beta L-L)+\frac{1}{2}E_{s2}tan\omega(\beta^2L^2-L^2) \qquad z = \beta L$$

Bending moment

$$M_1 = -\frac{1}{2}E_{s0}\Delta y_0(z^2)+\frac{1}{6}E_{s0}\Delta t(z^3)-\frac{1}{6}n\Delta y_0(z^3)+\frac{1}{12}n\Delta t(z^4) \qquad 0 < z < c_1$$

$$M_2 = p_{u0}\left(\frac{1}{2}z^2-c_1z+\frac{1}{2}c_1^2\right)+\frac{1}{2}m\left(\frac{1}{3}z^3-c_1^2z+\frac{2}{3}c_1^3\right)-E_{s0}\Delta y_0(c_1)(z-c_1)+\frac{1}{2}E_{s0}\Delta t(c_1^2)(z-c_1)$$
$$-\frac{1}{2}n\Delta y_0(c_1^2)(z-c_1)+\frac{1}{3}n\Delta t(c_1^3)(z-c_1)-\frac{1}{2}E_{s0}\Delta y_0(c_1^2)+\frac{1}{6}E_{s0}\Delta t(c_1^3)-\frac{1}{6}n\Delta y_0(c_1^3)+\frac{1}{12}n\Delta t(c_1^4) \qquad c_1 < z < \lambda L$$

$$M_3 = p_{u1}\left(\frac{1}{2}z^2-\lambda Lz+\frac{1}{2}\lambda^2L^2\right)+p_{u0}(\lambda L-c_1)(z-\lambda L)+\frac{1}{2}m(\lambda L^2-c_1^2)(z-\lambda L)-E_{s0}\Delta y_0(c_1)(z-\lambda L)$$
$$+\frac{1}{2}E_{s0}\Delta t(c_1^2)(z-\lambda L)-\frac{1}{2}n\Delta y_0(c_1^2)(z-\lambda L)+\frac{1}{3}n\Delta t(c_1^3)(z-\lambda L) \qquad \lambda L < z < c_2$$
$$+p_{u0}\left(\frac{1}{2}\lambda L^2-c_1\lambda L+\frac{1}{2}c_1^2\right)+\frac{1}{2}m\left(\frac{1}{3}\lambda L^3-c_1^2\lambda L+\frac{2}{3}c_1^3\right)-E_{s0}\Delta y_0(c_1)(\lambda L-c_1)+\frac{1}{2}E_{s0}\Delta t(c_1^2)(\lambda L-c_1)$$
$$-\frac{1}{2}n\Delta y_0(c_1^2)(\lambda L-c_1)+\frac{1}{3}n\Delta t(c_1^3)(\lambda L-c_1)-\frac{1}{2}E_{s0}\Delta y_0(c_1^2)+\frac{1}{6}E_{s0}\Delta t(c_1^3)-\frac{1}{6}n\Delta y_0(c_1^3)+\frac{1}{12}n\Delta t(c_1^4)$$

$$M_4 = -E_{s1}\Delta y_0\left(\frac{1}{2}z^2-bz+\frac{1}{2}b^2\right)+\frac{1}{2}E_{s1}\Delta t\cdot\left(\frac{1}{3}z^3-b^2z+\frac{2}{3}b^3\right)-pu1(b-\beta L)(z-b)-p_{u2}(\beta L-f)(z-b)$$
$$-E_{s2}y_0(f-g)(z-b)+\frac{1}{2}E_{s2}\tan\omega(f^2-g^2)(z-b)-p_{u2}(g-L)(z-b)-pu1\left(\frac{1}{2}b^2-\beta Lb+\frac{1}{2}\beta^2L^2\right) \qquad c_2 < z < b$$
$$-p_{u2}(\beta L-f)(b-\beta L)-E_{s2}y_0(f-g)(b-\beta L)+\frac{1}{2}E_{s2}\tan\omega(f^2-g^2)(b-\beta L)-p_{u2}(g-L)(b-\beta L)$$
$$-p_{u2}\left(\frac{1}{2}\beta^2L^2-f\beta L+\frac{1}{2}f^2\right)-E_{s2}y_0(f-g)(\beta L-f)+\frac{1}{2}E_{s2}\tan\omega(f^2-g^2)(\beta L-f)-p_{u2}(g-L)(\beta L-f)$$
$$-E_{s2}y_0\left(\frac{1}{2}f^2-gf+\frac{1}{2}g^2\right)-\frac{1}{2}E_{s2}\tan\omega\left(\frac{1}{3}f^3-g^2f+\frac{2}{3}g^3\right)+p_{u2}(g-L)(f-g)+p_{u2}\left(\frac{1}{2}g^2-Lg+\frac{1}{2}L^2\right)$$

$$M_5 = -pu1\left(\frac{1}{2}z^2-\beta Lz+\frac{1}{2}\beta^2L^2\right)-p_{u2}(\beta L-f)(z-\beta L)-E_{s2}y_0(f-g)(z-\beta L)$$
$$+\frac{1}{2}E_{s2}\tan\omega(f^2-g^2)(z-\beta L)-p_{u2}(g-L)(z-\beta L)-p_{u2}\left(\frac{1}{2}\beta^2L^2-f\beta L+\frac{1}{2}f^2\right) \qquad b < z < \beta L$$
$$-E_{s2}y_0(f-g)(\beta L-f)+\frac{1}{2}E_{s2}\tan\omega(f^2-g^2)(\beta L-f)-p_{u2}(g-L)(\beta L-f)$$
$$-E_{s2}y_0\left(\frac{1}{2}f^2-gf+\frac{1}{2}g^2\right)-\frac{1}{2}E_{s2}\tan\omega\left(\frac{1}{3}f^3-g^2f+\frac{2}{3}g^3\right)+p_{u2}(g-L)(f-g)+p_{u2}\left(\frac{1}{2}g^2-Lg+\frac{1}{2}L^2\right)$$

$$M_6 = -p_{u2}\left(\frac{1}{2}z^2 - fz + \frac{1}{2}f^2\right) - E_{s2}y_0(f-g)(z-f) + \frac{1}{2}E_{s2}\tan\omega\left(f^2 - g^2\right)(z-f)$$
$$- p_{u2}(g-L)(z-f) - E_{s2}y_0\left(\frac{1}{2}f^2 - gf + \frac{1}{2}g^2\right)$$
$$-\frac{1}{2}E_{s2}\tan\omega\left(\frac{1}{3}f^3 - g^2 f + \frac{2}{3}g^3\right) + p_{u2}(g-L)(f-g) + p_{u2}\left(\frac{1}{2}g^2 - Lg + \frac{1}{2}L^2\right)$$

βL < z < f

$$M_7 = -E_{s2}y_0\left(\frac{1}{2}z^2 - gz + \frac{1}{2}g^2\right) - \frac{1}{2}E_{s2}\tan\omega\left(\frac{1}{3}z^3 - g^2 z + \frac{2}{3}g^3\right)$$
$$+ p_{u2}(g-L)(z-g) + p_{u2}\left(\frac{1}{2}g^2 - Lg + \frac{1}{2}L^2\right)$$

f < z < g

$$M_8 = p_{u2}\left(\frac{1}{2}z^2 - Lz + \frac{1}{2}L^2\right)$$

g < z < L

CASE 9234E

Soil pressure distribution:

$p = -(E_{s0} + nz)(\Delta y_0 - z \cdot \Delta t)$ $\quad 0 < z < b_1$

$p = -p_{u0} - mz$ $\quad b_1 < z < b_2$

$p = -(E_{s0} + nz)(\Delta y_0 - z \cdot \Delta t)$ $\quad b_2 < z < \lambda L$

$p = -(E_{s1})(\Delta y_0 - z \cdot \Delta t)$ $\quad \lambda L < z < c$

$p = p_{u1}$ $\quad c < z < \beta L$

$p = -p_{u2}$ $\quad \beta L < z < f$

$p = -(E_{s2})(y_0 - z \cdot tan\omega)$ $\quad f < z < g$

$p = p_{u2}$ $\quad g < z < L$

Shear force equilibrium

$$-E_{s0}\Delta y_0(b_1) + \frac{1}{2}E_{s0}\Delta t(b_1^2) - \frac{1}{2}n\Delta y_0(b_1^2) + \frac{1}{3}n\Delta t(b_1^3) - p_{u0}(b_2 - b_1) - \frac{1}{2}m(b_2^2 - b_1^2)$$

$$-E_{s0}\Delta y_0(\lambda L - b_2) + \frac{1}{2}E_{s0}\Delta t(\lambda^2 L^2 - b_2^2) - \frac{1}{2}n\Delta y_0(\lambda^2 L^2 - b_2^2) + \frac{1}{3}n\Delta t(\lambda^3 L^3 - b_2^3)$$

$$-E_{s1}\Delta y_0(c - \lambda L) + \frac{1}{2}E_{s1}\Delta t(c^2 - \lambda^2 L^2) + p_{u1}(\beta L - c) - p_{u2}(f - \beta L) - E_{s2}y_0(g - f)$$

$$+\frac{1}{2}E_{s2}\tan\omega(g^2 - f^2) + p_{u2}(L - g) = 0$$

Bending moment equilibrium

$$-\frac{1}{2}E_{s0}\Delta y_0(b_1^2) + \frac{1}{3}E_{s0}\Delta t(b_1^3) - \frac{1}{3}n\Delta y_0(b_1^3) + \frac{1}{4}n\Delta t(b_1^4) - \frac{1}{2}p_{u0}(b_2^2 - b_1^2) - \frac{1}{3}m(b_2^3 - b_1^3)$$

$$-\frac{1}{2}E_{s0}\Delta y_0(\lambda^2 L^2 - b_2^2) + \frac{1}{3}E_{s0}\Delta t(\lambda^3 L^3 - b_2^3) - \frac{1}{3}n\Delta y_0(\lambda^3 L^3 - b_2^3) + \frac{1}{4}n\Delta t(\lambda^4 L^4 - b_2^4)$$

$$-\frac{1}{2}E_{s1}\Delta y_0(c^2 - \lambda^2 L^2) + \frac{1}{3}E_{s1}\Delta t(c^3 - \lambda^3 L^3) + \frac{1}{2}p_{u1}(\beta^2 L^2 - c^2) - \frac{1}{2}p_{u2}(f^2 - \beta^2 L^2)$$

$$-\frac{1}{2}E_{s2}y_0(g^2 - f^2) + \frac{1}{3}E_{s2}\tan\omega(g^3 - f^3) + \frac{1}{2}p_{u2}(L^2 - g^2) = 0$$

Shear force

$$T_1 = -E_{s0}\Delta y_0(z) + \frac{1}{2}E_{s0}\Delta t(z^2) - \frac{1}{2}n\Delta y_0(z^2) + \frac{1}{3}n\Delta t(z^3) \quad 0 < z < b_1$$

$$T_2 = -p_{u0}(z - b_1) - \frac{1}{2}m(z^2 - b_1^2) - E_{s0}\Delta y_0(b_1) + \frac{1}{2}E_{s0}\Delta t(b_1^2) - \frac{1}{2}n\Delta y_0(b_1^2) + \frac{1}{3}n\Delta t(b_1^3) \quad b_1 < z < b_2$$

$$T_3 = -E_{s0}\Delta y_0(z - b_2) + \frac{1}{2}E_{s0}\Delta t(z^2 - b_2^2) - \frac{1}{2}n\Delta y_0(z^2 - b_2^2) + \frac{1}{3}n\Delta t(z^3 - b_2^3)$$
$$- p_{u0}(b_2 - b_1) - \frac{1}{2}m(b_2^2 - b_1^2) - E_{s0}\Delta y_0(b_1) + \frac{1}{2}E_{s0}\Delta t(b_1^2) - \frac{1}{2}n\Delta y_0(b_1^2) + \frac{1}{3}n\Delta t(b_1^3) \quad b_2 < z < \lambda L$$

$$T_4 = -E_{s1}\Delta y_0(z - c) + \frac{1}{2}E_{s1}(z^2 - c^2)\cdot\Delta t T + p_{u1}(c - \beta L)$$
$$- p_{u2}(\beta L - f) - E_{s2}y_0(f - g) + \frac{1}{2}E_{s2}\tan\omega(f^2 - g^2) + p_{u2}(g - L) \quad \lambda L < z < c$$

$$T_5 = p_{u1}(z - \beta L) - p_{u2}(\beta L - f) - E_{s2}y_0(f - g) + \frac{1}{2}E_{s2}\tan\omega(f^2 - g^2) + p_{u2}(g - L) \quad c < z < \beta L$$

$$T_6 = -p_{u2}(z - f) - E_{s2}y_0(f - g) + \frac{1}{2}E_{s2}\tan\omega(f^2 - g^2) + p_{u2}(g - L) \quad \beta L < z < f$$

$$T_7 = -E_{s2}y_0(z-g)+\frac{1}{2}E_{s2}\tan\omega(z^2-g^2)+p_{u2}(g-L) \qquad f < z < g$$

$$T_8 = p_{u2}(z-L) \qquad g < z < L$$

$$T_\beta = -p_{u2}(\beta L-f)-E_{s2}y_0(f-g)+\frac{1}{2}E_{s2}\tan\omega(f^2-g^2)+p_{u2}(g-L) \qquad z = \beta L$$

Bending moment

$$M_1 = -\frac{1}{2}E_{s0}\Delta y_0(z^2)+\frac{1}{6}E_{s0}\Delta t(z^3)-\frac{1}{6}n\Delta y_0(z^3)+\frac{1}{12}n\Delta t(z^4) \qquad 0 < z < b_1$$

$$M_2 = -p_{u0}\left(\frac{1}{2}z^2-b_1z+\frac{1}{2}b_1^2\right)-\frac{1}{2}m\left(\frac{1}{3}z^3-b_1^2z+\frac{2}{3}b_1^3\right)-E_{s0}\Delta y_0(b_1)(z-b_1)$$
$$+\frac{1}{2}E_{s0}\Delta t(b_1^2)(z-b_1)-\frac{1}{2}n\Delta y_0(b_1^2)(z-b_1)+\frac{1}{3}n\Delta t(b_1^3)(z-b_1) \qquad b_1 < z < b_2$$
$$-\frac{1}{2}E_{s0}\Delta y_0(b_1^2)+\frac{1}{6}E_{s0}\Delta t(b_1^3)-\frac{1}{6}n\Delta y_0(b_1^3)+\frac{1}{12}n\Delta t(b_1^4)$$

$$M_3 = -E_{s0}\Delta y_0\left(\frac{1}{2}z^2-b_2z+\frac{1}{2}b_2^2\right)+\frac{1}{2}E_{s0}\Delta t\left(\frac{1}{3}z^3-b_2^2z+\frac{2}{3}b_2^3\right)$$
$$-\frac{1}{2}n\Delta y_0\left(\frac{1}{3}z^3-b_2^2z+\frac{2}{3}b_2^3\right)+\frac{1}{3}n\Delta t\left(\frac{1}{4}z^4-b_2^3z+\frac{3}{4}b_2^4\right)-p_{u0}(b_2-b_1)(z-b_2)$$
$$-\frac{1}{2}m(b_2^2-b_1^2)(z-b_2)-E_{s0}\Delta y_0(b_1)(z-b_2)+\frac{1}{2}E_{s0}\Delta t(b_1^2)(z-b_2)-\frac{1}{2}n\Delta y_0(b_1^2)(z-b_2) \qquad b_2 < z < \lambda L$$
$$+\frac{1}{3}n\Delta t(b_1^3)(z-b_2)-p_{u0}\left(\frac{1}{2}b_2^2-b_1b_2+\frac{1}{2}b_1^2\right)-\frac{1}{2}m\left(\frac{1}{3}b_2^3-b_1^2b_2+\frac{2}{3}b_1^3\right)$$
$$-E_{s0}\Delta y_0(b_1)(b_2-b_1)+\frac{1}{2}E_{s0}\Delta t(b_1^2)(b_2-b_1)-\frac{1}{2}n\Delta y_0(b_1^2)(b_2-b_1)+\frac{1}{3}n\Delta t(b_1^3)(b_2-b_1)$$
$$-\frac{1}{2}E_{s0}\Delta y_0(b_1^2)+\frac{1}{6}E_{s0}\Delta t(b_1^3)-\frac{1}{6}n\Delta y_0(b_1^3)+\frac{1}{12}n\Delta t(b_1^4)$$

$$M_4 = -E_{s1}\Delta y_0\left(\frac{1}{2}z^2-cz+\frac{1}{2}c^2\right)+\frac{1}{2}E_{s1}\Delta t\left(\frac{1}{3}z^3-c^2z+\frac{1}{3}z^3c^3\right)$$
$$+(z-c)*[p_{u1}(c-\beta L)-p_{u2}(\beta L-f)-E_{s2}y_0(f-g)+\frac{1}{2}E_{s2}\tan\omega(f^2-g^2)+p_{u2}(g-L)]$$
$$p_{u1}\left(\frac{1}{2}c^2-\beta Lc+\frac{1}{2}\beta^2L^2\right)-p_{u2}(\beta L-f)(c-\beta L)-E_{s2}y_0(f-g)(c-\beta L)+\frac{1}{2}E_{s2}\tan\omega(f^2-g^2)(c-\beta L) \qquad \lambda L < z < c$$
$$+p_{u2}(g-L)(c-\beta L)-p_{u2}\left(\frac{1}{2}\beta^2L^2-f\beta L+\frac{1}{2}z^2\right)-E_{s2}y_0(f-g)(\beta L-f)$$
$$+\frac{1}{2}E_{s2}\tan\omega(f^2-g^2)(\beta L-f)+p_{u2}(g-L)(\beta L-f)$$
$$-E_{s2}y_0\left(\frac{1}{2}f^2-gf+\frac{1}{2}g^2\right)+\frac{1}{2}E_{s2}\tan\omega\left(\frac{1}{3}f^3-g^2f+\frac{2}{3}g^3\right)+p_{u2}(g-L)(f-g)+p_{u2}\left(\frac{1}{2}g^2-Lg+\frac{1}{2}L^2\right)$$

$$M_5 = p_{u1}\left(\frac{1}{2}z^2 - \beta L z + \frac{1}{2}\beta^2 L^2\right) - p_{u2}(\beta L - f)(z - \beta L) - E_{s2}y_0(f - g)(z - \beta L)$$
$$+\frac{1}{2}E_{s2}\tan\omega\left(f^2 - g^2\right)(z - \beta L) + p_{u2}(g - L)(z - \beta L) - p_{u2}\left(\frac{1}{2}\beta^2 L^2 - f\beta L + \frac{1}{2}f^2\right)$$
$$- E_{s2}y_0(f - g)(\beta L - f) + \frac{1}{2}E_{s2}\tan\omega\left(f^2 - g^2\right)(\beta L - f) + p_{u2}(g - L)(\beta L - f)$$
$$- E_{s2}y_0\left(\frac{1}{2}f^2 - gf + \frac{1}{2}g^2\right) + \frac{1}{2}E_{s2}\tan\omega\left(\frac{1}{3}f^3 - g^2 f + \frac{2}{3}g^3\right) + p_{u2}(g - L)(f - g) + p_{u2}\left(\frac{1}{2}g^2 - Lg + \frac{1}{2}L^2\right)$$

$c < z < \beta L$

$$M_6 = -p_{u2}\left(\frac{1}{2}z^2 - fz + \frac{1}{2}f^2\right) - E_{s2}y_0(f - g)(z - f) + \frac{1}{2}E_{s2}\tan\omega\left(f^2 - g^2\right)(z - f)$$
$$+ p_{u2}(g - L)(z - f) - E_{s2}y_0\left(\frac{1}{2}f^2 - gf + \frac{1}{2}g^2\right) + \frac{1}{2}E_{s2}\tan\omega\left(\frac{1}{3}f^3 - g^2 f + \frac{2}{3}g^3\right)$$
$$+ p_{u2}(g - L)(f - g) + p_{u2}\left(\frac{1}{2}g^2 - Lg + \frac{1}{2}L^2\right)$$

$\beta L < z < f$

$$M_7 = -E_{s2}y_0\left(\frac{1}{2}z^2 - gz + \frac{1}{2}g^2\right) + \frac{1}{2}E_{s2}\tan\omega\left(\frac{1}{3}z^3 - g^2 z + \frac{2}{3}g^3\right)$$
$$+ p_{u2}(g - L)(z - g) + p_{u2}\left(\frac{1}{2}g^2 - Lg + \frac{1}{2}L^2\right)$$

$f < z < g$

$$M_8 = p_{u2}\left(\frac{1}{2}z^2 - Lz + \frac{1}{2}L^2\right)$$

$g < z < L$

CASE 7234E

Soil pressure distribution:

$p = -(E_{s0} + nz)(\Delta y_0 - z \cdot \Delta t)$ $\quad 0 < z < b_1$

$p = -p_{u0} - mz$ $\quad b_1 < z < \lambda L$

$p = -p_{u1}$ $\quad \lambda L < z < b_2$

$p = -(E_{s1})(\Delta y_0 - z \cdot \Delta t)$ $\quad b_2 < z < c$

$p = p_{u1}$ $\quad c < z < \beta L$

$p = -p_{u2}$ $\quad \beta L < z < f$

$p = -(E_{s2})(y_0 - z \cdot tan\omega)$ $\quad f < z < g$

$p = p_{u2}$ $\quad g < z < L$

Shear force equilibrium

$$-E_{s0}\Delta y_0(b_1) + \frac{1}{2}E_{s0}\Delta t(b_1^2) - \frac{1}{2}n\Delta y_0(b_1^2) + \frac{1}{3}n\Delta t(b_1^3) - p_{u0}(L_0 - b_1) - \frac{1}{2}m(L_0^2 - b_1^2)$$

$$-p_{u1}(b_2 - L_0) - E_{s1}\Delta y_0(c - b_2) + \frac{1}{2}E_{s1}\Delta t(c^2 - b_2^2) + p_{u1}(\beta L - c) - p_{u2}(f - \beta L)$$

$$-E_{s2}y_0(g - f) + \frac{1}{2}E_{s2}\tan\omega(g^2 - f^2) + p_{u2}(L - g) = 0$$

Bending moment equilibrium

$$-\frac{1}{2}E_{s0}\Delta y_0(b_1^2) + \frac{1}{3}E_{s0}\Delta t(b_1^3) - \frac{1}{3}n\Delta y_0(b_1^3) + \frac{1}{4}n\Delta t(b_1^4)$$

$$-\frac{1}{2}p_{u0}(L_0^2 - b_1^2) - \frac{1}{3}m(L_0^3 - b_1^3) - \frac{1}{2}p_{u1}(b_2^2 - L_0^2)$$

$$-\frac{1}{2}E_{s1}\Delta y_0(c^2 - b_2^2) + \frac{1}{3}E_{s1}\Delta t(c^3 - b_2^3) + \frac{1}{2}p_{u1}(\beta^2 L^2 - c^2) - \frac{1}{2}p_{u2}(f^2 - \beta^2 L^2)$$

$$-\frac{1}{2}E_{s2}y_0(g^2 - f^2) + \frac{1}{3}E_{s2}\tan\omega(g^3 - f^3) + \frac{1}{2}p_{u2}(L^2 - g^2) = 0$$

Shear force:

$T_1 = -E_{s0}\Delta y_0(z) + \frac{1}{2}E_{s0}\Delta t(z^2) - \frac{1}{2}n\Delta y_0(z^2) + \frac{1}{3}n\Delta t(z^3)$ $\quad 0 < z < b_1$

$T_2 = -p_{u0}(z - b_1) - \frac{1}{2}m(z^2 - b_1^2) - E_{s0}\Delta y_0(b_1) + \frac{1}{2}E_{s0}\Delta t(b_1^2) - \frac{1}{2}n\Delta y_0(b_1^2) + \frac{1}{3}n\Delta t(b_1^3)$ $\quad b_1 < z < \lambda L$

$T_3 = -p_{u1}(z - L_0) - p_{u0}(L_0 - b_1) - \frac{1}{2}m(L_0^2 - b_1^2)$

$-E_{s0}\Delta y_0(b_1) + \frac{1}{2}E_{s0}\Delta t(b_1^2) - \frac{1}{2}n\Delta y_0(b_1^2) + \frac{1}{3}n\Delta t(b_1^3)$ $\quad \lambda L < z < b_2$

$T_4 = -E_{s1}\Delta y_0(z - c) + \frac{1}{2}E_{s1}(z^2 - c^2) \cdot \Delta tT + p_{u1}(c - \beta L) - p_{u2}(\beta L - f)$

$-E_{s2}y_0(f - g) - \frac{1}{2}E_{s2}\tan\omega(f^2 - g^2) + p_{u2}(g - L)$ $\quad b_2 < z < c$

$T_5 = p_{u1}(z - \beta L) - p_{u2}(\beta L - f) - E_{s2}y_0(f - g) - \frac{1}{2}E_{s2}\tan\omega(f^2 - g^2) + p_{u2}(g - L)$ $\quad c < z < \beta L$

$T_6 = -p_{u2}(z - f) - E_{s2}y_0(f - g) - \frac{1}{2}E_{s2}\tan\omega(f^2 - g^2) + p_{u2}(g - L)$ $\quad \beta L < z < f$

$T_7 = -E_{s2}y_0(z - g) - \frac{1}{2}E_{s2}\tan\omega(z^2 - g^2) + p_{u2}(g - L)$ $\quad f < z < g$

$T_8 = p_{u2}(z - L)$ $\quad g < z < L$

$$T_\beta = -p_{u2}(\beta L - f) - E_{s2} y_0 (f - g) - \frac{1}{2} E_{s2} \tan\omega (f^2 - g^2) + p_{u2}(g - L) \qquad z = \beta L$$

Bending moment

$$M_1 = -\frac{1}{2} E_{s0} \Delta y_0 (z^2) + \frac{1}{6} E_{s0} \Delta t (z^3) - \frac{1}{6} n \Delta y_0 (z^3) + \frac{1}{12} n \Delta t (z^4) \qquad 0 < z < b_1$$

$$M_2 = -p_{u0}\left(\frac{1}{2} z^2 - b_1 z + \frac{1}{2} {b_1}^2\right) - \frac{1}{2} m\left(\frac{1}{3} z^3 - {b_1}^2 z + \frac{2}{3} {b_1}^3\right) - E_{s0} \Delta y_0 (b_1)(z - b_1)$$
$$+ \frac{1}{2} E_{s0} \Delta t ({b_1}^2)(z - b_1) - \frac{1}{2} n \Delta y_0 ({b_1}^2)(z - b_1) + \frac{1}{3} n \Delta t ({b_1}^3)(z - b_1) \qquad b_1 < z < \lambda L$$
$$- \frac{1}{2} E_{s0} \Delta y_0 ({b_1}^2) + \frac{1}{6} E_{s0} \Delta t ({b_1}^3) - \frac{1}{6} n \Delta y_0 ({b_1}^3) + \frac{1}{12} n \Delta t ({b_1}^4)$$

$$M_3 = -p_{u1}\left(\frac{1}{2} z^2 - L_0 z + \frac{1}{2} {L_0}^2\right)$$
$$+ (z - L_0)[0 - p_{u0}(L_0 - b_1) - \frac{1}{2} m({L_0}^2 - {b_1}^2) - E_{s0} \Delta y_0 (b_1) + \frac{1}{2} E_{s0} \Delta t ({b_1}^2) - \frac{1}{2} n \Delta y_0 ({b_1}^2) \qquad \lambda L < z < b_2$$
$$+ \frac{1}{3} n \Delta t ({b_1}^3)] - p_{u0}\left(\frac{1}{2} {L_0}^2 - b_1 L_0 + \frac{1}{2} {b_1}^2\right) - \frac{1}{2} m\left(\frac{1}{3} {L_0}^3 - {b_1}^2 L_0 + \frac{2}{3} {b_1}^3\right)$$
$$- E_{s0} \Delta y_0 (b_1)(L_0 - b_1) + \frac{1}{2} E_{s0} \Delta t ({b_1}^2)(L_0 - b_1) - \frac{1}{2} n \Delta y_0 ({b_1}^2)(L_0 - b_1)$$
$$+ \frac{1}{3} n \Delta t ({b_1}^3)(L_0 - b_1) - \frac{1}{2} E_{s0} \Delta y_0 ({b_1}^2) + \frac{1}{6} E_{s0} \Delta t ({b_1}^3) - \frac{1}{6} n \Delta y_0 ({b_1}^3) + \frac{1}{12} n \Delta t ({b_1}^4)$$

$$M_4 = -E_{s1} \Delta y_0 \left(\frac{1}{2} z^2 - cz + \frac{1}{2} c^2\right) + \frac{1}{2} E_{s1} \Delta t \left(\frac{1}{3} z^3 - c^2 z + \frac{1}{3} z^3 c^3\right)$$
$$+ (z - c) * [p_{u1}(c - \beta L) - p_{u2}(\beta L - f) - E_{s2} y_0 (f - g) + \frac{1}{2} E_{s2} \tan\omega (f^2 - g^2) + p_{u2}(g - L)]$$
$$p_{u1}\left(\frac{1}{2} c^2 - \beta L c + \frac{1}{2} \beta^2 L^2\right) - p_{u2}(\beta L - f)(c - \beta L) - E_{s2} y_0 (f - g)(c - \beta L) \qquad b_2 < z < c$$
$$+ \frac{1}{2} E_{s2} \tan\omega (f^2 - g^2)(c - \beta L)$$
$$+ p_{u2}(g - L)(c - \beta L) - p_{u2}\left(\frac{1}{2} \beta L^2 - f \beta L + \frac{1}{2} f^2\right) - E_{s2} y_0 (f - g)(\beta L - f)$$
$$+ \frac{1}{2} E_{s2} \tan\omega (f^2 - g^2)(\beta L - f) + p_{u2}(g - L)(\beta L - f) - E_{s2} y_0 \left(\frac{1}{2} f^2 - gf + \frac{1}{2} g^2\right)$$
$$+ \frac{1}{2} E_{s2} \tan\omega \left(\frac{1}{3} f^3 - g^2 f + \frac{2}{3} g^3\right) + p_{u2}(g - L)(f - g) + p_{u2}\left(\frac{1}{2} g^2 - Lg + \frac{1}{2} L^2\right)$$

$$M_5 = p_{u1}\left(\frac{1}{2} z^2 - \beta L z + \frac{1}{2} \beta^2 L^2\right) - p_{u2}(\beta L - f)(z - \beta L) - E_{s2} y_0 (f - g)(z - \beta L)$$
$$+ \frac{1}{2} E_{s2} \tan\omega (f^2 - g^2)(z - \beta L) + p_{u2}(g - L)(z - \beta L) \qquad c < z < \beta L$$
$$- p_{u2}\left(\frac{1}{2} \beta^2 L^2 - f \beta L + \frac{1}{2} f^2\right) - E_{s2} y_0 (f - g)(\beta L - f)$$
$$+ \frac{1}{2} E_{s2} \tan\omega (f^2 - g^2)(\beta L - f) + p_{u2}(g - L)(\beta L - f) - E_{s2} y_0 \left(\frac{1}{2} f^2 - gf + \frac{1}{2} g^2\right)$$
$$+ \frac{1}{2} E_{s2} \tan\omega \left(\frac{1}{3} f^3 - g^2 f + \frac{2}{3} g^3\right) + p_{u2}(g - L)(f - g) + p_{u2}\left(\frac{1}{2} g^2 - Lg + \frac{1}{2} L^2\right)$$

$$M_6 = -p_{u2}\left(\frac{1}{2}z^2 - fz + \frac{1}{2}f^2\right) - E_{s2}y_0(f-g)(z-f) + \frac{1}{2}E_{s2}\tan\omega\left(f^2 - g^2\right)(z-f) + p_{u2}(g-L)(z-f)$$

$$- E_{s2}y_0\left(\frac{1}{2}f^2 - gf + \frac{1}{2}g^2\right) + \frac{1}{2}E_{s2}\tan\omega\left(\frac{1}{3}f^3 - g^2 f + \frac{2}{3}g^3\right) + p_{u2}(g-L)(f-g) + p_{u2}\left(\frac{1}{2}g^2 - Lg + \frac{1}{2}L^2\right) \qquad \beta L < z < f$$

$$M_7 = -E_{s2}y_0\left(\frac{1}{2}z^2 - gz + \frac{1}{2}g^2\right) + \frac{1}{2}E_{s2}\tan\omega\left(\frac{1}{3}z^3 - g^2 z + \frac{2}{3}g^3\right)$$

$$+ p_{u2}(g-L)(z-g) + p_{u2}\left(\frac{1}{2}g^2 - Lg + \frac{1}{2}L^2\right) \qquad f < z < g$$

$$M_8 = p_{u2}\left(\frac{1}{2}z^2 - Lz + \frac{1}{2}L^2\right) \qquad g < z < L$$

CASE 12634E

Soil pressure distribution:

$p = p_{u0} + mz$	0 < z < c1
$p = -(E_{s0} + nz)(\Delta y_0 - z \cdot \Delta t)$	c1 < z < c2
$p = p_{u0} + mz$	c2< z < λL
$p = p_{u1}$	λL < z < βL
$p = -p_{u2}$	βL < z < f
$p = -(E_{s2})(y_0 - z \cdot tan\omega)$	f < z < g
$p = p_{u2}$	g < z < L

Shear force equilibrium

$$p_{u0}c_1 + \frac{1}{2}mc_1^{\,2} - E_{s0}\Delta y_0(c_2 - c_1) + \frac{1}{2}E_{s0}\Delta t\left(c_2^{\,2} - c_1^{\,2}\right) - \frac{1}{2}n\Delta y_0\left(c_2^{\,2} - c_1^{\,2}\right) + \frac{1}{3}n\Delta t\left(c_2^{\,3} - c_1^{\,3}\right)$$

$$p_{u0}(\lambda L - c_2) + \frac{1}{2}m\left(\lambda^2 L^2 - c_2^{\,2}\right) + p_{u1}(\beta L - \lambda L) - p_{u2}(f - \beta L)$$

$$-E_{s2}y_0(g - f) + \frac{1}{2}E_{s2}\tan\omega\left(g^2 - f^2\right) + p_{u2}(L - g) = 0$$

Bending moment equilibrium

$$\frac{1}{2}p_{u0}c_1^{\,2} + \frac{1}{3}mc_1^{\,3} - \frac{1}{2}E_{s0}\Delta y_0\left(c_2^{\,2} - c_1^{\,2}\right) + \frac{1}{3}E_{s0}\Delta t\left(c_2^{\,3} - c_1^{\,3}\right) - \frac{1}{3}n\Delta y_0\left(c_2^{\,3} - c_1^{\,3}\right) + \frac{1}{4}n\Delta t\left(c_2^{\,4} - c_1^{\,4}\right)$$

$$\frac{1}{2}p_{u0}\left(\lambda^2 L^2 - c_2^{\,2}\right) + \frac{1}{3}m\left(\lambda^3 L^3 - c_2^{\,3}\right) + \frac{1}{2}p_{u1}\left(\beta^2 L^2 - \lambda^2 L^2\right) - \frac{1}{2}p_{u2}\left(f^2 - \beta^2 L^2\right)$$

$$-\frac{1}{2}E_{s2}y_0\left(g^2 - f^2\right) + \frac{1}{3}E_{s2}\tan\omega\left(g^3 - f^3\right) + \frac{1}{2}p_{u2}\left(L^2 - g^2\right) = 0 = 0$$

Shear force

$T_1 = p_{u0}z + \frac{1}{2}mz^2$	0 < z < c_1
$T_2 = -E_{s0}\Delta y_0(z - c_1) + \frac{1}{2}E_{s0}\left(z^2 - c_1^{\,2}\right)\cdot\Delta t - \frac{1}{2}\Delta y_0 n\left(z^2 - c_1^{\,2}\right) + \frac{1}{3}n\Delta t\left(z^3 - c_1^{\,3}\right) + p_{u0}c_1 + \frac{1}{2}mc_1^{\,2}$	c1 < z < c2
$T_3 = p_{u0}(z - \lambda L) + \frac{1}{2}m(z^2 - \lambda^2 L^2) + p_{u1}(\lambda L - \beta L) - p_{u2}(Ls - f) - E_{s2}y_0(f - g) + \frac{1}{2}E_{s2}\tan\omega\left(f^2 - g^2\right) + p_{u2}(g - L)$	c2< z < λL
$T_4 = p_{u1}(z - \beta L) - p_{u2}(Ls - f) - E_{s2}y_0(f - g) + \frac{1}{2}E_{s2}\tan\omega\left(f^2 - g^2\right) + p_{u2}(g - L)$	λL < z <βL
$T = -p_{u2}(z - f) - E_{s2}y_0(f - g) + \frac{1}{2}E_{s2}\tan\omega\left(f^2 - g^2\right) + p_{u2}(g - L)$	βL< z < f
$T = -E_{s2}y_0(z - g) + \frac{1}{2}E_{s2}\tan\omega\left(z^2 - g^2\right) + p_{u2}(g - L)$	f < z < g
$T = p_{u2}(z - L)$	g < z < L

Bending moment

$$M_1 = \frac{1}{2} p_{u0} z^2 + \frac{1}{6} m z^3 \qquad 0 < z < c_1$$

$$M_2 = -E_{s0}\Delta y_0\left(\frac{1}{2}z^2 - cz + \frac{1}{2}c^2\right) + \frac{1}{2}E_{s0}\left(\frac{1}{3}z^3 - c^2 z + \frac{2}{3}c^3\right)\cdot\Delta t - \frac{1}{2}\Delta y_0 n\left(\frac{1}{3}z^3 - c^2 z + \frac{2}{3}c^3\right) \qquad c_1 < z < c2$$
$$+\frac{1}{3}n\Delta t\left(\frac{1}{4}z^4 - c^3 z + \frac{3}{4}c^4\right) + p_{u0}c(z-c) + \frac{1}{2}mc^2(z-c) + \frac{1}{2}p_{u0}c^2 + \frac{1}{6}mc^3$$

$$M_3 = p_{u0}\left(\frac{1}{2}z^2 - \lambda L z + \frac{1}{2}\lambda^2 L^2\right) + \frac{1}{2}m\cdot\left(\frac{1}{3}z^3 - \lambda L^2 z + \frac{2}{3}\lambda L^3\right) + p_{u1}(\lambda L - \beta L)(z - \lambda L) - p_{u2}(Ls - f)(z - \lambda L)$$
$$-E_{s2}y_0(f-g)(z-\lambda L) + \frac{1}{2}E_{s2}\tan\omega\left(f^2 - g^2\right)(z-\lambda L) + p_{u2}(g-L)(z-\lambda L) \qquad c2 < z < \lambda L$$
$$p_{u1}\left(\frac{1}{2}\lambda^2 L^2 - \beta L\lambda L + \frac{1}{2}\beta^2 L^2\right) + (\lambda L - Ls)[-p_{u2}(Ls-f) - E_{s2}y_0(f-g) + \frac{1}{2}E_{s2}\tan\omega\left(f^2-g^2\right) + p_{u2}(g-L)]$$
$$-p_{u2}\left(\frac{1}{2}Ls^2 - fLs + \frac{1}{2}f^2\right) - E_{s2}y_0(f-g)(Ls-f) + \frac{1}{2}E_{s2}\tan\omega\left(f^2-g^2\right)(Ls-f) + p_{u2}(g-L)(Ls-f)$$
$$-E_{s2}y_0\left(\frac{1}{2}f^2 - gf + \frac{1}{2}g^2\right) + \frac{1}{2}E_{s2}\tan\omega\left(\frac{1}{3}f^3 - g^2 f + \frac{2}{3}g^3\right) + p_{u2}(g-L)(f-g) + p_{u2}(\frac{1}{2}g^2 - gL + \frac{1}{2}L^2)$$

$$M_4 = p_{u1}\left(\frac{1}{2}z^2 - \beta L z + \frac{1}{2}\beta^2 L^2\right) + (z - Ls)[-p_{u2}(Ls-f) - E_{s2}y_0(f-g)$$
$$+\frac{1}{2}E_{s2}\tan\omega\left(f^2-g^2\right) + p_{u2}(g-L)] - p_{u2}\left(\frac{1}{2}Ls^2 - fLs + \frac{1}{2}f^2\right) \qquad \lambda L < z < \beta L$$
$$-E_{s2}y_0(f-g)(Ls-f) + \frac{1}{2}E_{s2}\tan\omega\left(f^2-g^2\right)(Ls-f) + p_{u2}(g-L)(Ls-f)$$
$$-E_{s2}y_0\left(\frac{1}{2}f^2 - gf + \frac{1}{2}g^2\right) + \frac{1}{2}E_{s2}\tan\omega\left(\frac{1}{3}f^3 - g^2 f + \frac{2}{3}g^3\right)$$
$$+p_{u2}(g-L)(f-g) + p_{u2}(\frac{1}{2}g^2 - gL + \frac{1}{2}L^2)$$

$$M_5 = -p_{u2}\left(\frac{1}{2}z^2 - fz + \frac{1}{2}f^2\right) - E_{s2}y_0(f-g)(z-f) + \frac{1}{2}E_{s2}\tan\omega\left(f^2-g^2\right)(z-f) \qquad \beta L < z < f$$
$$+p_{u2}(g-L)(z-f) - E_{s2}y_0\left(\frac{1}{2}f^2 - gf + \frac{1}{2}g^2\right)$$
$$+\frac{1}{2}E_{s2}\tan\omega\left(\frac{1}{3}f^3 - g^2 f + \frac{2}{3}g^3\right) + p_{u2}(g-L)(f-g) + p_{u2}(\frac{1}{2}g^2 - gL + \frac{1}{2}L^2)$$

$$M_6 = -E_{s2}y_0\left(\frac{1}{2}z^2 - gz + \frac{1}{2}g^2\right) - \frac{1}{2}E_{s2}\tan\omega\left(\frac{1}{3}z^3 - g^2 z + \frac{2}{3}g^3\right) \qquad f < z < g$$
$$+p_{u2}(g-L)(z-g) + p_{u2}\left(\frac{1}{2}g^2 - Lg + \frac{1}{2}L^2\right)$$
$$M_7 = p_{u2}\left(\frac{1}{2}z^2 - Lz + \frac{1}{2}L^2\right) \qquad g < z < L$$

CASO P1234

Soil pressure distribution:

$p = p_{u0} + mz$ $\quad 0 < z < c_1$

$p = -(E_{s0} + nz)(\Delta y_0 - z \cdot \Delta t)$ $\quad c_1 < z < \lambda L$

$p = -(E_{s1})(\Delta y_0 - z \cdot \Delta t)$ $\quad \lambda L < z < c_2$

$p = p_{u1}$ $\quad c_2 < z < \beta L$

$p = -p_{u2}$ $\quad \beta L < z < f$

$p = -(E_{s2})(y_0 - z \cdot tan\omega)$ $\quad f < z < g$

$p = p_{u2}$ $\quad g < z < L$

Shear forces equilibrium:

$$p_{u0}c1 + \frac{1}{2}mc1^2 - E_{s0}\Delta y_0(\lambda L - c1) + \frac{1}{2}E_{s0}\Delta t(\lambda^2 L^2 - c1^2) - \frac{1}{2}n\Delta y_0(\lambda^2 L^2 - c1^2) + \frac{1}{3}n\Delta t(\lambda^3 L^3 - c1^3)$$
$$- E_{s1}\Delta y_0(c2 - \lambda L) + \frac{1}{2}E_{s1}\Delta t(c2^2 - \lambda^2 L^2) + p_{u1}(\beta L - c2) - p_{u2}(f - \beta L)$$
$$- E_{s2}y_0(g - f) + \frac{1}{2}E_{s2}\tan\omega(g^2 - f^2) + p_{u2}(L - g) = 0$$

Bending moment equilibrium

$$\frac{1}{2}p_{u0}c1^2 + \frac{1}{3}mc1^3 - \frac{1}{2}E_{s0}\Delta y_0(\lambda^2 L^2 - c1^2) + \frac{1}{3}E_{s0}\Delta t(\lambda^3 L^3 - c1^3) - \frac{1}{3}n\Delta y_0(\lambda^3 L^3 - c1^3) + \frac{1}{4}n\Delta t(\lambda^4 L^4 - c1^4)$$
$$- \frac{1}{2}E_{s1}\Delta y_0(c2^2 - \lambda^2 L^2) + \frac{1}{3}E_{s1}\Delta t(c2^3 - \lambda^3 L^3) + \frac{1}{2}p_{u1}(\beta^2 L^2 - c2^2) - \frac{1}{2}p_{u2}(f^2 - \beta^2 L^2)$$
$$- \frac{1}{2}E_{s2}y_0(g^2 - f^2) + \frac{1}{3}E_{s2}\tan\omega(g^3 - f^3) + \frac{1}{2}p_{u2}(L^2 - g^2) = 0$$

Shear forces

$$T = p_{u0}z + \frac{1}{2}mz^2 \qquad 0 < z < c_1$$

$$T = -E_{s0}\Delta y_0(z - c1) + \frac{1}{2}E_{s0}(z^2 - c1^2)\cdot\Delta t - \frac{1}{2}\Delta y_0 n(z^2 - c1^2) + \frac{1}{3}n\Delta t(z^3 - c1^3) + p_{u0}c1 + \frac{1}{2}mc1^2 \qquad c_1 < z < \lambda L$$

$$T = -E_{s0}\Delta y_0(\lambda L - c1) + \frac{1}{2}E_{s0}(\lambda^2 L^2 - c1^2)\cdot\Delta t - \frac{1}{2}\Delta y_0 n(\lambda^2 L^2 - c1^2) + \frac{1}{3}n\Delta t(\lambda^3 L^3 - c1^3) + p_{u0}c1 + \frac{1}{2}mc1^2 - E_{s1}\Delta y_0(z - \lambda L) + \frac{1}{2}E_{s1}(z^2 - \lambda^2 L^2)\cdot\Delta t \qquad \lambda L < z < c_2$$

$$T = -E_{s0}\Delta y_0(\lambda L - c1) + \frac{1}{2}E_{s0}(\lambda^2 L^2 - c1^2)\cdot\Delta t - \frac{1}{2}\Delta y_0 n(\lambda^2 L^2 - c1^2) + \frac{1}{3}n\Delta t(\lambda^3 L^3 - c1^3) + p_{u0}c1 + \frac{1}{2}mc1^2 - E_{s1}\Delta y_0(c2 - \lambda L) + \frac{1}{2}E_{s1}(c2^2 - \lambda^2 L^2)\cdot\Delta t + p_{u1}(z - c2) \qquad c_2 < z < \beta L$$

$$T = -p_{u2}(z - f) - E_{s2}y_0(f - g) + \frac{1}{2}E_{s2}\tan\omega(f^2 - g^2) + p_{u2}(g - L) \qquad \beta L < z < f$$

$$T = -E_{s2}y_0(z - g) + \frac{1}{2}E_{s2}\tan\omega(z^2 - g^2) + p_{u2}(g - L) \qquad f < z < g$$

$$T = p_{u2}(z - L) \qquad g < z < L$$

Bending moments

$$M_1 = \frac{1}{2} p_{u0} z^2 + \frac{1}{6} m z^3 \qquad 0 < z < c_1$$

$$M_2 = -E_{s0}\Delta y_0\left(\frac{1}{2}z^2 - c1z + \frac{1}{2}c1^2\right) + \frac{1}{2}E_{s0}\left(\frac{1}{3}z^3 - c1^2 z + \frac{2}{3}c1^3\right)\cdot\Delta t$$
$$-\frac{1}{2}\Delta y_0 n\left(\frac{1}{3}z^3 - c1^2 z + \frac{2}{3}c1^3\right) + \frac{1}{3}n\Delta t\left(\frac{1}{4}z^4 - c1^3 z + \frac{3}{4}c1^4\right)$$
$$+ p_{u0}c1(z - c1) + \frac{1}{2}mc1^2(z - c1) + \frac{1}{2}p_{u0}c1^2 + \frac{1}{6}mc1^3 \qquad c_1 < z < \lambda L$$

$$M_3 = -E_{s1}\Delta y_0\left(\frac{1}{2}z^2 - \lambda L z + \frac{1}{2}\lambda^2 L^2\right) + \frac{1}{2}E_{s1}\Delta t\left(\frac{1}{3}z^3 - \lambda^2 L^2 z + \frac{1}{3}z^3\lambda^3 L^3\right)$$
$$- E_{s0}\Delta y_0(\lambda L - c1)(z - \lambda L) + \frac{1}{2}E_{s0}\Delta t\left(\lambda^2 L^2 - c1^2\right)(z - \lambda L) - \frac{1}{2}n\Delta y_0\left(\lambda^2 L^2 - c1^2\right)(z - \lambda L)$$
$$+ \frac{1}{3}n\Delta t\left(\lambda^3 L^3 - c1^3\right)(z - \lambda L) + p_{u0}c1(z - \lambda L) + \frac{1}{2}mc1^2(z - \lambda L) \qquad \lambda L < z < c_2$$
$$- E_{s0}\Delta y_0\left(\frac{1}{2}\lambda^2 L^2 - c1\lambda L + \frac{1}{2}c1^2\right) + \frac{1}{2}E_{s0}\left(\frac{1}{3}\lambda^3 L^3 - c1^2\lambda L + \frac{2}{3}c1^3\right)\cdot\Delta t - \frac{1}{2}\Delta y_0 n\left(\frac{1}{3}\lambda^3 L^3 - c1^2\lambda L + \frac{2}{3}c1^3\right)$$
$$+ \frac{1}{3}n\Delta t\left(\frac{1}{4}\lambda^4 L^4 - c1^3\lambda L + \frac{3}{4}c1^4\right) + p_{u0}c1(\lambda L - c1) + \frac{1}{2}mc1^2(\lambda L - c1) + \frac{1}{2}p_{u0}c1^2 + \frac{1}{6}mc1^3$$

$$M_4 = p_{u1}\left(\frac{1}{2}z^2 - c_2 z + \frac{1}{2}{c_2}^2\right) - E_{s0}\Delta y_0(\lambda L - c1)(z - c_2) + \frac{1}{2}E_{s0}\Delta t\left(\lambda^2 L^2 - c1^2\right)(z - c_2)$$
$$- \frac{1}{2}n\Delta y_0\left(\lambda^2 L^2 - c1^2\right)(z - c_2) + \frac{1}{3}n\Delta t\left(\lambda^3 L^3 - c1^3\right)(z - c_2) + p_{u0}c1(z - c_2) + \frac{1}{2}mc1^2(z - c_2)$$
$$- E_{s1}\Delta y_0(c2 - \lambda L)(z - c_2) + \frac{1}{2}E_{s1}\Delta t\left(c2^2 - \lambda^2 L^2\right)(z - c_2) - E_{s1}\Delta y_0\left(\frac{1}{2}{c_2}^2 - \lambda L c_2 + \frac{1}{2}\lambda^2 L^2\right) \qquad c_2 < z < \beta L$$
$$+ \frac{1}{2}E_{s1}\Delta t\left(\frac{1}{3}{c_2}^3 - \lambda^2 L^2 c_2 + \frac{1}{3}{c_2}^3\lambda^3 L^3\right) - E_{s0}\Delta y_0(\lambda L - c1)(c_2 - \lambda L) + \frac{1}{2}E_{s0}\Delta t\left(\lambda^2 L^2 - c1^2\right)(c_2 - \lambda L)$$
$$- \frac{1}{2}n\Delta y_0\left(\lambda^2 L^2 - c1^2\right)(c_2 - \lambda L) + \frac{1}{3}n\Delta t\left(\lambda^3 L^3 - c1^3\right)(c_2 - \lambda L) + p_{u0}c1(c_2 - \lambda L) + \frac{1}{2}mc1^2(c_2 - \lambda L)$$
$$- E_{s0}\Delta y_0\left(\frac{1}{2}\lambda^2 L^2 - c1\lambda L + \frac{1}{2}c1^2\right) + \frac{1}{2}E_{s0}\left(\frac{1}{3}\lambda^3 L^3 - c1^2\lambda L + \frac{2}{3}c1^3\right)\cdot\Delta t - \frac{1}{2}\Delta y_0 n\left(\frac{1}{3}\lambda^3 L^3 - c1^2\lambda L + \frac{2}{3}c1^3\right)$$
$$+ \frac{1}{3}n\Delta t\left(\frac{1}{4}\lambda^4 L^4 - c1^3\lambda L + \frac{3}{4}c1^4\right) + p_{u0}c1(\lambda L - c1) + \frac{1}{2}mc1^2(\lambda L - c1) + \frac{1}{2}p_{u0}c1^2 + \frac{1}{6}mc1^3$$

$$M = -p_{u2}\left(\frac{1}{2}z^2 - fz + \frac{1}{2}z^2\right) - E_{s2}y_0(f - g)(z - f) + \frac{1}{2}E_{s2}\tan\omega\left(f^2 - g^2\right)(z - f) + p_{u2}(g - L)(z - f) \qquad \beta L < z < f$$
$$-E_{s2}y_0\left(\frac{1}{2}f^2 - gf + \frac{1}{2}g^2\right) + \frac{1}{2}E_{s2}\tan\omega\left(\frac{1}{3}f^3 - g^2 f + \frac{2}{3}g^3\right) + p_{u2}(g - L)(f - g) + p_{u2}\left(\frac{1}{2}g^2 - Lg + \frac{1}{2}L^2\right)$$

$$M_6 = -E_{s2}y_0\left(\frac{1}{2}z^2 - gz + \frac{1}{2}g^2\right) - \frac{1}{2}E_{s2}\tan\omega\left(\frac{1}{3}z^3 - g^2 z + \frac{2}{3}g^3\right) \qquad f < z < g$$
$$+ p_{u2}(g - L)(z - g) + p_{u2}\left(\frac{1}{2}g^2 - Lg + \frac{1}{2}L^2\right)$$

$$M_7 = p_{u2}\left(\frac{1}{2}z^2 - Lz + \frac{1}{2}L^2\right) \qquad g < z < L$$

CASE 56234E (Corresponding to B1C)

Soil pressure distribution:

$p = -p_{u0} - mz$ $\quad 0 < z < b$

$p = -(E_{s0} + nz)(\Delta y_0 - z\Delta t)$ $\quad b < z < c$

$p = p_{u0} + mz$ $\quad c < z < \lambda L$

$p = p_{u1}$ $\quad \lambda L < z < \beta L$

$p = -p_{u2}$ $\quad \beta L < z < f$

$p = -E_{s2}(y_0 - z\tan\omega)$ $\quad f < z < g$

$p = p_{u2}$ $\quad g < z < L$

Shear force equilibrium

$$-p_{u0}b - \frac{1}{2}mb^2 - E_{s0}\Delta y_0(c-b) + \frac{1}{2}E_{s0}\Delta t(c^2-b^2) - \frac{1}{2}\Delta y_0 n(c^2-b^2) + \frac{1}{3}n\Delta t(c^3-b^3) + p_{u0}(\lambda L - c)$$
$$+\frac{1}{2}m(\lambda^2L^2 - c^2) + p_{u1}(\beta L - \lambda L) - p_{u2}(f - \beta L) - E_{s2}y_0(g-f) + \frac{1}{2}E_{s2}\tan\omega(g^2-f^2) + p_{u2}(L-g) = 0$$

Bending moment equilibrium

$$-\frac{1}{2}p_{u0}b^2 - \frac{1}{3}mb^3 - \frac{1}{2}E_{s0}\Delta y_0(c^2-b^2) + \frac{1}{3}E_{s0}\Delta t(c^3-b^3) - \frac{1}{3}\Delta y_0 n(c^3-b^3)$$
$$+\frac{1}{4}n\Delta t(c^4-b^4) + \frac{1}{2}p_{u0}(\lambda^2L^2-c^2) + \frac{1}{3}m(\lambda^3L^3-c^3) + \frac{1}{2}p_{u1}(\beta^2L^2-\lambda^2L^2)$$
$$-\frac{1}{2}p_{u2}(f^2-\beta^2L^2) - \frac{1}{2}E_{s2}y_0(g^2-f^2) + \frac{1}{3}E_{s2}\tan\omega(g^3-f^3) + \frac{1}{2}p_{u2}(L^2-g^2) = 0$$

Congruence

$$b = \frac{n\Delta y_0 - m - E_{s0}\Delta t - \sqrt{(n\Delta y_0 - m - E_{s0}\Delta t)^2 + 4n\Delta t(E_{s0}\Delta y_0 - p_0)}}{2n\Delta t}$$ (if n=0, $E_{s0}=E_{s1}$, $b = \frac{\Delta y_0 - p_{u0}/E_{s1}}{\Delta t + m/E_{s1}}$)

$$c = \frac{n\Delta y_0 + m - E_{s0}\Delta t - \sqrt{(n\Delta y_0 + m - E_{s0}\Delta t)^2 + 4n\Delta t(E_{s0}\Delta y_0 + p_0)}}{2n\Delta t}$$

$$f = \frac{y_0 - p_{u2}/E_{s2}}{\tan\omega} \qquad g = \frac{y_0 + p_{u2}/E_{s2}}{\tan\omega}$$

Shear force

$T = -p_{u0}z - \frac{1}{2}mz^2$ $\quad 0 < z < b$

$T = -p_{u1}(z-b) - p_{u0}b - \frac{1}{2}mb^2$ $\quad b < z < c$

$T = -E_{s1}\Delta y_0(z-c) + \frac{1}{2}E_{s1}\Delta t(z^2-c^2) - p_{u1}(c-b) - p_{u0}b - \frac{1}{2}mb^2$ $\quad c < z < \lambda L$

$T = p_{u1}(z-\lambda L) - E_{s1}\Delta y_0(\lambda L - c) + \frac{1}{2}E_{s1}\Delta t(\lambda^2L^2-c^2) - p_{u1}(c-b) - p_{u0}b - \frac{1}{2}mb^2$ $\quad \lambda L < z < \beta L$

$T_5 = -p_{u2}(z-f) - E_{s2}y_0(f-g) + \frac{1}{2}E_{s2}\tan\omega(f^2-g^2) + p_{u2}(g-L)$ $\quad \beta L < z < f$

$T_6 = -E_{s2}y_0(z-g) + \frac{1}{2}E_{s2}\tan\omega(z^2-g^2) + p_{u2}(g-L)$ $\quad f < z < g$

$T_7 = p_{u2}(z-L)$ $\quad g < z < L$

Bending moment

$M = -\frac{1}{2}p_{u0}z^2 - \frac{1}{6}mz^3$ $\quad 0 < z < b$

$$M = -p_{u1}\left(\frac{1}{2}z^2 - bz + \frac{1}{2}b^2\right) - p_{u0}b(z-b) - \frac{1}{2}mb^2(z-b) - \frac{1}{2}p_{u0}b^2 - \frac{1}{6}mb^3 \qquad b < z < c$$

$$M = -E_{s1}\Delta y_0\left(\frac{1}{2}z^2 - cz + \frac{1}{2}c^2\right) + \frac{1}{2}E_{s1}\Delta t\left(\frac{1}{3}z^3 - c^2z + \frac{2}{3}c^3\right) - p_{u1}(c-b)(z-c)$$

$$- p_{u0}b(z-c) - \frac{1}{2}mb^2(z-c) \qquad c < z < \lambda L$$

$$- p_{u1}\left(\frac{1}{2}c^2 - bc + \frac{1}{2}b^2\right) - p_{u0}b(c-b) - \frac{1}{2}mb^2(c-b) - \frac{1}{2}p_{u0}b^2 - \frac{1}{6}mb^3$$

$$M = p_{u1}\left(\frac{1}{2}z^2 - \lambda Lz + \frac{1}{2}\lambda^2L^2\right) - E_{s1}\Delta y_0(\lambda L - c)(z-c) + \frac{1}{2}E_{s1}\Delta t\left(\lambda^2L^2 - c^2\right)(z-c)$$

$$- p_{u1}(c-b)(z-c) - p_{u0}b(z-c) - \frac{1}{2}mb^2(z-c) \qquad \lambda L < z < \beta L$$

$$- E_{s1}\Delta y_0\left(\frac{1}{2}z^2 - cz + \frac{1}{2}c^2\right) + \frac{1}{2}E_{s1}\Delta t\left(\frac{1}{3}z^3 - c^2z + \frac{2}{3}c^3\right)$$

$$- p_{u1}(c-b)(z-c) - p_{u0}b(z-c) - \frac{1}{2}mb^2(z-c)$$

$$- p_{u1}\left(\frac{1}{2}c^2 - bc + \frac{1}{2}b^2\right) - p_{u0}b(c-b) - \frac{1}{2}mb^2(c-b) - \frac{1}{2}p_{u0}b^2 - \frac{1}{6}mb^3$$

$$M_5 = -p_{u2}\left(\frac{1}{2}z^2 - fz + \frac{1}{2}f^2\right) - E_{s2}y_0(f-g)(z-f) + \frac{1}{2}E_{s2}\tan\omega\left(f^2 - g^2\right)(z-f)$$

$$+ p_{u2}(g-L)(z-f) - E_{s2}y_0\left(\frac{1}{2}f^2 - gf + \frac{1}{2}g^2\right) + \frac{1}{2}E_{s2}\tan\omega\left(\frac{1}{3}f^3 - g^2f + \frac{2}{3}g^3\right) \qquad \beta L < z < f$$

$$+ p_{u2}(g-L)(f-g) + p_{u2}\left(\frac{1}{2}g^2 - Lg + \frac{1}{2}L^2\right)$$

$$M_6 = -E_{s2}y_0\left(\frac{1}{2}z^2 - gz + \frac{1}{2}g^2\right) + \frac{1}{2}E_{s2}\,tan\omega\left(\frac{1}{3}z^3 - g^2z + \frac{2}{3}g^3\right) + p_{u2}(g-L)(z-g) \qquad f < z < g$$

$$+ p_{u2}\left(\frac{1}{2}g^2 - Lg + \frac{1}{2}L^2\right)$$

$$M_7 = p_{u2}\left(\frac{1}{2}z^2 - Lz + \frac{1}{2}L^2\right) \qquad g < z < L$$

CASE 17324E (Corresponding to B2C)

Soil pressure distribution:

$p = p_{u0} + mz$ $\quad 0 < z < c$

$p = -(E_{s0} + nz)(\Delta y_0 - z\Delta t)$ $\quad c < z < b$

$p = -p_{u0} - mz$ $\quad b < z < \lambda L$

$p = -p_{u1}$ $\quad \lambda L < z < \beta L$

$p = -p_{u2}$ $\quad \beta L < z < f$

$p = -E_{s2}(y_0 - z\tan\omega)$ $\quad f < z < g$

$p = p_{u2}$ $\quad g < z < L$

Shear force equilibrium

$$p_{u0}c + \frac{1}{2}mc^2 - E_{s0}\Delta y_0(b-c) + \frac{1}{2}E_{s0}\Delta t(b^2-c^2) - \frac{1}{2}\Delta y_0 n(b^2-c^2) + \frac{1}{3}n\Delta t(b^3-c^3) - p_{u0}(\lambda L - b)$$
$$-\frac{1}{2}m(\lambda^2 L^2 - b^2) - p_{u1}(\beta L - \lambda L) - p_{u2}(f - \beta L) - E_{s2}y_0(g-f) + \frac{1}{2}E_{s2}\tan\omega(g^2-f^2) + p_{u2}(L-g) = 0$$

Bending moment equilibrium

$$\frac{1}{2}p_{u0}c^2 + \frac{1}{3}mc^3 - \frac{1}{2}E_{s0}\Delta y_0(b^2-c^2) + \frac{1}{3}E_{s0}\Delta t(b^3-c^3) - \frac{1}{3}\Delta y_0 n(b^3-c^3)$$
$$+\frac{1}{4}n\Delta t(b^4-c^4) - \frac{1}{2}p_{u0}(\lambda^2L^2-b^2) - \frac{1}{3}m(\lambda^3L^3-b^3) - \frac{1}{2}p_{u1}(\beta^2L^2-\lambda^2L^2)$$
$$-\frac{1}{2}p_{u2}(f^2-\beta^2L^2) - \frac{1}{2}E_{s2}y_0(g^2-f^2) + \frac{1}{3}E_{s2}\tan\omega(g^3-f^3) + \frac{1}{2}p_{u2}(L^2-g^2) = 0$$

Congruence

$$c = \frac{n\Delta y_0 + m - E_{s0}\Delta t - \sqrt{(n\Delta y_0 - m - E_{s0}\Delta t)^2 + 4n\Delta t(E_{s0}\Delta y_0 + p_{u0})}}{2n\Delta t}$$

$$b = \frac{n\Delta y_0 - m - E_{s0}\Delta t - \sqrt{(n\Delta y_0 + m - E_{s0}\Delta t)^2 + 4n\Delta t(E_{s0}\Delta y_0 - p_{u0})}}{2n\Delta t}$$

$$f = \frac{y_0 - p_{u2}/E_{s2}}{\tan\omega} \qquad g = \frac{y_0 + p_{u2}/E_{s2}}{\tan\omega}$$

Shear force

$$T_1 = p_{u0}z + \frac{1}{2}mz^2 \qquad 0 < z < c$$

$$T_2 = -E_{s0}\Delta y_0(z-c) + \frac{1}{2}E_{s0}\Delta t(z^2-c^2) - \frac{1}{2}n\Delta y_0(z^2-c^2) \qquad c < z < b$$
$$+\frac{1}{3}n\Delta t(z^3-c^3) + p_{u0}c + \frac{1}{2}mc^2$$

$$T_3 = -p_{uo}(z-b) - \frac{1}{2}m(z^2-b^2) - E_{s0}\Delta y_0(b-c) + \frac{1}{2}E_{s0}\Delta t(b^2-c^2) \qquad b < z < \lambda L$$
$$-\frac{1}{2}n\Delta y_0(b^2-c^2) + \frac{1}{3}n\Delta t(b^3-c^3) + p_{u0}c + \frac{1}{2}mc^2$$

$$T_4 = -p_{u1}(z-\lambda L) - p_{uo}(\lambda L - b) - \frac{1}{2}m\left(\lambda^2 L^2 - b^2\right) - E_{s0}\Delta y_0 (b-c)$$
$$+\frac{1}{2}E_{s0}\Delta t\left(b^2 - c^2\right) - \frac{1}{2}n\Delta y_0\left(b^2 - c^2\right) + \frac{1}{3}n\Delta t\left(b^3 - c^3\right) + p_{u0}c + \frac{1}{2}mc^2 \qquad \lambda L < z < \beta L$$

$$T_5 = -p_{u2}(z-f) - E_{s2}y_0(f-g) + \frac{1}{2}E_{s2}\tan\omega\left(f^2 - g^2\right) + p_{u2}(g-L) \qquad \beta L < z < f$$

$$T_6 = -E_{s2}y_0(z-g) + \frac{1}{2}E_{s2}\tan\omega\left(z^2 - g^2\right) + p_{u2}(g-L) \qquad f < z < g$$

$$T_7 = p_{u2}(z-L) \qquad g < z < L$$

Bending moment

$$M = \frac{1}{2}p_{u0}z^2 + \frac{1}{6}mz^3 \qquad 0 < z < c$$

$$M_2 = -E_{s0}\Delta y_0\left(\frac{1}{2}z^2 - cz + \frac{1}{2}c^2\right) + \frac{1}{2}E_{s0}\Delta t\left(\frac{1}{3}z^3 - c^2 z + \frac{2}{3}c^3\right) - \frac{1}{2}n\Delta y_0\left(\frac{1}{3}z^3 - c^2 z + \frac{2}{3}c^3\right) \qquad c < z < b$$
$$+\frac{1}{3}n\Delta t\left(\frac{1}{4}z^4 - c^3 z + \frac{3}{4}c^4\right) + p_{u0}c(z-c) + \frac{1}{2}mc^2(z-c) + \frac{1}{2}p_{u0}c^2 + \frac{1}{6}mc^3$$

$$M_3 = -p_{uo}\left(\frac{1}{2}z^2 - bz + \frac{1}{2}b^2\right) - \frac{1}{2}m\left(\frac{1}{3}z^3 - b^2 z + \frac{2}{3}b^3\right) - E_{s0}\Delta y_0(b-c)(z-b) + \frac{1}{2}E_{s0}\Delta t\left(b^2 - c^2\right)(z-b)$$
$$-\frac{1}{2}n\Delta y_0\left(b^2 - c^2\right)(z-b) + \frac{1}{3}n\Delta t\left(b^3 - c^3\right)(z-b) + p_{u0}c(z-b) + \frac{1}{2}mc^2(z-b) \qquad b < z < \lambda L$$
$$-E_{s0}\Delta y_0\left(\frac{1}{2}b^2 - cb + \frac{1}{2}c^2\right) + \frac{1}{2}E_{s0}\Delta t\left(\frac{1}{3}b^3 - c^2 b + \frac{2}{3}c^3\right) - \frac{1}{2}n\Delta y_0\left(\frac{1}{3}b^3 - c^2 b + \frac{2}{3}c^3\right)$$
$$+\frac{1}{3}n\Delta t\left(\frac{1}{4}b^4 - c^3 b + \frac{3}{4}c^4\right) + p_{u0}c(b-c) + \frac{1}{2}mc^2(b-c) + \frac{1}{2}p_{u0}c^2 + \frac{1}{6}mc^3$$

$$M_4 = -p_{u1}\left(\frac{1}{2}z^2 - \lambda Lz + \frac{1}{2}\lambda^2 L^2\right) - p_{uo}(\lambda L - b)(z-\lambda L) - \frac{1}{2}m\left(\lambda^2 L^2 - b^2\right)(z-\lambda L)$$
$$-E_{s0}\Delta y_0(b-c)(z-\lambda L) + \frac{1}{2}E_{s0}\Delta t\left(b^2 - c^2\right)(z-\lambda L) - \frac{1}{2}n\Delta y_0\left(b^2 - c^2\right)(z-\lambda L)$$
$$+\frac{1}{3}n\Delta t\left(b^3 - c^3\right)(z-\lambda L) + p_{u0}c(z-\lambda L) + \frac{1}{2}mc^2(z-\lambda L) - p_{uo}\left(\frac{1}{2}\lambda^2 L^2 - b\lambda L + \frac{1}{2}b^2\right) \qquad \lambda L < z < \beta L$$
$$-\frac{1}{2}m\left(\frac{1}{3}\lambda^3 L^3 - b^2\lambda L + \frac{2}{3}b^3\right) - E_{s0}\Delta y_0(b-c)(\lambda L - b) + \frac{1}{2}E_{s0}\Delta t\left(b^2 - c^2\right)(\lambda L - b)$$
$$-\frac{1}{2}n\Delta y_0\left(b^2 - c^2\right)(\lambda L - b) + \frac{1}{3}n\Delta t\left(b^3 - c^3\right)(\lambda L - b) + p_{u0}c(\lambda L - b) + \frac{1}{2}mc^2(\lambda L - b)$$
$$-E_{s0}\Delta y_0\left(\frac{1}{2}b^2 - cb + \frac{1}{2}c^2\right) + \frac{1}{2}E_{s0}\Delta t\left(\frac{1}{3}b^3 - c^2 b + \frac{2}{3}c^3\right) - \frac{1}{2}n\Delta y_0\left(\frac{1}{3}b^3 - c^2 b + \frac{2}{3}c^3\right)$$
$$+\frac{1}{3}n\Delta t\left(\frac{1}{4}b^4 - c^3 b + \frac{3}{4}c^4\right) + p_{u0}c(b-c) + \frac{1}{2}mc^2(b-c) + \frac{1}{2}p_{u0}c^2 + \frac{1}{6}mc^3$$

$$M_5 = -p_{u2}\left(\frac{1}{2}z^2 - fz + \frac{1}{2}f^2\right) - E_{s2}y_0(f-g)(z-f)$$
$$+\frac{1}{2}E_{s2}\tan\omega\left(f^2 - g^2\right)(z-f) + p_{u2}(g-L)(z-f) \qquad \beta L < z < f$$
$$-E_{s2}y_0\left(\frac{1}{2}f^2 - gf + \frac{1}{2}g^2\right) + \frac{1}{2}E_{s2}\tan\omega\left(\frac{1}{3}f^3 - g^2 f + \frac{2}{3}g^3\right)$$
$$+p_{u2}(g-L)(f-g) + p_{u2}\left(\frac{1}{2}g^2 - Lg + \frac{1}{2}L^2\right)$$

$$M_6 = -E_{s2}y_0\left(\frac{1}{2}z^2 - gz + \frac{1}{2}g^2\right) + \frac{1}{2}E_{s2}\tan\omega\left(\frac{1}{3}z^3 - g^2z + \frac{2}{3}g^3\right) + p_{u2}(g-L)(z-g) + p_{u2}\left(\frac{1}{2}g^2 - Lg + \frac{1}{2}L^2\right) \qquad f < z < g$$

$$M_7 = p_{u2}\left(\frac{1}{2}z^2 - Lz + \frac{1}{2}L^2\right) \qquad g < z < L$$

Below, the four possible limit case type B1 and B2 are described:

LIMIT CASE B1-L1

Soil pressure distribution:

$p = -p_{u0} - mz$ $\quad 0 < z < \lambda L$

$p = -p_{u1}$ $\quad \lambda L < z < b$

$p = p_{u1}$ $\quad b < z < \beta L$

$p = -p_{u2}$ $\quad \beta L < z < f$

$p = p_{u2}$ $\quad f < z < L$

Shear force equilibrium

$$-p_{u0}\lambda L - \frac{1}{2}m\lambda^2 L^2 - p_{u1}(b-\lambda L) + p_{u1}(\beta L - b) - p_{u2}(f-\beta L) + p_{u2}(L-f) = 0$$

Bending moment equilibrium

$$-\frac{1}{2}p_{u0}\lambda^2 L^2 - \frac{1}{3}m\lambda^3 L^3 - \frac{1}{2}p_{u1}(b^2 - \lambda^2 L^2) + \frac{1}{2}p_{u1}(\beta^2 L^2 - b^2) - \frac{1}{2}p_{u2}(f^2 - \beta^2 L^2) + \frac{1}{2}p_{u2}(L^2 - f^2) = 0$$

Shear force

$T = -p_{u0}z - \frac{1}{2}mz^2$ $\quad 0 < z < \lambda L$

$T = -p_{u1}(z-\lambda L) - p_{u0}\lambda L - \frac{1}{2}m\lambda^2 L^2$ $\quad \lambda L < z < b$

$T = p_{u1}(z-b) - p_{u1}(b-\lambda L) - p_{u0}\lambda L - \frac{1}{2}m\lambda^2 L^2$ $\quad c < z < \beta L$

$T = -p_{u2}(z-f) + p_{u2}(f-L)$ $\quad \beta L < z < f$

$T = p_{u2}(z-L)$ $\quad f < z < L$

$T_\beta = p_{u2}(2f - L - \beta L)$ $\qquad \frac{T_\beta}{p_{u1}L} = k(2f_n - 1 - \beta)$ $\quad z = \beta L$

Bending moment

$M = -\frac{1}{2}p_{u0}z^2 - \frac{1}{6}mz^3$ $\quad 0 < z < \lambda L$

$M = -p_{u1}\left(\frac{1}{2}z^2 - \lambda L z + \frac{1}{2}\lambda^2 L^2\right) - p_{u0}\lambda L(z-\lambda L) - \frac{1}{2}m\lambda^2 L^2(z-\lambda L) - \frac{1}{2}p_{u0}\lambda^2 L^2 - \frac{1}{6}m\lambda^3 L^3$ $\quad \lambda L < z < b$

$M = p_{u1}\left(\frac{1}{2}z^2 - bz + \frac{1}{2}b^2\right) - p_{u1}(b-\lambda L)(z-b) - p_{u0}\lambda L(z-b) - \frac{1}{2}m\lambda^2 L^2(z-b)$

$-p_{u1}\left(\frac{1}{2}b^2 - \lambda L b + \frac{1}{2}\lambda^2 L^2\right) - p_{u0}\lambda L(b-\lambda L) - \frac{1}{2}m\lambda^2 L^2(b-\lambda L) - \frac{1}{2}p_{u0}\lambda^2 L^2 - \frac{1}{6}m\lambda^3 L^3$ $\quad b < z < \beta L$

$M = -p_{u2}\left(\frac{1}{2}z^2 - fz + \frac{1}{2}f^2\right) + p_{u2}(g-L)(z-f) + p_{u2}\left(\frac{1}{2}f^2 - Lf + \frac{1}{2}L^2\right)$ $\quad \beta L < z < f$

$M = p_{u2}\left(\frac{1}{2}z^2 - Lz + \frac{1}{2}L^2\right)$ $\quad g < z < L$

Numerical solution procedure:

fn is derived from the Shear force equilibrium

$$f_n = \frac{\beta}{2k} + \frac{\lambda}{4k}(1-k_0) - \frac{b_n}{k} + \frac{1+\beta}{2}$$

And the expression is put into the momentum equilibrium until convergence is reached

$$\frac{1}{2}\beta^2 + \frac{1}{6}\lambda^2(1-k_0) - b_n{}^2 + \frac{1}{2}k(\beta^2+1) - kf_n{}^2 = 0$$

i.e. : if β=0.5, λ=0.1, k0=0.5, k=2, η=1, it is obtained:

b_n=0.1111495 f_n=0.825675

CASE LIMIT B1-L2

Soil pressure distribution:

$p = -p_{u0} - mz$ $\quad 0 < z < b$

$p = p_{u0} + mz$ $\quad b < z < \lambda L$

$p = p_{u1}$ $\quad \lambda L < z < \beta L$

$p = -p_{u2}$ $\quad \beta L < z < f$

$p = p_{u2}$ $\quad f < z < L$

Shear force equilibrium

$$-p_{u0}b - \frac{1}{2}mb^2 + p_{u0}(\lambda L - b) + \frac{1}{2}m(\lambda^2 L^2 - b^2) + p_{u1}(\beta L - \lambda L) - p_{u2}(f - \beta L) + p_{u2}(L - f) = 0$$

Bending moment equilibrium

$$-\frac{1}{2}p_{u0}b^2 - \frac{1}{3}mb^3 + \frac{1}{2}p_{u0}(\lambda^2 L^2 - b^2) + \frac{1}{3}m(\lambda^3 L^3 - b^3) + \frac{1}{2}p_{u1}(\beta^2 L^2 - \lambda^2 L^2)$$

$$-\frac{1}{2}p_{u2}(f^2 - \beta^2 L^2) + \frac{1}{2}p_{u2}(L^2 - f^2) = 0$$

Shear force

$T_1 = -p_{u0}z - \frac{1}{2}mz^2$ $\quad 0 < z < b$

$T_2 = p_{u0}(z - b) + \frac{1}{2}m(z^2 - b^2) - p_{u0}b - \frac{1}{2}mb^2$ $\quad b < z < \lambda L$

$T_3 = p_{u1}(z - \lambda L) + p_{u0}(\lambda L - b) + \frac{1}{2}m(\lambda^2 L^2 - b^2) - p_{u0}b - \frac{1}{2}mb^2$ $\quad \lambda L < z < \beta L$

$T_4 = -p_{u2}(z - f) + p_{u2}(f - L)$ $\quad \beta L < z < f$

$T_5 = p_{u2}(z - L)$ $\quad f < z < L$

$T_\beta = p_{u2}(2f - L - \beta L)$ $\qquad \frac{T_\beta}{p_{u1}L} = k(2f_n - 1 - \beta)$ $\quad z = \beta L$

Bending moment

$M_1 = -\frac{1}{2}p_{u0}z^2 - \frac{1}{6}mz^3$ $\quad 0 < z < b$

$M_2 = -p_{u1}(c - b)(z - c) - p_{u0}b(z - c) - \frac{1}{2}mb^2(z - c)$

$-\frac{1}{2}mb^2(c - b) - \frac{1}{2}p_{u0}b^2 - \frac{1}{6}mb^3$ $\quad c < z < \lambda L$

$M_3 = p_{u1}\left(\frac{1}{2}z^2 - \lambda Lz + \frac{1}{2}\lambda^2 L^2\right) - E_{s1}\Delta y_0(\lambda L - c)(z - c) + \frac{1}{2}E_{s1}\Delta t(\lambda^2 L^2 - c^2)(z - c)$

$- p_{u0}b(z - c) - \frac{1}{2}mb^2(z - c) - \frac{1}{2}mb^2(c - b) - \frac{1}{2}p_{u0}b^2 - \frac{1}{6}mb^3$ $\quad \lambda L < z < \beta L$

$M_4 = -p_{u2}\left(\frac{1}{2}z^2 - fz + \frac{1}{2}f^2\right) + p_{u2}(g - L)(z - f) + p_{u2}\left(\frac{1}{2}f^2 - Lf + \frac{1}{2}L^2\right)$ $\quad \beta L < z < f$

$M_5 = p_{u2}\left(\frac{1}{2}z^2 - Lz + \frac{1}{2}L^2\right)$ $\quad f < z < L$

Numerical solution procedure:

fn is derived from the Shear force equilibrium

$$f_n = \frac{k_0(\lambda - 2b_n) + \frac{1-k_0}{\lambda}\left(\frac{1}{2}\lambda^2 - b_n{}^2\right) + (\beta - \lambda)}{2k} + \frac{1+\beta}{2}$$

And the expression is put into the momentum equilibrium until convergence is reached

$$\frac{\frac{1}{2}k_0\left(\lambda^2 - 2b_n{}^2\right) + \frac{1}{3}\frac{(1-k_0)}{\lambda}\left(\lambda^3 - 2b_n{}^3\right) + \frac{1}{2}\left(\beta^2 - \lambda^2\right)}{k} + \frac{1}{2}\beta^2$$

$$+\frac{1}{2} - \left(\frac{k_0(\lambda - 2b_n) + \frac{1}{2}\frac{1-k_0}{\lambda}\left(\lambda^2 - 2b_n{}^2\right) + (\beta - \lambda)}{2k} + \frac{1+\beta}{2}\right)^2 = 0$$

i.e., if β=0.6, λ=0.2, k0=0.2, k=5, η=1

bn=0.090442 fn=0.84511

CASE LIMIT B2-L1

Soil pressure distribution:

$p = p_{u0} + mz$ $\quad 0 < z < \lambda L$

$p = p_{u1}$ $\quad \lambda L < z < b$

$p = -p_{u1}$ $\quad b < z < \beta L$

$p = -p_{u2}$ $\quad \beta L < z < f$

$p = p_{u2}$ $\quad f < z < L$

Shear force equilibrium

$$p_{u0}\lambda L + \frac{1}{2}m\lambda^2 L^2 + p_{u1}(b-\lambda L) - p_{u1}(\beta L - b) - p_{u2}(f-\beta L) + p_{u2}(L-f) = 0$$

Bending momentum equilibrium:

$$\frac{1}{2}p_{u0}\lambda^2 L^2 + \frac{1}{3}m\lambda^3 L^3 + \frac{1}{2}p_{u1}(b^2 - \lambda^2 L^2) - \frac{1}{2}p_{u1}(\beta^2 L^2 - b^2) - \frac{1}{2}p_{u2}(f^2 - \beta^2 L^2) + \frac{1}{2}p_{u2}(L^2 - f^2) = 0$$

Shear force

$T = p_{u0}z + \frac{1}{2}mz^2$ $\quad 0 < z < \lambda L$

$T = p_{u1}(z-\lambda L) + p_{u0}\lambda L + \frac{1}{2}m\lambda^2 L^2$ $\quad \lambda L < z < b$

$T = -p_{u1}(z-b) + p_{u1}(b-\lambda L) + p_{u0}\lambda L + \frac{1}{2}m\lambda^2 L^2$ $\quad c < z < \beta L$

$T = -p_{u2}(z-f) + p_{u2}(f-L)$ $\quad \beta L < z < f$

$T = p_{u2}(z-L)$ $\quad f < z < L$

$T_\beta = p_{u2}(2f - L - \beta L)$ $\quad z = \beta L$

$$\frac{T_\beta}{p_{u1}L} = k(2f_n - 1 - \beta)$$

Bending moment

$M = \frac{1}{2}p_{u0}z^2 + \frac{1}{6}mz^3$ $\quad 0 < z < \lambda L$

$M_2 = p_{u1}\left(\frac{1}{2}z^2 - \lambda Lz + \frac{1}{2}\lambda^2 L^2\right) + p_{u0}\lambda L(z-\lambda L) + \frac{1}{2}m\lambda^2 L^2(z-\lambda L) + \frac{1}{2}p_{u0}\lambda^2 L^2 + \frac{1}{6}m\lambda^3 L^3$ $\quad \lambda L < z < b$

$M_3 = -p_{u1}\left(\frac{1}{2}z^2 - bz + \frac{1}{2}b^2\right) + p_{u1}(b-\lambda L)(z-b) + p_{u0}\lambda L(z-b) + \frac{1}{2}m\lambda^2 L^2(z-b)$ $\quad b < z < \beta L$

$+ p_{u1}\left(\frac{1}{2}b^2 - \lambda Lb + \frac{1}{2}\lambda^2 L^2\right) + p_{u0}\lambda L(b-\lambda L) + \frac{1}{2}m\lambda^2 L^2(b-\lambda L) + \frac{1}{2}p_{u0}\lambda^2 L^2 + \frac{1}{6}m\lambda^3 L^3$

$M_4 = -p_{u2}\left(\frac{1}{2}z^2 - fz + \frac{1}{2}f^2\right) + p_{u2}(f-L)(z-f) + p_{u2}\left(\frac{1}{2}f^2 - Lf + \frac{1}{2}L^2\right)$ $\quad \beta L < z < f$

$M_5 = p_{u2}\left(\frac{1}{2}z^2 - Lz + \frac{1}{2}L^2\right)$ $\quad g < z < L$

Numerical solution procedure:

fn is derived from the Shear force equilibrium

$$f_n = \frac{\lambda}{4k}(k_0 - 1) + \frac{b_n}{k} - \frac{\beta}{2k} + \frac{1}{2}(\beta + 1)$$

And the expression is put into the momentum equilibrium until convergence is reached

$$b_n{}^2 - \frac{1}{2}\beta^2 - \frac{1}{6}\lambda^2(1-k_0) + \frac{1}{2}k(\beta^2+1) - kf_n{}^2 = 0$$

i.e. : if β=0.7, λ=0.1, k0=0.5, k=2, η=0, it is obtained:

bn=0.293719 fn=0.815609

LIMIT CASE B2-L2

Soil pressure distribution:

$p = p_{u0} + mz$ $\quad 0 < z < b$

$p = -p_{u0} - mz$ $\quad b < z < \lambda L$

$p = -p_{u1}$ $\quad \lambda L < z < \beta L$

$p = -p_{u2}$ $\quad \beta L < z < f$

$p = p_{u2}$ $\quad f < z < L$

Shear force equilibrium

$$p_{u0}b + \frac{1}{2}mb^2 - p_{u0}(\lambda L - b) - \frac{1}{2}m\left(\lambda^2 L^2 - b^2\right) - p_{u1}(\beta L - \lambda L) - p_{u2}(f - \beta L) + p_{u2}(L - f) = 0$$

Bending moment equilibrium

$$\frac{1}{2}p_{u0}b^2 + \frac{1}{3}mb^3 - \frac{1}{2}p_{u0}\left(\lambda^2 L^2 - b^2\right) - \frac{1}{3}m\left(\lambda^3 L^3 - b^3\right) - \frac{1}{2}p_{u1}\left(\beta^2 L^2 - \lambda^2 L^2\right)$$

$$-\frac{1}{2}p_{u2}\left(f^2 - \beta^2 L^2\right) + \frac{1}{2}p_{u2}\left(L^2 - f^2\right) = 0$$

Shear force

$T = p_{u0}z + \frac{1}{2}mz^2$ $\quad 0 < z < b$

$T = -p_{u0}(z - b) - \frac{1}{2}m\left(z^2 - b^2\right) + p_{u0}b + \frac{1}{2}mb^2$ $\quad b < z < \lambda L$

$T = -p_{u1}(z - \lambda L) - p_{u0}(\lambda L - b) - \frac{1}{2}m\left(\lambda^2 L^2 - b^2\right) + p_{u0}b + \frac{1}{2}mb^2$ $\quad \lambda L < z < \beta L$

$T = -p_{u2}(z - f) + p_{u2}(f - L)$ $\quad \beta L < z < f$

$T = p_{u2}(z - L)$ $\quad f < z < L$

$T_\beta = p_{u2}(2f - L - \beta L)$ $\quad z = \beta L$

$$\frac{T_\beta}{p_{u1}L} = k(2f_n - 1 - \beta)$$

Bending moment

$M = \frac{1}{2}p_{u0}z^2 + \frac{1}{6}mz^3$ $\quad 0 < z < b$

$M = p_{u1}(c - b)(z - c) + p_{u0}b(z - c) + \frac{1}{2}mb^2(z - c) + \frac{1}{2}mb^2(c - b) + \frac{1}{2}p_{u0}b^2 + \frac{1}{6}mb^3$ $\quad c < z < \lambda L$

$M = p_{u1}\left(\frac{1}{2}z^2 - \lambda Lz + \frac{1}{2}\lambda^2 L^2\right) - p_{u0}b(z - c) - \frac{1}{2}mb^2(z - c)$

$- p_{u0}b(z - c) - \frac{1}{2}mb^2(z - c) - \frac{1}{2}mb^2(c - b) - \frac{1}{2}p_{u0}b^2 - \frac{1}{6}mb^3$ $\quad \lambda L < z < \beta L$

$M = -p_{u2}\left(\frac{1}{2}z^2 - fz + \frac{1}{2}f^2\right) + p_{u2}(g - L)(z - f) + p_{u2}\left(\frac{1}{2}f^2 - Lf + \frac{1}{2}L^2\right)$ $\quad \beta L < z < f$

$M = p_{u2}\left(\frac{1}{2}z^2 - Lz + \frac{1}{2}L^2\right)$ $\quad f < z < L$

Numerical solution procedure (if exists):

Assumed a $b < \lambda L$, f_n is derived from the Shear force equilibrium

$$f_n = \frac{k_0}{k} b_n - \frac{\beta}{2k} + \frac{(1-k_0)}{2k}\left(\frac{{b_n}^2}{\lambda} + \frac{1}{2}\lambda\right) + \frac{1}{2}(\beta+1)$$

And the expression is put into the momentum equilibrium until convergence is reached

$$-\frac{1}{2}\beta^2 + k_0 {b_n}^2 + \left(\frac{2}{3}\frac{{b_n}^3}{\lambda} + \frac{\lambda^2}{6}\right)(1-k_0) + \frac{1}{2}k\left(\beta^2+1\right) = k\left({f_n}^2\right)$$

i.e. : if β=0.7 λ=0.4 k0=0.5 k=2 η=0

b_n=0.34044 f_n=0.821329

ANALYSED CASES AND RELATIVE SOIL REACTION DISTRIBUTION

The following figures show the soil reaction distribution of all the different cases implemented into the model (blue line) in comparison with the ultimate soil pressure profile (dotted line).

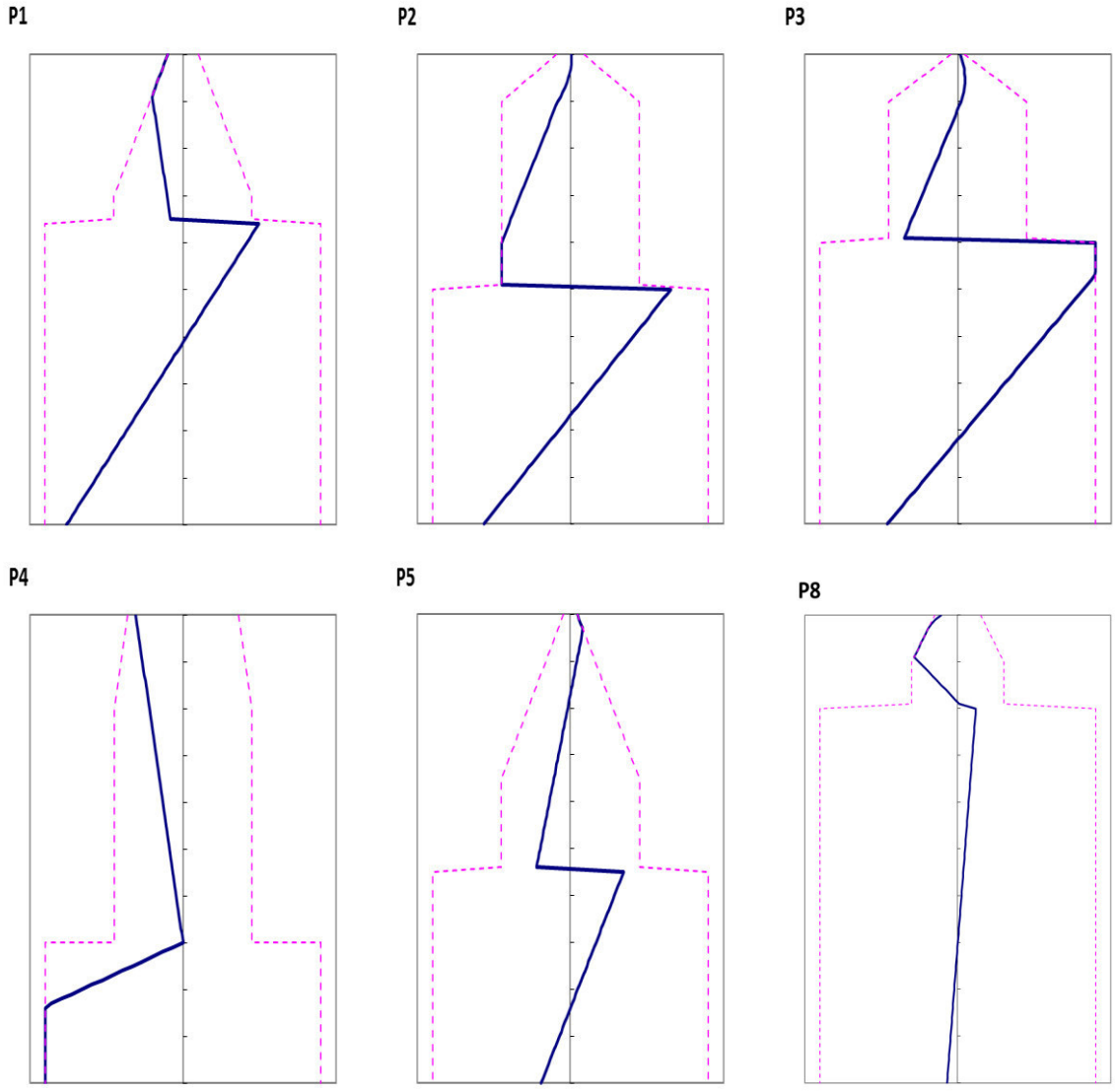

P86

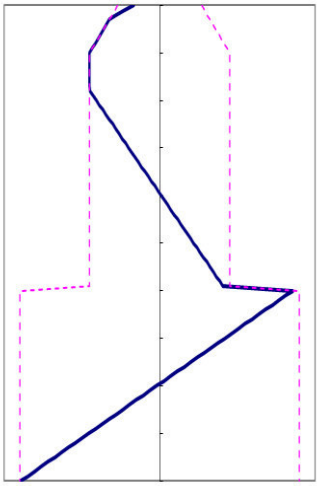

P16

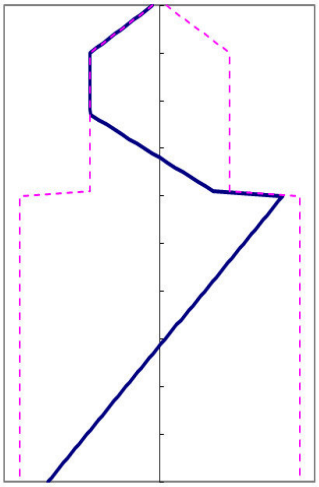

P26

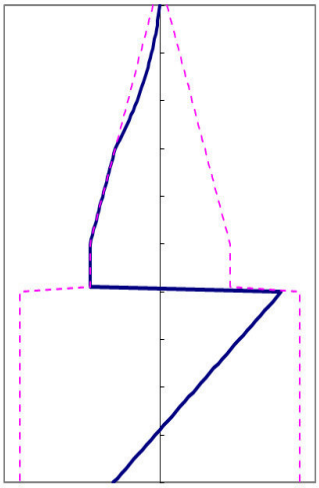

P57

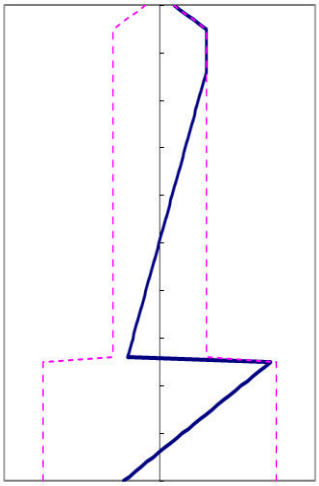

P12

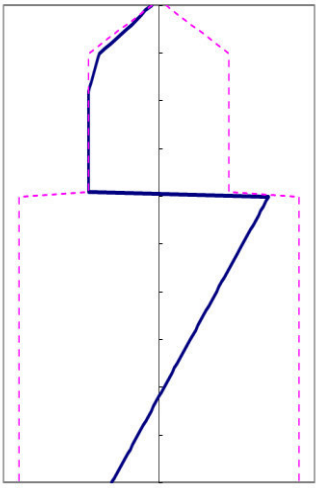

P13

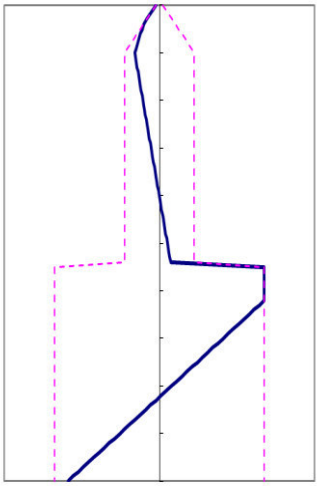

P14

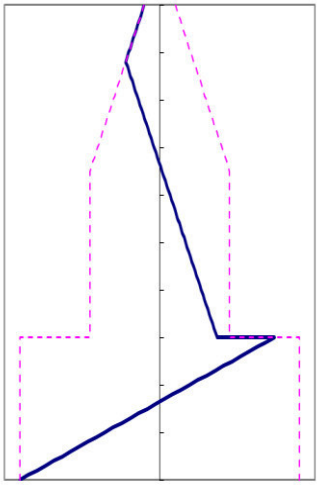

P23

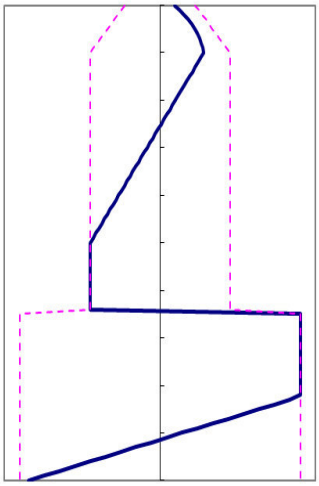

P34

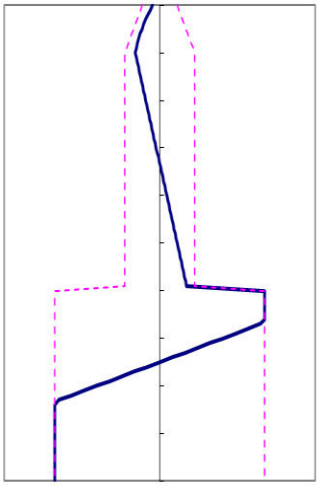

P52

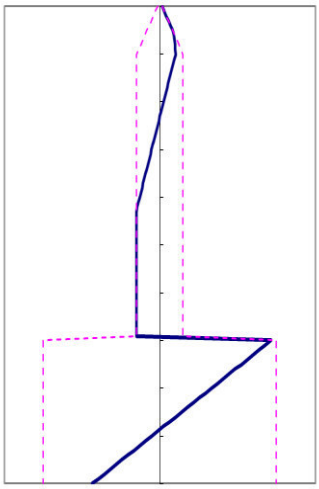

P53

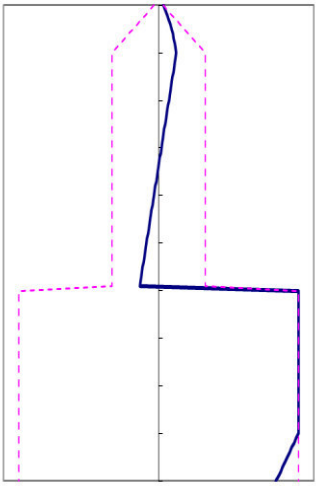

P83

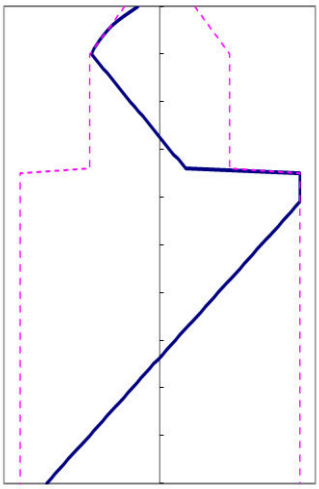

P163

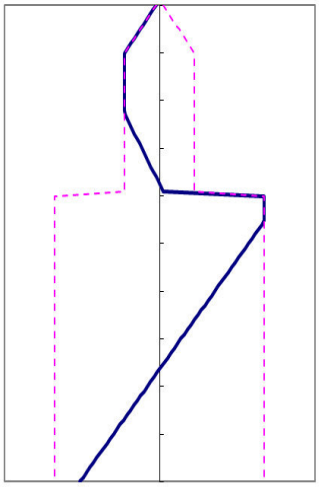

P263

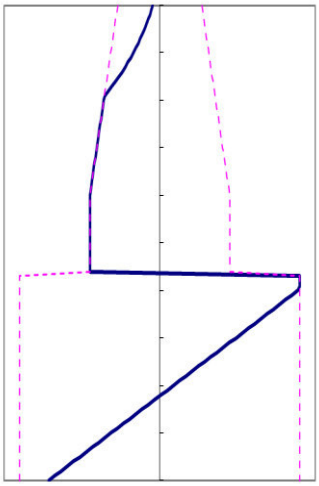

P123

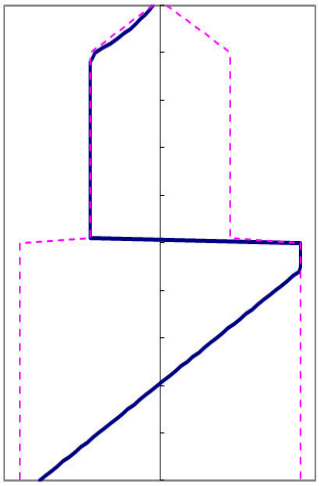

P863

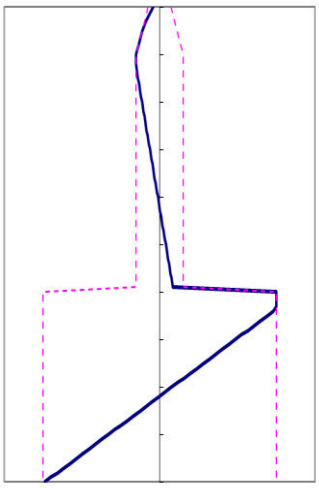

P8632

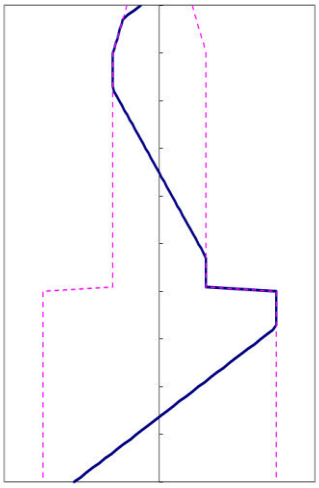

P572

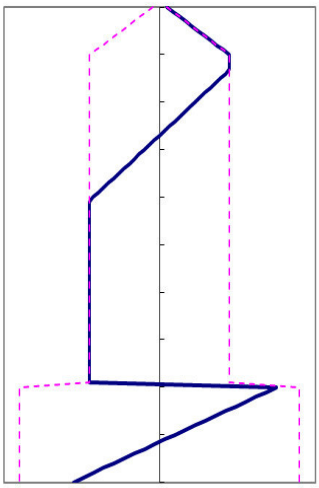

P562

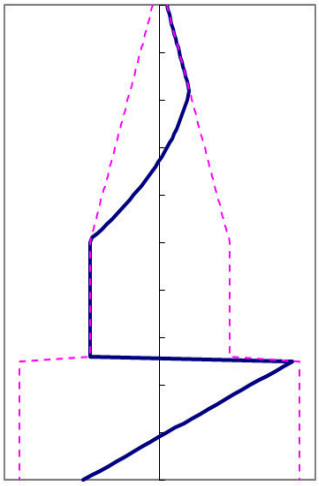

P132

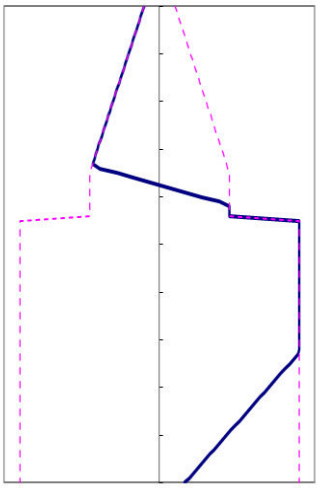

P134

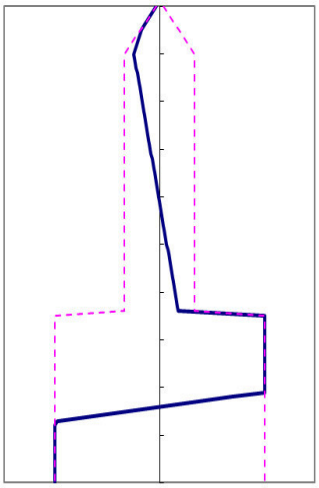

P234

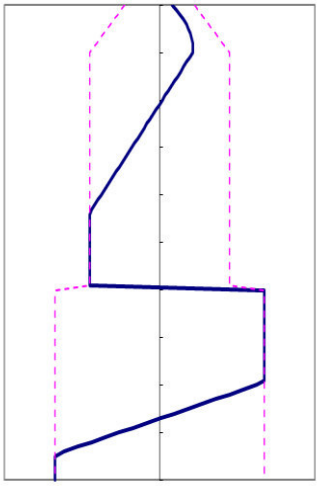

P523

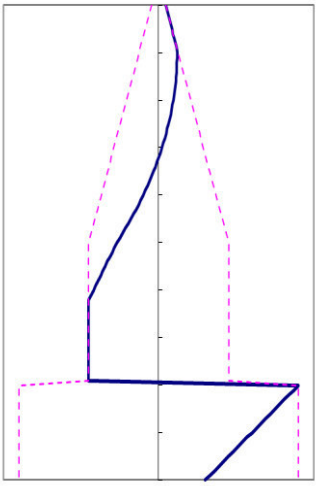

P834

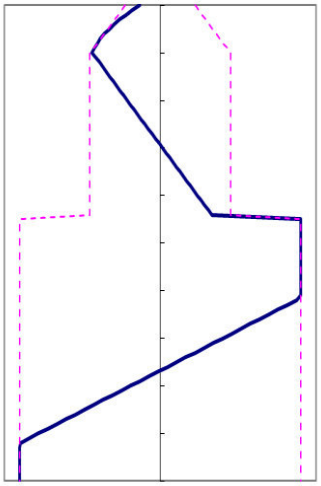

P923

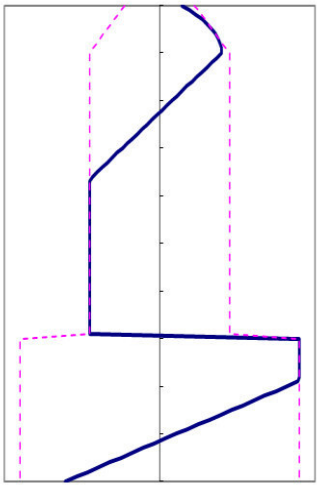

P324

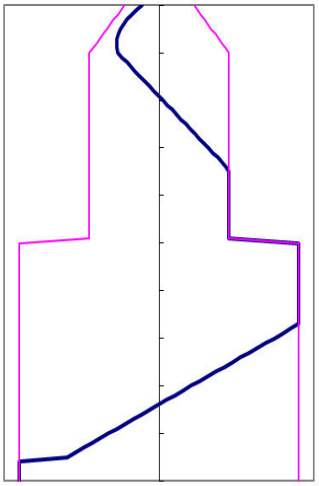

P1632

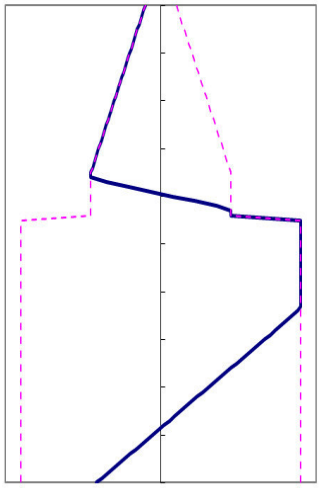

P1634

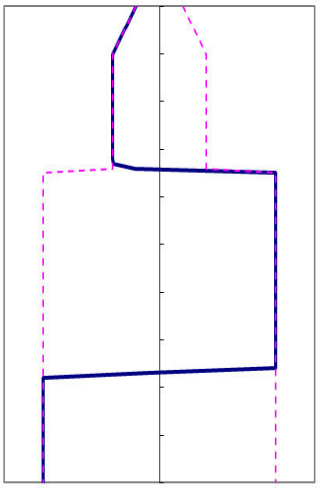

P2634

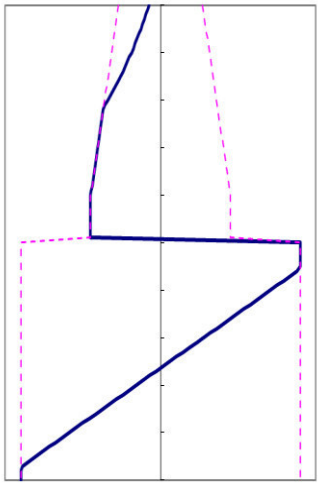

P723

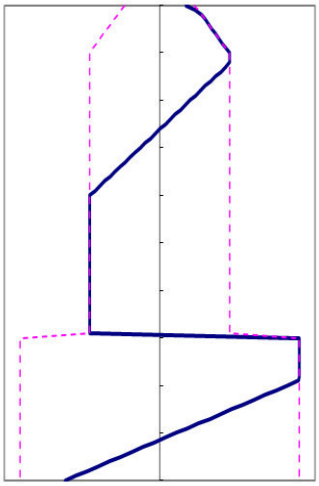

P8324

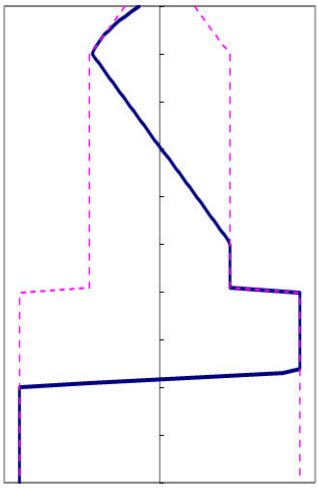

P8634

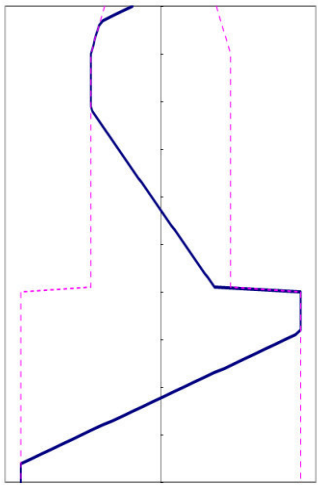

P5723

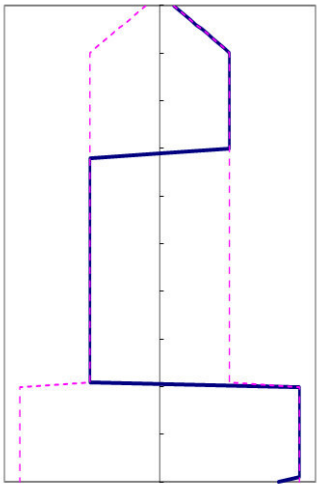

P5623

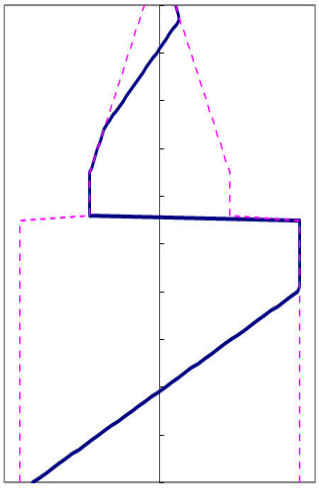

P7234

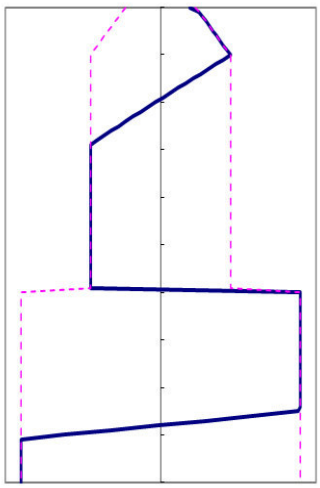

P9234

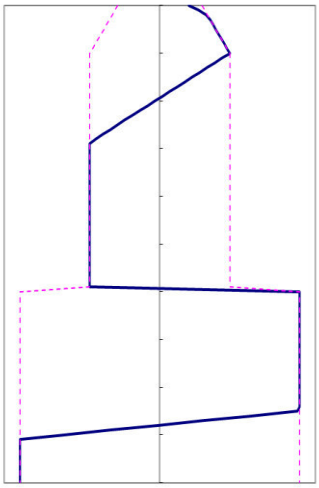

P12234

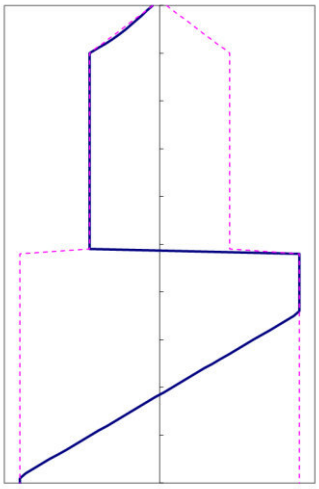

P86324

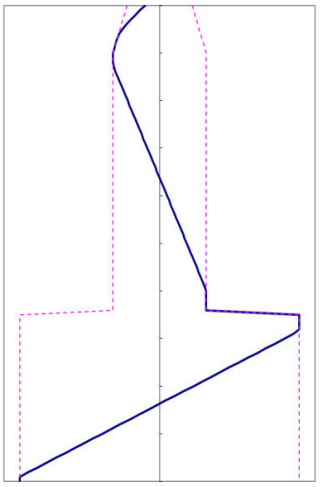

P32

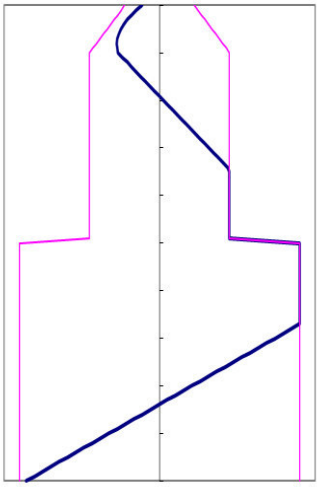

50234 = B1a

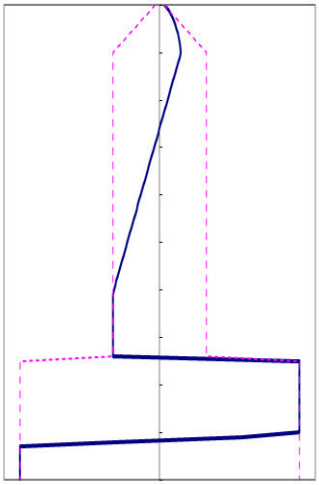

57234 = B1b

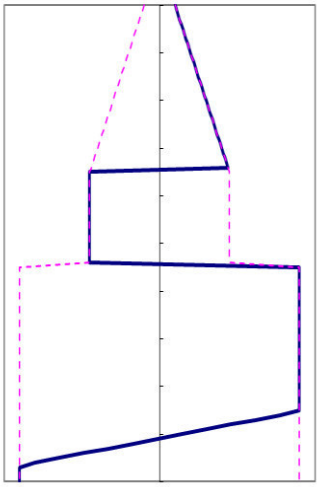

56234 = B1c

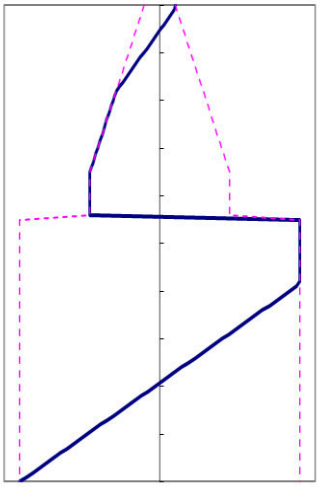

10324 = B2a

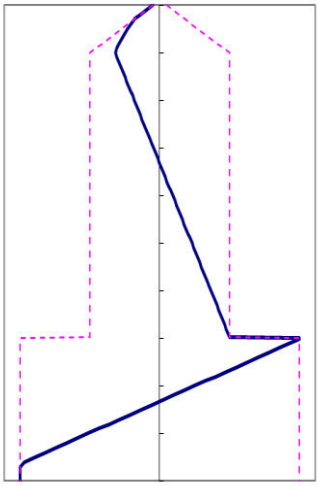

16324 = B2b

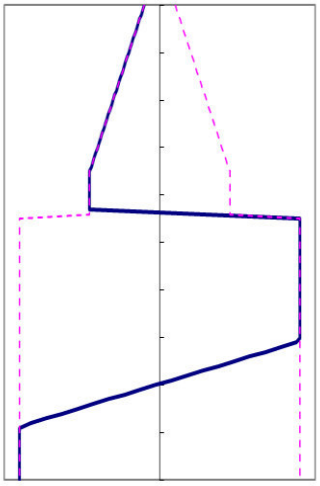

17324 = B2c

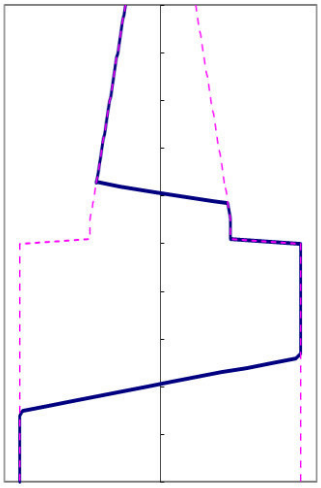

30000 = A1

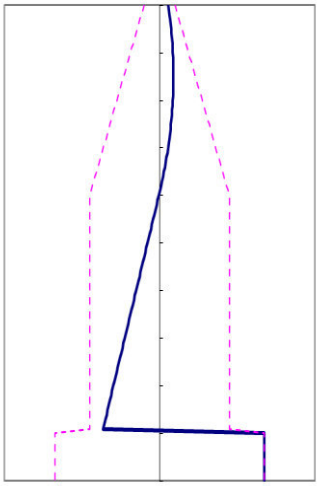

30200 = A2a

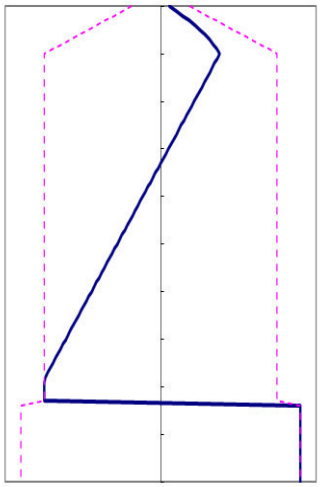

30260 = A2b

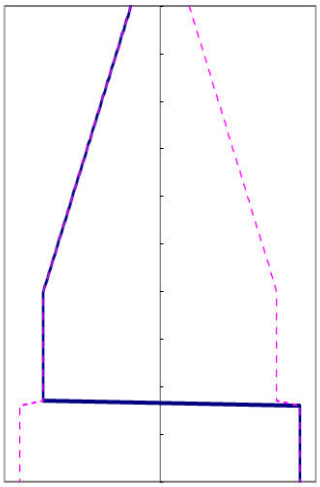

30500 = A2c

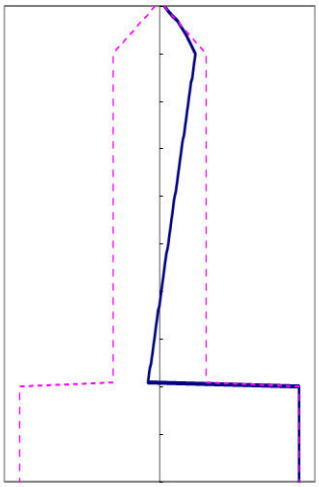

30570 = A2d

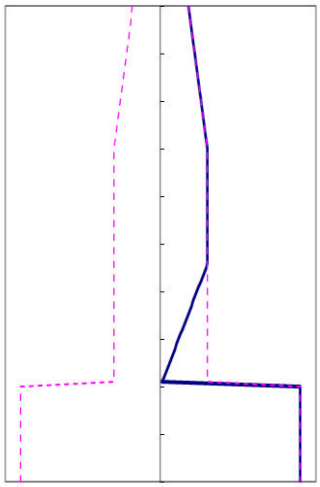

30572 = A3a

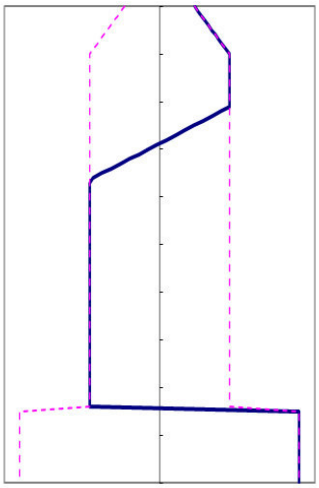

30502 = A3b

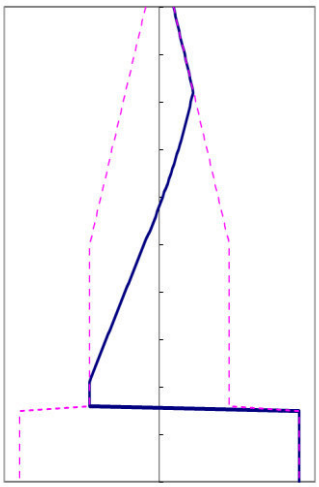

30562 = A3c

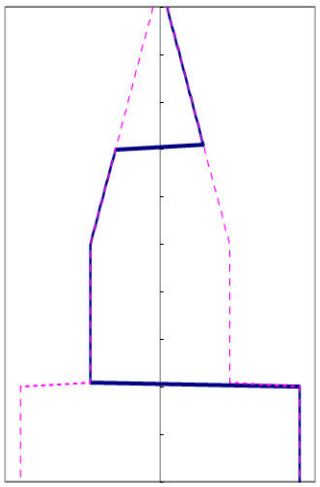

30072 = A72

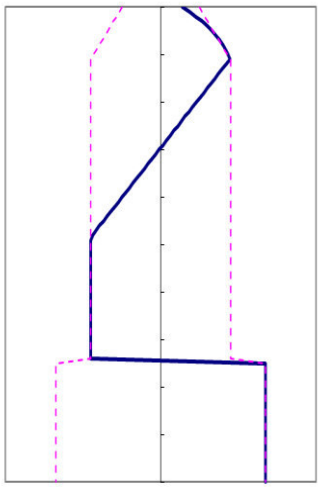

30092 = A92

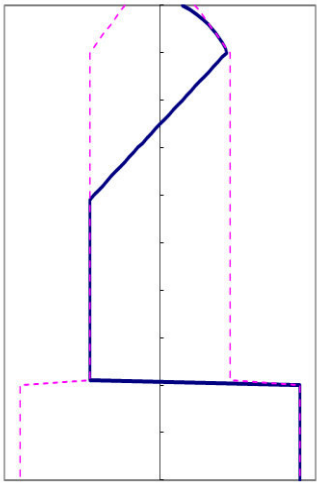

16200 = C1

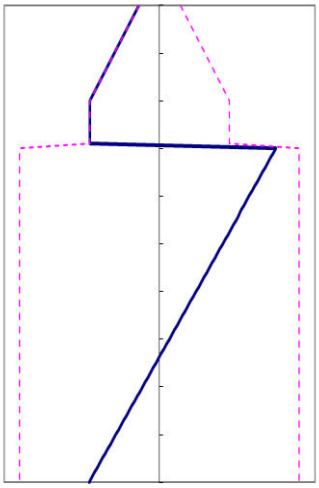

16230 = C2

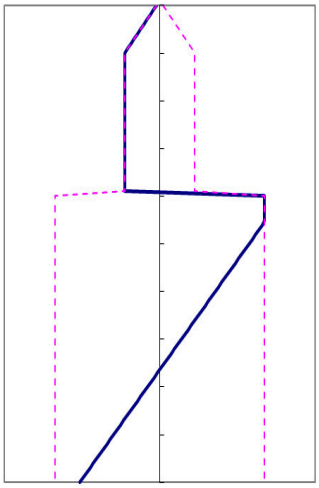

16234 = C3

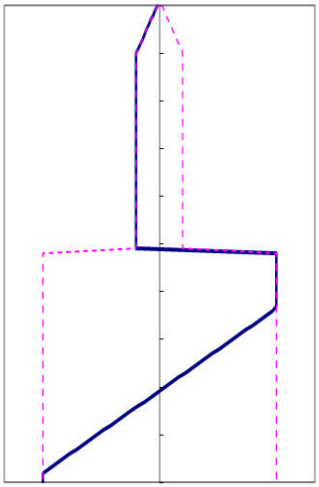

APPENDIX B
Cases for the elasto-plastic analysis of passive rigid piles in a homogeneous cohesionless soil

Since there exist several possible cases for given geometry and pile-soil properties, all analysed and implemented cases concerning the nonlinear analysis method for passive rigid piles in cohesive soils are presented as derived from two generalised cases, all named following the nomenclature used for the single configurations. Limit cases B1 and B2 are also presented.

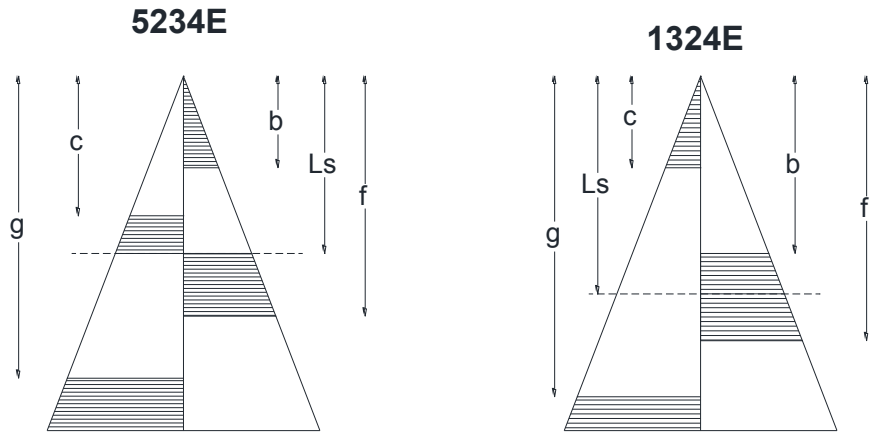

Figure B-1: Generalised cases used to derive all others configurations and their yielding zone with regards to the ultimate soil pressure distribution assumed in the model

The following tables describes the several main cases dependencies and the values to assign to the several parameters of the system in order to obtain every particular case.

Case	b	c	f	g	Case
5	b	Ls	Ls	L	5
2	0	c	Ls	L	2
52	b	c	Ls	L	52
53	b	Ls	f	L	53
23	0	c	f	L	23
523	b	c	f	L	523
234	0	c	f	g	234
B1	b	c	f	g	B1
A1	0	Ls	L	L	A1
A2	b	Ls	L	L	A2
A3	b	c	L	L	A3

Table B-1: Cases derived from the case 5234E (Corresponding to B1)

Case	b	c	f	g	Case
1	Ls	c	Ls	L	1
32	b	0	f	L	32
3	Ls	0	f	L	3
4	Ls	0	Ls	g	4
13	Ls	c	f	L	13
14	Ls	c	Ls	g	14
34	Ls	0	f	g	34
132	b	c	f	L	132
134	Ls	c	f	g	134
B2	b	c	f	g	B2
C1	Ls	Ls	Ls	L	C1
C2	Ls	Ls	f	L	C2
C3	Ls	Ls	f	g	C3

Table B-2: Cases derived from the case 1324E (Corresponding to B2)

The two generalised cases and their associated limit state are described as follow:

CASE 5234E (corresponding to B1)

(yielding in the regions between 0 and b; c and Ls, Ls and f; g and L)

Shear force equilibrium

$$\frac{1}{2}m\left(2L_s^{\,2}-f^2+L^2-g^2-b^2-c^2\right)-\frac{1}{2}ny_0\left(c^2-b^2+g^2-f^2\right)+\frac{1}{3}n\tan\omega\left(c^3-b^3+g^3-f^3\right)$$
$$+\frac{1}{2}ny_{s0}\left(c^2-b^2\right)-\frac{1}{3}n\tan\alpha\left(c^3-b^3\right)=0$$

Bending momentum equilibrium

$$\frac{1}{3}m\left(2L_s^{\,3}-f^3+L^3-g^3-b^3-c^3\right)-\frac{1}{3}ny_0\left(c^3-b^3+g^3-f^3\right)+\frac{1}{4}n\tan\omega\left(c^4-b^4+g^4-f^4\right)$$
$$+\frac{1}{3}ny_{s0}\left(c^3-b^3\right)-\frac{1}{4}n\tan\alpha\left(c^4-b^4\right)=0$$

Congruence in z = b; z = c; z = f e z = g

$$b=\frac{\Delta y_0-m/n}{\Delta\tan}\qquad c=\frac{\Delta y_0+m/n}{\Delta\tan}\qquad f=\frac{y_0-m/n}{\tan\omega}\qquad g=\frac{y_0+m/n}{\tan\omega}$$

Non-linear system of 6 equations in 6 variables (y_0, tanω, b, c, f, g)

Distributed loading $p_n=\frac{p}{nL^2}$

$$p_{n1}=-m_nz_n \qquad 0<z_n<b_n$$
$$p_{n2}=-(\Delta y_{0n})z_n+(\Delta\tan\omega)\cdot z_n^{\,2} \qquad b_n<z_n<c_n$$
$$p_{n3}=m_nz_n \qquad c_n<z_n<\beta$$
$$p_{n4}=-m_nz_n \qquad \beta<z_n<f_n$$
$$p_{n5}=-y_{0n}z_n+\tan\omega\cdot z_n^{\,2} \qquad f_n<z_n<g_n$$
$$p_{n6}=m_nz_n \qquad g_n<z_n<1$$

Shear force at $z_n=\beta$:

$$T_{n\beta}=-\frac{1}{2}(\Delta y_{0n})\left(c_n^{\,2}-b_n^{\,2}\right)+\frac{1}{3}(\Delta\tan)\cdot\left(c_n^{\,3}-b_n^{\,3}\right)+\frac{1}{2}\frac{m}{nL}\left(\beta^2-b_n^{\,2}-c_n^{\,2}\right)$$

Shear force $T_n=\frac{T}{nL^3}$

$$T_n=-\frac{1}{2}m_nz_n^{\,2} \qquad 0<z_n<b_n$$
$$T_{n2}=-\frac{1}{2}(\Delta y_{0n})\left(z_n^{\,2}-b_n^{\,2}\right)+\frac{1}{3}(\Delta\tan)\cdot\left(z_n^{\,3}-b_n^{\,3}\right)-\frac{1}{2}m_nb_n^{\,2} \qquad b_n<z_n<c_n$$
$$T_{n3}=-\frac{1}{2}(\Delta y_{0n})\left(c_n^{\,2}-b_n^{\,2}\right)+\frac{1}{3}(\Delta\tan)\cdot\left(c_n^{\,3}-b_n^{\,3}\right)+\frac{1}{2}m_n\left(z_n^{\,2}-b_n^{\,2}-c_n^{\,2}\right) \qquad c_n<z_n<\beta$$
$$T_{n4}=\frac{1}{2}m_n\left(g_n^{\,2}-1\right)-\frac{1}{2}m_n\left(z_n^{\,2}-f_n^{\,2}\right)-\frac{1}{2}y_{0n}\left(f_n^{\,2}-g_n^{\,2}\right)+\frac{1}{3}\tan\omega\cdot\left(f_n^{\,3}-g_n^{\,3}\right) \qquad \beta<z_n<f_n$$
$$T_{n5}=\frac{1}{2}m_n\left(g_n^{\,2}-1\right)-\frac{1}{2}y_{0n}\left(z_n^{\,2}-g_n^{\,2}\right)+\frac{1}{3}\tan\omega\cdot\left(z_n^{\,3}-g_n^{\,3}\right) \qquad f_n<z_n<g_n$$
$$T_{n6}=\frac{1}{2}m_n\left(z_n^{\,2}-1\right) \qquad g_n<z_n<1$$

Shear force at $z_n=\beta$:

$$T_{n\beta}=-\frac{1}{2}(\Delta y_{0n})\left(c_n^{\,2}-b_n^{\,2}\right)+\frac{1}{3}(\Delta\tan)\cdot\left(c_n^{\,3}-b_n^{\,3}\right)+\frac{1}{2}\frac{m}{nL}\left(\beta^2-b_n^{\,2}-c_n^{\,2}\right)$$

Normalised bending Moment $M_n = \frac{M}{nL^4}$

$$M_{n1} = -\frac{1}{6} m_n z_n^{\,3} \qquad 0 < z_n < b_n$$

$$M_{n2} = -\frac{1}{6} m_n b_n^{\,2}(3z_n - 2b_n) - \frac{1}{6}(\Delta y_{0n})\left(z_n^{\,3} - 3b_n^{\,2} z_n + 2b_n^{\,3}\right) + \frac{1}{12}\Delta tan\cdot\left(z_n^{\,4} - 4b_n^{\,3} z_n + 3b_n^{\,4}\right) \qquad b_n < z < c_n$$

$$M_{n3} = \frac{1}{6} m_n\left[z_n^{\,3} - 3\left(b_n^{\,2} + c_n^{\,2}\right)z_n + 2b_n^{\,3} + 2c_n^{\,3}\right] - \frac{1}{6}(\Delta y_{0n})\left[3\left(c_n^{\,2} - b_n^{\,2}\right)z_n - 2c_n^{\,3} + 2b_n^{\,3}\right]$$
$$\frac{1}{12}\Delta tan\left[4\left(c_n^{\,3} - b_n^{\,3}\right)z_n - 3c_n^{\,4} + 3b_n^{\,4}\right] \qquad c_n < z_n < \beta$$

$$M_{n4} = \frac{1}{6} m_n\left[3\left(g_n^{\,2} - 1\right)z_n - 2g_n^{\,3} + 2\right] - \frac{1}{6} m_n\left(z_n^{\,3} - 3f_n^{\,2} z_n + 2f_n^{\,3}\right)$$
$$-\frac{1}{6} y_{0n}\left[3\left(f_n^{\,2} - g_n^{\,2}\right)z_n - 2f_n^{\,3} + 2g_n^{\,3}\right] + \frac{1}{12} tan\,\omega\left[4\left(f_n^{\,3} - g_n^{\,3}\right)z_n - 3f_n^{\,4} + 3g_n^{\,4}\right] \qquad \beta < z_n < f_n$$

$$M_{n5} = \frac{1}{6} m_n\left(3g_n^{\,2} z_n - 3z_n - 2g_n^{\,3} + 2\right) - \frac{1}{6} y_{0n}\left(z_n^{\,3} - 3g_n^{\,2} z_n + 2g_n^{\,3}\right) + \frac{1}{12} tan\omega\cdot\left(z_n^{\,4} - 4g_n^{\,3} z_n + 3g_n^{\,4}\right) \qquad f_n < z_n < g_n$$

$$M_{6n} = \frac{1}{6} m_n\left(z_n^{\,3} - 3z_n + 2\right) \qquad g_n < z_n < 1$$

Maximum Bending Moment evaluation

Negative Bending Moment ($b_n < z_n < \beta$)

- $T_{n2} = -\frac{1}{2}\Delta y_{0n}\left(z_n^{\,2} - b_n^{\,2}\right) + \frac{1}{3}\Delta tan\cdot\left(z_n^{\,3} - b_n^{\,3}\right) - \frac{1}{2} m_n b_n^{\,2} = 0$

$z_{2n}^{\,3} - 0.75\left(b_n + c_n\right)z_{2n}^{\,2} + 0.5 b_n^{\,3} = 0$

If $b_n < z_{2n} < c_n$ the maximum Bending Moment is:

$$M_{max} = -\frac{1}{6} m_n b_n^{\,2}(3z_{2n} - 2b_n) - \frac{1}{6}\left(y_{0n} - y_{s0n}\right)\left(z_{2n}^{\,3} - 3b_n^{\,2} z_{2n} + 2b_n^{\,3}\right) + \frac{1}{12}\left(tan\omega - tan\alpha\right)\cdot\left(z_{2n}^{\,4} - 4b_n^{\,3} z_{2n} + 3b_n^{\,4}\right)$$

- $T_{3n} = -\frac{1}{2}\left(y_{0n} - y_{sn}\right)\left(c_n^{\,2} - b_n^{\,2}\right) + \frac{1}{3}\left(tan\omega - tan\alpha\right)\cdot\left(c_n^{\,3} - b_n^{\,3}\right) + \frac{1}{2} m_n\left(z_n^{\,2} - c_n^{\,2} - b_n^{\,2}\right) = 0$

$$z_{3n} = \sqrt{c_n^{\,2} + b_n^{\,2} + \frac{(\Delta y_{0n})}{m_n}\left(c_n^{\,2} - b_n^{\,2}\right) - \frac{2}{3}\frac{(\Delta tan)}{m_n}\cdot\left(c_n^{\,3} - b_n^{\,3}\right)} \qquad z_{3n} = \sqrt{\frac{1}{3}\frac{(\Delta tan)}{m_n}\left(c_n^{\,3} - b_n^{\,3}\right)}$$

if $c_n < z_{3n} < \beta$ the maximum Bending Moment is

$$M_{max} = \frac{1}{6} m_n\left[z_{3n}^{\,3} - 3\left(b_n^{\,2} + c_n^{\,2}\right)z_{3n} + 2b_n^{\,3} + 2c_n^{\,3}\right] - \frac{1}{6}\left(y_{0n} - y_{s0n}\right)\left[3\left(c_n^{\,2} - b_n^{\,2}\right)z_{3n} - 2c_n^{\,3} + 2b_n^{\,3}\right]$$
$$\frac{1}{12}\left(tan\,\omega - tan\,\alpha\right)\left[4\left(c_n^{\,3} - b_n^{\,3}\right)z_{3n} - 3c_n^{\,4} + 3b_n^{\,4}\right]$$

Positive Bending Moment ($\beta < z_n < g_n$)

- $T_{n4} = \frac{1}{2} m_n\left(g_n^{\,2} - 1\right) - \frac{1}{2} m_n\left(z_n^{\,2} - f_n^{\,2}\right) - \frac{1}{2} y_{0n}\left(f_n^{\,2} - g_n^{\,2}\right) + \frac{1}{3} tan\omega\cdot\left(f_n^{\,3} - g_n^{\,3}\right) = 0$

$$z_{4n} = \sqrt{f_n^{\,2} + g_n^{\,2} - 1 - \frac{1}{m_n} y_{0n}\left(f_n^{\,2} - g_n^{\,2}\right) + \frac{2}{3}\frac{1}{m_n} tan\,\omega\cdot\left(f_n^{\,3} - g_n^{\,3}\right)}$$

$$z_{4n} = \sqrt{\frac{\tan\omega}{3m_n}\cdot\left(g_n{}^3 - f_n{}^3\right) - 1} \quad \text{if } \beta < z_{4n} < f_n$$

$$M_{max} = \frac{1}{6}m_n\left[3\left(g_n{}^2 - 1\right)z_{4n} - 2g_n{}^3 + 2\right] - \frac{1}{6}m_n\left(z_{4n}{}^3 - 3f_n{}^2 z_{4n} + 2f_n{}^3\right)$$

$$-\frac{1}{6}y_{0n}\left[3\left(f_n{}^2 - g_n{}^2\right)z_{4n} - 2f_n{}^3 + 2g_n{}^3\right] + \frac{1}{12}\tan\omega\left[4\left(f_n{}^3 - g_n{}^3\right)z_{4n} - 3f_n{}^4 + 3g_n{}^4\right]$$

- $T_{n5} = \frac{1}{2}m_n\left(g_n{}^2 - 1\right) - \frac{1}{2}y_{0n}\left(z_n{}^2 - g_n{}^2\right) + \frac{1}{3}\tan\omega\cdot\left(z_n{}^3 - g_n{}^3\right) = 0$

If the solution of the expression $z_n{}^3 - 1.5a_n z_n{}^2 + \left(0.5g_n{}^3 - 1.5\frac{m_n}{\tan\omega}\right) = 0$ is within f_n and g_n, the maximum bending moment is:

$$M_{max} = -\frac{1}{6}y_{0n}\left(z_{5n}{}^3 - 3g_n{}^2 z_{5n} + 2g_n{}^3\right) + \frac{1}{12}\tan\omega\cdot\left(z_{5n}{}^4 - 4g_n{}^3 z_{5n} + 3g_n{}^4\right) + \frac{1}{6}m_n\left[3\left(g_n{}^2 - 1\right)z_{5n} - 2g_n{}^3 + 2\right]$$

LIMIT CASE B1

This limit case occurs for an infinite eternal displacement: $b = c = x$ e $f = g = y$

Shear force equilibrium

$$\frac{1}{2}m\left(2L_s^{\,2} - 2y^2 + L^2 - 2x^2\right) = 0$$

Bending momentum equilibrium

$$\frac{1}{3}m\left(2L_s^{\,3} - 2y^3 + L^3 - 2x^3\right) = 0$$

Normalised:

$$x_n^{\,2} + y_n^{\,2} = 0.5 + \beta^2$$

$$x_n^{\,3} + y_n^{\,3} = 0.5 + \beta^3$$

By combining the two equations the following equation is obtained:

$$y_n = \frac{x_n^{\,3} - 0.5 - \beta^3}{x_n^{\,2} - 0.5 - \beta^2}$$

And then:

$$x_n^{\,2} + y_n^{\,2} - 0.5 - \beta^2 = 0$$

$$x_n^{\,2} + \left(\frac{x_n^{\,3} - 0.5 - \beta^3}{x_n^{\,2} - 0.5 - \beta^2}\right)^2 - 0.5 - \beta^2 = 0$$

$$x_n^{\,6} - \left(\frac{1.5 + 3\beta^2}{2}\right)x_n^{\,4} - \left(\frac{1 + 2\beta^3}{2}\right)x_n^{\,3} + \left(\frac{0.75 + 3\beta^4 + 3\beta^2}{2}\right)x_n^{\,2} + \left(\frac{0.125 + \beta^3 - 1.5\beta^4 - 0.75\beta^2}{2}\right) = 0$$

x_n e y_n depend on β.

The solution is admissible if $0 < x_n < \beta$ and $\beta < y_n < 1$

The normalised shear force is:

$$\frac{T}{mL^2} = 0.5\beta^2 - x_n^{\,2}$$

In the following table, values of x_n e y_n over β are listed:.

β	x_n	y_n	T_{nm}
0.455	0.01560	0.84070	0.103269
0.460	0.04921	0.84213	0.103378
0.470	0.08343	0.84495	0.103490
0.480	0.10799	0.84778	0.103537
0.490	0.12845	0.85065	0.103552
0.500	0.14644	0.85355	0.103555
0.510	0.16277	0.85651	0.103556
0.520	0.17785	0.85952	0.103568
0.530	0.19197	0.86258	0.103598
0.540	0.20529	0.86571	0.103656
0.550	0.21795	0.86891	0.103748
0.560	0.23005	0.87217	0.103879
0.570	0.24164	0.87551	0.104060
0.580	0.25280	0.87892	0.104293
0.590	0.26356	0.88240	0.104585
0.600	0.27396	0.88597	0.104945
0.610	0.28404	0.88962	0.105374
0.620	0.29380	0.89335	0.105880
0.630	0.30329	0.89717	0.106468
0.640	0.31250	0.90108	0.107144

0.650	0.32146	0.90508	0.107916
0.660	0.33018	0.90917	0.108783
0.670	0.33867	0.91335	0.109754
0.680	0.34694	0.91763	0.110836
0.690	0.35499	0.92200	0.112031
0.700	0.36284	0.92647	0.113344
0.710	0.37050	0.93104	0.114781
0.720	0.37796	0.93571	0.116347
0.730	0.38523	0.94048	0.118045
0.740	0.39233	0.94535	0.119880
0.750	0.39924	0.95032	0.121855
0.760	0.40599	0.95539	0.123975
0.770	0.41256	0.96057	0.126244
0.780	0.41897	0.96585	0.128667
0.790	0.42521	0.97123	0.131242
0.800	0.43130	0.97672	0.133978
0.810	0.43723	0.98231	0.136876
0.820	0.44302	0.98800	0.139937
0.830	0.44865	0.99379	0.143166
0.840	0.45413	0.99968	0.146563

CASE 1324 E

(yieldng in regions between 0 and c; b and f ; g and L)

Shear force equilibrium

$$\frac{1}{2}m\left(b^2+c^2+L^2-f^2-g^2\right)-\frac{1}{2}ny_0\left(b^2-c^2+g^2-f^2\right)+\frac{1}{3}n\tan\omega\left(b^3-c^3+g^3-f^3\right)$$
$$+\frac{1}{2}ny_{s0}\left(b^2-c^2\right)-\frac{1}{3}n\tan\alpha\left(b^3-c^3\right)=0$$

Bending momentum equilibrium

$$\frac{1}{3}m\left(b^3+c^3+L^3-f^3-g^3\right)-\frac{1}{3}ny_0\left(b^3-c^3+g^3-f^3\right)+\frac{1}{4}n\tan\omega\left(b^4-c^4+g^4-f^4\right)$$
$$+\frac{1}{3}ny_{s0}\left(b^3-c^3\right)-\frac{1}{4}n\tan\alpha\left(b^4-c^4\right)=0$$

Congruence in z = b; z = c; z = f e z = g

$$b=\frac{y_0-y_s-m/n}{\tan\omega-\tan\alpha}\qquad c=\frac{y_0-y_s+m/n}{\tan\omega-\tan\alpha}\qquad f=\frac{y_0-m/n}{\tan\omega}\qquad g=\frac{y_0+m/n}{\tan\omega}$$

Non-linear system of 6 equations in 6 variables (y_0, tanω, b, c, f, g)

Distributed loading $p_n=\frac{p}{nL^2}$

$p_{n1}=m_n z_n$	$0 < z_n < c_n$
$p_{n2}=-(\Delta y_{0n})z_n+(\Delta\tan)\cdot z_n^{\,2}$	$c_n < z < b_n$
$p_{n3}=-m_n z_n$	$b_n < z_n < f_n$
$p_{n4}=-y_{0n}z_n+\tan\omega\cdot z_n^{\,2}$	$f_n < z_n < g_n$
$p_{n5}=m_n z_n$	$g_n < z_n < 1$

Shear force at $z_n = \beta$

$$T_{n\beta}=-\frac{1}{2}(y_{0n}-y_{sn})\left(b_n^{\,2}-c_n^{\,2}\right)+\frac{1}{3}(\tan\omega-\tan\alpha)\cdot\left(b_n^{\,3}-c_n^{\,3}\right)-\frac{1}{2}m_n\left(\beta^2-b_n^{\,2}-c_n^{\,2}\right)$$

Shear force $T_n=\frac{T}{nL^3}$

$T_n=\frac{1}{2}m_n z_n^{\,2}$	$0 < z_n < c_n$
$T_{n2}=-\frac{1}{2}(\Delta y_{0n})\left(z_n^{\,2}-c_n^{\,2}\right)+\frac{1}{3}(\Delta\tan)\cdot\left(z_n^{\,3}-c_n^{\,3}\right)+\frac{1}{2}m_n c_n^{\,2}$	$c_n < z < b_n$
$T_{n3}=-\frac{1}{2}m_n\left(z_n^{\,2}-b_n^{\,2}-c_n^{\,2}\right)-\frac{1}{2}(\Delta y_{0n})\left(b_n^{\,2}-c_n^{\,2}\right)+\frac{1}{3}(\Delta\tan)\left(b_n^{\,3}-c_n^{\,3}\right)$	$b_n < z_n < f_n$
$T_{n4}=\frac{1}{2}m_n\left(g_n^{\,2}-1\right)-\frac{1}{2}y_{0n}\left(z_n^{\,2}-g_n^{\,2}\right)+\frac{1}{3}\tan\omega\cdot\left(z_n^{\,3}-g_n^{\,3}\right)$	$f_n < z_n < g_n$
$T_{n5}=\frac{1}{2}m_n\left(z_n^{\,2}-1\right)$	$g_n < z_n < 1$

Shear force at $z_n = \beta$

$$T_{n\beta}=-\frac{1}{2}(y_{0n}-y_{sn})\left(b_n^{\,2}-c_n^{\,2}\right)+\frac{1}{3}(\tan\omega-\tan\alpha)\cdot\left(b_n^{\,3}-c_n^{\,3}\right)-\frac{1}{2}m_n\left(\beta^2-b_n^{\,2}-c_n^{\,2}\right)$$

Bending Moment $M_n = \frac{M}{nL^4}$

$M_{n1} = \frac{1}{6} m_n z_n^{\,3}$ $\quad 0 < z_n < c_n$

$M_{n2} = \frac{1}{6} m_n c_n^{\,2}(3z_n - 2c_n) - \frac{1}{6}(\Delta y_{0n})\left(z_n^{\,3} - 3c_n^{\,2} z_n + 2c_n^{\,3}\right) + \frac{1}{12}(\Delta tan\omega)\cdot\left(z_n^{\,4} - 4c_n^{\,3} z_n + 3c_n^{\,4}\right)$ $\quad c_n < z < b_n$

$M_{n3} = -\frac{1}{6} m_n\left[z_n^{\,3} - 3\left(b_n^{\,2} + c_n^{\,2}\right)z_n + 2b_n^{\,3} + 2c_n^{\,3}\right] - \frac{1}{6}(\Delta y_{0n})\left\{3\left(b_n^{\,2} - c_n^{\,2}\right)z_n - 2b_n^{\,3} + 2c_n^{\,3}\right\}$

$\frac{1}{12}(\Delta tan)\left\{4\left(b_n^{\,3} - c_n^{\,3}\right)z_n - 3b_n^{\,4} + 3c_n^{\,4}\right\}$ $\quad b_n < z_n < f_n$

$M_{n4} = -\frac{1}{6} y_{0n}\left(z_n^{\,3} - 3g_n^{\,2} z_n + 2g_n^{\,3}\right) + \frac{1}{12} tan\omega\cdot\left(z_n^{\,4} - 4g_n^{\,3} z_n + 3g_n^{\,4}\right) + \frac{1}{6} m_n\left(3g_n^{\,2} z_n - 3z_n - 2g_n^{\,3} + 2\right)$ $\quad f_n < z_n < g_n$

$M_{5n} = \frac{1}{6} m_n\left(z_n^{\,3} - 3z_n + 2\right)$ $\quad g_n < z_n < 1$

Maximum Bending Moment evaluation

- $T_{n2} = -\frac{1}{2}(\Delta y_{0n})\left(z_n^{\,2} - c_n^{\,2}\right) + \frac{1}{3}(\Delta tan\omega)\cdot\left(z_n^{\,3} - c_n^{\,3}\right) + \frac{1}{2} m_n c_n^{\,2} = 0$

$z_{2n}^{\,3} - 0.75(b_n + c_n) z_{2n}^{\,2} + 0.5 c_n^{\,3} = 0$ **IF** $c_n < z_n < b_n$

$M_{n2} = \frac{1}{6} m_n c_n^{\,2}(3z_n - 2c_n) - \frac{1}{6}(\Delta y_{0n})\left(z_n^{\,3} - 3c_n^{\,2} z_n + 2c_n^{\,3}\right) + \frac{1}{12}(\Delta tan)\cdot\left(z_n^{\,4} - 4c_n^{\,3} z_n + 3c_n^{\,4}\right)$

- $T_{n3} = -\frac{1}{2}(y_{0n} - y_{sn})\left(b_n^{\,2} - c_n^{\,2}\right) + \frac{1}{3}(tan\omega - tan\alpha)\cdot\left(b_n^{\,3} - c_n^{\,3}\right) - \frac{1}{2}\frac{m}{nL}\left(z_n^{\,2} - b_n^{\,2} - c_n^{\,2}\right) = 0$

$z_n = \sqrt{b_n^{\,2} + c_n^{\,2} - \frac{(y_{0n} - y_{sn})}{\overline{m}}\left(b_n^{\,2} - c_n^{\,2}\right) + \frac{2}{3}\frac{(tan\omega - tan\alpha)}{\overline{m}}\cdot\left(b_n^{\,3} - c_n^{\,3}\right)}$

$z_{3n} = \sqrt{c_n^{\,2} + b_n^{\,2} + \frac{(y_{0n} - y_{sn})}{\overline{m}}\left(c_n^{\,2} - b_n^{\,2}\right) - \frac{2}{3}\frac{(tan\omega - tan\alpha)}{\overline{m}}\cdot\left(c_n^{\,3} - b_n^{\,3}\right)}$

$z_{3n} = \sqrt{\frac{(\Delta tan)}{3m_n}\left(c_n^{\,3} - b_n^{\,3}\right)}$ $\quad$ if $b_n < z_n < f_n$

$M_{max} = -\frac{1}{6} m_n\left[z_{3n}^{\,3} - 3\left(b_n^{\,2} + c_n^{\,2}\right)z_{3n} + 2b_n^{\,3} + 2c_n^{\,3}\right] - \frac{1}{6}(\Delta y_{0n})\left\{3\left(b_n^{\,2} - c_n^{\,2}\right)z_{3n} - 2b_n^{\,3} + 2c_n^{\,3}\right\}$

$\frac{1}{12}(\Delta tan\,\omega)\left\{4\left(b_n^{\,3} - c_n^{\,3}\right)z_{3n} - 3b_n^{\,4} + 3c_n^{\,4}\right\}$

- $T_{n4} = \frac{1}{2} m_n\left(g_n^{\,2} - 1\right) - \frac{1}{2} y_{0n}\left(z_n^{\,2} - g_n^{\,2}\right) + \frac{1}{3} tan\omega\cdot\left(z_n^{\,3} - g_n^{\,3}\right) = 0$

$z_n^{\,3} - 1.5 a_n z_n^{\,2} + \left(0.5 g_n^{\,3} - 1.5\frac{m_n}{tan\,\omega}\right) = 0$ $\quad$ se $f_n < z_n < g_n$

$M_{n4} = -\frac{1}{6} y_{0n}\left(z_n^{\,3} - 3g_n^{\,2} z_n + 2g_n^{\,3}\right) + \frac{1}{12} tan\omega\cdot\left(z_n^{\,4} - 4g_n^{\,3} z_n + 3g_n^{\,4}\right) + \frac{1}{6}\frac{m}{nL}\left(3g_n^{\,2} z_n - 3z_n - 2g_n^{\,3} + 2\right)$

LIMIT CASE B2

This limit case occurs for an infinite eternal displacement: $b = c = x$ e $f = g = y$

Shear force equilibrium

$$\frac{1}{2}m\left(2x^2 + L^2 - 2y^2\right) = 0$$

Bending momentum equilibrium

$$\frac{1}{3}m\left(2x^3 + L^3 - 2y^3\right) = 0$$

Normalised:

$$2x_n^{\ 2} - 2y_n^{\ 2} + 1 = 0$$

$$2x_n^{\ 3} - 2y_n^{\ 3} + 1 = 0$$

By combining the two equations the following equation is obtained:

$$y_n = \frac{1 + 2x_n^{\ 3}}{1 + 2x_n^{\ 2}}$$

And then:

$$12x_n^{\ 4} - 8x_n^{\ 3} + 6x_n^{\ 2} - 1 = 0$$

x_n e y_n do not depend on β: $x_n \approx 0.4545$ $y_n \approx 0.84$

The solution is admissible if $x_n < \beta < y_n$

The normalised shear force, at $z_n = \beta$, is:

$$T_{n\beta} = -\frac{1}{2}\left(y_{0n} - y_{sn}\right)\left(b_n^{\ 2} - c_n^{\ 2}\right) + \frac{1}{3}\left(tan\omega - tan\alpha\right)\cdot\left(b_n^{\ 3} - c_n^{\ 3}\right) - \frac{1}{2}m_n\left(\beta^2 - b_n^{\ 2} - c_n^{\ 2}\right)$$

$$T_{n\beta} = -\frac{1}{2}m_n\left(\beta^2 - 2x_n^{\ 2}\right)$$

$$T_{m\beta} = \frac{T_\beta}{mL^2} = x_n^{\ 2} - 0.5\beta^2$$

ANALYSED CASES AND RELATIVE SOIL REACTION DISTRIBUTION

The following figures show the soil reaction distribution of all the different cases implemented into the model (blue line) in comparison with the ultimate soil pressure profile (dotted line).

P1

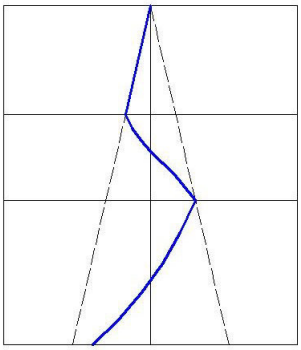

P2

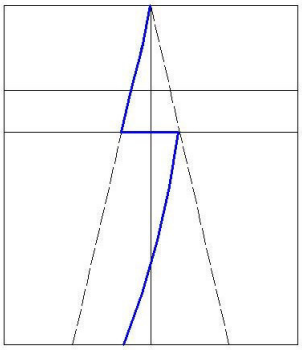

P3

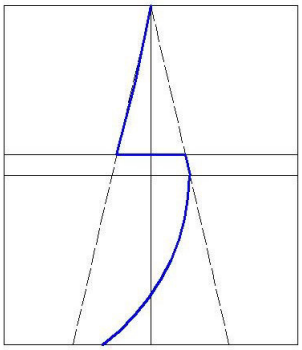

P4

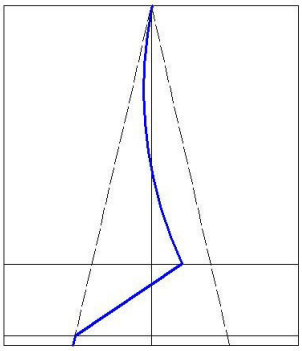

P5

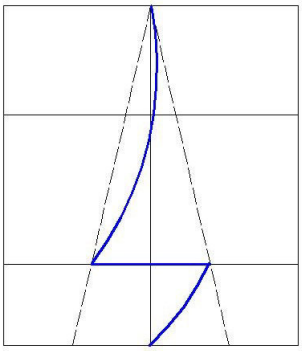

P13

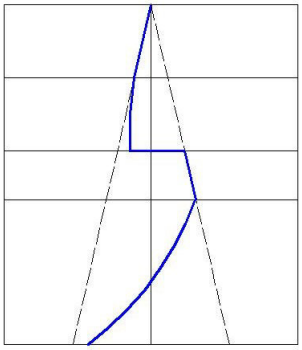

P14

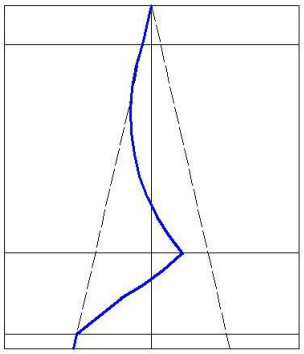

P16(132)

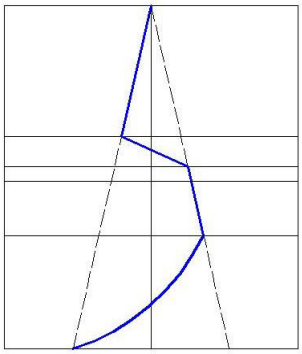

P52

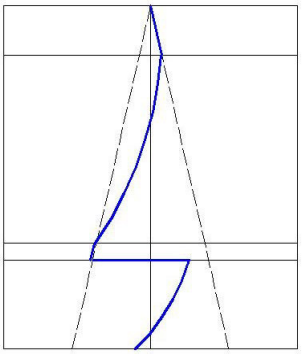

P53

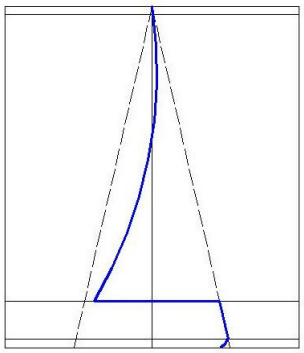

P23

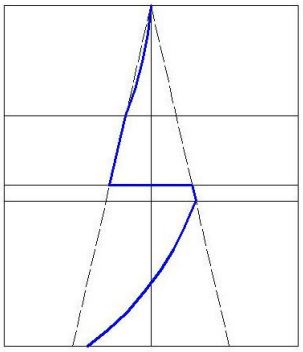

P34

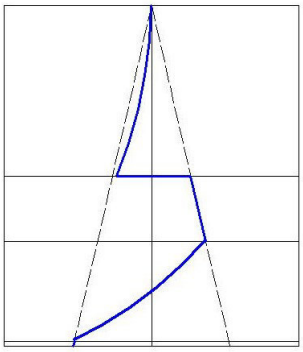

A1

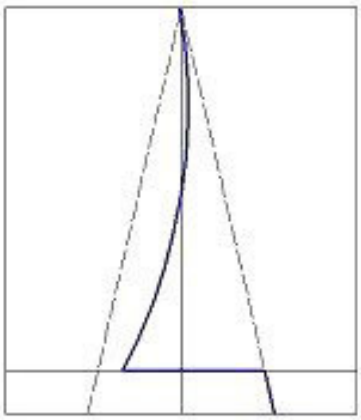

A2

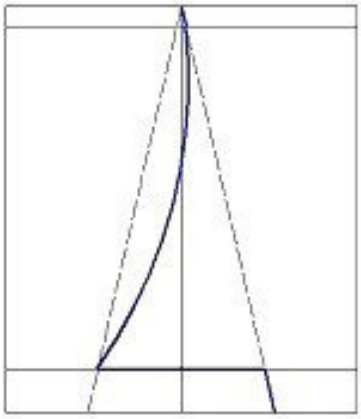

A3

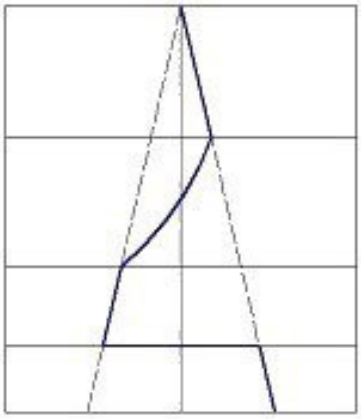

P523

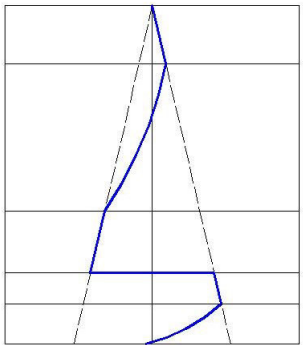

B1

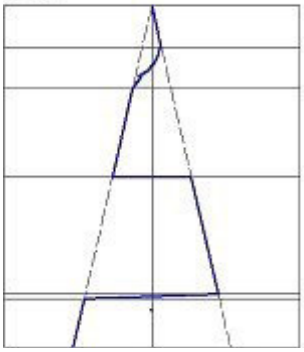

B2

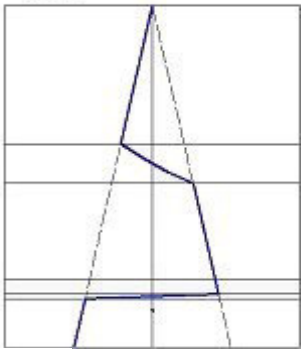

5234 EX b1

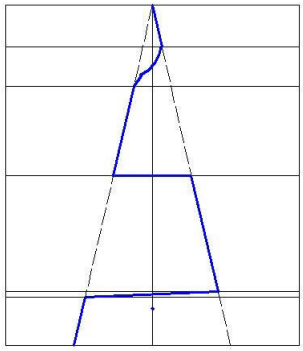

1234

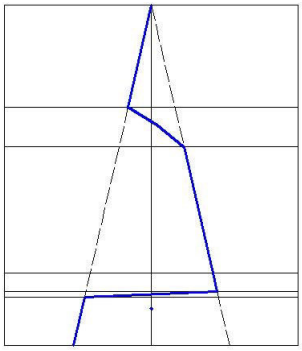

C1

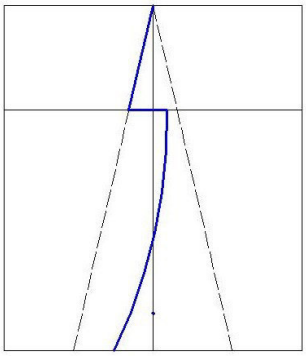

C2

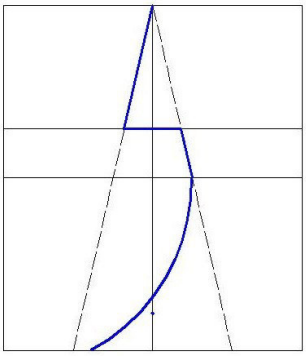

C3